ZooKeys 795: 1–12 (2018)
doi: 10.3897/zookeys.795.29339
http://zookeys.pensoft.net

RESEARCH ARTICLE

A peer-reviewed open-access journal
ZooKeys
Launched to accelerate biodiversity research

Fulfilling the taxonomic consequence after DNA Barcoding: *Carychium panamaense* sp. n. (Eupulmonata, Ellobioidea, Carychiidae) from Panama is described using computed tomographic (CT) imaging

Adrienne Jochum[1], Bernhard Ruthensteiner[2], Marian Kampschulte[3], Gunhild Martels[4], Jeannette Kneubühler[1], Adrien Favre[5]

1 *Naturhistorisches Museum der Burgergemeinde Bern, 3005 Bern, Switzerland and Institute of Ecology and Evolution, University of Bern, 3012 Bern, Switzerland* **2** *Zoologische Staatssammlung München, 81247 München, Germany* **3** *Department of Radiology, Universitätsklinikum Giessen und Marburg GmbH-Standort Giessen, Center for Radiology, 35385 Giessen, Germany* **4** *Department of Experimental Radiology, Justus-Liebig University Giessen, Biomedical Research Center Seltersberg (BFS), 35392 Giessen, Germany* **5** *Department of Entomology III, Senckenberg Research Institute and Natural History Museum, 60438 Frankfurt/M., Germany*

Corresponding author: *Adrienne Jochum* (Adrienne.jochum@gmail.com)

Academic editor: *T. Backeljau* | Received 27 August 2018 | Accepted 26 September 2018 | Published 5 November 2018

http://zoobank.org/07C35455-E66C-46D9-AB31-71CAC4CE9E01

Citation: Jochum A, Ruthensteiner B, Kampschulte M, Martels G, Kneubühler J, Favre A (2018) Fulfilling the taxonomic consequence after DNA Barcoding: *Carychium panamaense* sp. n. (Eupulmonata, Ellobioidea, Carychiidae) from Panama is described using computed tomographic (CT) imaging. ZooKeys 795: 1–12. https://doi.org/10.3897/zookeys.795.29339

Abstract

Five years ago, the Panamanian evolutionary lineage (EL) C12 was uncovered along with four other ELs in an integrative phylogenetic investigation of worldwide Carychiidae. Since EL C12 lacked shell material post-molecular analysis to serve as a museum voucher, it remained undescribed. Now, after recent collection efforts of C12 and the congener, *Carychium zarzaae* Jochum & Weigand, 2017 at their original Panamanian sites, C12 is morphologically described and formally assigned the name, *Carychium panamaense* Jochum, **sp. n.** In sync with recent taxonomic treatment of the genus, computed tomography (CT) is used in this work to differentiate shells of *C. panamaense* **sp. n.** from geographically-proximal, Caribbean, North and Central American congeners. Recent material of topotypic *Carychium jardineanum* (Chitty, 1853) and undamaged *C. zarzaae* were additionally CT-scanned and assessed in the comparative analyses.

Copyright *Adrienne Jochum et al.* This is an open access article distributed under the terms of the Creative Commons Attribution License (CC BY 4.0), which permits unrestricted use, distribution, and reproduction in any medium, provided the original author and source are credited.

Resumen

Hace cinco años, el linaje evolutivo (LE) panameño C12 fue descubierto junto con otros cuatro LEs en un estudio filogenético integrativo mundial de Carychiidae. El LE C12 permaneció sin ser descrito dado que, después de los análisis moleculares, no había conchas disponibles que sirvieran como material de referencia en museos.

Ahora, después de esfuerzos recientes para colectar C12 y el congénere, *Carychium zarzaae* Jochum & Weigand, 2017 en los sitios panameños originales, C12 es descrito morfológicamente y se le asigna formalmente un nombre, *Carychium panamaense* Jochum, **sp. n.** De acuerdo con el tratamiento taxonómico reciente del género, en este trabajo se emplea tomografía computarizada (TC) para diferenciar conchas de *C. panamaense* **sp. n.** de congéneres geográficamente cercanos del Caribe, Norte y Centro América. Además, en el análisis comparativo se escaneó con TC y se examinó material reciente del topotípico *Carychium jardineanum* (Chitty, 1853) y *C. zarzaae* en buen estado.

Keywords

microgastropoda, museum voucher, tropical ecology, conservation, Panamanian snails, Central America

Introduction

In an integrative phylogenetic investigation of worldwide Carychiidae, Weigand et al. (2013) uncovered four evolutionary lineages (ELs) of *Carychium* O.F. Müller, 1773 from North and Central America. These ELs were found to be molecularly distinct from the two known nominal species, *Carychium mexicanum* Pilsbry, 1891 and *C. costaricanum* E. von Martens, 1898. The consequential, morphological and taxonomic assessment of three of these molecularly uncovered lineages resulted in the recent description of three new species of *Carychium* by Jochum et al. (2017): *C. hardiei* Jochum & Weigand, 2017 from Georgia, USA, *C. belizeense* Jochum & Weigand, 2017 from Belize, and *C. zarzaae* Jochum & Weigand, 2017 from Panama. The fourth molecularly flagged EL (C12), also from Panama (Weigand et al. 2013), could not be fully assessed by Jochum et al. (2017, fig. 15) since no shells remained to serve as museum voucher material. Recent collection efforts by one of us (A.F.) at the topotypic locality, Parque International La Amistad in Chiriquí, Panama now enable full taxonomic treatment of lineage C12 (former morphospecies *C. mexicanum costaricanum* sensu Pilsbry (1948)) in Weigand et al. (2013, fig. 1). In congruence with Jochum et al. (2017), *Carychium panamaense* sp. n. is formally described in this work. In addition, since the protoconch and body whorl of the very fragile paratype material of Panama's recently described congener, *C. zarzaae* (NMBE 549927/1) was damaged in the initial CT-scanning process (Jochum et al. 2017, fig. 14), new images of the fresh topotypic material are presented here in the comparative analysis. Furthermore, although Jochum et al. (2017) presented the distinct molecular aspects of *C. jardineanum* (Chitty, 1853), the only known Caribbean (Jamaica) species of *Carychium*, computer tomographic (CT) images were not available at the time. Their inclusion in the comparative analysis of this work is beneficial for understanding both the spectrum of shell variability and diversity of the tropical American Carychiidae as well as the geographical context of *C. panamaense* sp. n. in particular (Fig. 1).

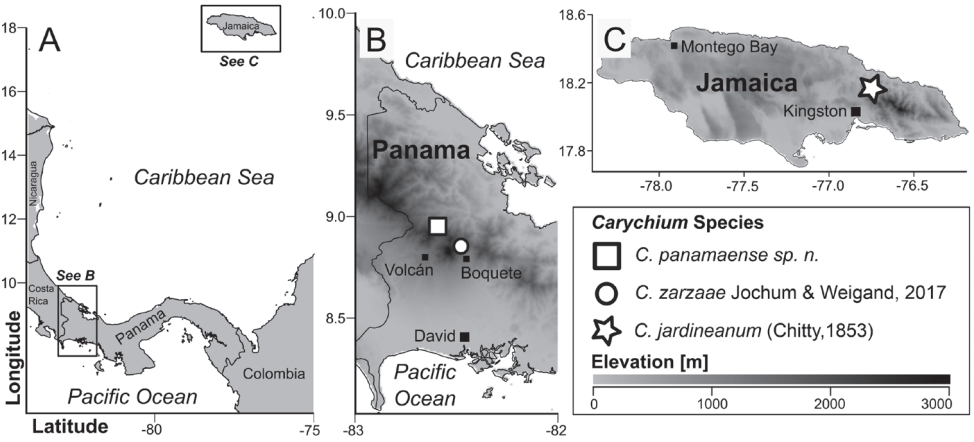

Figure 1. Map indicating type localities of the two Panamanian *Carychium* species, *C. panamaense* sp. n. and *C. zarzaae* Jochum & Weigand, 2017 and of the Jamaican allied species, *C. jardineanum* (Chitty, 1853). The grayscale indicates the local mean elevation. Map downloaded from WORLDCLIM (Hijmans et al. 2005); political borders retrieved from Esri Data and Maps (2002).

Material and methods

Carychium panamaense sp. n. was collected by A. Favre under the permit Ref. Nr. SE/PH-4-18 issued by the Ministerio de Ambiente, Balboa, Ancón, Panama.

Shell measurements include the shell width (**sw**), shell height (**sh**), aperture width (**aw**) and aperture height (**ah**) expressed in mm (Table 1). Whorl number was counted according to Kerney et al. (1979).

Qualitative aspects of shell morphology include peristome shape; whorl profile (whorl convexity); teleoconch sculpture; development of apertural dentition visible in frontal view; development of the columellar lamella as discernable in the CT images of the ventral, dorsal, side-left and side-right perspectives of the *C. panamaense* sp. n. adult shell.

Material is housed in the following collections:

AJC	Adrienne Jochum Collection: formerly Institute of Ecology, Evolution & Diversity, Phylogeny & Systematics Collection, Goethe-Universität, Frankfurt am Main, Germany
ANSP	Academy of Natural Sciences of Drexel University, Philadelphia, PA, USA
CM	Carnegie Museum of Natural History, Pittsburgh, PA, USA
MUPADI	Museo de Peces de Agua Dulce e Invertebrados, Universidad Autónoma de Chiriquí, David, Chiriquí, Panama
NMBE	Naturhistorisches Museum der Burgergemeinde Bern, Bern, Switzerland
RBINS	Royal Belgian Institute of Natural Sciences, Brussels, Belgium
SMF	Forschungsinstitut und Naturmuseum Senckenberg, Frankfurt am Main, Germany
UF	University of Florida, Florida Museum of Natural History, Gainesville, FL., USA

Table 1. Measurement data of *Carychium panamaense* sp. n., N=7. Abbreviations: sw – shell width, sh – shell height, aw – aperture width, ah – aperture height. All measurements in millimeters (mm).

***Carychium* specimen**	**Museum No.**	**Sample**	**sw**	**sh**	**aw**	**ah**
C. panamaense sp. n. holotype	NMBE 554428	1	0,91	2,12	0,70	0,80
C. panamaense sp. n. paratype	NMBE 554429	1	0,84	NA	0,64	0,77
C. panamaense sp. n. paratype	NMBE 554429	2	0,76	NA	0,60	0,71
C. panamaense sp. n. paratype (damaged)	NMBE 554429	3	NA	NA	NA	NA
C. panamaense sp. n. paratype, EtOH	NMBE 554432	1	0,93	2,03	0,68	0,73
C. panamaense sp. n. paratype, EtOH	NMBE 554432	2	0,91	1,98	0,69	0,77
C. panamaense sp. n. paratype, EtOH	NMBE 554432	3	0,97	2,09	0,74	0,83
Mean *C. panamaense*			0,89	2,06	0,67	0,77

Image acquisition

Digital images: *Carychium panamaense* sp. n. (Figs 2, 3) was imaged using a Leica DFC425 digital camera attached to a Leica M205 C stereo microscope (Wetzlar, Germany), using IMS Client analysis image system software (Imagic Bildverarbeitungs AG, Glattbrugg, Switzerland) for measurements.

Micro-CT: The two Panamanian species, *C. panamaense* sp. n. (Fig. 4A–J) and *C. zarzaae* (Fig. 4K–T), were imaged at the Zoologische Staatssammlung München, Munich, Germany. Scanning was performed with a Phoenix Nanotom m (GE Measurement & Control, Wunstorf, Germany) cone beam CT scanner at a voltage of 80 kV and a current of 325 mA using a tungsten ("Standard") target during a 360° rotation. *Carychium panamaense* sp. n. was captured in two longitudinal portions at 1200 projection images each at a total duration of 124 minutes; voxel size was 0.891 µm. *Carychium zarzaae* was captured at 1600 projections at a total duration of 205 minutes; voxel size was 0.919 µm. The 16-bit data sets, generated by reconstruction, were cropped and converted to 8-bit using VGStudio MAX 2.2 software (Volume Graphics, Heidelberg, Germany). Further visualization procedures were carried out with Amira 6.4 software (FEI Visualization Sciences Group, Burlington MA, USA) applying manual segmentation for discrimination of external and internal shell structures. Final visualization was enabled using the Volume Rendering tool. All grey-colored *Carychium* in the comparative analysis in this work (Fig. 5), except for *C. jardineanum*, were figured in Jochum et al. (2017). In congruence with Jochum et al. (2017), *C. jardineanum* was imaged using a SkyScan 2011 (Bruker MicroCT, Kontich, Belgium) micro-CT system, at the Department of Experimental Radiology, Justus-Liebig University Biomedical Research Center Seltersberg (BFS), Giessen, Germany. The *Carychium* were mounted and scanned 185° around their vertical axis in rotation steps of 0.23° at 80 kV tube voltage and 120 µA tube current. Reconstruction was performed using the Feldkamp cone beam reconstruction algorithm. Image resolution was 1.75 µm isotropic voxel side length with a grey scale resolution of 8 bit. Digital images, post processing and visualization (maximum intensity projection – MIP, volume compositing and summed voxel projection), were displayed using the ANALYZE software package (ANALYZE 11.0, Mayo Clinic, Rochester, MN, USA).

Taxonomy

Family Carychiidae Jeffreys, 1830
Genus *Carychium* O.F. Müller, 1773

***Carychium panamaense* Jochum, sp. n.**
http://zoobank.org/C70432C6-2FCD-4F9F-A48D-493E9F9E739D
Figures 2–4

Carychium panamaense: Weigand et al., 2013: 3, fig. 1 48|C12; Seq. ID: BARCA142-12, BARCA143-12, BARCA144-12

Material examined. Holotype (NMBE 554428/1 ex AJC 2383): Panama, Chiriquí Prov., Cerro Punta, La Amistad International Park, El Retoño Trail, near Las Nubes Ranger Station; 8.8934278°N, 82.6190528°W, elev. 2239 m, on moist broadleaf litter and twigs; 27 February 2018; leg. Adrien Favre.

Paratypes: locus typicus 3 damaged shells (NMBE 554429/3 ex AJC 2383); 7 specimens in ethanol (NMBE 554432 ex AJC 2382); 5 specimens in ethanol (SMF 349423 ex AJC 2382); 5 specimens in ethanol (MUPADI-Mol.-01-001 ex AJC 2382); 4 specimens in ethanol (ANSP A476441 ex AJC 2382); 5 specimens in ethanol (CM 159907 ex AJC 2382); 3 specimens in ethanol (UF 511987 ex. AJC 2382); data as for holotype.

Diagnosis. Shell ca. 2 mm in height, transparent, elongate-pupiform with an oblique, ovate-shaped and unequally thickened peristome, with a palatal callus, pronounced parieto-columellar callus and a prominent parietal denticle. Internal coiling of the lamella about the columellar spindle is wide rather than tight.

Description. Measurements are provided in Table 1. Shell minute, elongate pupiform, transparent when fresh, with about 4.1 convex whorls and a deeply incised suture; occasional, irregular striations or growth lines on the body whorl (see also Jochum et al. 2017, fig. 15). The shell is opaque with age and often superficially degraded with pock marks (due to acidity of the leaf litter). The protoconch is more nipple-like than bulbous. The teleoconch is smooth. Peristome is obliquely auriform, longer than wide, tending to be thinnest on the upper right-hand margin, where it slightly reflects from the body whorl and then curves into a relatively broad, shield-like aspect onto the body whorl (Figs 2A, E, 3A). The peristome is otherwise, uniform in thickness (Figs 2, 3) but becomes thinner towards the edges. A medium-sized parietal denticle is present, the base of which is in line horizontally with the widest, shield-like extension of the peristome onto the body whorl (Figs 2A, E, 3, 4F). Directly opposite the parietal denticle is a thickened palatal callus (Figs 2A, 4F). The lower left columellar margin has a prominently-thickened, parietal-columellar callus (Figs 2A, E, F, 3A–C, 4F). In aperture facing-right perspective, the peristome is sheer with the body whorl (Fig. 4G–H). The peristome curves back slightly at the base (Figs 2B, 4C) whereby, the layer of callus on the palatal side forms a small knob on the rim in the aperture facing-left (Fig. 2B) and dorsal (Fig. 4B) perspectives.

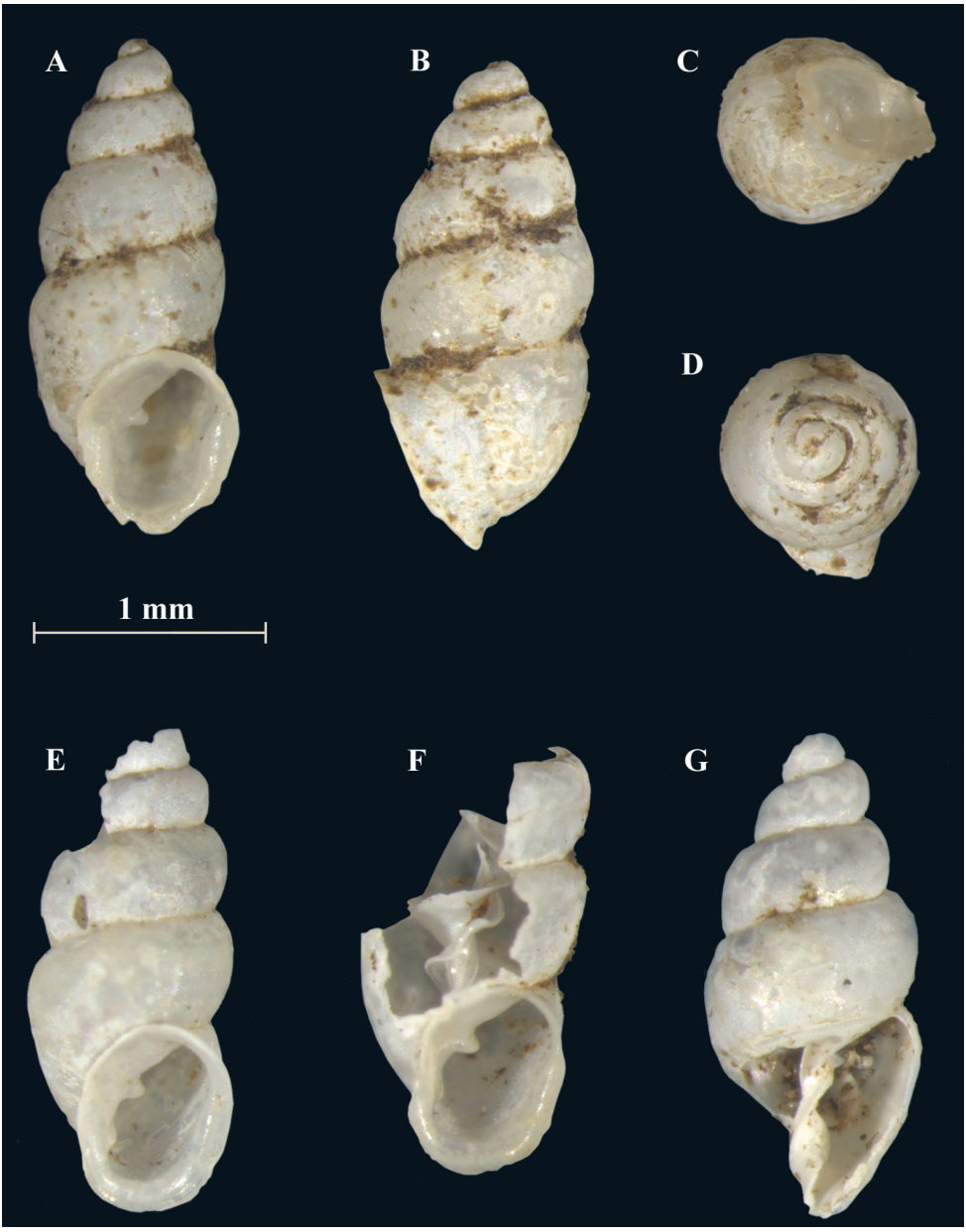

Figure 2. *Carychium panamaense* sp. n. **A–D** holotype (NMBE 554428/1) **E–G** paratype shells (NMBE 554429/3). Scale bar: 1 mm.

Internally, a widely spiraling, sinuous lamella starts at the top of the penultimate whorl (dorsal perspective) (Fig. 4B), which extends laterally in aperture facing-left and aperture facing-right perspectives (Fig. 4D, H). The degree of fullest sinuosity varies in the configuration of the lower primary lamella from an accentuated, oblique-elongated S-form (Fig. 2F) to a slightly curved aspect in the ventral perspective (Fig. 4F). The

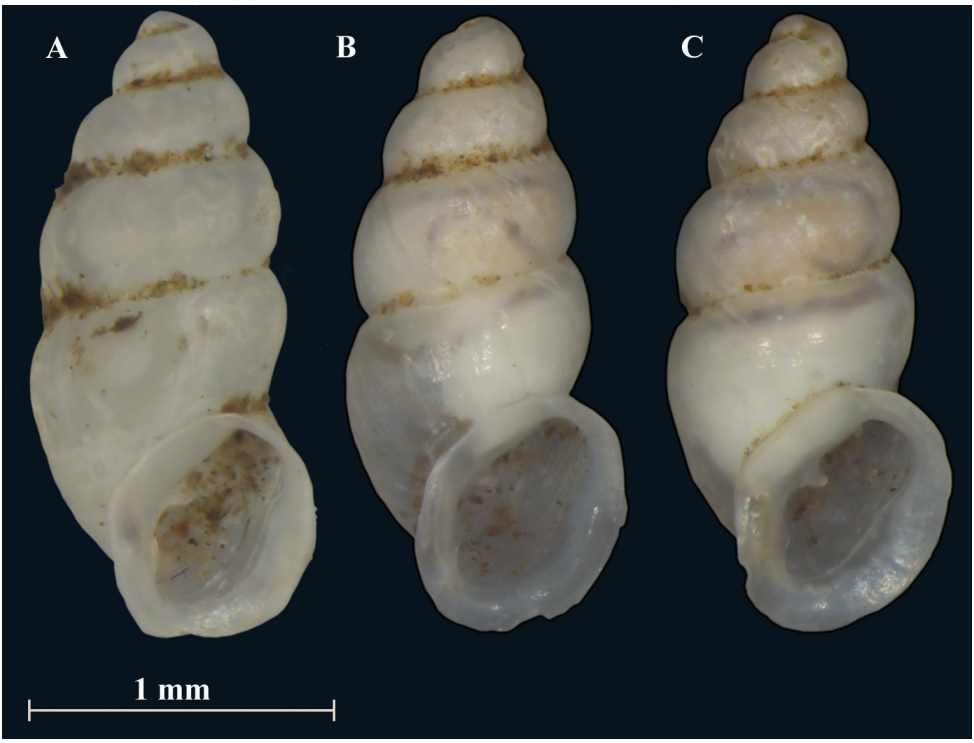

Figure 3. *Carychium panamaense* sp. n. **A–C** paratype shells preserved in alcohol (NMBE 554432). Scale bar: 1 mm.

thick, upper curvature of the lamella forms the upper part of the elongated S shape (Fig. 2F). The general curvature of the lamella about the columella is wider than narrow along the entire length of the columellar spindle. Viewed from the umbilical perspective (Fig. 4J), the rim of the peristome is thin and widely flared. In live individuals, the outmost edge of the peristome appears white (Fig. 6D).

Differential diagnosis. Differs from congeners presented in Jochum et al. (2017), imaged here (Figs 4K–T, 5), by its apertural morphology and large apertural size: long, obliquely-auriform, widely-flared aspect of the thinly-rimmed peristome (seen best from umbilical perspective) (Fig. 4) and the wide coiling of the lamella about the columellar spindle. Although the peristome mostly resembles that of *C. belizeense* (Jochum et al. 2017, fig. 11A, I), the generally broad, shield-like extension of the peristome onto the body whorl differentiates this species from *C. belizeense* as well as from its Southeastern USA, Caribbean and Central American congeners. Though the S-shaped configuration of the primary lamella (ventral view) (Fig. 2F) is closest to that of *C. belizeense* (Fig. 5), *C. hardiei* (Fig. 5) and *C. zarzaae* (Fig. 4P), the abapical onset of the lamella in the penultimate whorl and the general extant of sinuosity along the entire length of the columella in relation to the columellar spindle is unique to each species in both the ventral and dorsal perspectives. The tongue-like flexion of the primary lamella is a specific configuration occurring in three different perspectives within the shell of each of these species*: C. hardiei*

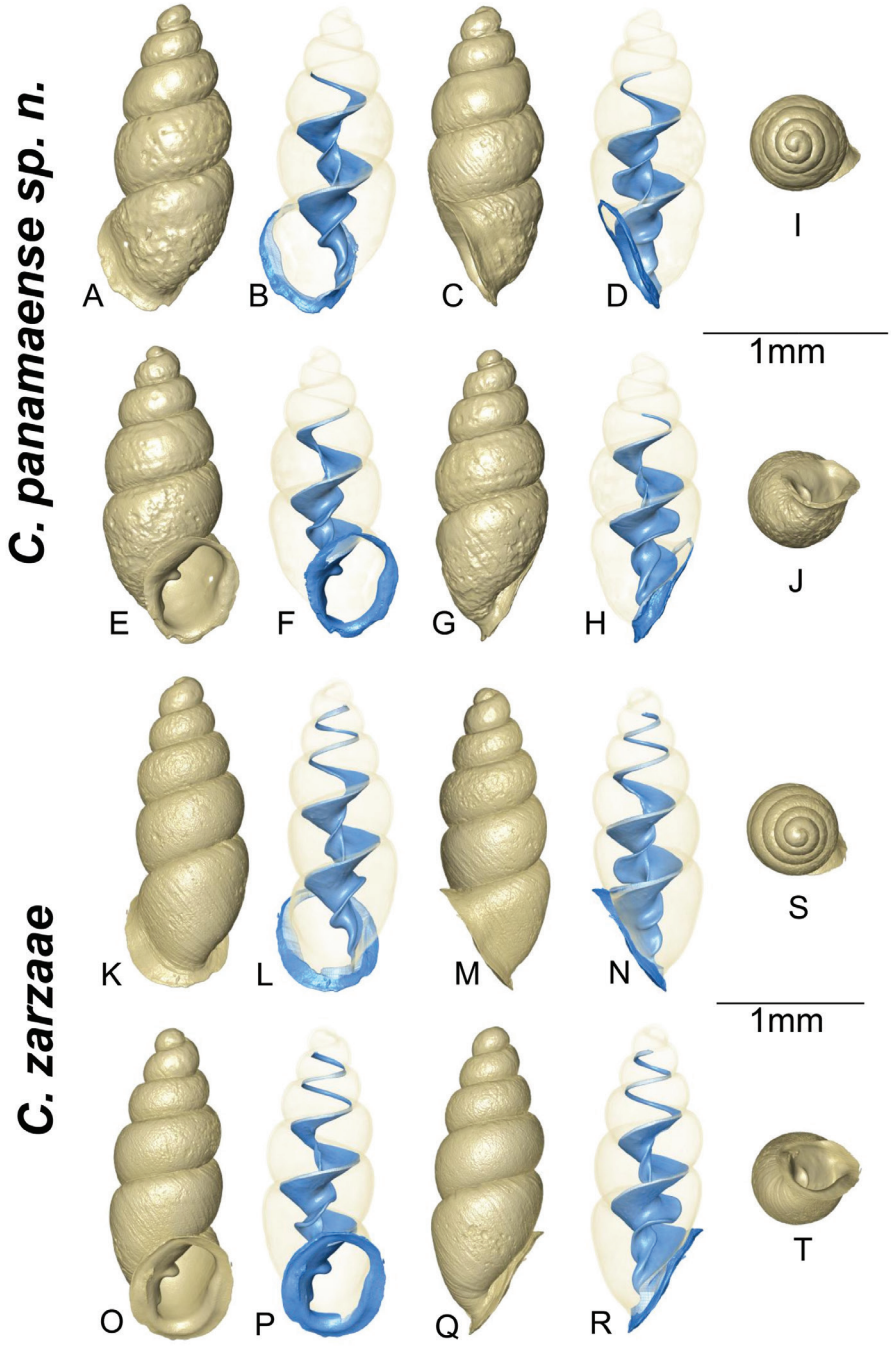

Figure 4.A–J *Carychium panamaense* sp. n. holotype (NMBE 554428/1), CT images, partly with external shell transparent to show columellar apparatus **I** aerial view of protoconch and spire **J** umbilical view **K–T** allied Panamanian species topotype, *Carychium zarzaae*, Jochum & Weigand, 2017 (AJC 2385). CT images, partly with external shell transparent to show columellar apparatus **S** aerial view of protoconch and spire **T** umbilical view. Scale bar: 1 mm.

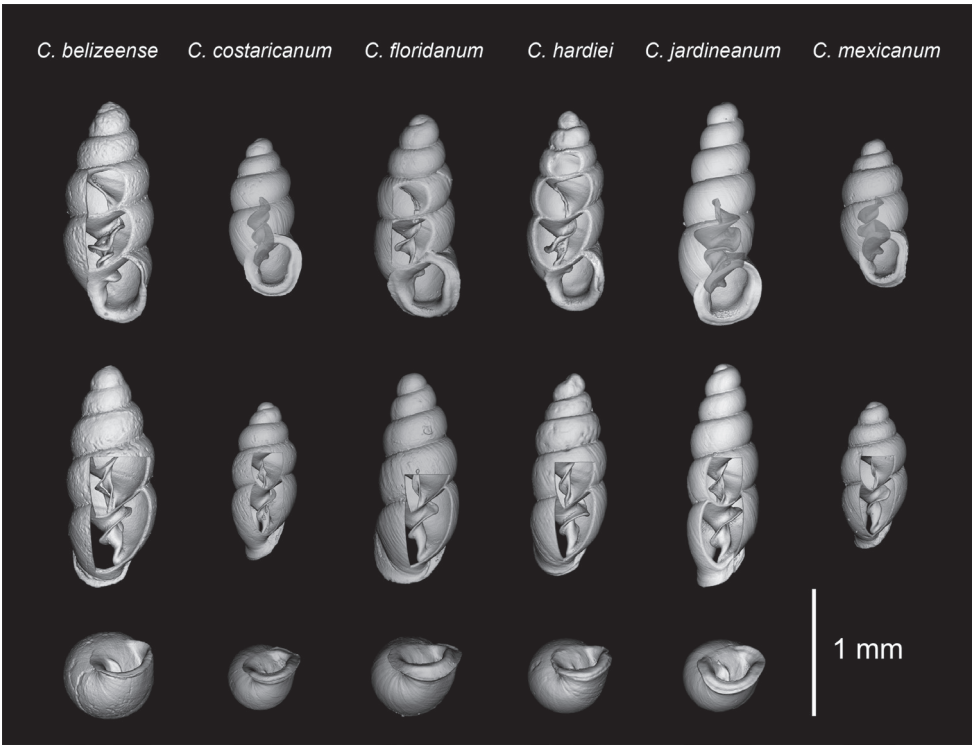

Figure 5. Comparative material (Jochum et al. 2017), *C. belizeense* Jochum & Weigand, 2017 paratype (NMBE 549924/8), *C. costaricanum* E. von Martens, 1898 (RBINS 10591), *C. floridanum* Clapp, 1918 (CM 46540), *C. hardiei* Jochum & Weigand, 2017 paratype (NMBE 549921/8), *C. jardineanum* (Chitty, 1853) (AJC 2321), *C. mexicanum* Pilsbry, 1891 (AJC 2092). CT images showing columellar apparatus, configuration of the columellar lamella and umbilical perspectives showing peristome configuration in allied Central American, Southeast USA and Caribbean species. Scale bar: 1 mm.

(dorsal perspective) (Fig. 5), *C. zarzaae* (aperture side-left perspective) (Fig. 4R) and *C. jardineanum* (ventral perspective) (Fig. 5). This down-turned, tongue-like flexion is not at all present in *C. panamaense* sp. n. (Fig. 4). The configuration of the lamella in *C. panamaense* is spatulate (Fig. 4H) rather than tongue-like in form (Fig. 4R).

DNA barcode data can clearly delineate *Carychium panamaense* sp. n. from all other North American, Caribbean and Central American taxa (Weigand et al. 2013, Jochum et al. 2017, fig. 3).

Etymology. The new species is named after Panama, the Central American country of origin.

Distribution. Only known from the type locality along the short distance, Retoño trail, ca. 50 m before the first river crossing, Parque International La Amistad, Chiriquí Prov., Panama.

Ecology. In moist broadleaf forest litter and twigs (*Quercus* and Lauraceae) at the base of trees and palm trees in secondary tropical rainforest (Fig. 6A–B).

Conservation. In the flat area of the Retoño trail, where water accumulates under trees during rainfall, live *Carychium panamaense* sp. n. was found in relative abundance,

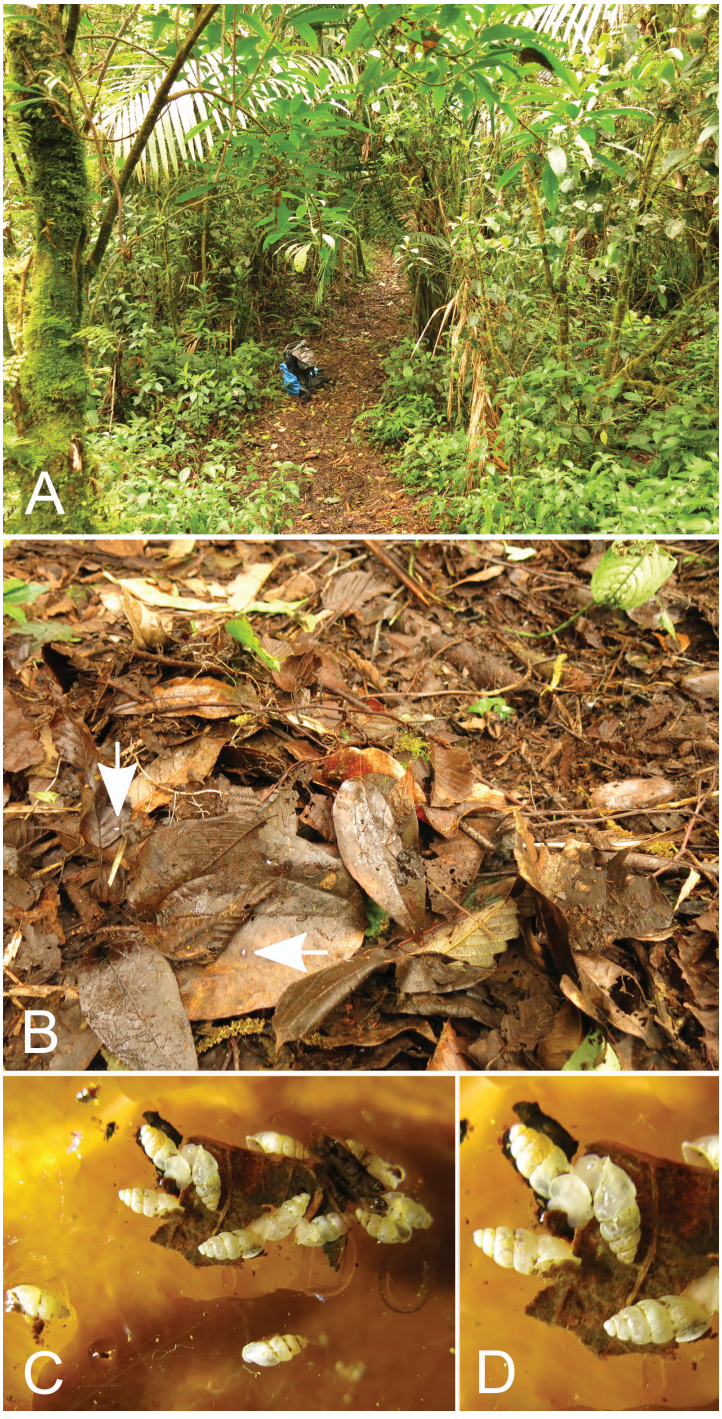

Figure 6. Type locality of *Carychium panamaense* sp. n., **A** El Retoño Trail, La Amistad International Park, Cerro Punta, Chiriquí Prov., Panama **B** broadleaf forest litter with white arrows indicating *C. panamaense* sp. n. on leaves **C–D** close-up view of live individuals crawling on leaf.

suggesting that it has optimum ecological conditions to survive there. *Carychium panamaense* sp. n. is only known from Parque International La Amistad, Chiriquí, Panama, a Bi-National Biosphere Reserve (RBA) located between Panama and Costa Rica and designated a UNESCO World Heritage Site. Despite its being found in a Biosphere Reserve, on a global scale, its current distribution may well be limited to the immediate area of Retoño trail. In conjunction with the Guidelines for the IUCN Red List (IUCN Standards and petitions Subcommittee 2014), it is considered a Critically Endangered narrow range endemic (CR B1) and as such, warrants immediate conservation priority.

Remarks. The type locality of the first recorded species of *Carychium* in Panama, *C. zarzaae* (Boquete), is approximately 97 km southeast of the type locality of *C. panamaense* sp. n. near the Las Nubes Ranger Station (Chiriquí). From the site of its closest known Central American relative, *C. costaricanum* (San Gerardo de Dota, San José, Costa Rica) (Weigand et al. 2013), the distance is 263 km.

Acknowledgements

We are very grateful to Tina Hoffmann (Universidad Autónoma de Chiriquí, Panama), Meike Piepenbring (Goethe-University, Frankfurt/M., Germany) and the Ministerio de Ambiente (Chiriquí, Panama) for their kind and expedient help in issuing us the collection permit for Panama. We thank Thomas Inäbnit (Naturhistorisches Museum der Burgergemeinde Bern, Bern, Switzerland (NMBE) for imaging and measuring the preserved material and Dorian Dörige (Goethe-University, Frankfurt/M., Germany) for technical help. We thank the editor, Thierry Backeljau, one anonymous reviewer and the reviewer, Barna Páll-Gergely for their comments towards improving the manuscript. Lastly, we gratefully acknowledge Eugenia Zarza (National Polytechnic Institute, Mexico City, Mexico) for her translation of the abstract into Spanish and Eike Neubert (NMBE) for his support.

References

Chitty E (1853) Descriptions of thirty supposed new species and varieties of land and fluviatile shells of Jamaica, with observations on some shells already described. Contributions to Conchology [series 2] 1: 1–19.

Clapp GH (1918) New southern forms of *Carychium* and *Thysanophora*. The Nautilus 31(3): 73–74.

Esri Data and Maps (2002) Redlands, California: Environmental Systems Research Institute.

IUCN (2014) Guidelines for Using the IUCN Red List Categories and Criteria. Version 11. Prepared by the Standards and Petitions Subcommittee 11: 16–59.

Hijmans RJ, Cameron SE, Parra JL, Jones PG, Jarvis A (2005) Very high resolution interpolated climate surfaces for global land areas. International Journal of Climatology 25: 1965–1978. http://dx.doi.org/10.1002/joc.1276

Jeffreys JG (1830) A synopsis on the testaceous pneumonobrancheous Mollusca of Great Britain. Transactions of the Linnean Society of London 16: 324–362. https://doi.org/10.1111/j.1095-8339.1829.tb00139.x

Jochum A, Weigand AM, Bochud E, Inäbnit T, Dörge DD, Ruthensteiner B, Favre A, Martels G, Kampschulte M (2017) Three new species of *Carychium* O.F. Müller from the Southeastern USA, Belize, and Panama are described using computer tomography (CT) (Eupulmonata, Ellobioidea, Carychiidae). ZooKeys 675: 97–127. https://doi.org/10.3897/zookeys.675.12453

Kerney MP, Cameron AD, Jungbluth JH (1979) Die Landschnecken Nord- und Mitteleuropas. Verlag Paul Parey, Hamburg and Berlin, 384 pp.

Martens von E (1898) Land and freshwater Mollusca. In: Godman FD, Salvin O (Eds) Biologia Centrali-Americana. RH Porter, London, 289–368.

Müller OF (1773) Vermivm terrestrium et fluviatilium, seu animalium infusoriorum, helminthicorum, et testaceorum, non marinorum, succincta historia. Volumen Imi pars Ima [1–33]. Heineck & Faber, Havniæ & Lipsiæ, 315 pp.

Pilsbry HA (1891) Preliminary notices of new Mexican shells. The Nautilus 5(1): 8–10.

Pilsbry HA (1891) Land and fresh-water molluscs collected in Yucatan and Mexico. Proceedings of the Academy of Natural Sciences of Philadelphia 43: 318–334.

Pilsbry HA (1948) Land Mollusca of North America (north of Mexico). Volume 2, Part 2. The Academy of Natural Sciences of Philadelphia, Monographs 3: 521–1113.

Weigand AM, Jochum A, Slapnik R, Schnitzler J, Zarza E, Klussmann-Kolb A (2013) Evolution of microgastropods (Ellobioidea, Carychiidae): Integrating taxonomic, phylogenetic and evolutionary hypotheses. BMC Evolutionary Biology 13(1): 18. https://doi.org/10.1186/1471-2148-13-18

ZooKeys 795: 13–30 (2018)
doi: 10.3897/zookeys.795.28412
http://zookeys.pensoft.net

RESEARCH ARTICLE

A peer-reviewed open-access journal
ZooKeys
Launched to accelerate biodiversity research

Sparsorythus sescarorum, new species from Mindoro, Philippines (Ephemeroptera, Tricorythidae)

Jhoana M. Garces[1], Ernst Bauernfeind[2], Hendrik Freitag[1]

1 *Department of Biology, School of Science and Engineering, Ateneo de Manila University, Quezon City, Philippines* **2** *2nd Zoological Department (Entomology), Natural History Museum Vienna, Burgring 7, Vienna, Austria*

Corresponding author: *Jhoana M. Garces* (jhoana.garces@obf.ateneo.edu)

Academic editor: *L. Pereira-da-Conceicoa* | Received 16 July 2018 | Accepted 19 September 2018 | Published 5 November 2018

http://zoobank.org/1E7C7F2B-0F53-4815-B12F-B89B132891B8

Citation: Garces JM, Bauernfeind E, Freitag H (2018) *Sparsorythus sescarorum*, new species from Mindoro, Philippines (Ephemeroptera, Tricorythidae). ZooKeys 795: 13–30. https://doi.org/10.3897/zookeys.795.28412

Abstract

A new mayfly species, *Sparsorythus sescarorum* **sp. n.** (Tricorythidae) is described from Mindoro Island, Philippines. Nymphs are characterized by the combination of the following characters: compound eyes of approximately equal size in both sexes, shape and setation of legs, presence of rudimentary gills on abdominal segment VII, and some details of mouthparts. Male imagines are characterized by the coloration pattern of wings and details of genitalia. The developmental stages are matched by DNA barcodes.

Keywords

COI, Key Biodiversity Area, mayfly, Taugad River, taxonomy

Introduction

The order Ephemeroptera (mayflies) is a monophyletic group of pterygote hemimetabolous insects with aquatic larvae and delicate membranous wings in the adult stage. The presence of a subimaginal winged instar is unique within recent pterygote insects. Despite the notable organismic diversity in the Philippine Archipelago, only 38 species of mayflies (Insecta: Ephemeroptera) have been recorded so far. The last catalog

Copyright *J.M. Garces et al.* This is an open access article distributed under the terms of the Creative Commons Attribution License (CC BY 4.0), which permits unrestricted use, distribution, and reproduction in any medium, provided the original author and source are credited.

by Hubbard and Pescador (1978) listed 20 species. New species and genera have been recorded afterwards from several parts of the Philippines by Flowers and Pescador (1984), and Müller-Liebenau (1980, 1982), with the most recent studies conducted by Braasch and Freitag (2008), Sroka and Soldán (2008), Braasch (2011) and Batucan et al. (2016). From these works, it can be inferred that there are eight families present in the Philippines: Baetidae, Caenidae, Ephemeridae, Heptageniidae, Leptophlebiidae, Prosopistomatidae, Teloganodidae and Tricorythidae. Some papers on mayflies of the country have been limited to ecological studies concerning mayfly nymphs (Realon 1979) and macroinvertebrate composition in certain freshwater bodies (e.g., Freitag 2004, Flores and Zafaralla 2012, Dacayana et al. 2013), albeit limited in number and scope as well. Nevertheless, the records regarding Philippines mayflies remain scattered and species diversity appears clearly underestimated.

In an effort to increase knowledge on the Philippine mayfly fauna, extensive sampling was done in Mindoro as part of the Baroc River Catchment Survey of the Ateneo de Manila University. The research group, as part of Bachelor of Science thesis, focused on the Key Biodiversity Area "69 Hinunduang Mt.", classified as terrestrial and inland water area of very high biological importance and extremely high critical conservation priority.

A new species, *Sparsorythus sescarorum* sp. n. belonging to the family Tricorythidae is described in this paper. The genus *Sparsorythus* Sroka & Soldán, 2008 (considered by Kluge 2010: 80 to represent a subgenus of *Tricorythus* Eaton, 1868) has been recorded from India, Indonesia, Sri Lanka, Vietnam and the Philippines, but is probably widespread in South and Southeast Asia. Listed below are the currently described species within the genus.

Genus *Sparsorythus* Sroka & Soldán, 2008

Sparsorythus bifurcatus Sroka & Soldán, 2008 (Vietnam)
Sparsorythus celebensis (Kluge, 2010) (Indonesia: Sulawesi)
Sparsorythus ceylonicus Sroka & Soldán, 2008 (Sri Lanka)
Sparsorythus dongnai Sroka & Soldán, 2008 (Vietnam)
Sparsorythus gracilis Sroka & Soldán, 2008 (India)
Sparsorythus grandis Sroka & Soldán, 2008 (Indonesia: Java)
Sparsorythus jacobsoni (Ulmer, 1913) (Indonesia: Java, Sumatra; Sri Lanka; Philippines)
Sparsorythus multilabeculatus Sroka & Soldán, 2008 (Vietnam)
Sparsorythus buntawensis Batucan, Nuñeza & Lin (in Batucan et al.) 2016 (Philippines: Mindanao)

Aside from the recently described *Sparsorythus buntawensis* Batucan et al., 2016 from Mindanao and the questionable record of *S. jacobsoni* (Ulmer, 1913) from Luzon (Ulmer 1924: 52), a female imago from Mindanao was reported as *Sparsorythus* sp. 4 by Sroka and Soldán (2008). A new species, *Sparsorythus sescarorum* sp. n. from Taugad River, Mindoro Island, Philippines is described in this paper.

Materials and methods

Nymphs were collected from rocks partially or fully submerged in the riffle section of the stream (Figs 10a–d). Winged specimens were attracted using a "black light" trap set-up from 6:30 PM to 8:00 PM under overcast skies near the streams or rivers. Insects were manually collected and stored in 96% ethanol to allow for genetic sequencing. Sample preparation for diagnosis under the dissecting microscope and compound microscope followed Braasch (2011) using Liquid de Faure (Adam and Czihak 1964) as mounting medium. Morphological examinations were performed using a Leica EZ4 stereo microscope and Olympus CX21 microscope. Processing and digital imaging of dissected parts was done using the latter stereo microscope equipped with DinoEye Eyepiece camera; the pictures were combined using CombineZP software (Hadley 2010) and were subsequently enhanced with Adobe Photoshop CS6. Full habitus photographs were taken under a Zeiss Axio Zoom V 16 microscope using diffuse LED lighting at magnifications up to 160×, with Canon 5D Mark II SLR attached to the microscope. Images were captured at various focus planes and subsequently stacked using the Zerene Stacker software. Morphological terminology followed Sroka and Soldán (2008) for nymph and imago, Koss and Edmunds (1974) for eggs and Edmunds and McCafferty (1988) for subimagines.

Specimens examined have been deposited in the following institutions: Museum of Natural History of the Philippine National Museum, Manila, Philippines (**PNM**); Ateneo de Manila University, Quezon City, Philippines (**AdMU**), Collection Jhoana Garces, Philippines (**CGM**), currently deposited in AdMU, and Museum für Naturkunde Berlin, Germany (**MNB**); and Naturhistorisches Museum Wien, Austria (**NMW**). Specimens at the latter repository are older and not collected by any of the authors, but they are presumably from the same locality.

Mitochondrial DNA extraction was done by elution with Qiagen DNeasy kit (Qiagen, Hilden, Germany) following the protocol for animal tissues (Qiagen 2002). For samples with successful DNA isolations, polymerase chain reactions (PCR) were performed using modified primers LC01490_mod (5'-TTTCAACAAACCATAAGGATATTGG-3') and HC02198_mod (5'-TAAACTTCAGGATGRCCAAAAAATCA-3') for amplification of a partition of the cytochrome c oxidase subunit (COI) gene. The PCR temperature progression was set: 180 s at 94 °C; 30 s at 94 °C, 30 s at 47 °C, 60 s at 72 °C (× 35 cycles); 300 s at 72 °C. Amplification success was checked by gel electrophoresis. PCR products of successful amplifications were sent to a commercial service for cleaning, cycle sequencing PCR and sequencing.

The sequences were manually traced and aligned using the software BIOEDIT version 7.2.5 (Hall 1999). Ends of each partition were trimmed to receive a complete matrix of all sequences used. The corresponding fragment of a COI sequence of *Sparsorythus gracilis* and *Sparsorythus buntawensis* available from GenBank (Table 1; Batucan et al. 2016; Selvakumar et al. 2016) were included in the statistical parsimony analysis conducted with TCS 1.21 (Clement et al. 2000). The network connection limit was set manually to 1000 steps in order to keep sub-networks of different species connected and show their inter-specific genetic distance.

Table 1. ENA/GenBank accession numbers of DNA sequences, geographical origins, collection sites, and organismic sample references of specimens used for molecular-genetic analyses.

Species	Locality	Code	Stage	Voucher	GenBank accession number
Sparsorythus sescarorum sp. n.	Mindoro	TR2L	Male Imago	EPH 2	MH595457
	Mindoro	HQCL	Female Subimago	EPH 42	MH595459
	Mindoro	HRCf	Nymph	EPH 43	MH595460
	Mindoro	369f	Nymph	EPH 5	MH595458
Sparsorythus gracilis	India				LC061853.1[1]
Sparsorythus buntawensis	Mindanao		Nymph	1.8.6	KT250142[2]

[1]Selvakumar et al. 2016; [2]Batucan et al. 2016.

Taxonomy

***Sparsorythus sescarorum* sp. n.**
http://www.zoobank.org/961534FC-BA4E-43F4-ABB9-A7097BA70B31
Figures 1–8

Type locality. Philippines, Oriental Mindoro, Municipality of Roxas, Barangay San Vicente: lower reach of Taugad River, a medium-sized mountain river and major tributary of the Baroc River, c. 12°37'18"N, 121°22'58"E, approximately 140 m asl (Figure 10c).

Type material. Holotype: ♂ nymph (PNM), labelled"PHIL:Or.Mindoro, Roxas, Brgy. San Vicente, Taugad River; submerged rock surface, riffle; sec. veget.; c.12°37'18"N, 121°222'58"E, c.140m asl; leg. PS Cagande, J Garces, H Freitag 28.Nov.2017 (TR2g)M", preserved in 95% ethanol, with complete set of gills and legs, one cercus partially broken near tip. **Paratypes**: 10 ♂ nymphs, same data as holotype [4 in MNB of which 1 on slide, 6 in CGM-AdMU of which 5 on slide]; 20 ♀ nymphs, same data as holotype [5 in PNM, 7 in MNB of which 1 on slide, 8 in CGM-AdMU of which 4 on slide]; 21 ♂ imagines, from exactly the same site as holotype collected using light trap on 28 Nov 2017 [7 in PNM, 4 in MNB of which 2 partly on slide, 10 in CGM-AdMU of which 6 partly on slide]; 24 ♀ subimagines, from exactly the same site as holotype collected using light trap on 28 Nov 2017 [8 in PNM, 5 in MNB of which 2 partly on slide, 11 in CGM-AdMU of which 2 partly on slide, 2 with corresponding eggs]; 1 ♂ subimago, from exactly same site as holotype, collected as nymph on 28 Nov 2017 and reared *in situ* in a mesh container [CGM-AdMU partly on slide]; 2 ♂ nymphs (NMW) labelled"Mindoro/ Mansalay/ Barok River 5km N Hinagdanan Fall/ coll. Mendoza 01-02-1995" [of which 1 on slide]; 2 ♀ nymphs (NMW) labelled as previous paratypes [of which 1 on slide]; 3 ♂ imagines (NMW) labelled as previous paratypes [of which 2 partly on slide]; 4 ♀ subimagines (NMW) labelled as previous paratypes [of which 1 partly on slide].

Description. *Nymph.* *Body* length 5.0–5.2 mm; ♂ cerci 0.8 and paracercus, 0.9 times body length; ♀ cerci and paracercus 0.9 times body length; head 1.9–2.0 times wider than long; antennae twice as long as head length (n = 10). General coloration of body brownish-yellow when preserved in alcohol.

Figure 1. *Sparsorythus sescarorum* sp. n., female nymph in dorsal view. Scale bar: 1.0 mm.

Head (Figure 1) pale brownish-yellow. Male compound eyes blackish. Antenna yellowish, pedicle approx. 2.5 times longer than scape, surface of scape with almost transparent ribbon-shaped bristles, a few hair like setae and a finely chagrined area

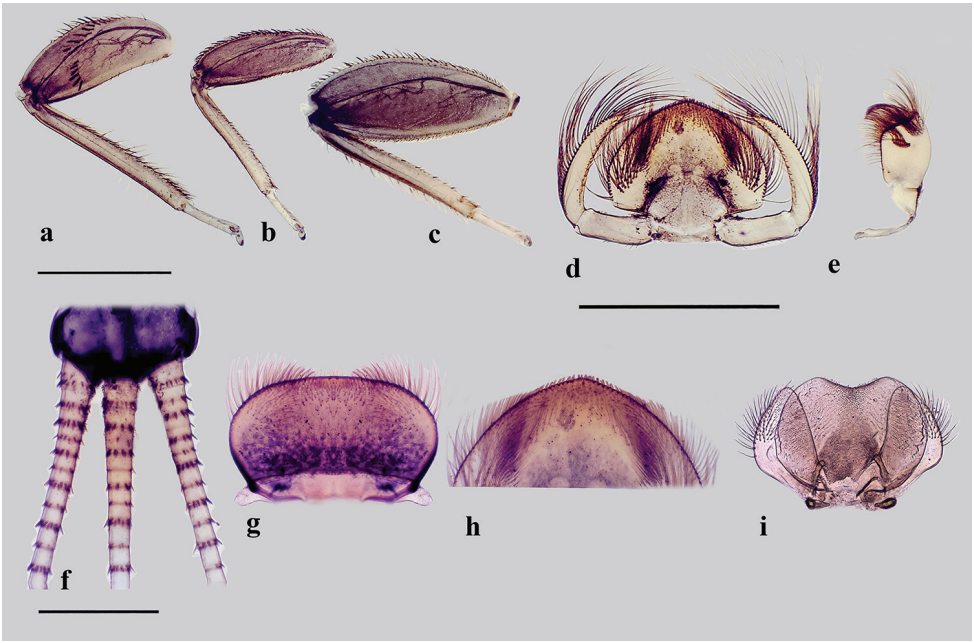

Figure 2. *Sparsorythus sescarorum* sp. n., nymph. **a** fore leg **b** mid leg **c** hind leg **d** labium **e** maxilla **f** cerci and paracercus **g** labrum **h** labium anterior without apicomedial indentation **i** hypopharyngeal lingua. Scale bars: 1.0 mm (**a–c**); 1.5 mm (**d–e**); 0.5 mm (**f–i**).

dorsally. Labrum (Figure 2g) oval; 2.8–3.0 times wider than long, with bristles medially diminishing in length along the anterior margin and laterally, uniformly scattered fine bristles on the dorsal surface. Two lateral groups of bristles on the ventral side. Hypopharyngeal lingua (Figure 2i) approximately as wide as long, with a short and shallow medio-longitudinal groove and wide apico-medial emargination; medial indentation relatively shallow, not exceeding 0.33 of hypopharyngeal lingua length, with uniformly scattered extremely small bristles; postero-lateral margin with 3–4 short, strong, evenly spaced bristles; superlingua rounded, bluntly pointed at apex, with a row of bristles in distal half of outer margin; bristles decreasing in length toward apex; inner margin of superlinguae straight (strongly concave in *S. buntawensis*). Mandibles (Figure 3a, b) as typical for the genus (Sroka and Soldán 2008); both outer incisors triangular; dorsal margin with numerous long filtering setae. Right prostheca (Figure 3d) 1/3 shorter than left, notched, expanded apically and bifurcate, with one long curved projection at distal part, bearing 3 finely fringed setae on the inner side. Distal part of left prostheca (Figure 3c) extended, with several short pointed teeth (blunt when worn); usually three long bristles (approximately ¾ of prostheca length) with feathery margins situated at base of prostheca (and frequently difficult to see). Maxilla (Figure 2e) oblong-shaped with truncate apex and anterolateral part with a group of strong bristles; a dense group of bristles medially and a regular oblique transversal row of slightly shorter bristles submarginally; maxillary palps absent; no sclerotized struc-

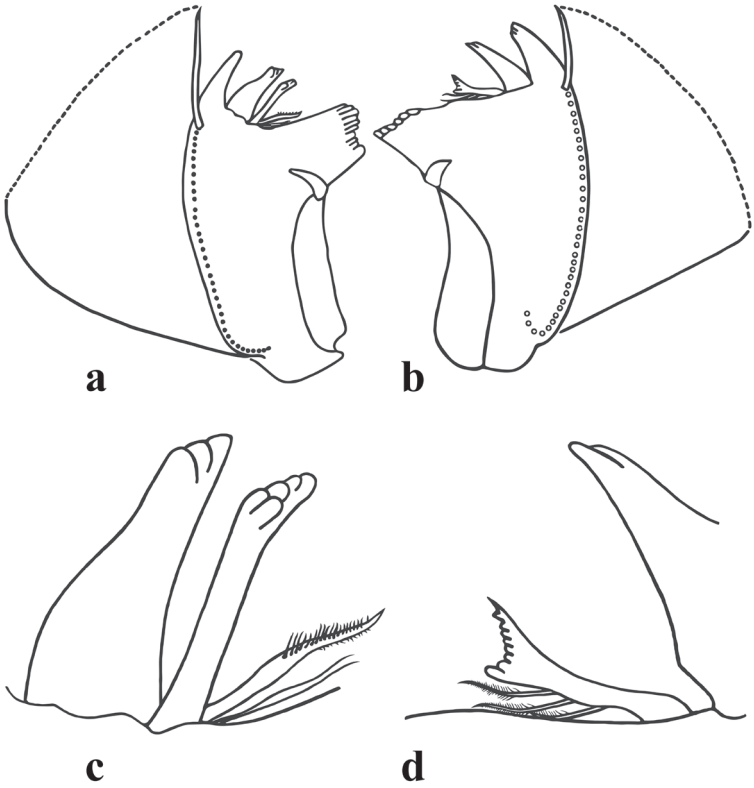

Figure 3. *Sparsorythus sescarorum* sp. n., nymph. Mandibles and details **a** left mandible **b** right mandible **c** left prostheca **d** right prostheca.

tures present. Labium (Figure 2d) with glossa and paraglossae fused into a rounded triangular plate; paraglossae with two groups of lateral submarginal bristles, the outer ones longer; labial plate without indentation or apico-medial incision (Figure 2h) (indentation present in *S. jacobsoni* sensu Ulmer 1939: Abb. 334); the whole plate surrounded by a regular row of setae diminishing apically in length; posterior margin of first segment of labial palp with 6 acutely pointed bristles.

Thorax (Figure 1) dorsally dull yellowish with blackish smudges and maculae, paler ventrally; pronotum laterally slightly enlarged with convex margins, distal margin more or less straight (in both sexes); wing pads dark, veins inconspicuous, in last instar larvae wing pads reaching the middle of abdominal segment II. Legs (Figures 2a–c) relatively robust; length ratio of femur : tibia : tarsus = 2.5 : 3.0 : 1.0 (fore legs), 2.5 : 2.5 : 1.0 (mid legs), 3.6 : 3.3 : 1.0 (hind legs). Fore femora (Figure 2a) flat, shorter than tibia; ratio length : width = 2.3 : 1.0; apically rounded strong spatulate bristles (Figure 4b), about 3.5–4.2 times longer than wide, arranged in a slightly irregular row almost perpendicularly crossing the femur, the row then abruptly bent basad and sinuously extending along the posterior margin of femur (somewhat similar to the "bow-shaped" arrange-

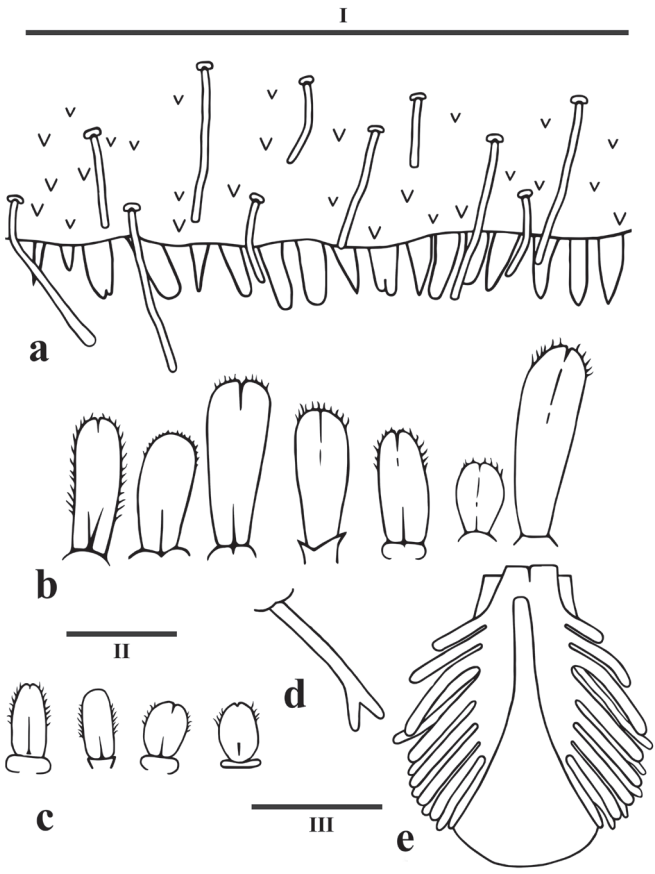

Figure 4. *Sparsorythus sescarorum* sp. n., nymph. **a** 1 mm section of segment VII abdominal terga with small denticles and ribbon-shaped bristles **b** Fore femora transverse row of setae **c** hind femora irregularly scattered setae **d** gill VI **e** gill V. Scale bars: I – 1 mm (**a**); II – 0.1 mm (**b, c**); III – 0.25 mm (**d, e**).

ment in *S. ceylonicus* Sroka & Soldán, 2008); transverse row usually consisting of five bristles; the median part of the posterior margin with a scattered row of strong pointed bristles, anterior margin with a few bifid hair-like setae and submarginally a few almost transparent ribbon-shaped bristles; otherwise surface of femur glabrous, without setae or bristles. Fore tibiae with conspicuous inner submarginal row of apically pointed bristles, slightly longer than tibia width and a few (4–7) long marginal bristles. Fore tarsus with a row of 6–10 strong pointed bristles along the inner margin and a few irregularly scattered bifid setae. Surface of middle and hind femora sparsely covered with stout spatulate bristles (Figures 4c, e) one-third of marginal bristle size and fine ribbon-shaped bristles. Middle femora (Figure 2b) with a dense row of blunt, slender spatulate (rarely pointed) bristles along the dorsal (posterior) margin, the basal half of posterior margin submarginally with some small spatulate bristles; ventral margin with a scanty row of medium sized blunt or slender spatulate bristles, more numerous and slightly longer in basal part; surface of femur with some very small oval bristles and fine transparent

ribbon-shaped bristles, the latter more numerous submarginally. Middle tibiae with an inner submarginal row of apically bluntly pointed bristles, about ½ of tibia width, outer margin with about a dozen long pointed bristles and scattered bifid setae. Hind femora (Figure 2c) with a dense row of blunt, slender spatulate (rarely pointed) bristles along the dorsal (posterior) margin, ventral (anterior) margin with several rows of distinctly smaller, slender spatulate and oval shaped bristles. Surface with scattered small oval bristles and fine ribbon-shaped bristles. Hind tibiae with inner marginal row of slender spatulate bristles, almost as long as bristles along posterior margin of femur; outer margin of tibia with a dense row of long, bluntly pointed bristles, interspersed with acutely pointed bristles (with finely feathery margins), scattered bifid setae and long hair-like setae (especially in distal half). Claws strongly hooked, with 2–3 teeth and a pair of strong pointed processes approximately in the middle. Dark tracheization conspicuous on all femora.

Abdominal terga (Figure 1) brownish with fine darker stippling, a small light medial dot and two pale yellowish brown paramedial patches; posterior part of terga VIII and IX darker; terga darker than sterna with greyish-black stippling; segments II–VII with gills. Gills on segments II–VI similar in shape (Figure 4e) and diminishing in size, each consisting of a dorsal ellipsoidal plate and two branched ventral membranous parts with dense filaments; gill plate on segment II reaches middle of abdominal segment IV, gill plate on segment VI reaches almost end of abdominal segment VII; gill plates simple, thin, not enforced, with scattered hair-like marginal bristles; rudimentary gill on segment VII (Figure 4d) small, tubular with bifurcate tip and frequently missing (or lost subsequent to collecting), without plate. Surface of terga with small denticles and ribbon-shaped bristles, the latter more densely distributed in lateral parts and a few scattered hair-like setae; posterior margin of terga (Figure 4a) with rather tongue-shaped teeth, acutely pointed, blunt or with somewhat frayed tips (worn). Abdominal terga without postero-lateral processes. Abdominal sterna with a few narrow ribbon shaped bristles in posterior lateral area, hind margin of sterna smooth. Posterior margin of sternum IX equally shaped in male and female larvae.

Paracercus (Figure 1) in male nymphs usually slightly longer than cerci, subequal in female nymphs; surface of segments without bristles; posterior margin of segments with strong, slender spatulate or bluntly pointed bristles of approx. ½ (basal segments) to $^1/_3$ of segment length (Figure 2f), tips of bristles extremely finely frayed. Sexual dimorphism in the spatial arrangement and width of cerci: ♂ with basal segments of cerci and paracercus broader and continuous; ♀ basal segments of cerci and paracercus distinctly more slender and not touching.

Male imago. *Body* length 4.5–4.8 mm; fore wing 4.0–4.5 mm; antenna 1.2 mm long; tibia 1.0 mm; cerci and paracercus length approx. 10–12 mm. General color of head and prothorax dark, blackish (Figure 5); antennal pedicle and posterior margin of eyes paler; mesothorax pale yellowish brown; abdomen white to pale greyish with black stippling and maculation on posterior margin; ventral thorax and abdomen paler, whitish and more transparent than dorsal side; tracheization not pigmented; cerci white to pale greyish, at least basal segments frequently with narrow black posterior border; forceps whitish to transparent; legs pale greyish, femora darker, finely stippled with

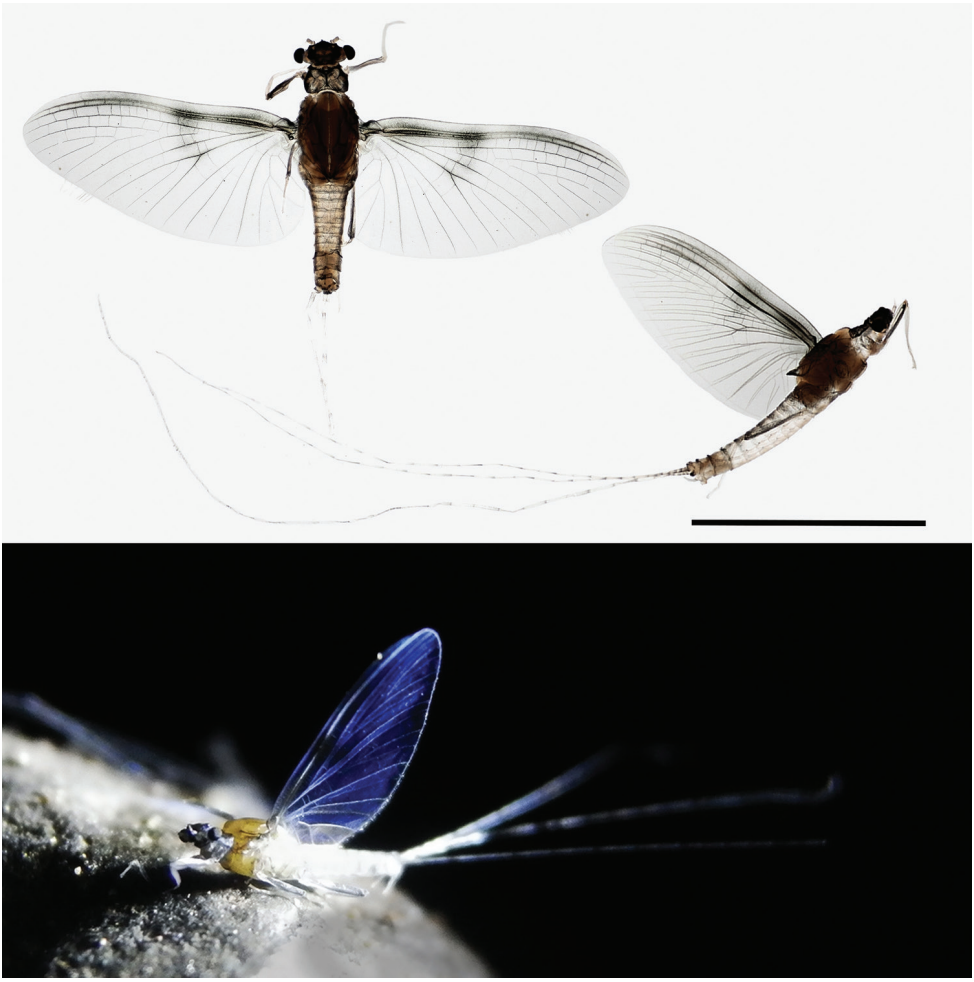

Figure 5. *Sparsorythus sescarorum* sp. n., male imago. Scale bar: 4.0 mm.

black along margins. Fore wings transparent with minimal dark grey smudges in basal half; most dark smudges in the costal and subcostalareas, clustered in basal and apical regions; pterostigmatic region milky, usually no cross veins in costal space discernible; venation mostly whitish, black in the center of the wing, almost transparent towards the margins; veins costa, subcosta and radius anterior rather transparent, broadly bordered with intense black stippling and conspicuous over all their length. Intensity of dark stippling on body, legs, and wings varies considerably between individuals.

Head (Figure 6b) with globular compound eyes, of approximately the same size as in females, distanced approximately half of mesothorax width; antennal pedicle approximately 2.5 times longer than scape. Prothorax (Figure 6b) slightly longer than head. Tarsal claws double on all legs; fore legs with two rounded claws, mid and hind legs with one claw rounded and the other pointed (ephemeroid). Femur slightly longer than tibia, length ratio 1.2 : 1. In the fore wing vein media forked at approximately ½ of its

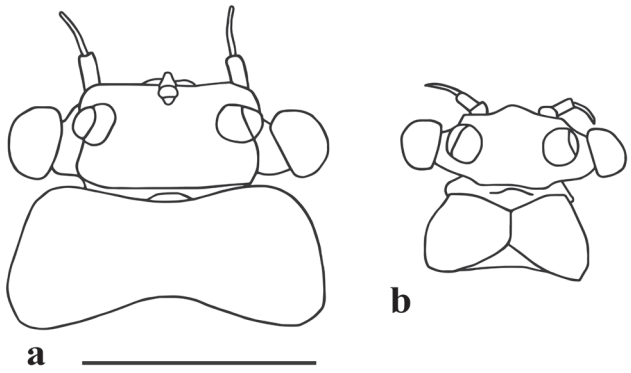

Figure 6. Head and prothorax of *Sparsorythus sescarorum* sp. n.: **a** female subimago **b** male imago. Scale bar: 1 mm.

length; veins cubitus posterior and analis frequently not visible along their entire length, transparent in apical part; posterior wing margin with fine setae, more scattered distally.

Genitalia (Figure 7) with subgenital plate entire. Forceps two-segmented; basal segment shorter than distal one, length ratio approximately 1.0 : 2.2; forceps segment I cylindrical, widest at base, slightly constricted in the middle; hind margin of forceps base sclerotized in medial part with a few tiny bristles; inner margin of segment two of forceps covered with numerous leaf-shaped attachment structures. Penis lobes simple, straight and tubular, slightly bent in dorsal direction, only slightly constricted subapically; penis apex reaching approximately the basal quarter of second forceps segment; apex of penis rounded with distinct medial emargination bisecting penal apex. Caudal filaments more than twice the body length, approx. 10–12 mm, cerci glabrous but paracercus sparsely covered with fine setae.

Male subimago. Similar to imago, but wings uniformly greyish and with microtrichae on wing surface; tarsus of fore leg with one pointed and one obtuse claw (= 'ephemeropteroid' sensu Kluge 2004: 34, Kluge 2010); fore femur slightly shorter than tibia, length ratio 0.9 : 1.0; cerci and paracercus longer than body, but distinctly shorter than in imago. Male genitalia almost as in imago, but forceps segment I stouter.

Female subimago. *Body* length 4.0–4.6 mm; fore wing 5.0–5.2 mm; cerci and paracercus length 3.5–4.0 mm. General coloration of head, prothorax, dorsal mesothorax and dorsal abdomen dark, brownish or blackish (Figure 8); ventral mesothorax yellowish brown; cerci whitish, densely covered with long setae. Head (Figure 6a) with globular compound eyes, of approximately the same size as in male imagines, distanced approximately half of mesothorax width; antennal pedicle approximately 2.5 times longer than scape. Femora blackish, basal end of fore femur paler than the rest, tibia and tarsus transparent. Tarsal claws double on all legs, one rounded and the other pointed (ephemeroid). Length ratio femur: tibia: tarsus = 3.0: 3.2: 1.0 (fore legs), 3.1: 3.0: 1.0 (middle legs), 4.8: 4.1: 1.0 (hind legs). Fore wings (Figure 8) gray with dark

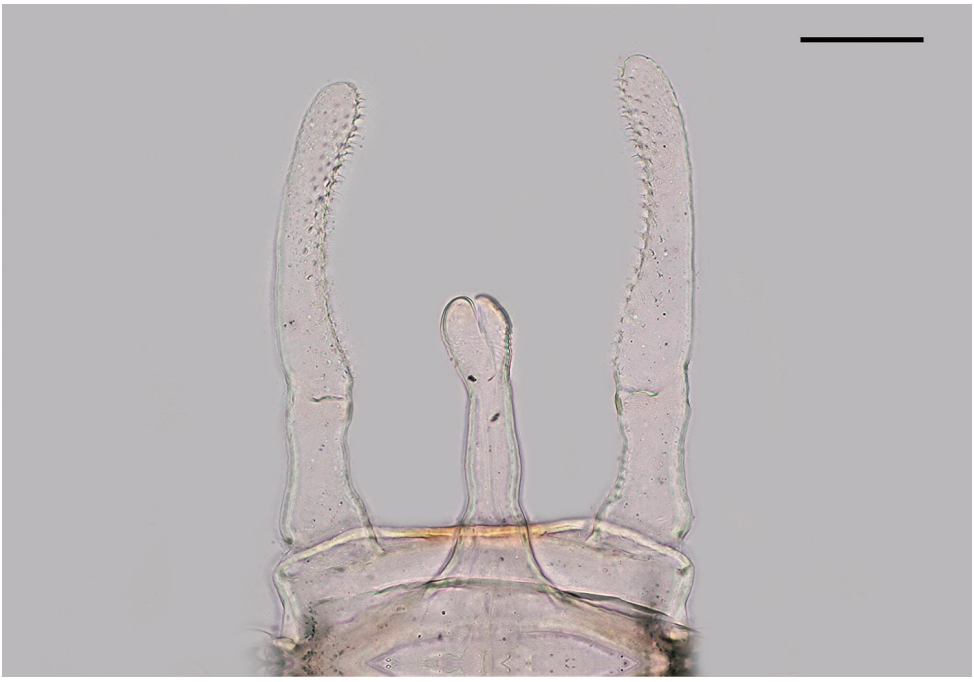

Figure 7. *Sparsorythus sescarorum* sp. n., male genitalia (imago). Scale bar: 0.1 mm.

Figure 8. *Sparsorythus sescarorum* sp. n., female subimago. Scale bar: 1 mm.

smudges in basal half; most dark smudges in the costal and subcostal space clustered in two regions; veins costa and subcosta distinctly darker and conspicuous over all their length; longitudinal venation darker anteriorly and proximally. Subimaginal falciform microtrichia present on wing surface, body surface, and legs. Outer and inner edges of wings (wing margin) with a seam of long and fine setae, slightly shorter towards the wing tip. Subanal plate (sternum IX) approximately as wide at base as long, smoothly rounded in distal half and more than one third longer than sternum VIII (compare Sroka and Soldán 2008: fig. 64).

Eggs. Approximately 190 × 120 µm, epithema (polar cap) covering approximately ⅕ of total egg length. Surface smooth, covered by typical shallow polygonal ridges (almost identical to Sroka and Soldán 2008: fig. 72). Micropyle very small, tagenoform.

The resulting network tree (Figure 9) demonstrates that the conspecific specimens of different life stages of *Sparsorythus sescarorum* sp. n. have only a maximum of five substitutions compared to the much higher divergence of the other *Sparsorythus* species sampled. This Statistical Parsimony tree is solely intended to provide evidence for matching larval and imaginal stages.

Differential diagnosis. The nymph of *Sparsorythus sescarorum* sp. n. differs from all known Oriental tricorythid taxa in the combination of the following characters: apex of hypopharyngeal lingua with wide medial indentation (similar in *S. buntawensis*), wing pads reaching the middle of abdominal segment II in last instar larvae, hind femora longer than tibia (length ratio of femur : tibia : tarsus = 3.6 : 3.3 : 1.0) with central femur surface glabrous (only a few tiny bristles submarginally) and bifurcate rudimentary gill on segment VII present. The new taxon in some respects somewhat resembles *S. bifurcatus* and *S. gracilis*, but leg ratio of hind femur : tibia : tarsus and setation of femora are distinctive. Unlike *S. jacobsoni* (sensu Ulmer 1939: Abb. 334), *S. sescarorum* has no small nick in the median anterior margin of its labial plate and possesses a specifically shaped transverse row of setae on fore femora, and the rudimentary gill is bifurcate instead of filamentous. Unlike *S. buntawensis, S. sescarorum* sp. n. has inner margin of superlinguae straight, bifurcate rudimentary gill and cerci and paracercus shorter than body length. They can be easily differentiated using leg ratios of femur : tibia : tarsus and fore femora length : width. The arrangement of apically rounded setae on fore femur resembles the bow-shaped arrangement of *S. ceylonicus*.

Male genitalia are comparatively similar within the genus *Sparsorythus*. The male imago of *Sparsorythus sescarorum* sp. n. can be differentiated from other Oriental tricorythid taxa based on the pattern of dark smudges in the fore wing, the medial sclerotization along the hind margin of forceps base and the length ratio of forceps segments. Color pattern of wings is rather similar in *S. multilabeculatus*, but male imagines of *S. sescarorum* are significantly larger (4.5–4.8 mm vs. 3 mm in *S. multilabeculatus*). Male imagines of *S. sescarorum* have globular compound eyes, of approximately the same size as in females, in contrast to *S. bifurcatus* and *S. dongnai* compound eyes which are distinctly larger than in females. Identification of female subimagines remains rather difficult (except by direct comparison of specimens), mainly based on coloration, color pattern of wings, length ratio of legs, shape of subanal plate (sternum IX) and exochorionic structures of eggs.

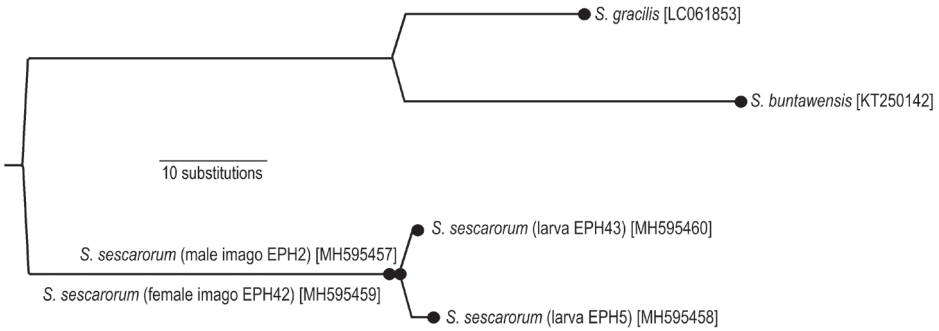

Figure 9. Statistical parsimony haplotype network of successfully sequenced samples, *Sparsorythus gracilis* and *Sparsorythus buntawensis* sequences from GenBank from aligned COI sequences of 523 bp. Filled circles represent haplotypes as labelled.

Distribution. The species is so far only known from the type locality, lower reach of Taugad River, Oriental Mindoro, Philippines.

Ecology. All material was collected from or near permanent rivers in Oriental Mindoro. This province has an equatorial monsoonal (Am) climate based on the Köppen-Geiger Classification and is nationally recognized as the Type III climate according to the Modified Corona Classification (Kintanar 1984), characterized by absence of a very pronounced maximum rain period and a short dry season, in Oriental Mindoro during the period of February to April. Average temperature is around 27.4 °C and the average annual rainfall about 2000 mm (PAGASA 2018), however with considerable annual and local variations. All collection sites are at low altitudes of 5–250 m a.s.l. at meandering alluvial rivers of small to medium size (2–12 m wide) comparable to the hyporhithral section (Figures 10a–c) with estimated water discharge ranging from 0.006 to 7.0 m^3/s during the respective times of collection. Most of these sites were surrounded by secondary vegetation, rarely secondary forest, with few houses and farmland in some distance from the river bed.

Larvae were collected in lotic river sections at water depth ranging from 3 to 35 cm, predominantly from mineral bottom substrates (typically small to medium-sized boulders in riffles (Figure 10d)), rarely from submerged wood. The water currents at these microhabitats were estimated to range from 0.08 to 0.79 m/s (usually ca. 0.2–0.4 m/s). The temperature of the water ranged from 23.0 to 28.7 °C, the pH from 6.8 to 8.3, dissolved oxygen from 3.8 to 8.3 mg/l (mostly, but not always near 100% saturation), biochemical oxygen demand (BOD_5) from 0.1 to 1.3 mg/l. The maximum values, respectively, measured for selected dissolved nutrients were as follows: phosphate 0.7 mg/l, ammonium 0.5 mg/l, nitrate 1.0 mg/l. Dissolved nitrites were always below detectable values (< 0.2 mg/l). Imagines and subimagines were collected from light traps placed along the same river sections. They seemed to be most attracted by black light used at a time shortly after sun set. No information on feeding, type of emergence and life cycle is available at present. Presumably subimagines emerge on the water surface and male subimagines moult almost immediately after emergence whereas females retain the subimaginal stage.

Figure 10. Collection sites of *Sparsorythus sescarorum* sp. n. in Roxas, Oriental Mindoro: **a** lower Hinundugan River, a tributary of the Baroc River **b** upper Hinundugan River **c** type locality, lower reach of Taugad River, a major tributary of the Baroc River **d** submerged rocks with nymphs (lifted above water surface), the typical larval habitat.

Etymology. The name of this new species is given to acknowledge the efforts of Baranggay Captain Ronel S. Sescar, Baranggay Kagawad for Environmental and Agriculture concerns Rodel S. Sescar and the rest of their family members who were instrumental for the protection and preservation of the Baroc River. Assessments of aquatic biodiversity and training of student researchers would not have been possible without their support for the past few years.

Discussion

Sroka and Soldán (2008) revised the hitherto known Tricorythidae from the Oriental Region, restricting the genus *Tricorythus* Eaton, 1868 to the Afrotropical Region and proposing the new genus *Sparsorythus* (type species *Sparsorythus bifurcatus* Sroka & Soldán, 2008) for Oriental tricorythid taxa. Kluge (2010) redescribed *Tricorythus varicauda* Pictet, 1843 (type species of *Tricorythus*) recognizing *Madecassorythus* Elouard & Oliarinony, 1997, *Spinirythus* Oliarinony & Elouard in Oliarinony et al., 1998, *Ranorythus* Oliarinony & Elouard, 1997 and *Sparsorythus* Sroka & Soldán, 2008 as

subgenera of *Tricorythus*. Lineages within Afrotropical *Tricorythus*, however, are still poorly known (Barber-James 2008) and for the present the opinion of Sroka and Soldán (2008) is followed in this paper.

Several characters of *Sparsorythus sescarorum* sp. n. merit comment. The nymphs of *S. sescarorum* sp. n. exhibit a sexual dimorphism in the spatial arrangement and width of cerci and paracercus as observed in other Tricorythidae. Size of eyes is about equal in male and female specimens in the larval and winged stages, whereas *S. bifurcatus* and *S. dongnai* exhibit distinctly larger eyes in male specimens. Kluge (2010) suggested that some species of *Tricorythus,* such as *T. exophthalmos,* show a correlation between enlarged male eyes and the sexually dimorphic shape of the pronotum, where the male pronotal fore margin expands medially forming a semicircular flap that overlaps the hind part of the head, while the female fore margin is straight. The fore margin of *S. sescarorum* sp. n. larval pronotum is more or less straight in both sexes, lending some support to the opinion of Kluge.

Female adults obviously retain the subimaginal stage. This has also been observed at least in *Tricorythus varicauda*, *Sparsorythus celebensis,* and some other tricorythid taxa (Kluge 2010). Male subimagines of the new species have never been collected at light traps, however a single specimen from the type locality is available which has been obtained by rearing nymphs and which obviously represents a subimago. This suggests that the subimaginal-imaginal molting of males occurs immediately after emergence before the first flight.

Acknowledgements

The study was made possible with the Gratuitous Permit (GP 0133-17) for the collection of aquatic wildlife in parts of Mindoro and Luzon as kindly issued by the Bureau of Fisheries and Aquatic Resources (BFAR), Quezon City. Prerequisite permissions were given by the local government units of San Vicente and the Municipality of Roxas, Baco and Puerto Galera, Oriental Mindoro, the indigenous Buhid community in San Vicente, PENRO Calapan, CENRO Roxas, and NCIP Oriental Mindoro. The authors are grateful to the unwavering support of the administration of San Vicente under the lead of Captain Mr. Ronel Sescar, Chief of the Barangay Police Mr. Rodel Sadiasa and field assistance of Mr. Allan Semaniano. Deep gratitude is dedicated to Ms. Princess Spica Cagande for helping the first author in conquering mountains of forests and funding applications during the preliminary stage of this study and to Mr. Clister Pangantihon for his valued support in the field study as well as Dr. Thomas von Rintelen and Robert Schreiber for advice and preliminary training of the first author in DNA taxonomy. Lastly, the authors are grateful to Michel Sartori and the anonymous reviewer for the constructive comments on the manuscript.

The authors are very thankful for the financial support of the field collections (student thesis) by the Philippine Commission on Higher Education (PHERNet program AdMU), the Advanced Science and Technology Human Resource Development Program (ASTHRDP) of the Department of Science and Technology (DOST) and the Office of Admission and Aid, Ateneo de Manila University. Trainings in taxonomy and

molecular genetics of the first author were kindly enabled thru funding by German Federal Ministry of Education and Research (BMBF project BIOPHIL 01DP14002) and the German Academic Exchange Service (DAAD project BIO-PHIL 57393541).

References

Adam H, Czihak G (1964) Arbeitsmethoden: der makroskopischen und mikroskopischen Anatomie. G. Fischer, Stuttgart, 583 pp.

Barber-James HM (2008) A synopsis of the Afrotropical Tricorythidae. In: Hauer FR, Stanford JA, Newell RL (Eds) International advances in the ecology, zoogeography and systematics of mayflies and stoneflies. University of California Publications in Entomology 128 [Proceedings of the 11th International Conference on Ephemeroptera and the 15th International Symposium on Plecoptera, Montana, USA, 22–29 August 2004], 187–203. https://doi.org/10.1525/california/9780520098688.003.0014

Batucan LS, Nuneza OM, Villanueva RJT, Lin CP (2016) A new species of mayfly (Ephemeroptera: Tricorythidae) from Mindanao Island, Philippines and association of life stages using DNA barcodes. Philippine Journal of Systematic Biology 10: 6–13.

Braasch D (2011) New species of the family Heptageniidae (Ephemeroptera) from Borneo and the Philippines. Deutsche Entomologische Zeitschrift 58(2): 201–219. https://doi.org/10.1002/mmnd.201100024

Braasch D, Freitag H (2008) *Palawaneuria*, a new subgenus of *Compsoneuria* and new species of *Compsoneuria* and *Afronurus* (Ephemeroptera, Heptageniidae) from Palawan, Philippines. Deutsche Entomologische Zeitschrift 55(1): 117–128. doi/10.1002/mmnd.200800009.

Clement M, Posada D, Crandall KA (2000) TCS: a computer program to estimate gene genealogies. Molecular Ecology 9: 1657–1659. https://doi.org/10.1046/j.1365-294x.2000.01020.x

Dacayana CML, Hingco JT, Del Socorro MML (2013) Benthic macroinvertebrate assemblage in bulod river, Lanao del Norte, Philippines. Journal of Multidisciplinary Studies 2(1): 398. https://doi.org/10.7828/jmds.v2i1.398

Eaton AE (1868) An outline of the re-arrangement of the genera of Ephemeridae. Entomologist's Monthly Magazine 5: 82–91.

Edmunds GF jr, McCafferty WP (1988) The Mayfly Subimago. Annual Review of Entomology 33: 509–529. https://doi.org/10.1146/annurev.en.33.010188.002453

Elouard J-M, Oliarinony R (1997) Biodiversité aquatique de Madagascar: 6. *Madecassorythus* un nouveau genre de Tricorythidae définissant la nouvelle sous-famille des Madecassorythinae (Ephemeroptera, Pannota). Bulletin de la Société entomologique de France 102(3): 225–232.

Flores MJL, Zafaralla MT (2012) Macroinvertebrate composition, diversity and richness in relation to the water quality status of mananga river, Cebu, Philippines. Philippine Science Letters 5(2): 103–113.

Flowers RW, Pescador ML (1984) A new *Afronurus* (Ephemeroptera: Heptageniidae) from the Philippines. International Journal of Entomology 26: 362–365.

Freitag H (2004) Composition and Longitudinal Patterns of Aquatic Insects Emergence in Small Rivers of Palawan Island, the Philippines. International Review of Hydrobiology 89(4): 375–391. https://doi.org/10.1002/iroh.200310710

Hadley A (2010) CombineZP. http://www.hadleyweb.pwp.blueyonder.co.uk/CZP/News.htm [Version of 6 June 2010]

Hall TA (1999) BioEdit: a user-friendly biological sequence alignment editor and analysis program for Windows 95/98/NT. Nucleic Acids Symposium Series 4: 95–98.

Hubbard MD, Pescador ML (1978) A catalog of the Ephemeroptera of the Philippines. Pacific Insects 19: 91–99.

Kintanar RL (1984) Climate of the Philippines, PAGASA report, Manila, 38 pp.

Kluge N (2004) The phylogenetic system of Ephemeroptera. Kluwer Academic Publishers, Dordrecht, 456 pp. https://doi.org/10.1007/978-94-007-0872-3

Kluge N (2010) Redescription of the taxon Tricorygnatha (Ephemeroptera, *Tricorythus* s.l.) based on new finding in Africa and Indonesia. Russian Entomological Journal 19(2): 79–104.

Koss RW, Edmunds GF Jr (1974). Ephemeroptera eggs and their contribution to phylogenetic studies of the order. Zoological Journal of the Linnean Society 55: 267–349. https://doi.org/10.1111/j.1096-3642.1974.tb01648.x

Müller-Liebenau I (1980) *Jubabaetis* gen.n. and *Platybaetis* gen.n., two new genera of the family Baetidae from the Oriental Region. In: Flannagan JF, Marshall KE (Eds) Advances in Ephemeroptera Biology. Plenum, New York, 103–114. https://doi.org/10.1007/978-1-4613-3066-0_8

Müller-Liebenau I (1982) New species of the family Baetidae from the Philippines (Insecta, Ephemeroptera). Archiv für Hydrobiologie 94(1): 70–82.

Oliarinony R, Elouard J-M, Raberiaka NH (1998). Biodiversité aquatique de Madagascar. 8. *Spinirythus* un nouveau genre de Tricorythidae (Ephemeroptera Pannota). Bulletin de la Société entomologique de France 103(3): 237–244.

PAGASA [Philippine Atmospheric, Geophysical and Astronomical Services Administration] (2018) Monthly rainfall, by Station, Year, and Month. http://philfsis.psa.gov.ph/index.php/id/15/matrix/J20FSMRI

Pictet FJ (1843) Histoire naturelle générale et particulière des insects névroptères, Famillie des éphémérines. J. Kessmann [et A. Cherbuliez], Genève, 319 pp.

Qiagen (2002) DNeasy Tissue Kit Handbook 05/2002. Hilden, Germany, 43 pp.

Realon CBR (1979) An ecological study of mayfly nymphs I Molawin Creek, Mt. Makiling, Laguna. The Philippine Entomologist 4(4): 233–291.

Selvakumar C, Sivaramakrishnan KG, Janarthanan S (2016) DNA barcoding of mayflies (Insecta: Ephemeroptera) from South India. Mitochondrial DNA Part B 1: 1, 651–655. https://doi.org/10.1080/23802359.2016.1219623

Sroka P, Soldán T (2008) The Tricorythidae of the Oriental Region. International Advances in the Ecology, Zoogeography and Systematics of Mayflies and Stoneflies. University of California Press, Oakland 128, 313–354. https://doi.org/10.1525/california/9780520098688.003.0021

Ulmer G (1913) Ephemeriden aus Java, gesammelt von Edw. Jacobson. Notes from the Leyden Museum 35: 102–120.

Ulmer G (1924) Ephemeropteren von den Sunda-Inseln und den Philippinen. Treubia 6: 28–91.

Ulmer G (1939) Eintagsfliegen (Ephemeropteren) von den Sunda-Inseln. Archiv für Hydrobiologie, Supplement 16: 443–692.

ZooKeys 795: 31–37 (2018)
doi: 10.3897/zookeys.795.28384
http://zookeys.pensoft.net

RESEARCH ARTICLE

A peer-reviewed open-access journal
ZooKeys
Launched to accelerate biodiversity research

Cnestus quadrispinosus, a new species of xyleborine ambrosia beetle from Thailand and Borneo (Coleoptera, Curculionidae, Scolytinae, Xyleborini)

Wisut Sittichaya[1], Roger A. Beaver[2]

1 *Department of Pest Management, Faculty of Natural Resources, Prince of Songkla University, Had Yai, Songkhla, 90112, Thailand* **2** *161/2 Mu 5, Soi Wat Pranon, T. Donkaew, A. Maerim, Chiangmai 50180, Thailand*

Corresponding author: *Wisut Sittichaya* (wisut.s@psu.ac.th)

Academic editor: *M. Alonso-Zarazaga* | Received 15 July 2018 | Accepted 12 September 2018 | Published 5 November 2018

http://zoobank.org/3AE1E82D-016A-4CC5-B73A-3EA0169AB8FD

Citation: Sittichaya W, Beaver RA (2018) *Cnestus quadrispinosus*, a new species of xyleborine ambrosia beetle from Thailand and Borneo (Coleoptera, Curculionidae, Scolytinae, Xyleborini). ZooKeys 795: 31–37. https://doi.org/10.3897/zookeys.795.28384

Abstract

A new species, *Cnestus quadrispinosus*, is described from Thailand, Brunei Darussalam, and East Malaysia (Sabah). It is compared to three related species of *Cnestus* which lack a mycangial tuft of hairs on the pronotum, and have an impressed elytral declivity.

Keywords

Ambrosia beetles, Brunei, Cnestus, new species, Sabah, Thailand

Introduction

The genus *Cnestus* Sampson was erected for a single species, *Cnestus magnus* Sampson, 1911, from Sri Lanka (Sampson 1911). Nunberg (1972) in a review of and key to the genus included 12 species. Wood (1986) included *Cnestus* in the tribe Xyleborini, and keyed it from other genera in the tribe. He considered that there are about 17 species in the Oriental region and Japan (Wood 1986). The catalog of Wood and Bright (1992) includes 21 species. However, some of these are synonyms or need to be transferred

Copyright *W Sittichaya, RA Beaver.* This is an open access article distributed under the terms of the Creative Commons Attribution License (CC BY 4.0), which permits unrestricted use, distribution, and reproduction in any medium, provided the original author and source are credited.

to other genera (Smith SM, Beaver RA, Cognato AI, unpublished data). Dole et al. (2010) discussed the phylogenetic relationship of the genus to other xyleborine genera, and Dole and Cognato (2010) transferred eleven more species to the genus, thereby extending its range to the Neotropical region. Hulcr and Cognato (2013) diagnose and describe the characters of the genus, and key 4 species found in New Guinea. Currently, we recognise 25 species in the Old World and Pacific islands, and 4 species in the Neotropical region. One Oriental species, *Cnestus mutilatus* (Blandford), has been imported to North America (Schiefer and Bright 2004, Gomez et al. 2018). All species are inbreeding and fungus-farming ambrosia beetles (Wood 1986, Hulcr and Cognato 2013). Recent collecting by the senior author in the far South of Thailand has revealed a new species, which also occurs on the island of Borneo.

Materials and methods

Specimens were collected using ethanol baited traps in the lowland tropical rain forest of the Hala-Bala Wildlife Sanctuary, Narathiwat province, Thailand. Specimens from Brunei Darussalam and East Malaysia (Sabah) were among material sent to RAB for identification by the Natural History Museum, London, and Dr. A. Floren. Photographs were taken with a Canon 6D digital Camera with a Canon MP-E 65mm Macro Photo Lens (Canon, Tokyo, Japan) and StackShot-Macrorail (Cognisys Inc, MI,USA) The photos were then combined with Helicon Focus 6.8.0. (Helicon Soft, Ukraine), all photos were improved with Adobe Photoshop CS6 (Adobe Systems, California, USA).

Abbreviations used for collections

NHMUK	Natural History Museum, London
NHMW	Naturhistorisches Museum Wien, Wien
PSUZC	Prince of Songkla University Zoological Collection, Songkhla
THNHM	Natural History Museum of the National Science Museum, Thailand
RAB	Private collection of Roger A. Beaver, Chiang Mai
WST	Private collection of Wisut Sittichaya, Songkhla

Taxonomy

***Cnestus quadrispinosus* sp. n.**
http://www.zoobank.org/FB70D798-BA22-425F-8281-AEC901EA88F9
Figure 1A-F

Type material. Holotype: female, THAILAND, Hala-Bala Wildlife Sanctuary, Narathiwat Province, lowland tropical rainforest, 5°47'44"N, 101°50'07"E, 01.iii.2014, ethanol baited trap (W. Sittichaya) (NHMW). Paratypes: 12 females, same data as hol-

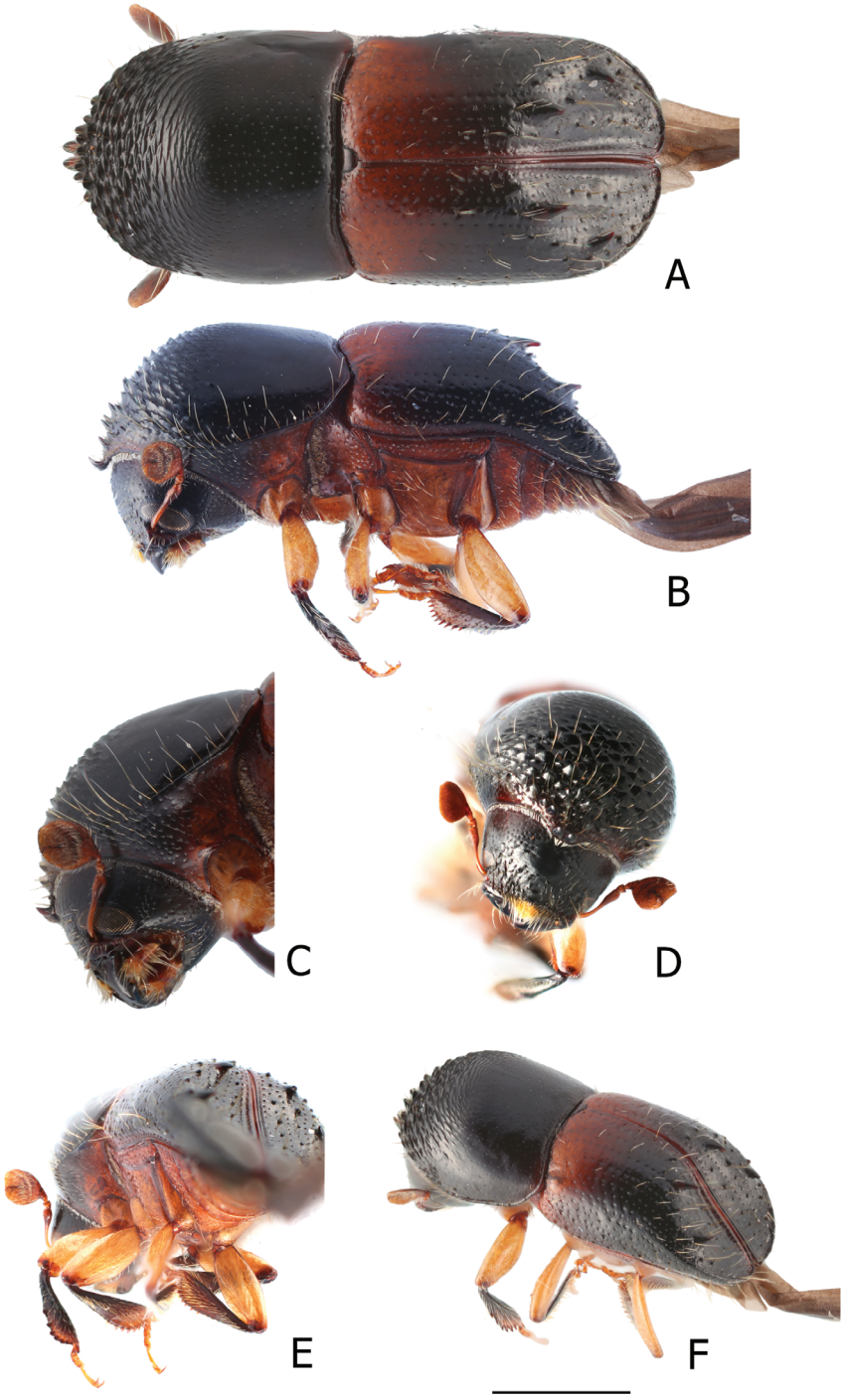

Figure 1 *Cnestus quadrispinosus* sp. n. A Dorsal view, B Ventro-lateral view, C Antenna, D front, E pro-, meso-, and meta-tibia, F posterolateral view. Scale bar: 2 mm.

otype (NHMW, 2; PSUZC, 2; THNHM, 2; RAB, 1; WST, 5). BRUNEI, Kuala Belalong FSC, E115°7', N4°34', Dipterocarp forest, *Dryobalanops beccarii*, Aerial F[light] I[ntercept]T[rap] 3, 220m alt., 30.v.[19]91, N. Mawdsley NM 178 (NHMUK, 1). [E. MALAYSIA], Sabah, Poring Spring, Lower montane mixed dipterocarp forest, *Xanthophyllum affine*, Fog XA11/F1, 12.v.1992, A. Floren (RAB, 1).

Diagnosis. The species is placed in *Cnestus* because it possesses the following combination of characters: body rather short and stout, with very sparse vestiture; antenna with four-segmented funicle (including pedicel), club truncate and flattened, its first segment covering the whole posterior surface; anterior margin of pronotum with two large, upcurved denticles, lateral margins of pronotum carinate, disc not asperate; scutellum flush with elytral surface; procoxae narrowly separated, intercoxal process spinelike, posterocoxal process not swollen; protibiae obliquely triangular, widest about one-fourth from apex, outer margin with 6−7 denticles in apical half, posterior face not tuberculate.

The species is distinguished from all other species of *Cnestus* by the large spine on interstriae III at the upper margin of the elytral declivity, and a second large spine on interstriae V on the lateral margin of the declivity. The species belongs to a small species group which lack a mycangial tuft of hairs at the base of the pronotal disc, and in which the elytral declivity is broadly impressed. The majority of *Cnestus* species have a mycangial tuft indicating the presence of a mesonotal mycangium, and a convex elytral declivity.

Description. *Female*. Length 4.25 mm (paratypes 3.45-4.50 mm), 2.30 times longer than wide (paratypes 2.20-2.56 times), body stout, shining, bicoloured, head dark brown to black, pronotum dorsally entirely black, laterally brown to dark brown, at least anterior part of elytral disc yellowish brown to dusky brown, area of paler colour varying individually from a small area at base of elytra to whole disc, remainder of elytral disc and declivity dark brown to black; ventrally yellowish brown, femora pale, tibiae dark brown, antennae and tarsi brown.

Head. Frons moderately convex, shining, with an indistinct small, smooth median swelling above epistoma, and a broader slightly raised smooth area towards vertex, lower part with scattered elongate rugae, arranged subconcentrically around lower swelling, upper part with fine punctures laterally; vestiture of fine hairs of variable length, longer and denser on lower part of frons; epistoma with dense brush of stiff, yellowish setae. Eyes shallowly emarginate at antennal insertion, lower portion distinctly larger. Antenna type 1 (Hulcr et al. 2007), scape long and slender, weakly spatulate, pedicel cup-shaped, funicle 3-segmented, the segments successively wider, antennal club large, subcircular and very flat, segment I covering posterior side, segment II corneous, visible only on anterior side.

Pronotum. Near type 7 in dorsal and lateral view (Hulcr et al. 2007), approximately as long as wide (holotype 1:1.03; paratypes 1:0.86-1.09), basal margin raised, shallowly, broadly emarginate; sides weakly curved in basal half, widest at about middle, more strongly curved anteriorly, anterior margin projecting over head with two large upcurved asperities at apex; anterior slope convex, armed with robust, pointed asperities anteriorly, the asperities becoming more transverse, more closely spaced and lower towards summit in middle; disc weakly shining, weakly reticulate, finely punctured, the punctures more closely spaced in the Thai than in the Bornean specimens, finer

and sparser posterolaterally; posterolateral margin acutely carinate from basal margin to middle of pronotum; vestiture on pronotal slope sparse, with long erect setae, disc glabrous, without mycangial tuft.

Scutellum. Small, flat, semicircular, impunctate.

Elytra. Holotype 1.13 times longer than wide (paratypes 1.05-1.33), 1.29 times longer than pronotum (paratypes 1.14-1.36), bases transverse, carinate from scutellum to humerus, a small longitudinal swelling at humerus; sides subparallel in basal two-thirds, then gradually rounded to apex; elytral disc shining, convex, striate-punctate, strial punctures fine, moderately dense, interstrial punctures uniseriate, coarser and a little more closely placed than those on striae, both sets of punctures more closely placed in Thai than in Bornean specimens, disc with a few long and fine yellowish interstrial setae; declivity commencing at about middle, steeply sloping, declivital face quite strongly, broadly, impressed, sub-shiny, the margins carinate from the apex to interstriae VII; upper margin of the declivity with a small spine on interstriae II and a much larger, posteriorly directed spine on interstriae III, another large spine of similar size on interstriae V at about mid-height of declivity, small spines or granules may also be present between these large spines on declivital margins; striae I and II impressed on the upper part of declivity, interstriae II and III much widened on declivity, almost flat, each with a row of widely separated granules or small spines bearing very long, fine hairs posteriorly.

Legs. Procoxae narrowly separated, anterocoxal process narrow, spine-like, posterocoxal process not swollen; protibia obliquely triangular, widest about one-fourth from apex, outer margin with 6–7 denticles in apical half, posterior face weakly convex, not tuberculate. Meso- and meta-tibiae more evenly rounded with 10-11 denticles on outer margin.

Male. Unknown.

Etymology. The Latin name is an adjective derived from the four (*quatuor*) spines (*spinae*) on the elytral declivity.

Distribution. Brunei Darussalam, East Malaysia (Sabah), Thailand.

Host plants. Unknown.

Discussion

Cnestus quadrispinosus is clearly related to three other species: *C. bicornis* (Eggers, 1923), *C. bicornioides* (Schedl, 1952), and *C. triangularis* (Schedl, 1975). All four species lack a mycangial tuft of hairs at the base of the pronotum, and have broadly impressed elytra. This combination of characters distinguishes them from all other species of *Cnestus*: *C. quadrispinosus* is easily distinguished from the other three species by the presence of two pairs of large spines on the declivity. *Cnestus bicornis* is distinguished by the more elongate, parallel-sided pronotum, and the fine, sparse punctures of the pronotal disc. We have been unable to find characters that will reliably separate *C. bicornioides* and *C. triangularis*, and suspect that the two species should be synonymised. However, further studies of the species are needed.

Key to the species of *Cnestus* lacking a pronotal mycangial tuft and with impressed elytral declivity

1 Interstriae III and V each with a single strong tooth on upper and lateral margins of elytral declivity respectively. Thailand, Brunei, East Malaysia ..... ***C. quadrispinosus* sp. n.**
– Interstriae III and V without large teeth on declivity 2
2 Pronotum parallel-sided, 1.25 times longer than wide. Pronotal disc very finely, very sparsely punctured. Length 2.2–2.6 mm. Indonesia (Java, Sumatra), Philippines ..... ***C. bicornis* (Eggers)**
– Pronotum with weakly curved sides, 1.0–1.1 times longer than wide. Pronotal disc more densely and coarsely punctured. Length 2.7−3.7 mm. China (Yunnan), India (Andaman Is., Bengal), Papua New Guinea, Philippines, Thailand, West Malaysia ..... ***C. bicornioides* (Schedl),= ? *C. triangularis* (Schedl)**

In the majority of *Cnestus* species, the females possess a mesonotal mycangium used to transport the ambrosial fungus on which the larvae feed (Stone et al. 2007, Hulcr and Cognato 2013). Its presence is indicated by a tuft of hairs at the base of the pronotum. It is not known whether the four species have lost this mycangium, or whether the mycangium is situated elsewhere in the body, most probably in the head. If the mycangium has been lost, the species may well be mycocleptic (Hulcr and Cognato 2010). In mycocleptic species, the female starts its gallery close to galleries of other ambrosia beetles. The fungus established by the 'host' species grows in the galleries of the mycoclept which consequently does not need to transport its own ambrosia fungus, and lacks mycangia (Hulcr and Cognato 2010).

Acknowledgements

We are most grateful to M. Barclay (NHMUK), L. Zerche (Senckenberg Deutsches Entomologisches Institut), A. Floren (University of Würzberg) and Dr. H. Schillhammer (NHMW) for access to specimens, and to J. Hulcr for photographs of the holotype of *C. triangularis*. Special thanks also go to Mr. Sunate Karapan, Ms. Chananrat Nuankaew, Ms. Kumaree Na-chalame and Mr. Phuchit Saekong for facilitation in specimen collecting in Hala-Bala Wildlife Sanctuary, Narathiwat Province. This research was supported by budget revenue of Prince of Songkla University, project number NAT570377S.

References

Dole SA, Cognato AI (2010) Revision of *Xylosandrus* Reitter (Curculionidae: Scolytinae). Proceedings of the California Academy of Science 61: 451–545.

Dole SA, Jordal BH, Cognato AI (2010) Polyphyly of *Xylosandrus* Reitter inferred from nuclear and mitochondrial genes (Coleoptera: Curculionidae: Scolytinae). Molecular Phylogenetics and Evolution 54: 773–782. https://doi.org/10.1016/j.ympev.2009.11.011

Eggers H (1923) Neue indomalayische Borkenkäfer (Ipidae). Zoologische Mededelingen 7: 129–220.

Gomez D, Rabaglia RJ, Fairbanks KEO, Hulcr J (2018) North American Xyleborini north of Mexico: a review and key to genera and species (Coleoptera, Curculionidae, Scolytinae). ZooKeys 768: 19–68. https://doi. org/10.3897/zookeys.768.24697

Hulcr J, Cognato AI (2010) Repeated evolution of theft in fungus farming ambrosia beetles. Evolution 64: 3205–3212. https://doi.org/10.1111/j.1558-5646.2010.01055.x

Hulcr J, Cognato AI (2013) Xyleborini of New Guinea: A Taxonomic Monograph. Thomas Say Publications in Entomology, Entomological Society of America, Annapolis, 176 pp.

Hulcr J, Dole SA, Beaver RA, Cognato AI (2007) Cladistic review of generic taxonomic characters in Xyleborina (Coleoptera: Curculionidae: Scolytinae). Systematic Entomology 32: 568–584. https://doi.org/10.1111/j.1365-3113.2007.00386.x

Nunberg M (1972) Die Gattung *Cnestus* Sampson (Coleoptera, Scolytidae). Annales Zoologici, Warszawa 29: 473–478.

Sampson FW (1911) On two new wood-boring beetles. Annals and Magazine of Natural History, Series 8, 8: 381–384. https://doi.org/10.1080/00222931108693046

Schedl KE (1952) Fauna Philippinensis VIII. Philippine Journal of Science 80: 363–371.

Schedl KE (1975) New Scolytidae and Platypodidae from Papua and New Guinea IV. Annalen des Naturhistorischen Museums in Wien 79: 337–399.

Schiefer TL, Bright DE (2004) *Xylosandrus mutilatus* (Blandford), an exotic ambrosia beetle (Coleoptera: Curculionidae: Scolytinae: Xyleborini) new to North America. The Coleopterists Bulletin 58: 431–438. https://doi.org/10.1649/760

Stone WD, Nebeker TE, Monroe WA, MacGown JA (2007) Ultrastructure of the mesonotal mycangium of *Xylosandrus mutilatus* (Coleoptera: Curculionidae). Canadian Journal of Zoology 85: 232–238. https://doi.org/10.1139/z06-205

Wood SL (1986) A reclassification of the genera of Scolytidae (Coleoptera). Great Basin Naturalist Memoirs 10: 1–126.

Wood SL, Bright DE (1992) A catalog of Scolytidae and Platypodidae (Coleoptera), Part 2: Taxonomic index. Great Basin Naturalist Memoirs 13: 1–1553.

ZooKeys 795: 39–48 (2018)
doi: 10.3897/zookeys.795.28543
http://zookeys.pensoft.net

RESEARCH ARTICLE

A peer-reviewed open-access journal
ZooKeys
Launched to accelerate biodiversity research

A new species of frog-biting midge from Papua New Guinea with a key to the described Corethrellidae of the Australopapuan region (Diptera, Corethrellidae, *Corethrella*)

Gunnar Mikalsen Kvifte[1], Ximena E. Bernal[1,2]

1 *Department of Biological Sciences, Purdue University, 913 West State Street, IN-47906 West Lafayette, USA*
2 *Smithsonian Tropical Research Institute, Apartado 0843-03092, Balboa, Ancón, Panamá, República de Panamá*

Corresponding author: *Gunnar Mikalsen Kvifte* (gkvifte@purdue.edu)

Academic editor: *Art Borkent* | Received 22 July 2018 | Accepted 18 September 2018 | Published 5 November 2018

http://zoobank.org/C5A51254-1520-4E42-9B52-B10BC4B0371D

Citation: Kvifte GM, Bernal XE (2018) A new species of frog-biting midge from Papua New Guinea with a key to the described Corethrellidae of the Australopapuan region (Diptera, Corethrellidae, *Corethrella*). ZooKeys 795: 39–48. https://doi.org/10.3897/zookeys.795.28543

Abstract

Corethrella oppositophila Kvifte & Bernal, **sp. n.** is described based on one male and six female specimens collected at 2200 m a.s.l. on Mount Wilhelm, Papua New Guinea. The species is the fourth species of frog-biting midge described from this country and appears similar to *Corethrella solomonis* Belkin based on pigmentation of legs and abdominal tergites. It differs from *C. solomonis*, however, in the shape of female flagellomeres I–III, and in the thorax which has a dark brown vertical stripe. The new species is named for its sexually dimorphic flagellomeres, which are short and squat in the female and elongate in the male. These differences in morphological characters are discussed in light of the likely sexual differences in functional uses of the antennae, as males use them for mating only whereas females use them both for mating and prey location. An emended key is presented to the described Australopapuan species of Corethrellidae.

Keywords

Culicoidea, Culicomorpha, Papua New Guinea, taxonomy

Copyright *G.M. Kvifte, X.E. Bernal.* This is an open access article distributed under the terms of the Creative Commons Attribution License (CC BY 4.0), which permits unrestricted use, distribution, and reproduction in any medium, provided the original author and source are credited.

Introduction

Frog-biting midges (Diptera: Corethrellidae; *Corethrella* Coquillett) are widespread in the tropics, noteworthy in their females being specialized micropredators of frogs and toads. Locating their hosts primarily by auditory cues (Borkent 2008, Bernal and de Silva 2015), they are an emerging study system in studying the ecology and evolution of acoustic eavesdropping behaviour (Bernal et al. 2006, Grafe et al. 2008, 2018, de Silva et al. 2015, Caldart et al. 2016, Legett et al. 2018). Their fossil record extends back to the early Cretaceous and their ancient age is reflected in their biogeography which suggests Gondwanan vicariate events (Borkent 2008, Baranov et al. 2016). Including the new species described herein, 110 species are known from the extant fauna; however, this family has received little taxonomic study across their broad worldwide distribution (Borkent 2008, Borkent and Grafe 2012, Fei-peng et al. 2015, Baranov et al. 2016, Caldart et al. 2016).

In particular, the frog-biting midges from the Afrotropical, Oriental, and Australasian regions have received little attention apart from limited regional treatments (Colless 1986, Borkent and Grafe 2012). Insufficient information from these biogeographic regions has ultimately hampered our understanding of this group's phylogeny and evolutionary history (Borkent 2008). Since the three earliest diverging extant lineages of frog-biting midges occur in Australasia (Borkent 2008, Baranov et al. 2016), lack of material from this region is particularly problematic. Only eleven species have been recorded from this region: three from Papua New Guinea, five from Australia, one from New Zealand, and two from the Solomon Islands. The rich tropical rainforests of the Australopapuan region are, however, likely to harbour much higher species diversity than currently recognized, as evident from the low number of specimens known for the described species (see discussion in Borkent 2008). Species richness comparable to those of Borneo or Costa Rica (Borkent 2008, Borkent and Grafe 2012), if not even higher, is to be expected in the Australopapuan region.

In this study, we examine Malaise trap material collected by Leponce et al. (2016) and describe *Corethrella oppositophila* Kvifte & Bernal, sp. n. based on an adult male and six adult females. This species is similar to *C. solomonis* Belkin, 1962 from the Solomon Islands, for which only the female has been described. The discovery of a male of this putative group of Australasian and Oceanic species could thus add phylogenetic information. We also provide a key to the frog-biting midges of the Australopapuan region. Finally, we reveal interesting sexual dimorphism in the antenna and discuss how these morphological characters may relate to their different functions in each sex.

Materials and methods

Specimens were collected in Malaise traps at Mount Wilhelm, Morobe province, in October 2012, as described by Leponce et al. (2016). All specimens were stored in 96% alcohol in the Royal Belgian Institute of Sciences (**RBINS**). Prior to examination

the specimens were cleared in 10% KOH at room temperature and mounted on slides in Canada balsam following methods outlined in Kirk-Spriggs (2017). Observations were performed using a Nikon Eclipse Ci compound microscope. Measurements were made using an ocular micrometer and are given in μm with an accuracy of +/- 2.5 μm, except wing length which is given in mm with an accuracy of 0.01 mm. When three or more specimens were available, measurements are given as ranges followed by means in parentheses. Photographs were taken with a Nikon DS-Fi2 camera and line drawings were prepared using a drawing tube from a Leitz Diaplan compound microscope attached to the Nikon Eclipse Ci.

Morphological characters and terminology mainly follows Borkent (2008). Additional characters, however, were also examined. The eyebridge, for instance, is of high taxonomic utility in Psychodinae, and both its width in facet rows and median extent are used here (Kvifte and Wagner 2017). The inner head skeleton of Corethrellidae, specifically the cibarium and tentorium appear to show some interspecific variation; terminology for these provisionally follows McAlpine (1981) and are labelled in figures 2a–b. Some chaetotaxic characters of the male and female postabdomen are also included: for males, the width/length proportions of tergite 8 and the width of the median hairless stripe on tergite 9 and, for females, the specialized setae on the proctiger.

***Corethrella oppositophila* Kvifte & Bernal, sp. n.**
http://zoobank.org/DB8CE9C3-BFA2-4560-9FE6-D2C2BB17478A
Figs 1–2

Type material. Holotype male. PAPUA NEW GUINEA: Morobe province, Mount Wilhelm, 5.758978°S, 145.18607°E, 2200 m a.s.l., 27.X.2012, leg. Mogia, Lilip, Vohotny & Leponce (Malaise trap). Six paratype females, same locality as holotype but collection dates 17.X.2012, 22.X.2012, 25.X.2012, 28.X.2012, and 31.X.2012 (two specimens). All specimens in collections of RBINS.

Diagnosis. Only extant species of Corethrellidae with the following combination of characters: wing with a mid-length band of dark pigmentation and scales, thorax brown with anterior two thirds of scutum, prosternum and katepisternum light brown, abdominal tergites light brown with anterior dark bands, dorsomedial seta of male gonocoxite parallel with proximalmost seta in dorsal row.

Description. Adult male (n = 1). ***Head*** (Figs 1a, 2a, 2c) broader than long. Eyebridge of five rows of facets, constricting towards median. Four frontal setae present. Antenna (Figure 1c) with pedicel dark brown, scape and flagellum paler. Pedicel without setae longer than length of pedicel. Length of flagellomeres 120, 62.5, 62.5, 85, 115, 132.5, 132.5, 130, 130, 125, 117.5, 82.5, 65, 80, terminal flagellomere bifurcate. Three sensilla coeloconica on flagellomere I, one sensillum coeloconicum on each of flagellomeres IX–XIII. Palpus uniformly pale brown with segment III of uniform width or slightly broader at mid length, length of palpal segments 37.5, 42.5, 100, 77.5, N/A (5th palpal segments missing in specimen). Palpal segment I with single lateral elongate seta, seg-

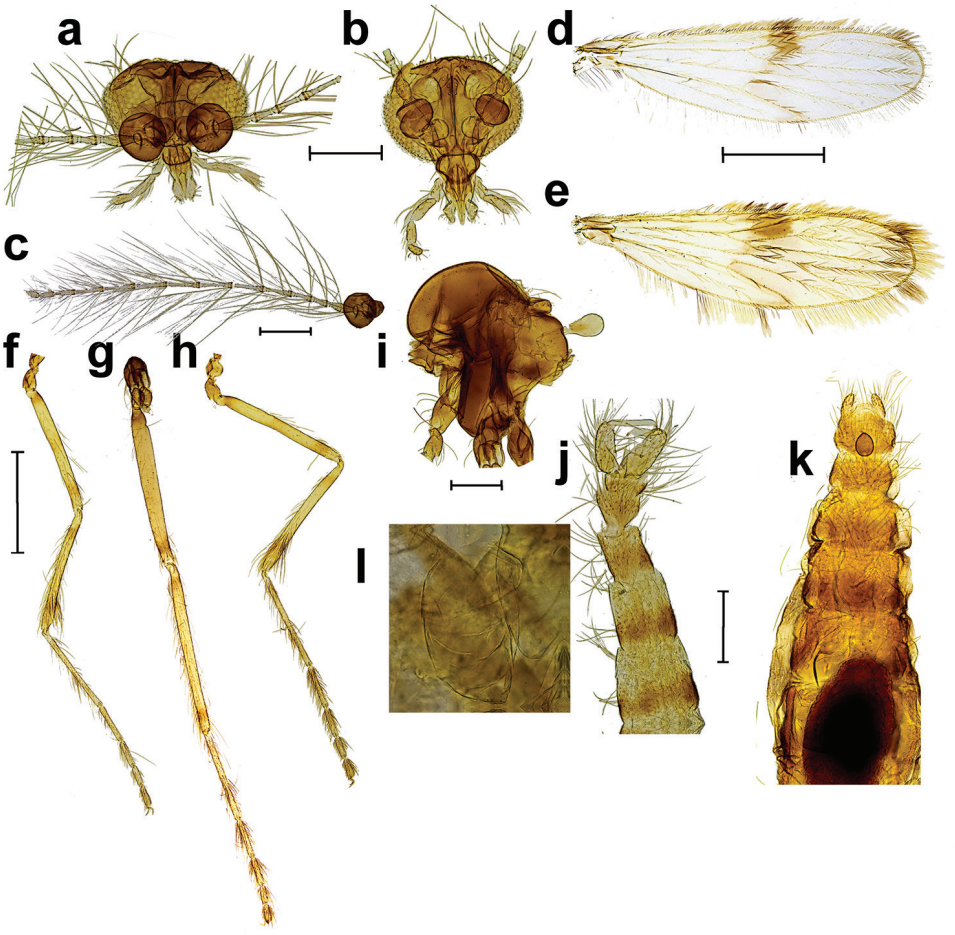

Figure 1. *Corethrella oppositophila* Kvifte & Bernal, sp. n., male and female **a** male head **b** female head **c** male antenna **d** male wing **e** female wing **f** hind leg of female **g** mid leg of female **h** fore leg of female **i** thorax of female **j** male abdomen **k** female abdomen with blood meal **l** egg in female abdomen. Scale bars: 200 μm (**a, b, c, i, j, k**); 500 μm (**d–g**). Views: frontal (**a, b**), dorsal (**d, e, j–l**), posterior (**f–h**).

ment II with two elongate setae, and one short. Clypeus broadly oval with single medial seta. Labellum oval. Cibarial pump, hypopharynx, tentorium and stipes as in Figure 2a.

Thorax brown with anterior two thirds of scutum, prosternum and katepisternum light brown. Dorsocentral row without elongate setae at posterior end. Prescutal suture narrow, extending more than two thirds of way to dorsocentral row. Anterior anepisternum divided diagonally into dorsal and ventral portions, dorsal portion about twice as large as ventral; posterior anepisternum undivided, posterior half without distinct setae. Haltere paler than thorax.

Wing (Figure 1d) 1.75 mm long, 0.48 mm wide, R_1 1.31 mm long. Apex of R_2 at level with M_1. Membrane with patch of dark infuscation from Sc to stem of R_{2+3}, paler

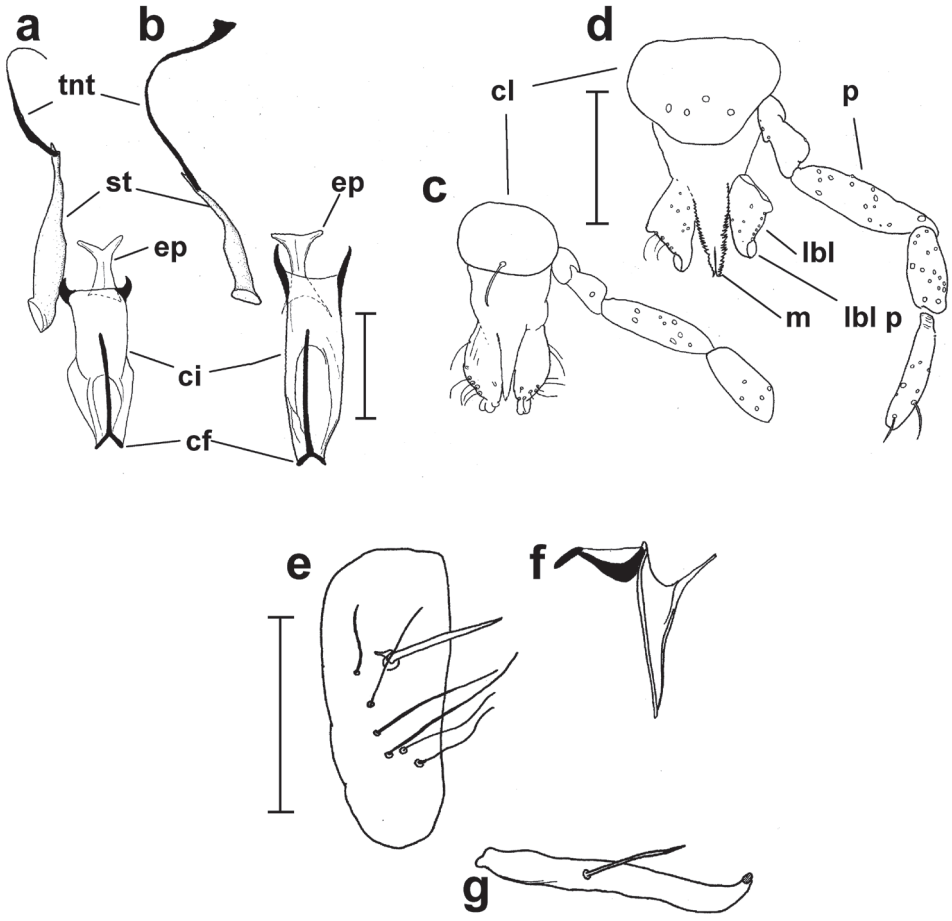

Figure 2. *Corethrella oppositophila* Kvifte & Bernal, sp. n., male and female **a** male hypopharynx, cibarium and stipes **b** female hypopharynx, cibarium and stipes **c** male clypeus and mouthparts **d** female clypeus and mouthparts **e** gonocoxite **f** paramere and aedeagus (only one paramere shown) **g** gonostylus. Scale bars 80 μm (**a, b**); 100 μm (**c–g**). Abbreviations: cf – cibarial fork, ci – cibarium, cl – clypeus, ep – epipharynx, lbl – labellum, lbl – labellar projection, m – mandible, p – palpal segment III, st – stipes, tnt – tentorium. Views: frontal (**a–d**), dorsal (**e–g**).

infuscation present over crossveins r-m and m-cu. Midlength and subapical bands of pigmented scales present. Wing scales narrow, those on C nearly twice as wide as those on other veins.

Legs light brown with rings of darker pigmentations basally and subbasally on all femora and tibiae, more indistinct on midtibia. Fore- and midtarsi with banding. With only slender setae, lacking scales. Claws on fore- and midlegs unequal, hind leg claws equal, all simple, without basal prongs or empodia. Ratio of foreleg Ta_3/Ta_4 = 1.56.

Abdomen (Figure 1j) Light brown with darker brown mottled bands anteriorly on each tergite, sternites I–II pale, other sternites light brown with darker brown mottled bands anteriorly. Tergites and sternites VIII and IX light brown; length of segment VIII 112.5, distally 2.5 times as wide as base; hairless stripe medially on tergite IX 35 μm wide.

Genitalia (Figure 2e–g). Gonocoxite uniformly pale brown, tapering gently towards apex; all setae of similar length; with well-defined dorsal row of six setae of uniform length and thickness. Dorsomedial seta stout, tapering from non-expanded base. Gonostylus sinuous, of equal thickness except tapering apically, one elongate, thick subbasal seta situated on inner surface (ventrally), with thick, blunt subapical peg; subbasal seta 0.4 length of gonostylus. Parameres comprised of a sclerotized S-shaped part and a less weakly sclerotized egg-shaped part. Aedeagus slender, tapering gradually to apex, reaching beyond dorsomedial seta, lateral margins meeting apically.

Adult female (n = 6) As for male, with following differences. *Head* (Figure 1b) Eyebridge of 5–6 rows of facets, constricting towards median. Coronal suture long, extending ventrally to between antennal bases. All available specimens with flagellum broken, length of preserved flagellomeres (n = 4) 70–80 (74), 42.5–45 (43), 45–50 (47), first flagellomere with three sensilla coeloconica. Length of palpal segments (n = 6, 6, 6, 4, 2) 35–50 (41), 40–47.5 (45), 87.5–97.5 (93), 70–80 (76), 80–95 . Clypeus broadly hexagonal, with anterior margin about half length of posterior margin,, with 1–5 setae in single row. Mandibular teeth small, pointed. Labellum rectangular with apicomedial projection. Cibarial pump, hypopharynx, tentorium, and stipes as in figure 2b.

Thorax (Figure 1i) brown with anterior third of scutum, prosternum, mediotergite, metaepisternum, scutellum, and metakatepisternum light brown.

Wing (Figure 1e) 1.73–2.00 (1.79) mm long, 0.46–0.60 (0.53) mm wide. R_1 1.19–1.35 (1.24) mm long.

Legs (Figure 1f–1h) Claws of each legs equal to those of others, equal on each leg, simple, with empodia slender, feather-shaped. Ratio of foreleg Ta_3 / Ta_4 = 1.35

Genitalia (Figure 1k) with 2–6 microseta subapically on proctiger.

Egg (n = 15, Figure 1I) length 240, width 127.5 mm.

Biology. Females have biting mouthparts and one paratype was collected with blood in its gut (Figure 1k). Another paratype female was preserved with 15 eggs in her abdomen; these were not preserved well enough, however, to allow morphological comparison with other described Corethrellidae eggs.

Distribution. Known only from the type locality on Papua New Guinea, where it was collected in a Malaise trap at 2200 m.a.s.l.

Etymology. From Latin *opposita*, opposite, and Greek φίλος *(philos*), friend. "Opposites attract" – referring to the stark sexual dimorphism of the basal flagellomeres of the male and female antennae.

Remarks. The new species keys to *C. solomonis* in Borkent (2008) but differs from that species by its thorax being more extensively brown (see description above and compare with Borkent 2008: fig. 38B) and having much shorter flagellomeres in the female. The male of *C. solomonis* is unknown.

The male and females of *C. oppositophila* Kvifte & Bernal sp. n. have been associated based on similarity of pigmentation, together with co-occurrence in the same Malaise trap at the same time.

Key to the described Corethrellidae of the Australopapuan region

1 Wings without pigmented markings **2**
– Wings with pigmented bands..... **3**
2 Wing veins largely without scales. Papua New Guinea ..... ***C. evenhuisi*** **Borkent, 2008**
– Wing veins with scales. Papua New Guinea..... ***C. pauciseta*** **Borkent, 2008**
3 At least hind tibia with dark band at base..... **4**
– Tibiae unicolorous or with well-defined dark bands only at apices **9**
4 Abdominal tergites uniformly pigmented. Hind tibia with dark band at base..... **5**
– Abdominal tergites with dark bands anteriorly. All tibiae with dark bands at base and subapically..... **6**
5 Wing with dark scales restricted to mid-length band and apical margin. Solomon Islands..... ***C. canningsi*** **Borkent, 2008**
– Wing with two bands of dark scales in addition to apical patch. Papua New Guinea ..... ***C. varia*** **Borkent, 2008**
6 Femora apically with pigmented dark band (fig. 1f–1h) 7
– Femora apically pale. Queensland (Australia) ..... ***C. mckeeveri*** **Colless, 1986**
7 Thorax with pleura pale with narrow brown stripes. Solomon Islands ..... ***C. solomonis*** **Belkin, 1962**
– Thorax with pleura mostly brown..... **8**
8 Wing with unicolorous scales on anterior margin. Thorax with some pale mottling on pleura, scutum unicolorous brown. Australia ..... ***C. collessi*** **Borkent, 2008**
– Wing with contrasting, i.e. both darker and lighter, scales on anterior margin. Thorax without mottling on pleura, scutum lighter on anterior two thirds. Papua New Guinea..... ***C. oppositophila*** **Kvifte & Bernal, sp. n.**
9 Abdominal tergites I–VII with dark pigmentation only apicolaterally, sternites completely pigmented. Tibiae without dark bands. New Zealand ..... ***C. novaezealandiae*** **Tonnoir, 1927**
– Abdominal tergites I–VII with entire hind margin darkly pigmented, sternites with incomplete pigmentation. Tibiae with apical dark bands. Australia **10**
10 Thorax dark brown. Wing with three distinct bands of pigmentation..... ***C. marksae*** **Colless, 1986**
– Thorax light brown. Wing with pigmentation restricted to single dark midlength band..... **11**
11 Head wider than long. Flagellomere I about four times as long as wide..... ***C. pallidula*** **Bugledich, 1999**
– Head circular in frontal view. Flagellomere I about twice as long as wide ..... ***C. alba*** **Borkent, 2008**

Discussion

Apart from its darker thorax and shorter female flagellomeres, the female of *C. oppositophila* resembles *C. solomonis*. Because of the overall similarity and geographical proximity of these two species, we consider it likely that these species are closely related, and possibly forming a group with *C. mckeeveri* Colless, 1994 as suggested by Borkent (2008) and Baranov et al. (2016).There is, however, currently no robust synapomorphic evidence available to support this group. These three species all have many plesiomorphic characters and are among the earliest diverging lineages of Corethrellidae, only the Australian *C. marksae* species group and the New Zealandian *C. novaezealandiae* are earlier divergences within the family (Borkent 2008, Baranov et al. 2016).

The male of *C. oppositophila* is similar to that of *C. mckeeveri* both in the shape of the parameres and the presence of an apical peg on the gonostylus, characters that also appear to be similar to those observed in *C. marksae* Colless, 1986. It can be separated from both of these species based on the gonocoxite having its dorsomedial setae on level with the proximalmost seta of the dorsomedial row, thus resembling the Afrotropical *C. harrisoni* Freeman, 1962.

Males and females of *C. oppositophila* appear to have highly pronounced sexual dimorphism in the length and width of the basal flagellomeres. These flagellomeres are elongate in the observed male, whereas in all observed females they are short and bead-shaped (Figure 1a–c). We deem it likely that these striking morphological differences translate into sex-specific adaptations to detect different acoustic cues and signals: in the one Corethrellidae species where courtship has been studied the most comprehensively, both sexes use sound in mate recognition (de Silva et al. 2015). Females in addition use auditory cues in locating frogs on which to feed, meaning their antennae have to respond to a broader range of acoustic stimuli than those of the males. Borkent (2008) showed that shortened basal flagellomeres in the female are apomorphic in Corethrellidae within Culicoidea, and that different conditions of basal flagellomere shortening have arisen on multiple occasions in frog-biting midges (characters 37, 59 and 77 in Borkent 2008, p. 216, 221 and 225). Judging from illustrations in Borkent (2008), however, sexual dimorphism in flagellomere length is not universal within the group, and even in the early diverging Australopapuan lineages there is considerable variation. More data are needed to ascertain how widespread these sexual dimorphisms are and how these morphological differences are related to the putative functional differences in both sexes as outlined above.

The material from which the new species was identified stems from the inventory project of Leponce et al. (2016), which sampled along the entire 3200 m elevational gradient of Mount Wilhelm, Papua New Guinea. For the present study, only material from 1200–3200 m a.s.l. was available for examination, and frog-biting midges were only present at the sampling station at 2200 m elevation. This observation is unlikely to reflect any real absence of *Corethrella* at lower elevations in Papua New Guinea, however, as the three previously described species from this island have been collected at 122, 1250, and 1300 m elevation (Borkent 2008). While *C. oppositophila* seems

to be a high-elevation species, further work that examines the distribution of Papuan frog-biting midges across the altitudinal gradient is necessary to understand the elevational distribution of these species. Overall, we are just starting to understand the Papuan fauna of frog-biting midges and systematic trapping for specimens from this group using sound-baited traps, for instance, will undoubtedly reveal interesting ecological patterns and many additional species than those currently described.

Acknowledgements

We are grateful to Maurice Leponce and Wouter Dekoninck for their hospitality during GMK's visit at RBINS, and for the loan of specimens. Greg Curler prepared the slides and Nigel K. Anderson took most of the photographs. This work was supported by NSF IOS#1433990 to XEB. The manuscript was improved by constructive and critical comments on an earlier draft by Art Borkent, and further comments by Viktor Baranov, Bill Grogan, and an anonymous reviewer.

References

Baranov V, Kvifte GM, Perkovsky EE (2016) Two new species of fossil *Corethrella* Coquillett from Late Eocene Rovno amber, with a species-level phylogeny for the family based on morphological traits (Diptera: Corethrellidae). Systematic Entomology 41: 531–540. https://doi.org/10.1111/syen.12172

Bernal XE, de Silva P (2015) Cues used in host-seeking behavior by frog-biting midges (*Corethrella* spp. Coquillet). Journal of Vector Ecology 40: 122–128. https://doi.org/10.1111/jvec.12140

Bernal XE, Rand AS, Ryan MJ (2006) Acoustic preferences and localization performance of blood-sucking flies (*Corethrella* Coquillett) to túngara frog calls. Behavioral Ecology 17: 709–715. https://doi.org/10.1093/beheco/arl003

Borkent A (2008) The Frog-Biting Midges of the World (Corethrellidae: Diptera). Zootaxa 1804: 1–456.

Borkent A, Grafe U (2012) The frog-biting midges of Borneo – from two to eleven species (Corethrellidae: Diptera). Zootaxa 3279: 1–45.

Caldart VM, dos Santos MB, Iop S, Pinho LC, Cechin SZ (2016) Hematophagous flies attracted to frog calls in a preserved seasonal forest of the austral Neotropics, with a description of a new species of *Corethrella* (Diptera: Corethrellidae). Zoological Science 33: 527–536. https://doi.org/10.2108/zs150173

Colless DH (1986) The Australian Chaoboridae (Diptera). Australian Journal of Zoology, Supplementary Series 124: 1–66. https://doi.org/10.1071/AJZS124

de Silva P, Nutter B, Bernal XE (2015) Use of acoustic signals in mating in an eavesdropping frog-biting midge. Animal Behaviour 103: 45–51 https://doi.org/10.1016/j.anbehav.2015.02.002

Fei-peng W, En-jiong H, Mei-qiong Y, Yi-xin Q, Ming-an O, Xiong G (2015) The frog-biting midges from China with description of two new species (Diptera: Corethrellidae). Journal of Fujian Agricultural and Forestry University (Natural Science Edition) 44: 245–249.

Grafe TU, Saat HBM, Hagen N, Kaluza B, Berudin ZBB, Wahab MABA (2008) Acoustic localisation of frog hosts by blood-sucking flies *Corethrella* Coquillet (Diptera: Corethrellidae) in Borneo. Australian Journal of Entomology 47: 350–354. https://doi.org/10.1111/j.1440-6055.2008.00667.x

Grafe TU, Ahmad Sah HH, Ahmad N, Borkent A, Meuche I, Konopik O (2018) Studying the sensory ecology of frog-biting midges (Corethrellidae: Diptera) and their frog hosts using ecological interaction networks. Journal of Zoology Early View, 11 pp. https://doi.org/10.1111/jzo.12612

Kirk-Spriggs AH (2017) Collection and preservation of Diptera. In: Kirk-Spriggs AH, Sinclair B (Eds) Manual of Afrotropical Diptera, Volume 1 – Introductory chapters and keys to Diptera families. South African National Biodiversity Institute, Pretoria, 69–87.

Kvifte GM, Wagner R (2017) 24. Psychodidae (sand flies, moth flies or owl flies). In: Kirk-Spriggs AH, Sinclair B (Eds) Manual of Afrotropical Diptera, Volume 2. Nematocerous Diptera and lower Brachycera. South African National Biodiversity Institute, Pretoria, 607–632.

Legett HD, Baranov VA, Bernal XE (2018) Seasonal variation in abundance and diversity of eavesdropping frog-biting midges (Diptera, Corethrellidae) in a neotropical rainforest. Ecological Entomology 43: 226–233. https://doi.org/10.1111/een.12492

Leponce M, Novotny V, Pascal O, Robillard T, Legendre F, Villemant C, Munzinger J, Molino J-F, Drew R, Ødegaard F, Schmidl J, Tishechkin A, Sam K, Bickel D, Dahl C, Damas K, Fayle TM, Gewa B, Jacquemin J, Keltim M, Klimes P, Koane B, Kua J, Mantilleri A, Mogia M, Molem K, Moses J, Nowatuo H, Orivel J, Pintaud J-C, Roisin Y, Sam L, Siki B, Soldati L, Soulier-Perkins A, Tulai S, Yombai J, Wardhaugh C, Basset Y (2016) Land module of Our Planet Reviewed – Papua New Guinea: aims, methods and first taxonomical results. In: Robillard T, Legendre F, Villemant C, Leponce M (Eds) Insects of Mount Wilhelm, Papua New Guinea. Publications Scientifiques du Muséum, Paris, 11–48.

McAlpine JF (1981) Morphology and terminology – adults. In: McAlpine JF, Peterson BV, Shewell GE, Teskey HJ, Vockeroth JR, Wood DM (Eds) Manual of Nearctic Diptera, Volume 1. Biosystematics Research Institute, Ottawa, Ontario, 9–64.

ZooKeys 795: 49–65 (2018)
doi: 10.3897/zookeys.795.28416
http://zookeys.pensoft.net

RESEARCH ARTICLE

A peer-reviewed open-access journal
ZooKeys
Launched to accelerate biodiversity research

Imaging natural history museum collections from the bottom up: 3D print technology facilitates imaging of fluid-stored arthropods with flatbed scanners

Patina K. Mendez[1], Sangyeon Lee[2], Chris E. Venter[3]

1 *130 Mulford Hall #3114, Department of Environmental Science, Policy & Management, University of California, Berkeley, Berkeley, CA 94720-3114, USA* **2** *Department of Mechanical Engineering, University of California, Berkeley, USA* **3** *207 Trinity Road, Brisbane, CA 94005, USA*

Corresponding author: *Patina K. Mendez* (patina.mendez@berkeley.edu)

Academic editor: *Pavel Stoev* | Received 17 July 2018 | Accepted 31 August 2018 | Published 5 November 2018

http://zoobank.org/F6627446-5C76-405C-A5A2-708AF4801EF9

Citation: Mendez PK, Lee S, Venter CE (2018) Imaging natural history museum collections from the bottom up: 3D print technology facilitates imaging of fluid-stored arthropods with flatbed scanners. ZooKeys 795: 49–65. https://doi.org/10.3897/zookeys.795.28416

Abstract

Availability of 3D-printed laboratory equipment holds promise to improve arthropod digitization efforts. A 3D-printed specimen scanning box was designed to image fluid-based arthropod collections using a consumer-grade flatbed scanner. The design was customized to accommodate double-width microscope slides and printed in both Polylactic Acid (PLA) and nylon (Polyamide). The workflow with two or three technicians imaged Trichoptera lots in batches of six scanning boxes. Individual images were cropped from batch imagess using an R script. PLA and nylon both performed similarly with no noticeable breakdown of the plastic; however, dyed nylon leeched color into the ethanol. The total time for handling, imaging, and cropping was ~8 minutes per vial, including returning material to vials and replacing ethanol. Image quality at 2400 dpi was the best and revealed several diagnostic structures valuable for partial identifications with higher utility if structures of the genitalia were captured; however, lower resolution scans may be adequate for natural history collection imaging. Image quality from this technique is similar to other natural history museum imaging techniques; yet, the scanning approach may have wider applications to morphometrics because of lack of distortion. The approach can also be applied to image vouchering for biomonitoring and other ecological studies.

Keywords

digitization, natural history collections, nylon, PLA, Trichoptera

Copyright *Patina K. Mendez et al.* This is an open access article distributed under the terms of the Creative Commons Attribution License (CC BY 4.0), which permits unrestricted use, distribution, and reproduction in any medium, provided the original author and source are credited.

Introduction

Specimen digitization efforts continue to be a high priority for natural history collections (Baird 2010). Specimens serve as exemplars of morphological variation in taxonomic studies and georeferenced collection records are required to build predictive models of species distributions (Dietrich et al. 2012, Johnson et al. 2013, Shah et al. 2014). When specimens are available digitally, risk of loss and damage to museum specimens can be reduced because only subsets of material may be requested by specialists and available images may facilitate remote identification of unknowns. Although various workflows and custom imaging systems have been developed to make museum material easier to access and manage, imaging museum specimens and digitizing associated information remains acutely laborious and expensive (Vollmar et al. 2010).

Arthropod imaging efforts are largely focused on pinned collections because challenges in imaging specimens stored in fluids is complicated by greater logistical difficulties, making their imaging a lower priority. Soft-bodied invertebrates such as larval insects, spiders, and adult aquatic insects are preferentially stored in ethanol or other preservatives so that shrinking during drying does not distort or obscure morphological structures required for identification. Vials are often stored within larger jars, and each vial often contains multiple specimens in a "lot" sometimes with free-floating dissections (e.g., genitalia) (Figure 1). Multiple labels must be removed from the vial and laid out when imaged. Fluid stored material can be messy and time-intensive to work with, often containing other preservatives that are toxic or noxious, and aged fluids often become yellowed or cloudy over time, requiring their replacement.

These curatorial activities during the imaging process results in longer handling times than pinned material when digitizing, thereby increasing digitization costs (Vollmar et al. 2010). The need to include fluid to support the soft-bodied specimens can make photographic imaging difficult because of surface reflections and distortion from the liquid. However, adoption of a process to image fluid collections is limited by a lack of standardized equipment, defined laboratory workflows, and the perceived inability to image multiple samples at the same time. Scanning material offers an opportunity to digitize fluid material because surface reflections become a non-issue, and scanners lack distortion that occurs in camera lenses because they scan each point by moving across the subject. Given that aquatic species are some of the most threatened under impending climate change (DeWalt et al. 2005, Shah et al. 2014) and their museum records exist primarily in fluid collections, digitization efforts of freshwater species are critical for identifying species and habitats most at risk.

3D printing technology can be used to develop custom equipment for research and can take advantage of available high-quality laboratory materials. Custom laboratory and field equipment is common in the life sciences because the materials are low cost and can be designed for the study goals. Although 3D printing has been common in prototyping in many industries, its adoption in the life sciences has just recently emerged: beetle decoys made on 3D printers can be used to visually attract emerald ash borers (Domingue et al. 2015), life history behavior of insets can be monitored with custom 3D-printed equipment (Berry et al. 2016), and field equipment can be

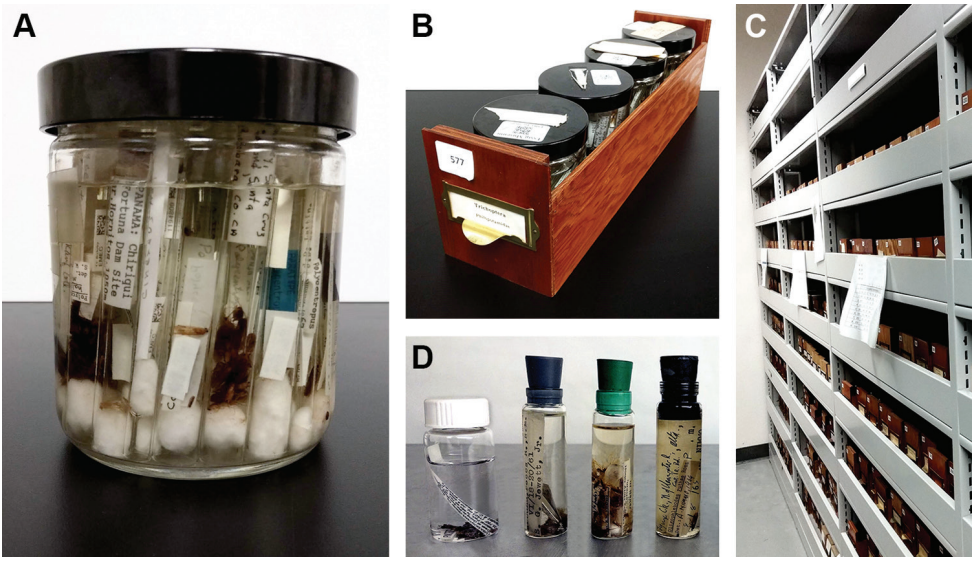

Figure 1. Fluid-stored arthropods in **A** a museum jar with shell vials **B** shell vials in a jar rack **C** racks in storage shelves at the Essig Museum of Entomology. Other fluid-based storage approaches include **D** screw-top scintillation vials and stoppered vials. Individually capped vials are commonly stored in racks on shelves.

repaired and improved with 3D-printed parts (Will and Steplowski 2016). 3D-printed equipment allows sizes and shapes to be specific to the application and can be designed to interface with existing equipment, be made from a wide range of materials, and compared to custom fabrication, can be relatively low cost.

The goal of this project was to design a standardized 3D-printed piece of laboratory equipment to streamline imaging of small invertebrates stored in fluid collections of natural history museums. Specifically, we designed the system to image on a flatbed scanner using standard, large, optically-clear 75 × 50 × 1 mm glass slides mounted into a 3D-printed plastic box. We also provide a basic scanning procedure with image resolution settings and an R script to subset the batch image scans. We tested our system using fluid-stored material from the Essig Museum of Entomology. We imaged specimen lots of Trichoptera because the wide range of body sizes and life forms provide a robust test of conditions found in wet collections.

Methods

Scanning box design and construction

To standardize the box size and reduce the need to cut custom glass, we designed the scanning box around a pair of large, double-wide microscope slides (75 × 50 × 1 mm, Fisher Scientific, Fisherbrand Plain Microscope Slides 12–550C). We selected this glass type and size because of its clarity, durability, relatively low cost (approx. $0.50/slide) and wide availability.

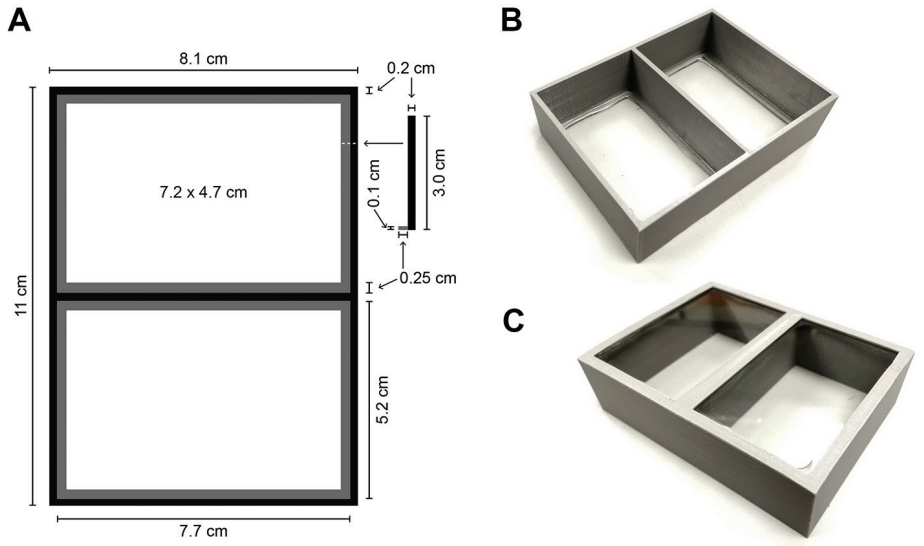

Figure 2. Fluid material scanning box: **A** dimensions of top-down and cross-section view of box plans, and finished box with glass affixed in **B** top and **C** bottom view.

The imaging design approach addresses issues with imaging in liquid, specifically to eliminate reflections on the surface from overhead shots by scanning through a clear-bottomed box. This design is based on an improvised glass-bottomed VWR pipet box lid-scanning approach used by some researchers for imaging voucher materials as required for the BOLD project (Milton et al. 2013). The final version of the scanning box design was also inspired by a design for photographing aquatic insects using microscope slides to create miniature aquaria for aquatic macrophotography (C Riley Nelson, pers. comm.).

Our approach used 3D print technology because of its ability to produce precise, low-volume runs in a variety of materials. Using Autodesk Meshmixer 2.9 (Autodesk 2015), we designed the box frame to have two panels, one for label information and one for specimens, resulting in a design box size of 8.1 cm × 11.0 cm × 3.0 cm with 0.2 cm walls (Figure 2). A 0.25 × 0.1 cm lip along the interior frame of the box bottom supports the slide once glued. We created the frame design and uploaded the StereoLithography (.stl) file to Shapeways (https://www.shapeways.com) for printing. This STL file is available from (https://github.com/pkmendez/museumscanbox) for download.

To compare frame materials, we printed the design in multiple materials, colors, and finishes at Shapeways. Polylactic Acid (PLA; Natureworks, Ingeo Biopolymer 4043D) designs are printed using Fused Deposition Modeling Technology by extruding melted PLA through a hot tip. Nylon (polyamide, Electro Optical Systems, PA2200) is printed through an ink-jet process and comes in unfinished (print lines visible) and polished (rough sides are abraded by blasting with polishing pellets). We printed PLA models in white, black, and grey (approx. $25 USD each). Nylon was available in white or dyed. We tested black and orange, both unfinished and polished (approx. $28 USD each). Although early prototypes also included prints in ABS-like materials, we did not include this material for further consideration because of the higher costs per print and

odors emitted during the materials testing phases. Instead tests were limited to PLA and nylon because of their similar cost and print time.

To complete each box, we fixed the slide into the box with two applications of E6000 silicone adhesive. To apply each layer, we used a wide-tip syringe loaded with adhesive, carefully tracing the margins of the slide and air-dried the box for 24 hours. E6000 shrinks when it dries and we found that two applications prevented most leaks.

Materials testing

We tested the completed scanning boxes by filling each box approximately 1/3 full of 75% ethanol. We examined the boxes every 20 minutes over the first hour, and then hourly thereafter for 4 hours. We recorded any leaking, softening of the material, staining, fading of colors, or odors.

Scanning workflow

The scanning workflow consisted of moving the specimen to the scanning boxes, placing them on the scanner, arranging and covering the specimens, acquiring a batch image, and then cropping the images in software (Figure 3A). To standardize scanning of the collection in the Essig Museum of Entomology similar to the CalBug project (CalBug 2017), we placed all labels into the upper panel of the scanning box with a unique Essig Museum of Entomology Catalog label (2D DataMatrix code) in the upper left corner of the box, followed by the collection label(s), then any determination, count, and habitat labels (Figure 4A). We covered the labels with a 4.8 × 7.3 cm piece of 1/8" thick acrylic Plexiglas in "sign white" (Tap Plastics, $1 each) to hold down the labels and serve as a background. In the lower panel, we arranged the specimens so that they did not overlap, added a 10 mm scale bar in the lower half of the panel, and covered the specimens with a white Plexiglas background. To both the label and specimen boxes, we added ethanol to submerge the white background and reduce imaging distortions caused by air bubbles (Figure 3B). We also replaced yellowed ethanol when necessary resullting in notable improvement to scans.

To improve the quality of the scans, we arranged specimen strategically and added supports in the specimen box. For larvae, we lined up the caddisfly cases, but did not remove larvae from cases, and for adults with genitalic dissections, we often paired the body and dissections within a ring (a plumbing slip joint washer) to keep the material from floating and to serve as a standoff for the background (Figure 3D). For larger specimens, such as large-cased limnephilids, we used polished Plexiglas cubes 3/8" on a side in each corner of the panel to keep the white background panel from rocking (Figure 3B). To prevent buildup of oils on the scan boxes, we washed the scanning boxes in tap water and dish soap at the end of each daily scanning session and left them to air dry overnight. Before beginning the next scanning session, we cleaned both the scanner glass and the exterior slide glass of the scanning box using household glass cleaner.

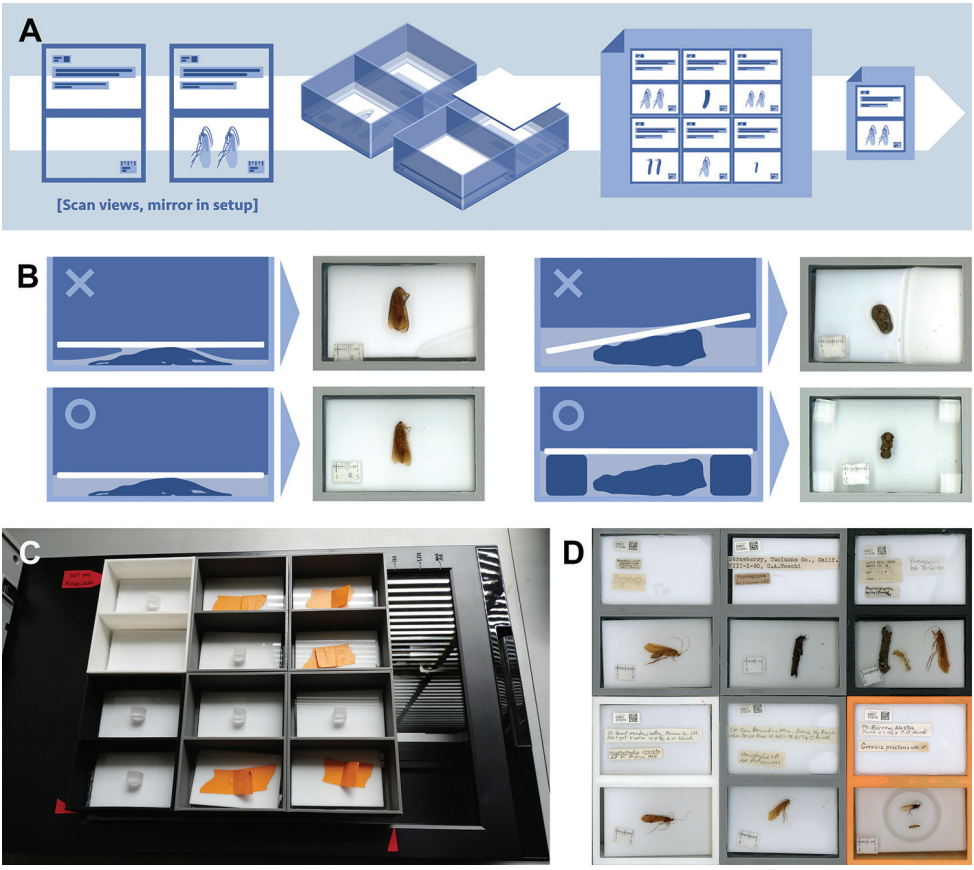

Figure 3. Scanning process images: **A** scanning process with scan view setup, box covers, full scan, and cropped image **B** required fill levels of fluid for box covers to prevent bubbles and standoffs (left) to prevent an uneven scan (right) **C** six boxes set up on scanner; and **D** resulting full scan. Clear Plexiglas cube standoffs **B** and slip-joint rings **D** (lower-right) improve scans.

To image specimens efficiently, and reduce overall handling time, we imaged batches of 6 boxes (Figure 3 C, D) on an Epson Perfection C600 Photo Scanner connected to a workstation (Lenovo Ideacentre Q190, 1.60 GHz Intel Celeron, 4GB Ram, Windows 8). We arranged the boxes in a compact 2 × 3 grid with no spacing between boxes. The set of boxes was aligned with tape-marks on the scanner for the outer boundaries (Figure 3C) and we set the marquee scanning area to capture only the 6 boxes in one scan. Once set, this marquee box did not need to be repositioned between scans.

To determine the most appropriate resolution and file size to image batches, we scanned a representative batch at 600 dpi, 1200 dpi, and 2400 dpi, compared file characteristics and determined the resolvable structures at each resolution. To determine resolvable structures, we compared images of *Rhyacophila harmstoni* Ross, 1944 (UC BERKELEY EMEC 41255), a caddisfly with an overall adult body length of approximately 1 cm, but also examined other images scanned at 2400 dpi to identify

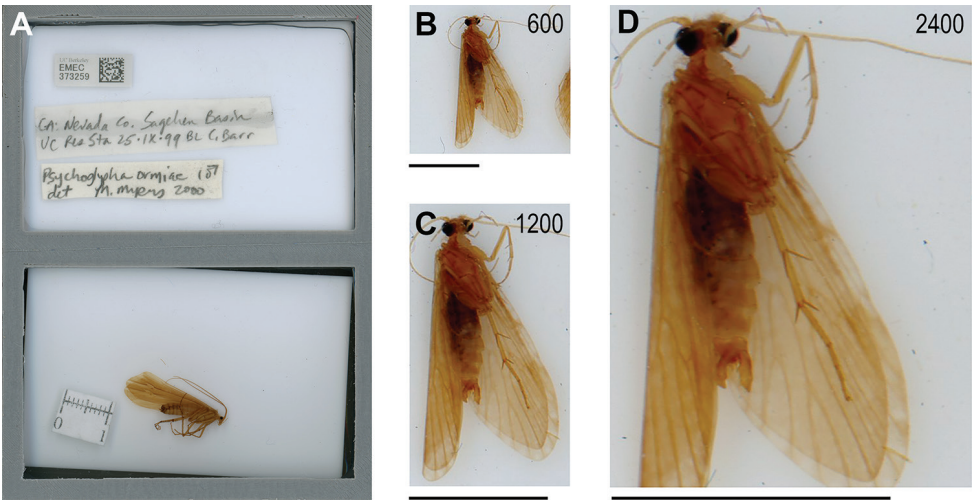

Figure 4. Cropped scan and scan resolution comparison: **A** final cropped scan of EMEC 37259, *Psychoglypha ormiae* (Ross, 1938) ♂, with standard layout of labels and specimens **B–D** comparison of scan resolution settings of 600 dpi, 1200 dpi, and 2400 dpi to show 100% scale display quality differences. Black scale bar is 5 mm for *Rhyacophila harmstoni* Ross, 1944 ♂ (EMEC 41255, NV: White Pine Co.) in all images. Images are unmodified in software (e.g., no sharpening, white balance, or color correction).

resolvable structures from other species. Although higher dpi options were available for the scanner, settings above 2400 dpi exceeded the capabilities of the workstation and file sizes became too large to process efficiently. For the final archived version, we scanned each batch at 2400 dpi in color and saved images as JPG files. In early phases of the project, we saved images as TIFF files, but file sizes were too large to store and process. For most scans, we pre-scanned to check label and specimen positioning with a preview.

Imaging technicians worked in teams of 2–3 for 3-hour scanning sessions with a set of 12 scanning boxes in two batches of 6. 1–2 technicians loaded batches of scanning boxes by working one vial at a time to load the label panel and the specimen panel. Fluid-stored material in the Essig Museum of Entomology is stored in thin, long shell vials (mostly 8 × 90 mm and 12 × 90 mm) stoppered with a firm piece of cotton and inserted cotton-side down in wide-mouth pint jars of ethanol. Each sample scanned required that a vial was selected from pint jar, the cotton was removed, and the contents of the vial emptied into the scanning box, and the vial rinsed with ethanol to make sure all small parts were moved to the scanning box. A batch was then passed to a technician who operated the scanning station.

The scanning technician moved the boxes to the scanner, arranged and covered the specimens, previewed the scans and then completed the high-resolution scans. While the scanning technician scanned the batch, the loading technicians either loaded a new batch if it was the first run, or unloaded the batch that came off the scanner, and then loaded the new batch. Unloading the scanning boxes required technicians to carefully return

the material and labels (including the new 2D DataMatrix code label) to the shell vials, completely search the scanning boxes for small parts, refill ethanol, re-stopper the vials with cotton and return them to a pint jar. As part of this process, we often curated the material by replacing ethanol, replacing chipped shell vials, and re-copying faded labels. But, we avoided replacing all ethanol in every sample to reduce the chance of losing small parts of specimens. The estimates for the handling time include these activities.

Image processing

To process the 6-box batch image into a single file for each image, we bulk-processed the 6-panel images using an R script (available from: https://github.com/pkmendez/museumscanbox) (R Core Team 2016) using package 'magick' (v. 0.4) (Ooms 2017). We loaded each image, cropped the image into 6 separate files, rotated the image to portrait, and renamed each file as a subname of the original image. The script uses the dimensions of the marquee panel to determine where to crop the image to make 6 equivalent panels. We did not perform edge detection or rotate each image by hand in software, instead relying on high-quality, well-aligned scans with accurate marquee boxes. Because of the size of each of the images, we increased the memory limit of our R workspace to 20000 MB, rotated after cropping, and removed all images from the R workspace after each loop iteration.

We later manually renamed files to the Essig Museum naming convention (e.g., EMEC41255 Rhyacophila harmstoni.jpg). To keep archive images directly comparable and avoid the need to recalibrate scale bars between photos for morphometric measurements, we did not standardize the archive image dimensions, instead leaving each at the native dimensions after cropping. We also did not make any color corrections to the images to avoid increasing processing time by having to manually interact with each cropped scan. Images were resized to be comparable in dimensions to images of the pinned material and deposited into the Essig Museum of Entomology's custom MySQL database and later transcribed in the workflow along with images of pinned material.

Results

Materials performance

Of the three materials tested, PLA performed best with no reaction to the ethanol during the 4-hour test with leaks only occurring when the slide did not form a good seal with the adhesive (Table 1). We sealed leaks with an additional application of E6000 at the slide perimeter. Polished white nylon performed acceptably, with no softening of materials or odors, yet some ethanol eventually moved up and over the sides because of the surface texture. This effect occurred more quickly in the unpolished nylon because it has a rougher surface, increasing the surface area for the liquid to cling. The nylon

Table 1. 3D materials and response to 4-hour ethanol test. PLA (white, black, and grey) and nylon (white, black, orange, both unfinished and polished versions) exposed to 75% ethanol.

Material	Material Information	Performance in EtOH test
PLA	Fused Deposition Modeling Technology. Heat-extruded, hard plastic, unpolished. Lines visible between layers.	No odors, softening, leaking, or creep of ethanol. No color change to model or ethanol.
Nylon (strong and flexible)	Inkjet-like process, requires support material when printing, unfinished or polished. Unfinished noticeably rougher (layer lines) than polished nylon.	No odors or softening. Creep of ethanol up and over side. Extreme leeching of color into ethanol in black and orange models.

boxes in orange and black leeched the dye used to stain the boxes, staining the ethanol. Because we aimed to avoid staining collection material from the mobilized stain, we only recommend nylon in white.

Scanning size and quality

Scanning time and file size increased with increasing dpi setting on the scanner (Table 2). Scan times ranged from <15 s to 3.4 m. File size for TIFF were ~25–37× larger than JPG files at the same dpi. File size at the highest resolution of 2400 dpi for JPGs was 16× larger than the 600 dpi scan. All resolutions recovered basic features such general wing venation, tibial spurs, and determining if individuals were likely males or females based on the shape of the abdomen if visible through the wings (Figure 4). As resolution increased, the detail increased on all structures and allowed for individual segments of maxillary and labial palps, antennae and tarsi to be identified, ocelli presence and location, setae and spines (e.g., head, thorax, wings, legs), sutures and individual segments of thorax and abdomen, and shape of larger structure of male genitalia to be discerned at the highest resolution (Figs. 4B–D, 5C). In general, scans at 2400 dpi were the clearest. In most cases, however, family-level diagnostic features such as setal warts on the head and thorax were not apparent, often because of positioning of the specimen. In some cases, images were informative to identify some specimens that were missing determinations in the collection.

For larvae, materials and structure of the case were identifiable (Figure 5E, I), as well as head shape, mandibles and some leg features (Figure 5B, D). Cases often obscured abdominal detail and we did not remove caddisflies from cases to keep material associated and minimize disruption for later activities for experts. For pupae, abdominal gills and hook-plates, as well as facial setal warts and other features of segments were visible (Figure 5F).

Scan quality decreased when scanner glass and exterior surfaces of slide glass were not cleaned and dried between sessions resulting in condensation on the slide surface. Yellowed ethanol also made for poor scans. When specimens were large (e.g., cased limnephilids), scans were darker than shallower scans. Dark-bodied specimens often lacked detail.

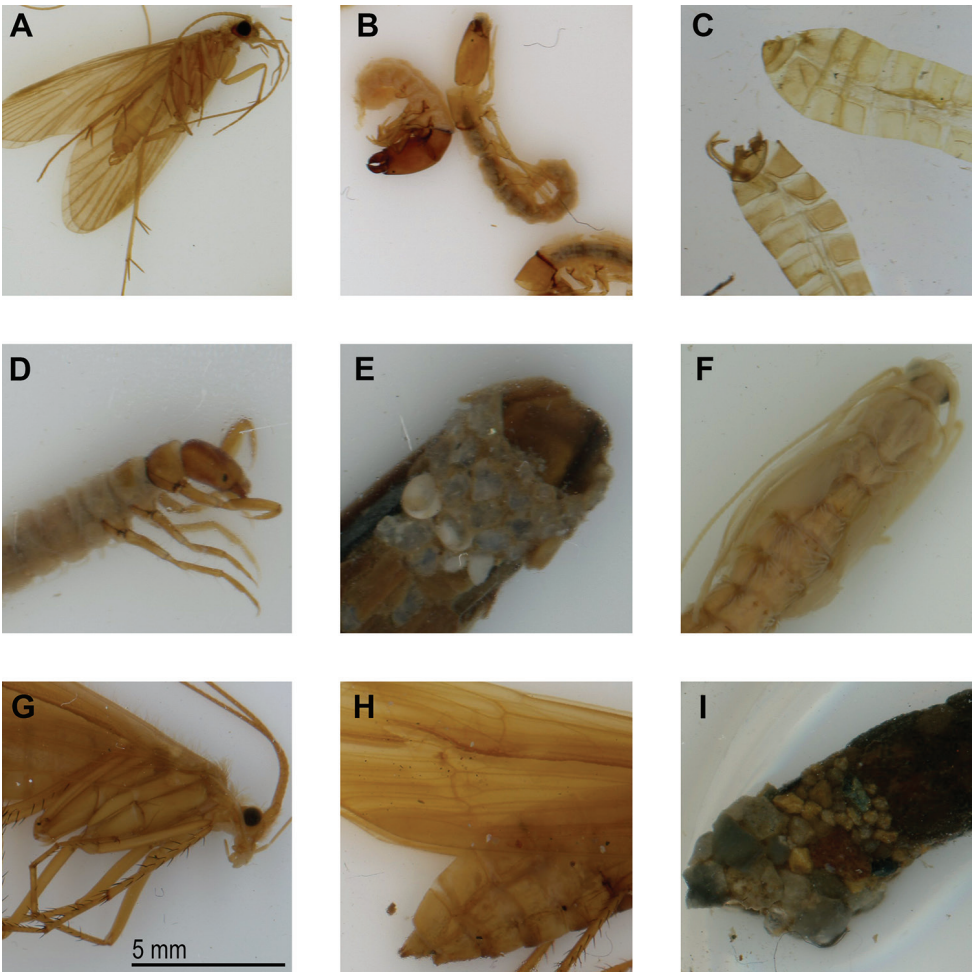

Figure 5. Example scans of different species and life stages of Essig Museum of Entomology Trichoptera showing detail of morphological features **A** *Dolophilodes novusamericana* (Ling, 1938) ♂, CA: Marin Co., EMEC 373433 **B** *Wormaldia* sp. larvae, CA: Nevada Co., EMEC 1194742 **C** *Limnephilus frijole* Ross, 1944 genitalic dissections of ♀♂, CA: Modoc Co., EMEC 373223 **D** larva and **E** case of *Yphria californica* (Banks, 1907), CA: El Dorado Co., EMEC 373355 **F** Limnephilidae pupa, no location data, EMEC 373316 **G** *Psychoglypha ormiae* ♀ (Ross, 1938), CA: Nevada Co., EMEC 373259 **H** *Psychoglypha* sp. ♀, CA: Nevada Co., EMEC 373266 and **I** *Hesperophylax designatus* (Walker, 1852) case, CA: Mono Co., EMEC 373246. All scans are unmodified in software (no sharpening, white balance, or color correction). Scale bar: 5mm.

Scanning workflow

When technicians worked in teams of two or three, they scanned 3–4 batches/hour (12–20 mins per batch) resulting in a rate of ~7 mins/vial/worker from the unloading step through rehousing the material, including routine curatorial activities. Although

Table 2. Scanning details and resolvable structures of Trichoptera at different resolutions. All dimensions are approximate for one set of 6 boxes in one scanning pass.

Scanning resolution (dpi)	Scanning time	Dimensions (pixels)	JPG file size	TIFF file size	Resolvable Structures in adults
600	< 15s	5091 × 3714	3.4 MB	83.2 MB	Tibial spurs, wing venation major veins, abdominal shape to determine sex, large male genitalic structures.
1200	1m 10s	10183 × 11428	10.2 MB	333 MB	The same structures @ 600 dpi, but greater detail on shape and count of tibial spurs, detail in wing pigment, shape detail on male genitalic structures, shape of maxillary and labial palp segments sometimes possible to discern.
2400	3m 40s	20366 × 22856	34 MB	1.29 GB	The same structures available @ 1200 dpi, but also segments of antennae, individual setae on the head and abdomen, and additional detail on male genitalic structures. Tibial spines, ocelli, and setae on wings was also discernable for some taxa.

increasing the team to three members increased the speed of loading and unloading, the scanning step was often the time limiting step in the process because the specimen had to be arranged and previewed before scanning.

Image processing

Large file sizes increased image processing times often exceeding the available memory on our scanning computer and we had to perform most image processing on a computer with higher specifications (Razer RZ09-01302E21, 2.60 GHz Intel Core i7-4720HQ, 16GB Ram, Windows 10). Processing took ~1.5 mins to cut and rotate the 6 individual scanning box images per batch resulting in individual files of 5MB each (~3.5–7.5 MB). Alignment issues occurred occasionally when the marquee was misaligned in the bulk scan as a result of technician error. These errors were sometimes correctable by realigning and hand-cropping in image editing software.

Discussion

Using 3D print technology in research workflows is an opportunity to reduce costs for customized laboratory equipment as well as provide standardized and reproducible components available anywhere that it can be printed. For imaging arthropod natural history collections, low-cost PLA and nylon performed well in a bulk scanning workflow. Images were more than adequate for museum documentation and also recorded features at a high enough resolution for a partial identification of Trichoptera in some instances. We recommend this equipment and workflow as a low-cost method to image natural history museum fluid collections.

Performance of scanning box

Valued for its wide availability on consumer-level 3D printers, PLA is a desirable material for fabrication of the museum scanning boxes because of the low cost (~$2/box on home or campus printers). When printed at 100% infill, leaks between layers never occurred. As a material advertised for its biodegradable and compostable properties, the key concern as a material for the scanning box would be degradation of the PLA over time as a result of its interaction with the 70–75% ethanol solution. Hydrolysis of PLA into lactic acid occurs when the material interacts with ethanol and water with increased breakdown occurring more at lower concentrations of ethanol (Iñiguez-Franco et al. 2016). Lactic acid is commonly used at its 85% reagent strength concentration at 130 °C when clearing male genitalia of caddisflies because it dissolves soft internal abdominal structures and loosens phallic structures critical for species identifications (Blahnik et al. 2007). During this process, the lactic acid is rinsed from the structures completely before the specimen is returned to ethanol for curation.

We hypothesize that lactic acid resulting from the breakdown of PLA during the short scanning sessions, often occurring with ethanol changes when rehousing the specimens, should minimize retention of lactic acid or at least keep at it low levels similar to rinsed specimen after the clearing process. In the scanning box application, room temperatures are much lower than the 40 °C temperature of PLA hydrolysis conducted by Iñiguez-Franco et al. (2016). We doubt that any resultant lactic acid would continue to clear specimens once they have been permanently stored. Moreover, lactic acid generally does not affect recovery of DNA from specimens that have been exposed to it (Paquin and Vink 2009). Although field studies at high summer temperatures report color changes in PLA over months of outdoor exposure (Will and Steplowski 2016), the scanning boxes for this project remained unchanged after 1.5 years of use at room temperatures in the laboratory.

Nylon (polyamide) serves as a viable alternative because of its wide availability and chemical resistance for the non-dyed models. However, we did not have access to printers that printed in nylon other than through web vendors, limiting our ability to inexpensively prototype and test, making it the more expensive of the two materials. Nylon scanning boxes remained stable after 1.5 years of use in the laboratory.

Imaging efficiency and workflow

The efficiency of imaging through a scanning approach was similar to other fluid-based approaches yet required double the handling time of pinned material. Volunteers working in teams of 2–3 processed vials at a rate of ~8 vials/worker/hour (~7 mins per vial + <1min/image of digital processing) from unloading and positioning specimen to scanning and rehousing. This rate is similar to imaging samples from ichthyology and herpetology museums, where 41% of the museums reported 6–10 mins/sample and 22% reported 11–15 mins/sample (Vollmar et al. 2010). However, fluid sample

scanning was slower compared to imaging pinned material. The latter ranging from 1.3 mins/museum object for the CalBug project (P Oboyski, pers. comm.) to 3–4 mins/pinned specimen including short data entry at the Australian Museum (Flemons and Berents 2012). This difference in handling time for fluid compared to pinned material results from the time required to remove the material from the vial, position the labels and specimens on the scanner, and then curate and rehouse the specimens. Over tens of thousands of specimens, this summed small difference in overall time required to image a collection may be on the order of years or decades, depending on the size of the collection.

Compared to whole drawer imaging approaches such as SatScan (Blagoderov et al. 2012), DScan (Schmidt et al. 2012) or GigaPan (Bertone et al. 2012), imaging the fluid-based collection is considerably slower. Yet the resolution of the information associated with each specimen is much finer-grained and can serve broader functions. All labels are spread out for each sample lot compared to the whole drawer which may have stacked labels and obscured information (Dietrich et al. 2012). Identifications often include the year identified in the handwriting of the worker—this handwriting can be diagnostic for estimating the accuracy of the determination (Flemons and Berents 2012). Unfortunately, other approaches such as multi-vial imaging on a scanner used at InvertNet (Dietrich et al. 2012) could not be applied to the Essig Museum collection because label information is often obscured: up to 40 narrow vials closed with cotton are bulk stored in lots of 20–40 in pint jars (Figure 1A).

Image quality

Scanning at 2400 dpi created high-quality scans appropriate to resolve some taxonomically-informative structures in many groups of Trichoptera. In most images, diagnostic structures such as tibial spurs, and labial and maxillary palps were clear enough to provide basic level information that is helpful for narrowing-down to the family level, with the exception of dorsal features of the head and thorax. Ocelli and dorsal setal warts were visible if the specimen was positioned on its dorsum for scanning. Some wing venation was clear enough to see major veins, patterning, and scale-like setae, but this detail is certainly not enough for wing-keys that rely on detail such as miniscule hooks and hind-wings (e.g., Ruiter 2000). Unfortunately, Trichoptera preserved in ethanol are often faded or discolored and color was unreliable for identification. Scans of darker-bodied specimen often had contrast issues that may need to be corrected in digital editing software if used for purposes beyond recordkeeping. In most cases, the wings obscured detail on the abdomen, but Trichoptera wings are generally transparent and it was often possible to estimate if the specimens were male or female based on the shape of the abdomen. For specimens with cleared genitalia, some diagnostic characters on genitalia were visible, however for the vast majority of taxa, identification can only be determined by viewing structures of cleared genitalia under a compound microscope, and no mass digitization imaging technique to date would be able to accomplish this task.

Scans have the potential to be used beyond identifications and museum record-keeping. Wing measurements derived from imaging pinned specimens with a camera lens are not reliable for morphometric analyses, especially for larger specimens where error increases if the wing is not aligned with the measurement plane or if there is distortion from the lens used to acquire the image (Hall et al. 2014, Trueman and Yeates 2015). However, caddisfly images acquired by scanning may have value for morphometric analysis of forewings because they are imaged flat and their measurements may be comparable to slide-mounted forewings. In this scanning technique, all images are at the same scale and measurements can be made on all images with a single calibration. Unfortunately, wings were sometimes curled and folded in the vials, and the overlap between wing layers may make it difficult to determine the correct wing to measure. Given the high image resolution and data quality, we expect that these research grade images should be able to be identified digitally when integrated into resources such as iNaturalist or other systems that use machine learning algorithms.

Considerations for scanning conditions based on application

Although 2400 dpi produced the highest quality scans, the final selection of the scanning settings should be determined based on the desired utility of the scan and how the image files will be stored. For natural history museums, if the scans are primarily a snapshot of the material that provides visual verbatim label information and the count and condition of loan material, a lower resolution and smaller file size may be more desirable. However, acquiring lower resolution scans may not measurably speed up the imaging process because the handling time per vial is so high. If wider utility is desired, such as for identification, teaching, or morphometrics, higher resolution scans are worthwhile. We approached this project from the perspective of wanting to determine the highest quality scans we could get though the scanning method. In our case, the size of the Essig Trichoptera Collection is relatively small (~2,500 sample lots) compared to other fluid collections. We scanned at the higher resolution for longer term research purposes, and later batch downscaled images for museum archiving and display images. These downscaled images are comparable in size and resolution with those taken for the pinned collection with much lower file storage requirements.

The scanning box applications are not limited to museum imaging and this method may serve as a tool that can be used more widely to archive aquatic ecology specimens. For example, samples taken for biological monitoring are not often stored long term, representing a lost opportunity to permanently archive life history condition (e.g., body size, life stage) of aquatic taxa which may ultimately be useful in long-term ecological studies. Images may also be able to provide easily examinable records when physical material is unavailable or as part of a workflow for QA/QC by remote reviewers or experts. Other fluid-based bulk samples such as those from malaise or pitfall traps can be imaged and sent to experts to share samples. This method is appropriate

for image-based vouchering to accompany DNA sequences such as those archived by BOLD (Milton et al. 2013).

The design size for this fluid-based application for natural history arthropod collections was based on the wide variability in label sizes for fluid-based collections. Compared to pinned collections, which usually have much smaller labels (e.g., 1.5 cm x 0.75 cm) to fit under the insect body to maximize the number of individuals that fit in a museum drawer, fluid collections have no such constraint. The size of vials used for storage in collections range from wide scintillation vials with caps, to stoppered vials, to very thin shell vials. Many labels tend to be larger because of the need to write by hand with pencil and archival pigment inks to prevent loss of label information in ethanol. The double wide museum slide best accommodated the label and specimen lots of collection material, yet a standard slide sized scanning box may be more appropriate for other collections.

The scanning boxes are a 3D printable design, and with software the design can be modified to change the dimensions of the scanning box for alternative imaging purposes. Smaller scannable areas, such as those designed around a standard microscope slide or even microscope cover slips, may be viable for digital archiving, especially for projects such as BOLD vouchering where label information is not required and the frame needs to only accommodate one specimen; the 3D-printed boxes may be single and mobile, or have a fused layout for batch imaging could match indexing of DNA samples to reduce laboratory errors. The number of images captured would be dependent on the printing size capabilities of the 3D printer and the overall scan area. Larger area scans, such as for large benthic samples or ichthyology, are also possible but there may be challenges in finding high-quality glass that is thin enough not to reduce image quality and inexpensive enough to be used in this application.

Conclusions

The value of developing a standardized method and equipment for imaging fluid-based museum material should not be underestimated. In natural history collections, freshwater aquatic species, with the exception of odonates, are some of the least documented with digital images, mainly restricted to images of pinned adult forms. Most museums have not embarked on digitizing fluid material, and this method represents a clear opportunity for a low-cost approach that can be integrated into existing workflows. The scanning box and laboratory workflow performed well with few leaks and used a simple approach for technicians. Compared to other systems, the components are inexpensive, available, and replaceable. Boxes can be printed in-house or ordered with the cost of 12 boxes (2 batches) for well under $400 USD and can be used with existing scanners and computers. Because the design is fairly simple and designed to make use of available laboratory materials, it can be made to accommodate smaller slides or customized to the imaging needs of the museum or for other research needs.

Acknowledgements

We thank Milo Fedane, Jessica Garcia-Reyes, Gregory Gladkov, Chloe Kapanen, Stella Li, Soledad Soto, Sonja Stott, and Michelle Yang for scanning and organizing material. Kipling Will and Charles Griswold encouraged pursuit of the project. We thank Vincent H. Resh for laboratory facilities, Peter Oboyski for access to the Essig Museum Trichoptera collection, Joshua Steiner for printing additional prototypes, and Marilyn Myers for her work in the Essig collection. The Sponsored Projects for Undergraduate Research (SPUR) and Undergraduate Research Apprenticeship Program (URAP) at the University of California, Berkeley provided funding for this project.

References

Autodesk (2015) Autodesk Meshmixer, Version 2.6. http://www.meshmixer.com

Baird R (2010) Leveraging the fullest potential of scientific collections through digitization. Biodiversity Informatics 7: 130–136. https://doi.org/10.17161/bi.v7i2.3987

Berry D, Selby RD, Horvath JC, Cameron RH, Porqueras D, Stouthammer R (2016) A modular system of 3D printed emergence traps for studying the biology of shot hole borers and other Scolytinae. Journal of Economic Entomology 109: 969–972. https://doi.org/10.1093/jee/tov407

Bertone MA, Blinn RL, Stanfield TM, Dew KJ, Seltmann KC, Deans AR (2012) Results and insights from the NCSU Insect Museum GigaPan project. ZooKeys 209: 115–132. https://doi.org/10.3897/zookeys.209.3083

Blagoderov V, Kitching IJ, Livermore L, Simonsen TJ, Smith VS (2012) No specimen left behind: industrial scale digitization of natural history collections. ZooKeys 209: 133–146. https://doi.org/10.3897/zookeys.209.3178

Blahnik RJ, Holzenthal RW, Prather AL (2007) The lactic acid method for clearing Trichoptera genitalia. In: Bueno-Soria J, Barba-Álvarez R, Armitage BJ (Eds) Proceedings of the 12th International Symposium on Trichoptera. The Caddis Press, Columbus, Ohio, 9–14.

CalBug: Terrestrial Arthropod Database (2017) http://calbug.berkeley.edu [accessed 19 Jun 2017].

Dietrich CH, Hart J, Raila D, Ravaioli U, Sobh N, Sobh O, Taylor C (2012) InvertNet: a new paradigm for digital access to invertebrate collections. ZooKeys 209: 165–181. https://doi.org/10.3897/zookeys.209.35711

DeWalt RE, Favret C, Webb DW (2005) Just How Imperiled Are Aquatic Insects? A Case Study of Stoneflies (Plecoptera) in Illinois. Annals of the Entomological Society of America 98: 941–950. https://doi.org/10.1603/0013-8746(2005)098[0941:JHIAAI]2.0.CO;2

Dominugue MJ, Pulsifer DP, Lakhtakia A, Berkebile J, Steiner KC, Lelito JP, Hall LP, Barker TC (2015) Detecting emerald ash borers (*Agrilus planipennis*) using branch traps baited with 3D-printed beetle decoys. Journal of Pest Science 88:267–279. https://doi.org/10.1007/s10340-014-0598-y

Flemons P, Berents P (2012) Image based Digitisation of Entomology Collections: Leveraging volunteers to increase digitization capacity. ZooKeys 209: 203–217. https://doi.org/10.3897/zookeys.209.3146

Hall MJR, MacLeod N, Wardhana AH (2014) Use of wing morphometrics to identify populations of the Old World screwworm fly, *Chrysomya bezziana* (Diptera: Calliphoridae): A preliminary study of the utility of museum specimens. Acta Tropica 138: S49–S55. https://doi.org/10.1016/j.actatropica.2014.03.023

Iñiguez-Franco F, Auras R, Burgess G, Holmes D, Fang X, Rubino M, Soto-Valdez H (2016) Concurrent solvent induced crystallization and hydrolytic degradation of PLA by water-ethanol solutions. Polymer 99: 315–323. https://doi.org/10.1016/j.polymer.2016.07.0188

Johnson L, Mantle BL, Gardner JL, Backwell PRY (2013) Morphometric measurements of dragonfly wings: The accuracy of pinned, scanned and detached measurement methods. ZooKeys 276: 77–84. https://doi.org/10.3897/zookeys.276.4207

Milton M, Pierossi P, Ratnasingham S (2013) BOLD SYSTEMS: Barcode of Life Data Systems Handbook, v. 3.6. BOLD Systems, Biodiversity Institute of Ontario, Guelph, 34 pp. http://www.boldsystems.org/libhtml_v3/static/BOLD_Handbook_Oct2013.pdf

Ooms J (2017) magick: Advanced Image-Processing in R. R package version 0.4. https://CRAN.R-project.org/package=magick

Paquin P, Vink CJ (2009) Testing compatibility between molecular and morphological techniques for arthropod systematics: A minimally destructive DNA extraction method that preserves morphological integrity, and the effect of lactic acid on DNA quality. Journal of Insect Conservation 13: 453–457. https://doi.org/10.1007/s10841-008-9183-0

R Core Team (2016) R: A language and environment for statistical computing. R Foundation for Statistical Computing, Vienna. https://www.R-project.org

Ruiter DE (2000) Generic key to the adult ocellate Limnephiloidea of the Western Hemisphere (Insecta: Trichoptera). Ohio Biological Survey, Columbus, Ohio, 22 pp.

Schmidt S, Balke M, Lafogler S (2012) DScan – a high-performance digital scanning system for entomological collections. ZooKeys 209: 183–191. https://doi.org/10.3897/zookeys.209.3115

Shah DN, Domisch S, Pauls SU, Haase P, Jähnig SC (2014) Current and future latitudinal gradients in stream macroinvertebrate richness across North America. Freshwater Science 33: 1136–1147. https://doi.org/10.1086/678492

Trueman JWH, Yeates DK (2015) Can whole-drawer images measure up? A reply to Johnson et al. (2013). ZooKeys 500: 141–149. https://doi.org/10.3897/zookeys.500.9139

Vollmar A, Macklin JA, Ford LS (2010) Natural history specimen digitization: Challenges and concerns. Biodiversity Informatics 7: 93–112. https://doi.org/10.17161/bi.v7i2.3992

Will K, Steplowski I (2016) A 3D printed malaise trap head. The Pan-Pacific Entomologist 92: 86–91. https://doi.org/10.3956/2016-92.2.86

ZooKeys 795: 67–76 (2018)
doi: 10.3897/zookeys.795.26870
http://zookeys.pensoft.net

RESEARCH ARTICLE

A peer-reviewed open-access journal
ZooKeys
Launched to accelerate biodiversity research

Chroma+, a new automontage method of image background selection for Insects and other structurally complex objects

Pavel Jakubec[1], Martin Novák[1], Jarin Qubaiová[1]

1 *Faculty of Environmental Sciences, Czech University of Life Sciences Prague, Kamýcká 129, Praha – Suchdol, 165 00, Czech Republic*

Corresponding author: *Pavel Jakubec* (jakubecp@fzp.czu.cz)

Academic editor: *Pavel Stoev* | Received 22 May 2018 | Accepted 10 September 2018 | Published 5 November 2018

http://zoobank.org/24E615AA-CFD2-4691-9DB1-C5BBA388C756

Citation: Jakubec P, Novák M, Qubaiová J (2018) Chroma+, a new automontage method of image background selection for Insects and other structurally complex objects. ZooKeys 795: 67–76. https://doi.org/10.3897/zookeys.795.26870

Abstract

Obtaining taxonomic-grade images is a vital part of probably every present-day morphological study of insects, even though the task itself is perceived as a "necessary evil" due to high investment of both time and effort to produce representable images. Cleaning the background and making it appear as a solid color of known properties is probably one of the most time-demanding tasks. Several techniques have been developed to reduce the time requirement; the most convenient and cost-effective one presumably being the chroma isolation. This method uses a green background that can be isolated and conveniently replaced with another picture or solid color, as used in the film industry. However, the main drawback of this technique is spilling of color onto the object, which is unavoidable and can be corrected only by sacrificing the true color of the object to some extent. Our improved Chroma+ method is based on classical chroma isolation workflow and helps to overcome this problem by taking an additional image of the object with a neutral color background and applying a selection obtained from the chroma-isolated picture on it. This technique is, in terms of the resulting image quality, superior to classical chroma isolation, while the time difference between these two methods is negligible. Furthermore, it does not require any additional equipment (hardware or software), thus being accessible to both employed taxonomists, low budget laboratories, and enthusiasts.

Keywords

Automontage, entomology, methodology, photography, retouching, species digitalization

Copyright *Pavel Jakubec et al.* This is an open access article distributed under the terms of the Creative Commons Attribution License (CC BY 4.0), which permits unrestricted use, distribution, and reproduction in any medium, provided the original author and source are credited.

Introduction

A picture is worth a thousand words. This is very true in the field of comparative biology, a scientific discipline, which supports many others like community ecology, conservation biology, pest management, biosecurity, and biological control (Balke et al. 2013). All who work in these fields need to accurately identify species of interest and an image is the simplest and the most effective tool of how to pass the information, necessary for the task, on.

Techniques of photography have been evolving rapidly in the recent past and specifically macrophotography has seen an accelerated development in the last few decades. The rise of digital cameras opened many possibilities for creating perfect pictures and easily sharing them with others. These possibilities are still expanding beyond new horizons thanks to discoveries of new tools and work-flows. A perfect example of this phenomenon is the focus-stacking technique that enables widening of the available focus depth of the camera. This is achieved by merging several pictures with different focus distances together into one final sharp image, thus bypassing focus depth restrictions posed by the laws of optics (Thomson 2010). Due to these restrictions, it used to be impossible to create sharp images of very small objects (like insect specimens) in their entirety. However in the recent years, it has become a gold standard of good morphological descriptions to provide fully sharp image of the specimens that are discussed (Arino and Galicia 2005, Theodor and Furr 2009).

Once the perfect image is captured there is often an issue with the background. Many people prefer solid, well-defined colors (black, white, gray or another color according to their taste), which do not draw the attention of the viewer away from the photographed object and make placement of such images next to another easy; with backgrounds of the neighboring images blending together smoothly. This is, nevertheless, difficult to achieve directly with a camera. Overcoming these obstacles is often easier when using photo-retouching methods, where the image of the specimen is traced and the background is deleted or hidden by masking. That way, it can be replaced with an exactly defined RGB or CMYK color. Thanks to this technique, composing several images into one final figure is thus easy and straight forward.

Unfortunately, there is a price to pay. Common techniques used for background isolation are time-consuming and often largely rely on the user's skill as one has to trace the whole contour of the specimen and erase the original background. This problem can be solved by using chroma isolation technique. The method uses a background that can be isolated (usually green or other color that is not occurring on the photographed object) and digitally replaced with another picture or solid color. Although chroma isolation can help in overcoming all of these issues, it often leaves colored halos around and on the object (Arino and Galicia 2005). These halos or color spills are practically impossible to remove from the image without affecting the original colors and therefore this method is not widely used in entomology.

However, chroma isolation, despite its obvious flaws, is a promising technique, being time efficient and fairly easy to use. In this paper we propose an improved chroma isolation method "Chroma+", which deals with the main issue, the color spill, and further improves reliability of the specimen selection against its background.

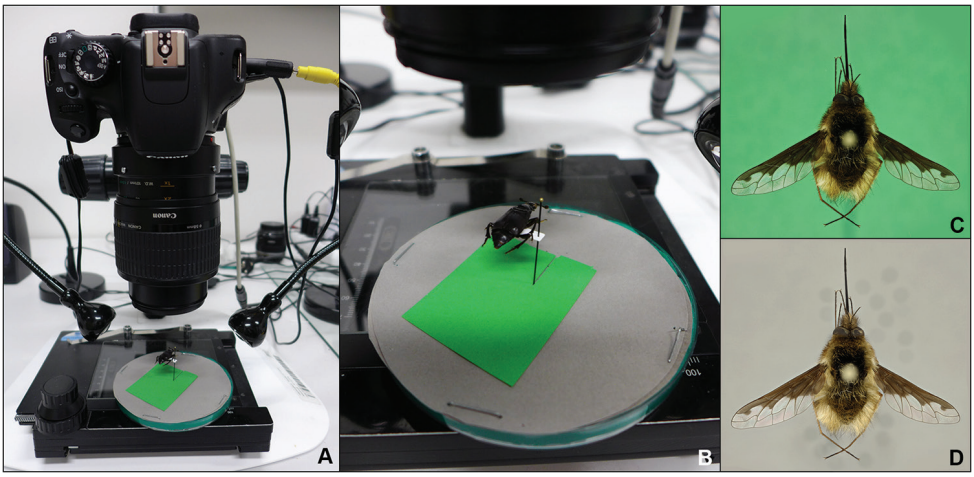

Figure 1. Chroma+ working space setup. **A** Overall setup of camera, light sources, and mounting plate for photographing the object **B** detail of mounting plate; green sheet can be removed by a simple pull (as it is cut near the pin) **C** resulting chroma-background image **D** resulting desired-background image.

Methodology

The specimens used were obtained from the personal collection of the first author and from the collection provided by Jan Růžička (Prague). They were relaxed, unmounted, repositioned, and cleaned in an ultrasonic bath when needed, following standard protocols (Harrison 2012).

To obtain the pictures of our test specimens, we used a slightly modified Canon Cognisys setup (Canon EOS 550D with Canon MP-E 65 mm 1:2.8 1–5× Macro Photo Lens mounted on an automated macro rail for focus stacking (Cognisys StackShot)), which represents a standard setup in the field of macrophotography of insects (Brecko et al. 2014). For shooting image sequences of our specimens for consequent stacking, we used the Auto-distance mode, and the distance between steps (μm) was determined by magnification and F-stop used according to the depth-of-field table for Canon MP-E 65 mm 1:2.8 1–5× Macro Photo Lens, thus ensuring optimal number of images per stack.

The specimens were mounted on a pin and the setup allowed us to change the color of the background by simply placing colored paper in the space between the specimen and the polyurethane foam sheet (see Figure 1A–B). We made two image stacks for each specimen. The first one with a chroma background (Figure 1C) and the second one with a gray background (Figure 1D).

For focus-stacking the final images we used Zerene Stacker 1.04 software, as recommended by (Brecko et al. 2014) using PMax algorithm.

For isolation of the background we used GIMP 2.8.16 software (GIMP) and Photoshop CS5 (12.0) (PS) (versions for Windows). GIMP is a freeware and therefore a good choice for low budget laboratories and citizen scientists. It can also operate on wide variety of platforms like UNIX, MS Windows, Mac OS X. Photoshop is a pur-

chased software, but provides more editing features with a larger level of sensitivity and sophistication of its tools.

We compared manual and semi-automated approaches using *Eraser* (PS) and *Background eraser* (PS) tools with automated methods *Color range* selection (PS) and *Refine edge* (PS) in classic chroma isolation and ultimately in our improved Chroma+ technique that can be deployed in both Photoshop and GIMP.

Retouching workflow used in time efficiency testing

a) Eraser

1. Select Eraser tool and manually erase the background pixels or pixel groups. Accuracy is improved by making the tool smaller and by lowering the hardness (creating gradient between center of the tool and its edge).
2. Create new layer filled with desired color to serve as the new background.

b) Background eraser

1. Select Background Eraser tool (BE), set optimal value of the strength (lower values for backgrounds of similar color to the specimen, higher values for more differing backgrounds) and size of the tool.
2. Using this tool, erase the background around the circumference of the specimen. Several rounds of deleting with Background Eraser in different values may be needed. In cases where similar color of background and specimen require low values of BE, the background is often not deleted completely. Another round of BE with higher set value is thus required to get rid of the remnants of the background without simultaneously deleting parts of the specimen.
3. Delete the rest of the background with the simple Eraser tool, since it does not directly touch the specimen.
4. Create new layer filled with desired color to serve as a new background.

c) Chroma isolation

1. Load picture with chroma background (File -> Open...).
2. Define a chroma background using the Select Color Range (Select -> Color Range) in Photoshop or Select By Color tool (Select -> By Color) in GIMP. The selection is made by selecting specific shades of background and can be increased or subtracted in Photoshop by changing the level of Fuzziness within Select Color Range window as well as in GIMP by Shift + click or Ctrl + click. Selection is made instantly, so observe if the fit is improving or not and adjust accordingly.
3. (optional) Selection can be further improved by using other tools that allow edge feathering of the selection (Select -> Feather...) or shift it (Select -> Shrink... / Select -> Growth...).

4. The last step is using the created selection on the chroma image background. An option that allows good amount of flexibility is to use the selection for creation of the mask (in Photoshop, select the layer, and click New Layer Mask button in the Layers panel; in GIMP select the layer -> right click -> Add Layer Mask... -> Initialize Layer Mask to: Selection (check the box Invert mask) -> Add). Now the part of the image where the background should be is translucent and only the specimen with all its features should be visible.

d1) Chroma+ (Photoshop)

1. Load both pictures with chroma background and neutral background as layers of the same project and align them (Edit -> Auto-Align layers) using default settings.
2. Define a chroma background using steps 2 (optionally step 3) described in c) Chroma isolation method.
3. Once the chroma background is selected and the edge touching the specimen smoothed to a desirable level, remove it from the neutral background image by either directly deleting it or using a mask (step 4 in c) Chroma isolation method).

d2) Chroma+ (GIMP)

1. Load both pictures with chroma background and the neutral background (NB) (File -> Open as Layers...) and align them with Image Registration plug-in (Tools -> Image Registration...).
2. Define a chroma background using steps 2 (optionally step 3) described in c) Chroma isolation method.
3. Once the chroma background is selected and the edge touching the specimen smoothed to a desirable level, remove it from the neutral background image by either directly deleting it or using a mask (step 4 in c) Chroma isolation method).

Results

Manual and semi-automated selection

The manual and semi-automated approach for creating a selection of the object of interest is a straight forward method. The retoucher has to trace the whole contour of the object and delete everything that is not a part of it. Usually, the *Pen* tool or *Eraser* tool are used, but Photoshop also offers more sophisticated tools like the *Background eraser*, where the user selects the threshold and the tool itself determines what the object is and what the background is. This is what we consider a semi-automated approach.

The *Eraser* tool was used to create Figure 2A–B and the image is a result of 45 minutes of work. In comparison, the semi-automated approach using the *Background*

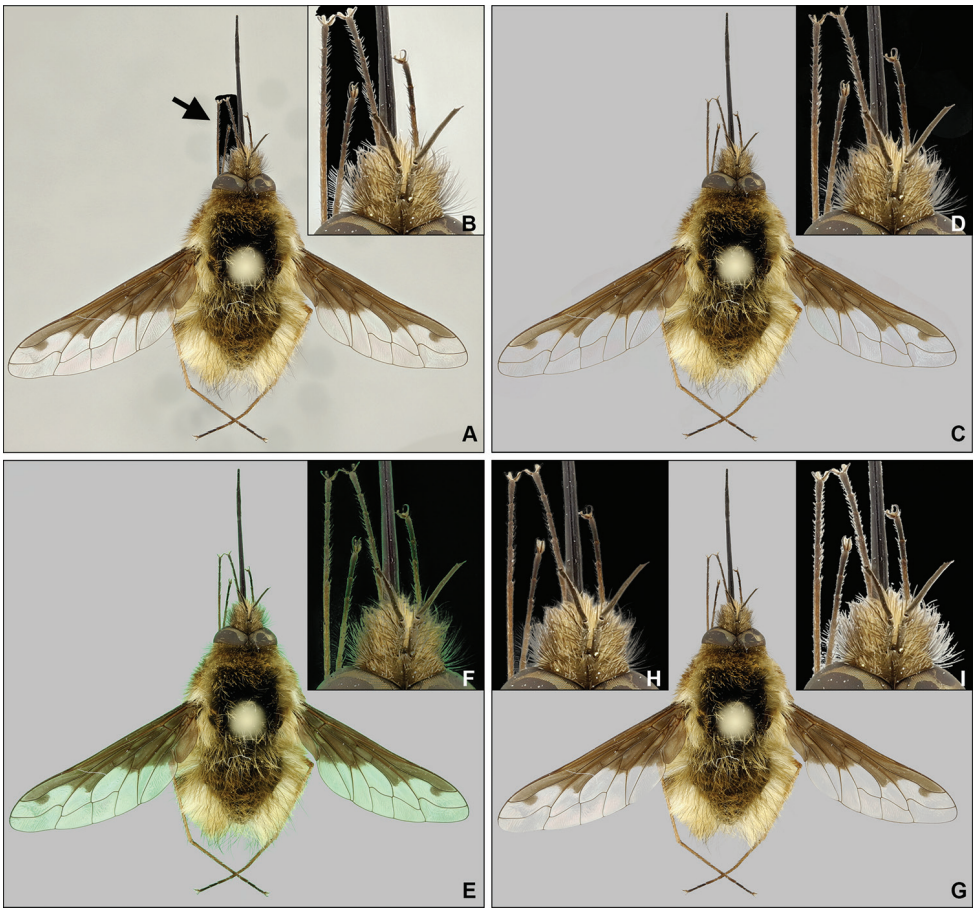

Figure 2. Comparison among methods of background selection. **A** Manual Eraser method; resulting image, arrow showing the amount of background removed after 45 min. **B** Manual Eraser method; magnified detail of removed background. **C** Background Eraser method; resulting image. **D** Background Eraser method; magnified detail showing imperfections in cropping and artefacts in the background. **E** Chroma method; resulting image, object with green halo. **F** Chroma method; magnified detail. **G** Chroma+ method, resulting image (Photoshop). **H** Chroma+ method; magnified detail after using Photoshop. **I** Chroma+ method; magnified detail after using GIMP.

eraser tool resulted in a completely uniform background around the whole object (Figure 2C–D) in the same amount of time.

From a qualitative perspective, it is worth mentioning that the *Background eraser* tool is unable to perform as a stand-alone tool and some parts of the background had to be removed by the basic *Eraser* tool as the semi-automated tool is unable to distinguish the background from the object when they are of similar color or brightness.

We did not use the *Pen* tool despite the fact that it is a much praised tool by professional retouchers. Due to the complex shape of our object, the time spent would be similar to the manual *Eraser* approach, meaning tedious work with doubtful results.

Automated selection

Chroma isolation. The time required for making a selection and refining it consists of only several minutes. However, a background that is not fully out of focus is unsuitable for this method as it is necessary to deal with scratches and dust spots on its surface. If the specimen is pinned, being at a sufficient distance from its background, the selection can be done in less than a minute.

The quality of the results is strongly limited by the properties of the specimen itself. If the object is covered with fine hairs along the edges or has translucent parts like wings, the color of the background will spill over or under these structures (Figures 2E–F and 3C) and removing it without affecting the original coloration of the specimen will become impossible. Even objects with round edges are prone to color spill as can be seen on Figure 2E.

We found two main advantages of this method, the first one being indisputably its speed, while the second is the surprising simplicity of the whole selection process. However, the above mentioned quality issues make this method practically useless for production of high quality images for publications.

Chroma+. Both speed and efficiency of the chroma isolation method are clearly superior in comparison to all other methods, but the quality issues are limiting it in its usefulness for descriptive morphology. The Chroma+ technique is based on the fact that we are working with stationary objects and the background can be changed between the shots. Therefore, we can create two pictures; one with a chroma background (green, blue, red, etc.) and the second with a background similar to the one that we would like to have in our final image (usually white, black, or gray). The object in these two images should be perfectly aligned (this can be fixed to some extent by using software automated alignment tools), thus when opened in the graphical software as layers, the chroma background image can be used to create the selection in the same way as in chroma isolation method. This selection is then used on the second image with the desired background color. In that way we can obtain the selection around the object without any color alternation caused by the spill from the chroma background.

From a qualitative perspective this approach enables dealing with complex edges and is comparable to the manual and semi-automated methods (Figure 2G–I). Timewise, this approach is slower than chroma isolation, because you have to make a second image. However, when we compare the Chroma+ with methods that are producing images of similar quality, it easily surpasses them without much difficulty. The various differences between these methods can be observed in Table 1.

Table 1. Comparison of various approaches for isolating an object from its background performed by the same person on the same specimen of Bee fly (Bombyliidae) (N = 1). See Figure 2 for results.

Traits	Manual	Semi-automated	Chroma isolation	Chroma+ (PS)	Chroma+ (GIMP)
Photo acquisition time (in minutes)	10	10	10	15	15
Creating the selection (in minutes)	45+ *	45	1	1	5
Total time	55+	55	11	16	20

* see Figure 2A–B for actual extent of selection accomplished within 45 mins.

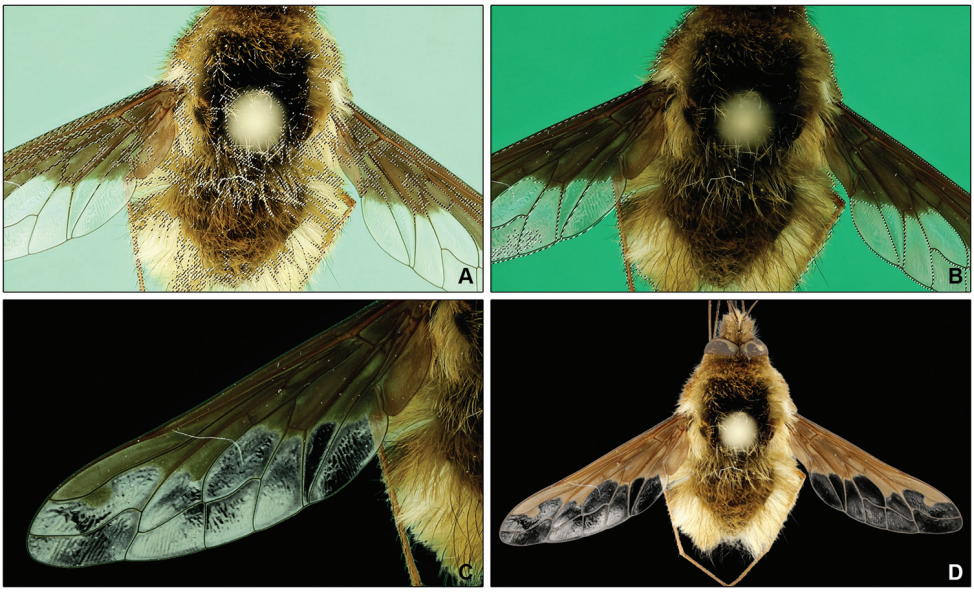

Figure 3. Limitations and troubleshooting. **A** Excessive color selection caused by a low-contrast chroma image **B** correct color selection due to a high-contrast chroma image **C** disadvantage of simple chroma method; green halo over object and color spill in translucent areas **D** unnatural halo around the object, caused by significant difference between photographed and assigned backgrounds.

Discussion

Chroma isolation represents one of the automated selection methods where the human element is supervising the final result, assisting the computer program only by choosing the appropriate shades of the background that should be selected. Both Photoshop and GIMP offer tools (e.g., Color Range tool (PS) and Select by Color tool (GIMP)) that allow isolation of the background based on a specified color range.

The Chroma+ technique inherited one crucial trait of its predecessor and that is its simplicity. Here, the user's input in creating the selection is minimal, thus facilitating more consistent results among the users. This distinguishes it from manual and semi-automated methods where the quality of the results is highly dependent on the user's experiences and skills.

Chroma isolation is often called "green screen", but green is not the only color that can be used. We highly recommend using colors that are not present on any part of the object. Therefore, a green object can be photographed against blue or red backgrounds.

Possible limitations and troubleshooting of Chroma+

One of the possible issues with the two-picture approach of Chroma+ is the position shift that occurs due to the physical interaction with the specimen or camera. The shift

causes a misalignment between the two pictures and the mask created over the chroma image will not fit on the second image with the desired background. This issue can be greatly mitigated by avoiding physical contact with both the specimen and the camera. When this is not possible, alignment of the two images using graphical software is an option. However, such a solution is suitable only for a horizontal shift in position and the tool is incapable of correcting the angular shift.

Isolation of the object is rarely perfect and we are striving to a selection that is as close as possible to the object itself without cropping it. Ultimately, there is always a small halo (often in range of a few pixels) around the object. When the object is photographed on a white background this halo can be observed when we replace the background of the image with a dark color such as black or dark gray (Figure 3D). Although, it may be seen as a flaw of the selection function, it is an inevitable result of the background color spill over the object. Cropping it would be a mistake resulting in alternation of the specimen shape and possible loss of some features such as fine hairs. To prevent this issue, we suggest using at least a similar color of the background as the one you desire in the final image. This will allow you to blend in the halo and the background in an inconspicuous way.

The color selection of the chroma background appears to be more accurate on slightly underexposed images as the contrast between the object and the background increases. This is often used in the classical chroma isolation technique, but the limited dynamic range of the camera sensor dictates how much underexposure can be achieved in one image without compromising quality of the result (underexposed image of the specimen is unacceptable). The Chroma+ allows you to underexpose the first image as much as necessary, since it is only used in creating the selection and will not show up in the final image. This allows full freedom to create enough contrast between the object and the chroma background (Figure 3A–B). We achieved the best results with contrast levels making the object appear almost like a silhouette.

The selection can be adjusted with other tools available in the used software. You can add or subtract some areas where the selection algorithm did not work properly. There are often translucent parts (e.g. wings, elytra, etc.) where the color selection tool has difficulty differentiating them from the shades of the chroma background. A wide range of tools is available in each program such as the *Quick selection* tool (PS), *Free selection* tool (GIMP) or *Background eraser* tool (PS). After the selection is made, you are additionally allowed to adjust the hardness of the transition between the object and background. We prefer a slightly softer look of the edges as they seem to blend with the background more naturally. This look can be achieved by using the *Refine edge* tool (PS) or applying the feather function (GIMP) on your final selection (feathering 3 pixels is usually more than sufficient).

In conclusion, the Chroma+ method can be performed with basic macrophotography equipment, using freeware such as GIMP. This makes our method a viable option for both employed taxonomists in low budget laboratories and insect photography enthusiasts.

Acknowledgments

We would like to thank Jan Růžička for providing specimens for photography and Christopher A. Harding for language corrections. The project was supported by the Ministry of the Interior of the Czech Republic (grant no. VI20152018027) and Internal Grant Agency of the Faculty of Environmental Sciences, CULS Prague (4211013123141).

References

Arino AH, Galicia D (2005) Taxonomic-grade images. In: Häuser CL, Steiner A, Holstein J, Scoble MJ (Eds) Digital imaging of biological type specimens. A manual of best practice. Results from a study of the European Network for Biodiversity Information, Stuttgart, 87–124.

Balke M, Schmidt S, Hausmann A, Toussaint EF, Bergsten J, Buffington M, Häuser CL, Kroupa A, Hagedorn G, Riedel A, Polaszek A, Ubaidillah R, Krogmann L, Zwick A, Fikáček M, Hájek J, Michat MC, Dietrich C, La Salle J, Mantle B, Ng PK, Hobern D (2013) Biodiversity into your hands - A call for a virtual global natural history "metacollection". Frontiers in Zoology 10: 55. https://doi.org/10.1186/1742-9994-10-55

Brecko J, Mathys A, Dekoninck W, Leponce M, VandenSpiegel D, Semal P (2014) Focus stacking: Comparing commercial top-end set-ups with a semi-automatic low budget approach. A possible solution for mass digitization of type specimens. ZooKeys 464: 1–23. https://doi.org/10.3897/zookeys.464.8615

Harrison JG (2012) Cleaning and preparing adult beetles (Coleoptera) for light and scanning electron microscopy. African Entomology 20: 395–401. https://doi.org/10.4001/003.020.0209

Theodor JM, Furr RS (2009) High Dynamic Range imaging as applied to paleontological specimen photography. Palaeontologia Electronica 12: 1–30.

Thomson GH (2010) Digital camera performance where spatial resolution is determined by the optical component. Photogrammetric Record 25: 42–46. https://doi.org/10.1111/j.1477-9730.2009.00566.x

ZooKeys 795: 77–81 (2018)
doi: 10.3897/zookeys.795.28218
http://zookeys.pensoft.net

SHORT COMMUNICATION

A peer-reviewed open-access journal
ZooKeys
Launched to accelerate biodiversity research

A broadly distributed species instead of an insular endemic? A new find of the poorly known Hainan gymnure (Mammalia, Lipotyphla)

Alexei V. Abramov[1,2], Anna A. Bannikova[3], Vladimir S. Lebedev[4], Viatcheslav V. Rozhnov[2,5]

1 *Zoological Institute, Russian Academy of Sciences, Universitetskaya nab. 1, Saint Petersburg 199034, Russia* **2** *Joint Vietnamese-Russian Tropical Research and Technological Centre, Nguyen Van Huyen, Nghia Do, Cau Giay, Hanoi, Vietnam* **3** *Lomonosov Moscow State University, Vorobievy Gory, Moscow 119992, Russia* **4** *Zoological Museum of Lomonosov Moscow State University, B. Nikitskaya 6, Moscow 125009, Russia* **5** *A.N. Severtsov Institute of Ecology and Evolution, Russian Academy of Sciences, Leninskii pr. 33, Moscow 119071, Russia*

Corresponding author: *Alexei V. Abramov* (alexei.abramov@zin.ru)

Academic editor: *E. Eizirik* | Received 6 July 2018 | Accepted 1 August 2018 | Published 5 November 2018

http://zoobank.org/8A875979-C83A-46FB-B49D-6580E9674B5D

Citation: Abramov AV, Bannikova AA, Lebedev VS, Rozhnov VV (2018) A broadly distributed species instead of an insular endemic? A new find of the poorly known Hainan gymnure (Mammalia, Lipotyphla). ZooKeys 795: 77–81. https://doi.org/10.3897/zookeys.795.28218

Abstract

The Hainan gymnure *Neohylomys hainanensis* (Mammalia, Lipotyphla), endemic to Hainan Island (China), is one of the rarest and least-known species within the family Galericidae. The IUCN Red List inferred it as an endangered species due to ongoing population decline caused by natural habitat loss. A recent biodiversity survey has revealed *N. hainanensis* to be rather common in northern Vietnam. This is the first record of the species outside Hainan Island. New data have allowed us to re-assess the conservation status of this poorly known mammal. The occurrence of *N. hainanensis* in mainland Vietnam also supports the hypothesis that Hainan Island could have been previously connected to Guangxi and northern Vietnam rather than to neighbouring Guangdong.

Keywords

Distribution, *Neohylomys hainanensis*, new findings, Vietnam

Copyright *Alexei V. Abramov et al.* This is an open access article distributed under the terms of the Creative Commons Attribution License (CC BY 4.0), which permits unrestricted use, distribution, and reproduction in any medium, provided the original author and source are credited.

Introduction

The family Galericidae (Mammalia, Lipotyphla) comprises six recent genera and 8–10 species of gymnures and moonrats inhabiting tropical and subtropical forests of southern China and SE Asia, including the Philippines and the Sunda Islands (Hutterer 2005, Bannikova et al. 2014). The majority of its species are listed as endemics, having very small distributional ranges restricted to some islands (*Podogymnura truei*, *P. aureospinula*, *Neohylomys hainanensis*) or small mountainous areas (*Hylomys parvus*, *Otohylomys megalotis*).

The Hainan gymnure *Neohylomys hainanensis* Shaw & Wong, 1959 is usually regarded as one of the rarest and least-known species of all the Galericidae (Stone 1995, Johnston and Smith 2016). This species remains known from a few museum specimens only (Stone 1995). The recent IUCN Red List recognized the Hainan gymnure as an endangered species, because it is known from the island of Hainan only, and its range is less than 5,000 km² (Johnston and Smith 2016). According to published data (Corbet 1988, Hoffmann and Lunde 2008), this species occurs in tropical rainforests and subtropical evergreen forests. During the last decades, the forests of Hainan Island have been under considerable anthropogenic pressure due to logging and agricultural use. It is agreed that the population of *N. hainanensis* is in decline due to habitat loss (Johnston and Smith 2016).

Materials and methods

During the 2018 small mammal surveys conducted by the Joint Vietnamese-Russian Tropical Research and Technological Centre in northern Vietnam, five specimens of small gymnures were collected in Cao Bang Province, approximately 22°37'41"N, 105°54'41"E, at elevation 300–700 m a.s.l. (Figure 1). All specimens were obtained from local villagers during studies of rodent distribution and pest control. Voucher specimens (coll. numbers AVA 18-134, AVA 18-125, AVA 18-136, AVA 18-137, AVA 18-138) are kept in the Zoological Institute of the Russian Academy of Sciences (Saint Petersburg, Russia).

Results and discussion

A morphological analysis of Vietnamese specimens has revealed their identity as *N. hainanensis*. These are small-sized, vole-like gymnures with a heavily built body and slightly stout, pointed rostrum. Head and body length 120–142 mm, tail length 30–40 mm. Tail is approximately 26.3% of head and body length, whereas it is 70–80% in *Otohylomys*, ca. 50% in *Neotetracus* and 10–15% in *Hylomys*. *Neohylomys hainanensis* from Hainan has its head and body length 120–147 mm, tail length 36–43 mm; relative tail length is 28.9% (Shaw and Wong 1959, Hoffmann and Lunde 2008). Dorsum dull olive-brown; ventral pelage yellowish, lighter than dorsal; there is a longitudinal black line on

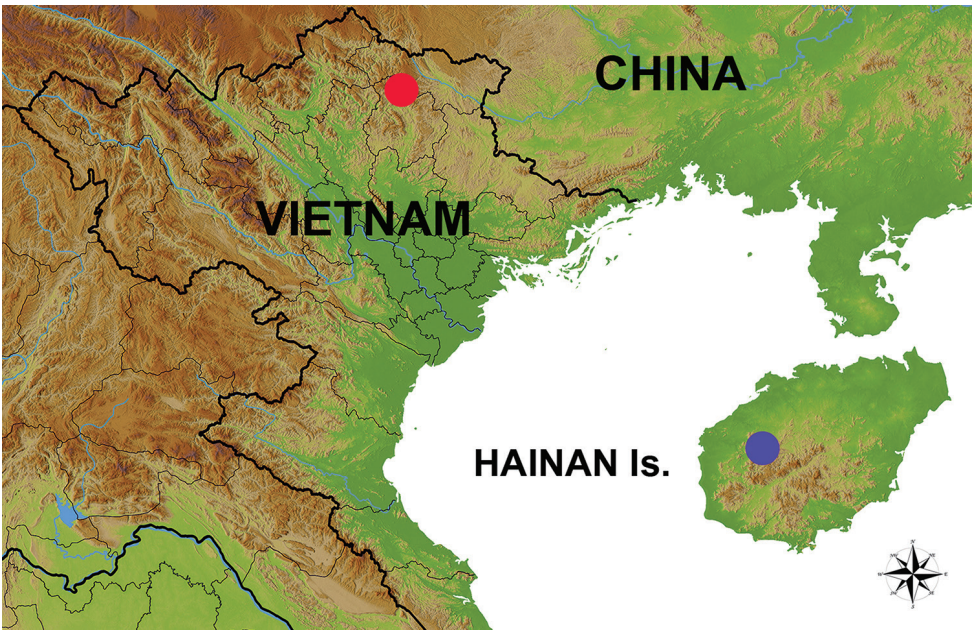

Figure 1. Distribution map of *Neohylomys hainanensis*. Previously known records from Hainan Island are marked with blue, new findings in Vietnam are marked with red.

anterior midback (Figure 2A). Tail bicoloured, dark above and much lighter below. Dental formula: 3.1.4.3/3.1.3.3 = 42. There are four upper and three lower premolars (Figure 2B). First upper incisor is very large. Upper canine teeth only slightly larger than adjacent incisors and premolars. The dentition of Vietnamese specimens in full concordance with that of *N. hainanensis* (Shaw and Wong 1959, Engesser and Jiang 2011).

All the Vietnamese specimens were collected from evergreen mixed forest at the elevations of 300–700 m a.s.l. It was not recorded at higher elevations (1500–1800 m a.s.l. in Phia Oac – Phia Den National Park). According to the information from local villagers, this species is rather common, both in slightly disturbed forests and in primary forests.

In Hainan, the species is recorded from the Jianfengling Nature Reserve and may also occur in the Jiaxi and Wuzhishan nature reserves (Johnston and Smith 2016). The small distributional area and population decline make the species quite vulnerable. In Vietnam, the species has been recorded in and around the Phia Oac – Phia Den National Park in Cao Bang Province (Figure 1). Additional research is needed to estimate the distribution, population and habitat status, and threats to *N. hainanensis* in Vietnam. Little is known about the biology and ecology of this species (Stone 1995). New distribution findings have allowed us to gain additional data on the species' natural history.

Hainan Island is widely recognized as one of the world's biodiversity hotspots (Myers et al. 2000). The geological history of Hainan Island, as well as the Indo-Malaysian or East Asian affinity of its biota, is still poorly understood. Some authors suppose it was previously connected to mainland China (Guangdong), whereas others

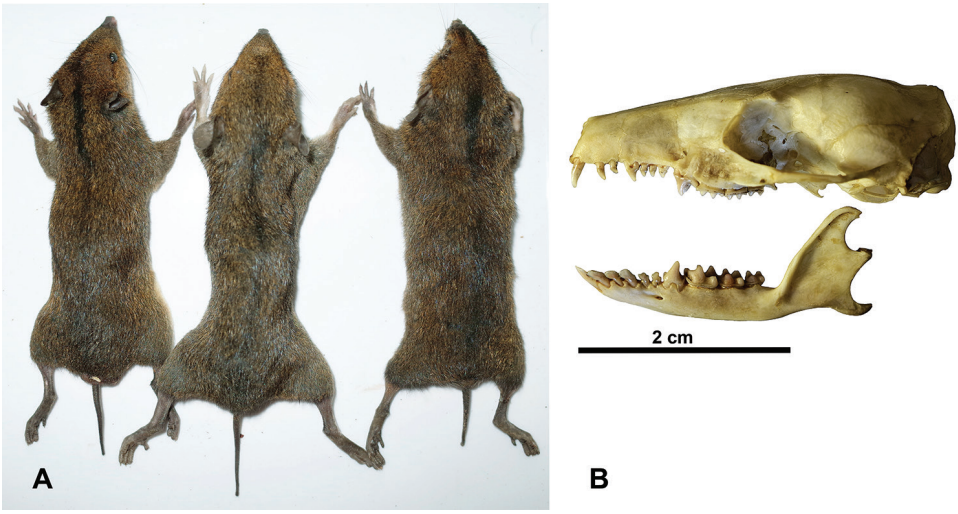

Figure 2. *Neohylomys hainanensis* from Vietnam. **A** total view **B** skull.

argue that Hainan Island was originally located near Guangxi and northern Vietnam during the early Cenozoic (see Zhu 2016). Vertebrate animal studies have revealed the island to have a higher species diversity and endemism in comparison to adjacent mainland China, which could be related to the geological origin of Hainan (Chen and Bi 2007, Chen 2008, 2009). A comprehensive analysis of seed plant distribution (Zhu 2016) showed that the Hainan flora indeed has a tropical Asian affinity and very low endemism at generic and species levels, which seems to imply its continental origin. Moreover, the Hainan flora shows strong similarities to that of Vietnam and Guangxi, but less so to the adjacent Guangdong Province (Zhu 2016). Our discovery of the Hainan gymnure also supports the idea that Hainan Island could have been connected to northern Vietnam.

Acknowledgements

Fieldwork was supported by the Joint Vietnamese-Russian Tropical Research and Technological Centre. We thank AN Kuznetsov, Nguyen Dang Hoi, and Le Xuan Son, who made considerable efforts in preparing for the field works. We are grateful to the administration of the Phia Oac – Phia Den National Park for providing us with an opportunity to carry out field surveys. Fieldwork took place under the administrative permission of the Vietnam Administration of Forestry of the Vietnamese Ministry of Agriculture and Rural Development and People's Committee of Cao Bang Province. We are very grateful to Paula Jenkins and Yuri LR Leite for their helpful and constructive comments on an earlier version of the manuscript. This study was supported in part by the Russian Foundation for Basic Research (16-04-00085).

References

Bannikova AA, Lebedev VS, Abramov AV, Rozhnov VV (2014) Contrasting evolutionary history of hedgehogs and gymnures (Mammalia: Erinaceomorpha) as inferred from a multigene study. Biological Journal of Linnean Society 112: 499–519. https://doi.org/10.1111/bij.12299

Chen YH (2008) Avian biogeography and conservation on Hainan Island, China. Zoological Science 25: 59–67. https://doi.org/10.2108/zsj.25.59

Chen Y (2009) Distribution patterns and faunal characteristic of mammals on Hainan Island of China. Folia Zoologica 58: 372–384.

Chen YH, Bi JF (2007) Biogeography and hotspots of amphibian species of China: implications to reserve selection and conservation. Current Science 92: 480–489.

Corbet GB (1988) The family Erinaceidae: a synthesis of its taxonomy, phylogeny, ecology and zoogeography. Mammal Review 18: 117–172. https://doi.org/10.1111/j.1365-2907.1988.tb00082.x

Engesser B, Jiang J (2011) Odontological and craniological comparisons of the recent hedgehogs *Neotetracus* with *Hylomys* and *Neohylomys* (Erinaceidae, Insectivora, Mammalia). Vertebrata Palasiatica 49: 406–422.

Johnston C, Smith AT (2016) *Neohylomys hainanensis*. The IUCN Red List of Threatened Species 2016, e.T10588A22326961. https://doi.org/10.2305/IUCN.UK.2016-1.RLTS.T10588A22326961.en [accessed on 20 June 2018]

Hoffmann RS, Lunde D (2008) Order Erinaceomorpha. In: Smith AT, Xie Y (Eds) A Guide to the Mammals of China. Princeton University Press, Princeton & Oxford, 292–297.

Hutterer R (2005) Order Erinaceomorpha. In: Wilson DE, Reeder DA (Eds) Mammal Species of the World. A Taxonomic and Geographic Reference (3rd edn). Johns Hopkins University Press, Baltimore, 212–219.

Myers N, Mittermeier RA, Mittermeier CG, da Fonseca GAB, Kent J (2000) Biodiversity hotspots for conservation priorities. Nature 403: 853–858. https://doi.org/10.1038/35002501

Stone RD (1995) Eurasian Insectivores and Tree Shrews. An Action Plan for their Conservation. IUCN, Gland, Switzerland, 109 pp.

Shaw TH, Wong S (1959) A new insectivore from Hainan. Acta Zoologica Sinica 11: 422–429.

Zhu H (2016) Biogeographical evidences help revealing the origin of Hainan Island. PLoS ONE 11: e0151941. https://doi.org/10.1371/journal.pone.0151941

ZooKeys 795: 83–91 (2018)
doi: 10.3897/zookeys.795.28036
http://zookeys.pensoft.net

RESEARCH ARTICLE

A peer-reviewed open-access journal
ZooKeys
Launched to accelerate biodiversity research

Australobius tracheoperspicuus sp. n., the first subterranean species of centipede from southern China (Lithobiomorpha, Lithobiidae)

Qing Li[1], Su-jian Pei[2], Xuan Guo[1], Hui-qin Ma[3], Hui-ming Chen[1]

1 *Guizhou Institute of Biology, Guiyang, Guizhou 550001, PR China* **2** *School of Life Sciences, Hengshui University, Hengshui, Hebei 053000, PR China* **3** *Scientific Research Office, Hengshui University, Hengshui, Hebei 053000, PR China*

Corresponding authors: *Hui-qin Ma* (mhq008@yahoo.com); *Hui-ming Chen* (mei601@126.com)

Academic editor: *M. Zapparoli* | Received 28 June 2018 | Accepted 5 September 2018 | Published 8 November 2018

http://zoobank.org/B1D0C7E4-8AAE-4A07-B193-F33761C27D4F

Citation: Li Q, Pei S-j, Guo X, Ma H-q, Chen H-m (2018) *Australobius tracheoperspicuus* sp. n., the first subterranean species of centipede from southern China (Lithobiomorpha, Lithobiidae). ZooKeys 795: 83–91. https://doi.org/10.3897/zookeys.795.28036

Abstract

Australobius tracheoperspicuus **sp. n.** (Lithobiomorpha: Lithobiidae) was recently discovered from the Cave of the brickyard of Gaofeng village, in the Guizhou Province, southwest China, and it is described here. Morphologically the new species is similar to *A. magnus* (Trozina, 1894) from north-western China. The new species can be easily distinguished from those by the trachea connected to the valve of the TIII clearly visible from the dorsal side, the absence of ocelli on each side of the cephalic plate, the DaC spine being only present on the XIIIth–XVth legs. Numbers of examined specimens, distribution and the main morphological characters and an identification key to the known Chinese species of genus *Australobius* based on adult specimens is given.

Keywords

Australobius, cave Lithobiomorpha, China, new species

Introduction

The World Catalogue of Centipedes (Bonato et al. 2016) currently records 33 species/subspecies for the genus *Australobius* Chamberlin, 1920, mostly in South-East Asia and East Australia (Zapparoli and Edgecombe 2011). The genus is characterized by possessing the following traits (Eason 1978, 1997, Edgecombe 2002, Zapparoli

Copyright *Qing Li et al.* This is an open access article distributed under the terms of the Creative Commons Attribution License (CC BY 4.0), which permits unrestricted use, distribution, and reproduction in any medium, provided the original author and source are credited.

and Edgecombe 2011): antenna mostly with 20 articles, some species more than 24; ocelli few (e.g., 1+3–1+6), some species more than 8; forcipular coxosternal teeth at least 3+3; tergites with more or less distinct posterior triangular projections; female gonopods with uni-, bi- or tridentate claw, 3+3–4+4 spurs, rarely more than 4; tarsal articulation of legs I–XIII indistinct in some species.

The myriapoda fauna of China is still poorly known and this is especially the case with centipedes of the order Lithobiomorpha. Only 80 species/subspecies of lithobiomorphs are to date known from the country (Ma et al. 2014a, b, 2015, 2018; Pei et al. 2014, 2015, 2016, 2018; Qin et al. 2014, 2017; Qiao et al. 2018; Chao et al. 2018). Altogether, only five species of *Australobius* have been recorded from China (Ma et al. 2008a, b, 2014b, Qin et al. 2014). However, none of them have been recorded from subterranean environment. The present note is devoted to the description of a new cave-dwelling *Australobius* from southern China, as well as the first subterranean species of Lithobiomorpha from China. An identification key is also given to all six species of *Australobius* known to occur in China.

Materials and methods

All specimens were hand-collected in cave and preserved in 75 % ethanol. Illustrations and measurements were produced using a ZEISS SteREO Discovery. V20 microscope equipped with an Abbe drawing tube and an ocular micrometer and axiocam 512 color. The colour description is based on specimens fixed in 75% ethanol. The body length is measured from the anterior margin of the cephalic plate to the posterior end of the postpedal tergite. Type specimens are deposited in the School of Life Sciences, Hengshui University, Hengshui, China (**HUSLS**). The terminology of the external anatomy follows Bonato et al. (2010). Measurements are shown in millimeters (mm).

The following abbreviations are used in the text and the tables:

T, TT	tergite, tergites;	**Ti**	tibia,
S, SS	sternite, sternites;	**a**	anterior,
C	coxa,	**m**	median,
Tr	trochanter,	**p**	posterior,
P	prefemur,	**DaC spine**	anterior dorsal spine of coxa.
F	femur,		

Taxonomy

***Australobius tracheoperspicuus* sp. n.**
http://zoobank.org/98D3BEF9-A361-40BF-BDE0-2B9400875C49
Figs 1–11, Table 1

Material. *Type material.* Holotype: male, Cave of the brickyard of Gaofeng village, Yancang Town, Yi-Hui-Miao Autonomous County of Weining , Bijie City, Guizhou Province, 26°54'30.95"N, 104°24'13.78"E, alt. 2430 m a.s.l., 19 V 2017, Huiming

Table 1. Leg plectrotaxy of *Australobius tracheoperspicuus* sp. n.

Legs	Ventral side					Dorsal side				
	C	Tr	P	F	Ti	C	Tr	P	F	Ti
I–XII			mp	amp	am			amp	ap	ap
XIII			amp	amp	am	a		amp	ap	ap
XIV		m	amp	amp	a	a		amp	ap	ap
XV		m	amp	am	a	a		amp	a	

Chen leg. Paratypes: 1 ♀, 1 ♂, same data as holotype. *Other material.* 4♂♂(larvae), the Gaodiping Cave of Dashan village, shaanqiao street, Yi-Hui-Miao Autonomous County of Weining , Bijie City, Guizhou Province, 26°50'55.03"N, 104°17'08.81"E, alt. 2175 m a.s.l., 23 IV 2017, Huiming Chen leg.

Diagnosis. Antennae with 26 articles, no ocelli, anterior margin of the coxosternite with 5+5 teeth, more or less developed, porodonts slender, between fourth and fifth outer teeth. Tergites without posterior triangular projections, trachea connected to the valve of the T III clearly visible from the dorsal side. Coxal pores 4–6. Tarsal articulation well defined on legs I–XV. No secondary sexual modifications on legs XIV and XV of male. Female gonopods with simple claw, 2+2 spurs. Male gonopods short and small blunt cone bulge, apically slightly sclerotized.

Description. Body length 17.43 –19.24 mm, cephalic plate 1.76–1.93 mm long, 1.77–1.97 mm wide; the whole body pale yellow–brownish, tarsus II of all legs more darker, proximal parts of forcipules and the teeth of the anterior margin of the coxosternite brown, all claws of legs yellow–brown.

Antennae with 26+26 articles; basal article slightly longer than wide, subsequent articles markedly longer than wide, distal article up to 2.5 times as long as wide. Abundant long setae on antennal surface, less so on basal articles, gradual increase in density of setae to about the fourth article, then more or less constant. Length of antenna 7.3–7.4 times width of cephalic plate, and often extending close to posterior edge of T XI (Figure 1).

No ocelli on each side of the cephalic plate. Tömösváry's organ ovate, situated at anterolateral margin of the cephalic plate (Figure 2).

Cephalic plate smooth, convex, very slightly wider than long; tiny setae emerging from pores scattered very sparsely over whole surface; frontal marginal ridge with shallow anterior median furrow; from short to long setae scattered along marginal ridge of cephalic plate, there more setae close to the antenna; lateral marginal ridge discontinuous (Figure 3).

Forcipular coxosternite subtrapezoidal (Figure 4), anterior margin broad, external side lightly longer than internal side; median diastema moderately narrow, deeply V–shaped; anterior margin with 5+5 blunt teeth; porodonts slender, lying between the fourth and fifth outer teeth, and more closer to the fourth tooth, the innermost tooth more posterior, and the interdental distance gradually increases from the internal side to the external side (Figure 5); some short setae scattered on the ventral side of coxosternite; usually there are more setae near the dental margin.

All tergites with wrinkles, central backside slightly hunched, T I posterolaterally narrower than anterolaterally, generally trapeziform, narrower than cephalic plate, broader than T III. Trachea connected to the valve of the T III is clearly visible from

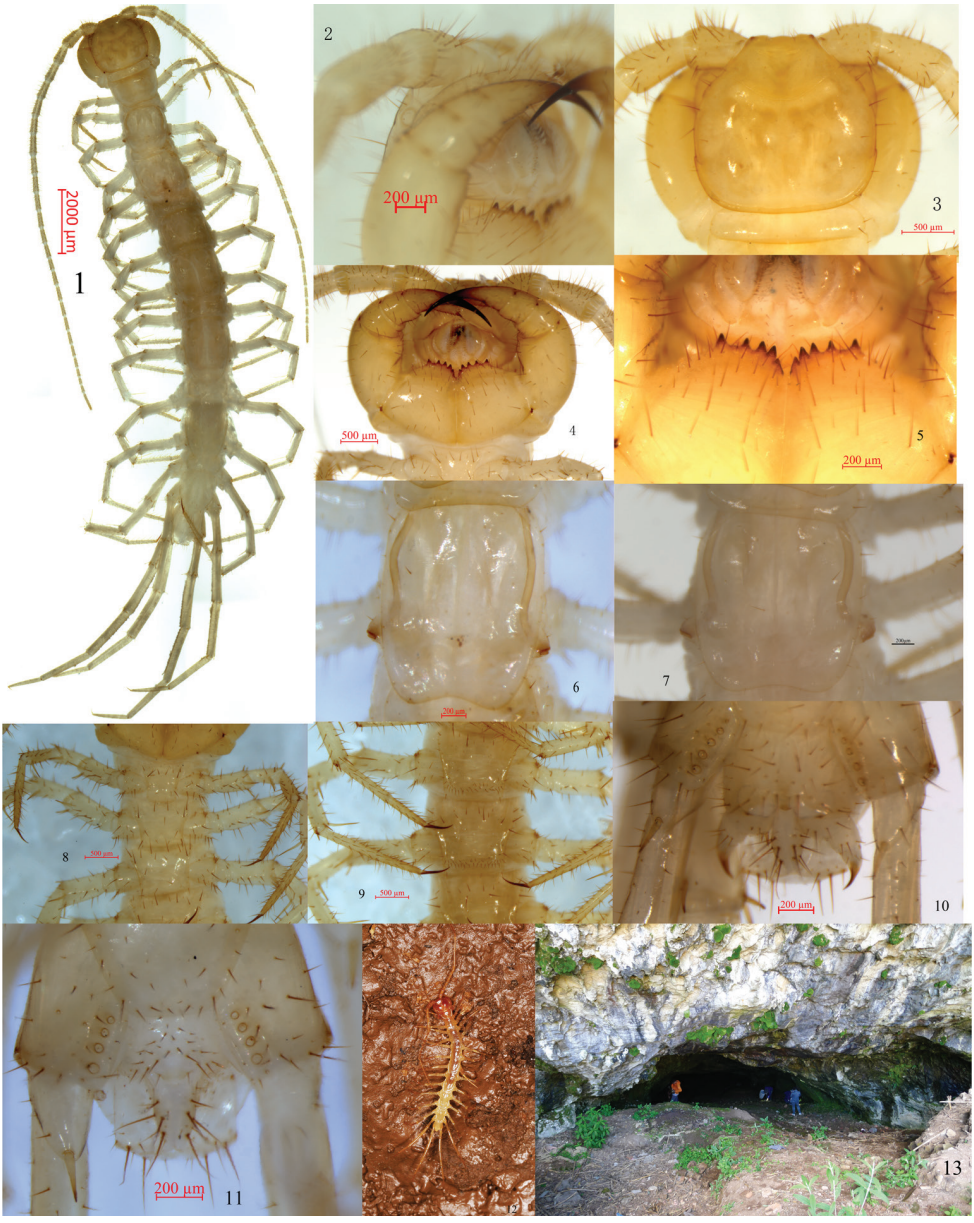

Figures 1–12. *Australobius tracheoperspicuus* sp. n. (holotype male **1–5, 7–9, 11–12** paratype female **6** and **10**) **1** Habitus, dorsal view **2** Tömösváry's organ, lateral view **3** Cephalic plate, dorsal view **4** Cephalic plate, ventral view **5** Forcipular coxosternite, ventral view **6** T III of female **7** T III of male **8** SS I–V **9** SS VI and VII **10** Posterior segments and gonopods of female, ventral view **11** Posterior segments and gonopods in male, ventral view **12** Living specimen of *Australobius tracheoperspicuus* sp. n. **13** Cave of the brickyard of Gaofeng village.

the dorsal side (Figs 6–7). Posterior margin of T I slightly concave, posterior margin of TT III, V, VII, VIII, X, XII, XIV and XV concave. Marginal ridge of TT II , IV, VI, IX, X, XI, XII , XIII, XIV and XV bulging; lateral marginal ridge of all tergites

continuous; all posterior angles generally rounded, without triangular projections; tiny setae scattered very sparsely over surface, more densely on anterior and posterior angles (Figure 1). All the tergites more longer than the congeneric species, T X is the longest, at most up to 1.3 times as long as wide.

Posterior side of sternites narrower than anterior one, generally trapeziform, comparatively smooth, long and thick setae emerging from pores scattered sparsely on surface, more setae on surface of the SS I–V (Figure 8), there are two irregular rows short and slightly thinker setae along the posterior margin of the SS VI and VII (Figure 9), few setae on surface of the following SS.

Legs long and slender, tarsal articulation well defined on legs I-IV; all legs with fairly long curved claws; anterior and posterior accessory spurs on legs I–XIII anterior accessory spurs moderately long and slender, forming an angle of about 45° with tarsal claws; posterior one slightly strong, forming an angle of about 30° with tarsal claws; no accessory spurs on legs XIV and XV. Comparatively long setae scattered very sparsely over surface of prefemur, femur, tibia and tarsus of legs I–XIII, more setae scattered on surface of tarsus; dorsal setae slightly longer than ventral, however, more setae in ventral; setae scattered on surface of legs XIV and XV clearly scarcer and short and fine than on other legs. Legs XIV and XV hardly thicker and stronger in both male and female, tarsus I about 6.3–6.6 times as long as wide in legs XV. Tarsus I of legs XV 5.0–5.6 times as long as wide in male, tarsus I of legs XV 5.0–5.6 times as long as wide in male. Leg plectrotaxy as in Table 1.

Coxal pores 4–6, most of them round, few ovate, 5-5-6-5 or 5-6-5-5 in female, 4-5-5-4 or 4-4-4-4 in male, coxal pore field set in a relatively shallow groove, fringe of coxal pore field with eminence, moderately long setae scattered sparsely over surface of eminence.

Female S XV anterolaterally broader than posterolaterally, generally trapeziform, posteromedially straight; sternite of genital segment usually well chitinised; posterior margin of genital sternite deeply concave between condyles of gonopods, except for a small, median bulge; long setae scattered over ventral surface of genital segment, regularly fringed, with longer setae along posterior margin. Gonopods: first article fairly broad, second moderately long and slender, coniform spurs in right, inner spur obviously larger than outer one (Figure 10); apical claw of third article simple, slender and sharp (Figure 11). Many long setae on surface of all segments of gonopods.

Male S XV posterolaterally narrower than anterolaterally, posterior edge straight, sparsely covered with long setae; sternite of genital segment smaller than in female, usually well sclerotised. Posterior margin quite deeply concave between gonopods, without a medial bulge; comparatively long setae scattered on ventral surface of genital segment, few slender setae near S XV, setae gradually increasing in density from anterior to posterior, gonopods short and small blunt cone bulge, apically slightly sclerotised (Figure 10).

Etymology. The specific name refers to the trachea connected to the valve of the T III that is clearly visible from the dorsal side.

Habitat. The specimens were collected on the limestone walls and bedrock floor of the cave.

Discussion. The new species resembles *A. magnus* (Trozina, 1894) from North-Western China in having the coxal pores numbering 6–7, no accessory spurs on legs

Table 2. Numbers of examined specimens, distribution and main morphological characters of the have known Chinese species of *Australobius* Chamberlin, 1920. Abbreviation: DaC spine, anterior spine of dorsal of coxa.

	A. anamagnus	***A. apicicornis***	***A. magnus***	***A. nodulus***	***A. tetrophthalmus***	***A. tracheoperspicuus* sp. n.**
Original description	Ma et al. 2008a	Qin et al. 2014	Trotzina 1894	Ma et al. 2008b	Loksa 1960	This paper
Specimens examined	2♀1♂	3♀2♂	1♀	4♀2♂	1♂	1♀2♂(4♂larvae)
Other sources	no	no	Eason 1997, Dyachkov 2017	no	Eason 1978	no
Specimens examined	no	no	13♀6♂, 34♀8♂	no	1♂	no
Distribution	Qinghai-Tibet Plateau China (Tibet)	Qinghai-Tibet Plateau China (Sichuan)	Qinghai-Tibet Plateau China (Tibet), Kirghizia and Kazakhstan	Qinghai-Tibet Plateau, China (Tibet)	China S (Guangxi)	China S (Guizhou)
Body length (mm)	15.9 – 26.6	17.6 – 22.5	16.0 – 30.0	17.1 – 22.1	19.0	17.4 –19.2
Number of antennal articles	26+26, rarely 25+26	24+24	25+25 – 30+30	31+31 – 33+33	29	26+26
Number and arrangement of ocelli	10, in 2 rows	7 – 9, in 2 rows	8 – 9, in 2 rows	9 – 11, in 2 rows	4, in 2 rows	None
Tömösváry's organ	Nearly round, smaller than adjoining ocelli	Round, smaller than adjacent ocellus	Round, smaller than adjacent ocellus	Smaller than adjoining ocelli	Ovate, larger than adjoining ocelli	Ovate
Number and arrangement of coxosternal teeth	3+3, 3+4, 4+4	8+6, 5+5, 6+6, 5+6, Roughly triangular	2+2 – 7+7, few 3+4, 6+7, small, blunt	6+6 or 6+5, small and of	5+5, small blunt	5+5
Porodont	Comparatively thick and strong, situated between outer two teeth, few between second and third	Absent	Short and pointed, situated between outer two teeth, or between second and third	Situated between outer third and fourth teeth, rarely between second and third teeth	Not reported	slender, lying between the fourth and fifth outer teeth, and more closer to the fourth tooth
Number of coxal pores	4 – 9 Females: 5-6-7-6, 5-7-7-7, 6-7-7-6,	5 – 8, usually 6-6-6-6, 6-6-6-5, 8-8-8-8, 6-7-7-6, 6-7-7-7, 6-7-8-7, 6-7-9-7	3 – 7, rarely 8	4 – 7 arranged into an irregular row, 5-6-6-5, 4-5-5-5, 6-7-7-6, 6-7-7-5	3-3-3-3	4 – 6, 5-5-6-5 or 5-6-5-5 in female, 4-5-5-4 or 4-4-4-4 in male
DaC spine	On XIIth (present or absent) –XVth legs	On XIIIth – XVth legs	On VIIIth –Xth present or absent, on XIth –XV 15th legs present	On VIIth –XVth legs	Absent	On XIIIth –XVth legs
legs XIVth accessory spur	Absent	Present	Absent	Absent	Not reported	Absent
legs XVth accessory spur	Absent	Absent	Absent	Absent	Not reported	Absent
Number and shape of spurs on female gonopods	3+3, 3+4, 4+4 moderately small, inner coniform spurs, inner one much smaller	3+3 or 4+4 coniform spurs, ones smaller than outer spurs	2+2 – 4+4, rarely 4+5	2+2 or 4+4 moderately small, coniform spurs, inner spur clearly smaller than outer one	Not reported	2+2 moderately long and slender, coniform spurs, inner spur larger than outer one,
Apical claw of female gonopods and lateral denticles	Broad, simple	Simple	Simple	Broad, simple	Not reported	simple, slender and sharp
Male gonopods	A small hemispherical protuberance, with a single long seta, distal region slightly sclerotised	small, indistinct swellings, with one or two long setae	small, spherical	Small hemispheroid protuberance, with3 – 4 long setae, apically slightly sclerotized	Not reported	small small blunt cone bulge, apically slightly sclerotised

XIV and XV, DaC spine present on legs XIII–XV, apical claw of female gonopods simple. However, the new species can be easily distinguished by the following characters: trachea connected to the valve of the TIII clearly visible from the dorsal side in new species instead of the trachea connected to the valve of the TIII is invisible from the dorsal side in *A. magnus*; absence of ocellus on each side of the cephalic plate vs. 8–9 ocelli in *A. magnus*; DaC spine being only present on the XIIIth–XVth legs in contrast to being present or absent on VIIIth–Xth legs, present on Xth –XVth legs in *A. magnus*.

On the other hand, several diagnostic features of the recently described Chinese species that are routinely used in the diagnosis of species of *Australobius* Chamberlin, 1920 are variable within the framework of the original description, perhaps the most conspicuous variation pertains to the number of teeth on the anterior margin of the coxosternite and the numbers of the antennal articles and the ocelli. For example, in the original description of the genus *Australobius*, the number of antennal articles is mostly 20, some species more than 24 articles, whereas in many species occurring in China it is higher (Table 2). The same is true for the number of the ocelli, which is few (e.g., 1+3–1+6) or in some species more than 8 in the original description of the genus, whereas in many species occurring in China it is higher (Table 2), and for the number of coxosternal teeth, which is at least 3+3 in the original description, whereas in many species occurring in China it is more variable (Table 2).

To assist in the identification of the Chinese species of *Australobius*, numbers of examined specimens, distribution and main morphological characters of the known species of this genus in China is presented (Table 2) and key to the known Chinese species of the genus is presented, these characters are specific only to adults of the taxa occurring in China.

Key to the known Chinese species of the genus *Australobius* Chamberlin, 1920

1 No ocelli on each side of cephalic plate ..... ***A. tracheoperspicuus* sp. n.**
– At least four ocelli on each side of cephalic plate **2**
2 Four ocelli on each side of cephalic plate, Tömösváry's organ larger than adjacent ocelli ..... ***A. tetrophthalmus* (Loksa, 1960)**
– More than seven ocelli on each side of cephalic plate, Tömösváry's organ smaller than adjacent ocelli **3**
3 No prodonts ..... ***A. apicicornis* Qin, Lin, Zhao, Li, Xie, Ma, Su & Zhang, 2014**
– Porodonts present **4**
4 Large posterior tergites wrinkled; bulge present on terminal part of tarsus ..... ***A. magnus* (Trozina, 1894)**
– Large posterior tergites smooth; no bulge on the terminal part of tarsus **5**
5 Antenna with at most 26 articles and 2+2 or 4+4 forcipular coxosternal teeth ..... ***A. anamagnus* Ma, Song & Zhu, 2008**
– Antenna with at least 31 articles and at most 6+6 forcipular coxosternal teeth ..... ***A. nodulus* Ma, Song & Zhu, 2008**

Acknowledgements

This study was supported by the National Natural Science Foundation of China (NSFC grant No. 31572239), the Talents Introduction Foundation of the Guizhou Academy of Sciences (2009-2); the Foundation of Biologic Resource and Environment Big Data ([2015] 4013); the scientific investigation of Caohai lake National Nature Reserve (2016GZCH-012); the innovative Talent Team (2015) 4012; and the innovative Talent Plan (2016) 5666. We are grateful to Gregory D Edgecombe, London, UK, Pavel Stoev, Sofia, Bulgaria, and Marzio Zapparoli, Viterbo, Italy, for their hospitality and continuous help during our research. We thank Rowland M Shelley, North Carolina, USA, and Dr His–Te Shih, Taichung, China, for providing us with invaluable literature.

References

Bonato L, Chagas Junior A, Edgecombe GD, Lewis JGE, Minelli A, Pereira LA, Shelley RM, Stoev P, Zapparoli M (2016) ChiloBase 2.0 – A World Catalogue of Centipedes (Chilopoda). http://chilobase.biologia.unipd.it

Bonato L, Edgecombe GD, Lewis JGE, Minelli A, Pereira LA, Shelley RM, Zapparoli M (2010) A common terminology for the external anatomy of centipedes (Chilopoda). ZooKeys 69: 17–51. https://doi.org/10.3897/zookeys.69.737

Chao J, Lee K, Chang H (2018) *Lithobius* (*Monotarsobius*) *meifengensis,* a new species of centipede from high altitude forest in central Taiwan (Chilopoda, Lithobiomorpha, Lithobiidae). Zookeys 741: 181–192. https://doi.org/10.3897/zookeys.741.21036

Dyachkov YuV (2017) New data on the *Australobius magnus* (Trotzina, 1894) (Chilopoda: Lithobiomorpha: Lithobiidae) from Southern Kazakhstan. Ukrainian Journal of Ecology 7(4): 440–443. http://dx.doi.org/10.15421/2017_139

Eason EH (1997) On some Lithobiomorpha from the mountains of Kirghizia and Kazakhstan (Chilopoda). Arthropoda Selecta 6(1–2): 117–121.

Eason EH (1978) On Lithobiidae from the Seychelles with description of two new species of the subgenus *Australobius*, genus *Lithobius* (Chilopoda: Lithobiomorpha). Journal of Zoology 184: 21–34. https://doi.org/10.1111/j.1469-7998.1978.tb03263.x

Edgecombe GD (2002) Morphology and distribution of *Australobius scabrior* (Chilopoda: Lithobiomorpha: Lithobiidae). Memoirs of the Queensland Museum 48: 103–118. http://www.nhm.ac.uk/resources-rx/files/edgecombe--hollington-2002-australobius-94124.pdf

Loksa I (1960) Einige neue Diplopoden-und Chilopoden-Arten aus Chinesischen Höhlen. Acta Zoologica Academiae Scientiarum Hungaricae 6: 135–148.

Ma H, Lu Y, Liu H, Hou X, Pei S (2018) *Hessebius luculentus*, a new species of the genus *Hessebius* Verhoeff, 1941 from China (Lithobiomorpha, Lithobiidae). Zookeys 741: 193–202. https://doi.org/10.3897/zookeys.741.20061

Ma H, Pei S, Hou X, Zhu T (2014a) *Lithobius* (*Monotarsobius*) *zhangi* sp. n., a new species from Eastern China (Chilopoda, Lithobiomorpha, Lithobiidae). ZooKeys 459: 1–10. https://doi.org/10.3897/zookeys.459.8169

Ma H, Pei S, Hou X, Zhu T, Gai Y (2015) *Lithobius* (*Ezembius*) *anabilineatus* sp. nov., a new species (Lithobiomorpha: Lithobiidae) from Eastern China. Oriental Insects 49(3–4): 256–263. https://doi.org/10.1080/00305316.2015.1081647

Ma H, Pei S, Hou X, Zhu T, Wu D, Gai Y (2014b) An annotated checklist of Lithobiomorpha of China. Zootaxa 3847(3): 333–358. http://dx.doi.org/10.11646/zootaxa.3847.3.2

Ma H, Song D, Zhu M (2008a) A new species of the genus *Australobius* Chamberlin, 1920 (Lithobiomorpha: Lithobiidae) from Tibet, China. Entomological News 2: 171–177. https://doi.org/10.3157/0013-872X(2007)118[77:HPBTCT]2.0.CO;2

Ma H, Song D, Zhu M (2008b) A new species of *Australobius* Chamberlin, 1920 (Lithobiomorpha: Lithobiidae) from China. Oriental Insects 42: 335–340. https://doi.org/10.1080/00305316.2008.10417558

Pei S, Lu Y, Liu H, Hou X, Ma H (2018) *Lithobius* (*Ezembius*) *tetraspinus*, a new species of centipede from northwest China (Lithobiomorpha, Lithobiidae). ZooKeys 741: 203–217. https://doi.org/10.3897/zookeys.741.19980

Pei S, Lu Y, Liu H, Hou X, Ma H, Zapparoli M (2016) *Lithobius* (*Ezembius*) *multispinipes* n. sp., a new species of centipede from Northwest China (Lithobiomorpha: Lithobiidae). Zootaxa 4169(2): 390–400. http://dx.doi.org/10.11646/zootaxa.4169.2.12

Pei S, Ma H, Zhu T, Gai Y (2014) A new species of *Lithobius* (*Ezembius*) Chamberlin (Lithobiomorpha: Lithobiidae) from China. Oriental Insects 48(1–2): 102–107. https://doi.org/10.1080/00305316.2014.959787

Pei S, Ma H, Hou X, Zhu T, Gai Y (2015) *Lithobius* (*Ezembius*) *laevidentata* sp. n., a new species (Chilopoda: Lithobiomorpha: Lithobiidae) from the Northwest region of China. Biologia 70(8): 1113–1117. https://doi.org/10.1515/biolog-2015-0124

Qiao P, Qin W, Ma H, Su J, Zhang T (2018) Two new species of the genus Hessebius Verhoeff, 1941 from China (Lithobiomorpha, Lithobiidae). Zookeys 735: 65–82. https://doi.org/10.3897/zookeys.735.22237

Qin W, Lin G, Zhao X, Li B, Xie J, Ma H, Su J, Zhang T (2014) A new species of *Australobius* (Lithobiomorpha: Lithobiidae) from the Qinghai–Tibet Plateau, China. Biologia 69(11): 1601–1605. https://doi.org/10.2478/s11756-014-0459-4

Qin W, Qiao P, Huang Y, Lin G, Su J, Zhang T (2017) A new species of *Bothropolys* and a new record of *Lithobius magnitergiferous* (Lithobiidae) from the Qinghai-Tibet Plateau, China. Biologia 72(11): 1314–1319. https://doi.org/10.1515/biolog-2017-0151

Trotzina A (1894) Vier neue *Lithobius*-Arten aus Central Asia. Horae Societatis Entomologicae Rossicae 28: 247–253.

Zapparoli M, Edgecombe GD (2011) Lithobiomorpha. – In: Minelli A (Ed.) Treatise on Zoology – Anatomy, Taxonomy, Biology – The Myriapoda, Volume 1. Jordaan Luchtmans, Brill, Leiden/Boston, 371–389.

ZooKeys 795: 93–103 (2018)
doi: 10.3897/zookeys.795.27619
http://zookeys.pensoft.net

RESEARCH ARTICLE

A peer-reviewed open-access journal
ZooKeys
Launched to accelerate biodiversity research

First continental troglobiont *Cylindroiulus* millipede (Diplopoda, Julida, Julidae)

Ana Sofia P.S. Reboleira[1], Henrik Enghoff[1]

1 *Natural History Museum of Denmark, University of Copenhagen, Universitetsparken 15, DK-2100 København Ø, Denmark*

Corresponding author: *Ana Sofia P.S. Reboleira* (sreboleira@snm.ku.dk)

Academic editor: *Nesrine Akkari* | Received 20 June 2018 | Accepted 25 September 2018 | Published 8 November 2018

http://zoobank.org/EC1CAED3-DAAC-4AE7-8779-44DB3164EECE

Citation: Reboleira ASPS, Enghoff H (2018) First continental troglobiont *Cylindroiulus* millipede (Diplopoda, Julida, Julidae). ZooKeys 795: 93–103. https://doi.org/10.3897/zookeys.795.27619

Abstract

The new species of millipede *Cylindroiulus villumi* is described from a cave in the Estremenho karst massif in central Portugal. It is the first cave-adapted species of its genus with a strict subterranean life-style in continental Europe, and is the fifth blind species of the genus. The new species is illustrated with photographs and diagrammatic drawings. It is tentatively placed in the purely Iberian *Cylindroiulus perforatus*-group. The differences between the new species and its relatives are discussed, as well as its adaptations to a subterranean life-style.

Keywords

cave fauna, Julida, karst, Portugal, troglobiont

Introduction

The genus *Cylindroiulus* Verhoeff, 1894 belongs to the Palaeartic family Julidae and has more than 100 species distributed in Macaronesia and Europe (Kime and Enghoff 2017), North Africa (Read 2005, Akkari and Enghoff 2008), Turkey, the Caucasus region and Iran (Read 1992), and Central Asia (Read 1994). The genus can be recognized by the lack of frontal and metazonital setae, expanded mandibular stipites in males, gonopods with a flagella, and free, unforked mesomerites separated by a deep and wide incision from the opisthomerite (Read 1990).

Cave-adapted species of *Cylindroiulus* species were only known from Madeira Island, whereas in continental Europe only two anophthalmic, but not troglobiont, species were known (Reboleira and Enghoff 2014a, Read 2007).

Copyright *A.S.P.S. Reboleira, H. Enghoff*. This is an open access article distributed under the terms of the Creative Commons Attribution License (CC BY 4.0), which permits unrestricted use, distribution, and reproduction in any medium, provided the original author and source are credited.

Nine species of *Cylindroiulus* are currently known from mainland Portugal: *C. anglilectus* Read, 2007, *C. boreoibericus* Read, 2007, *C. britannicus* (Verhoeff, 1891), *C. caeruleocinctus* (Wood, 1864), *C. fenestratus* Read, 1989, *C. latestriatus* (Curtis, 1845), *C. perforatus* Verhoeff, 1905, *C. propinquus* (Porat, 1870), and *C. truncorum* (Silvestri, 1896) (Read 2007, Kime and Enghoff 2017).

Only very recently cave-adapted species of millipedes from Portugal have started to dig out of the dark and become known to science (Enghoff and Reboleira 2013, Reboleira and Enghoff 2013a, b, 2014a, b, c, 2017). Recently, a new species of *Cylindroiulus* has been found in a cave in the Estremenho massif in central Portugal. This is the largest karst area of Portugal, mainly composed of Jurassic limestone; a considerable part of its area is included in the Serra de Aire e Candeeiros Natural Park. We here describe this first cave-adapted species of *Cylindroiulus* from the European continent.

Materials and methods

Sampling was performed by direct search in the cave Algar do Pena in Estremenho karst massif, central Portugal.

Specimens were examined under a binocular stereomicroscope Leica M165C, and measurements were made with the software Leica Application Suite V4.12. Gonopods, vulvae, legs and antennae were dissected and mounted on temporary slides in glycerine or lactic acid for study under light microscopy in a Leica DM2500 microscope. Measurements were made following the methodology described by Enghoff (1982). Images of the gonopods and vulvae were stacked with the software Zerene Stacker. For scanning electron microscopy (SEM) one head, gonopod, leg, and tail were mounted on aluminium stubs, coated for 110 seconds with platinum/palladium, and studied in a JEOL JSM-6335F microscope. The background of some SEM images was processed with Adobe Photoshop CS6.

The type material is deposited in the collection of the Natural History Museum of Denmark, University of Copenhagen (**NHMD**, formerly ZMUC).

Results

Order Julida Brandt, 1833
Family Julidae Leach, 1814
Genus *Cylindroiulus* Verhoeff, 1894

***Cylindroiulus villumi* sp. n.**
http://zoobank.org/79A57B30-7ABF-4FCB-9B94-CB0A459DB129
Figs 1–5

Type material. Holotype, male, Portugal, Estremenho karst massif, Algar do Pena Cave (Coordinates: 39°27'54.40"N, 8°48'25.24"W), ASPS Reboleira leg., 04 Nov

Figure 1. *Cylindroiulus villumi* sp. n. **A** habitus of live female **B** habitus of subadult male. The partly darker colouration in 1B is due to gut contents seen by transparency. Scale bar: 1 mm.

2014. **Paratypes**: Portugal, Estremenho karst massif, Algar do Pena Cave, ASPS Reboleira leg., 04 Nov 2014, 1 male, 2 females, 4 juvenile males and 1 juvenile; same data but 28 Mar 2018, 1 female and 1 juvenile.

Diagnosis. A medium to small, blind, and unpigmented species of the *Cylindroiulus perforatus*-group. Anterior constriction pronounced and pilosity of the telson scarce. Differs from all other species in the group by the lack of eyes and by the shape of the gonopod mesomerite which is shorter than the promerite (>< *C. fenestratus* Read, 1989, *C. perforatus* Verhoeff, 1905, and *C. ventanaea* Read, 2007) and apically rounded (>< *C. anglilectus* Read, 2007). Further differs from other group members except *C. anglilectus* by the much shorter paracoxal process.

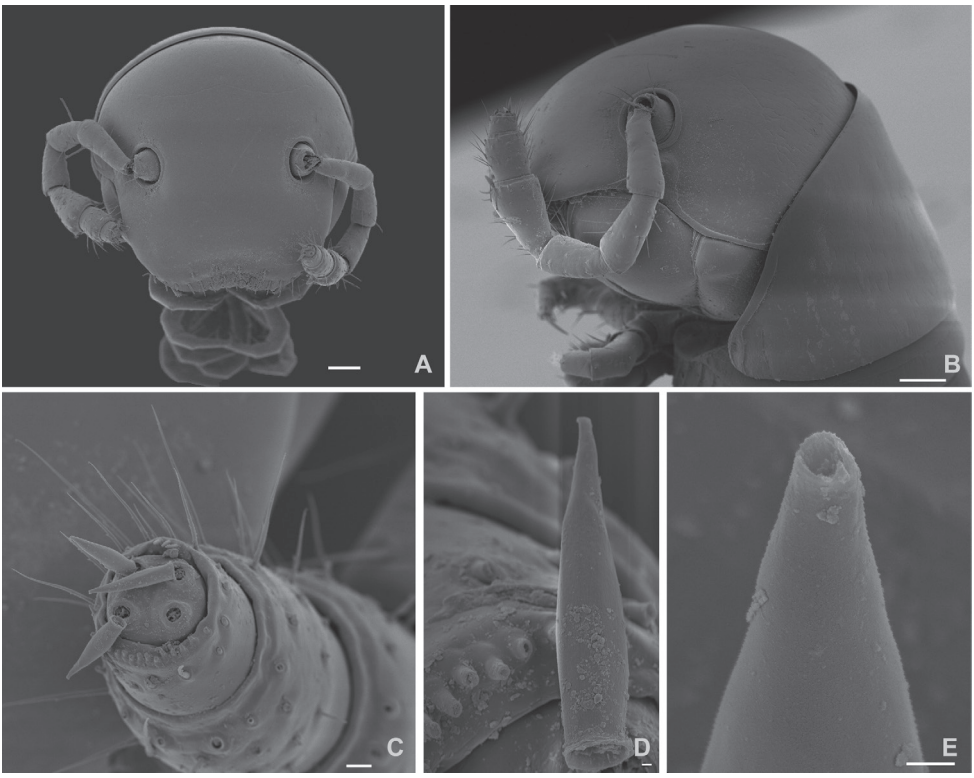

Figure 2. *Cylindroiulus villumi* sp. n. female paratype, SEM. **A** anterior view of the head **B** lateral view of the head **C** tip of the antenna **D** detail of a sensory cone of the antenna **E** tip of the sensory cone. Scale bars: 100 μm (**A, B**); 10 μm (**C**); 1 μm (**D, E**).

Description. Male holotype: 37 podous + 1 apodous rings + telson; females up to 41 podous + 1 apodous rings + telson.

Body length up to 13 mm in females and 11.4 mm in males. Vertical body diameter (H): 0.9 mm (females) and 0.7 mm (males). Integument unpigmented (Figure 1); eyes absent (Figs 1, 2A, B). Length of antennae 0.8 mm (Figure 2B), with sensory cones elongated and with a fine longitudinal striation (Figure 2C, D) ending in a pore as shown in Figure 2E. Anterior constriction of body pronounced in dorsal view. Limbus of the the normal type *sensu* Enghoff (1982), i.e., with simple marginal cells without denticles on the free margin. Length of legs (Figure 3A) 1.8 mm, tarsus being the longest podomere. Length of claw 9.6% of total leg length. Accessory claw exceptionally short: 92% shorter than the claw (Figure 3B). Preanal ring with a very short blunt projection, almost glabrous, only with 5 lateral setae (Figure 3C, D), subanal scale with two setae, anal valves with two long ventral setae on the lateral part of the posterior margin, rarely up to two additional setae were observed, however the number is variable and may even differ between right and left valve of the same specimen (Figure 3C). Male first pair of legs modified as typical of the genus, hook-like.

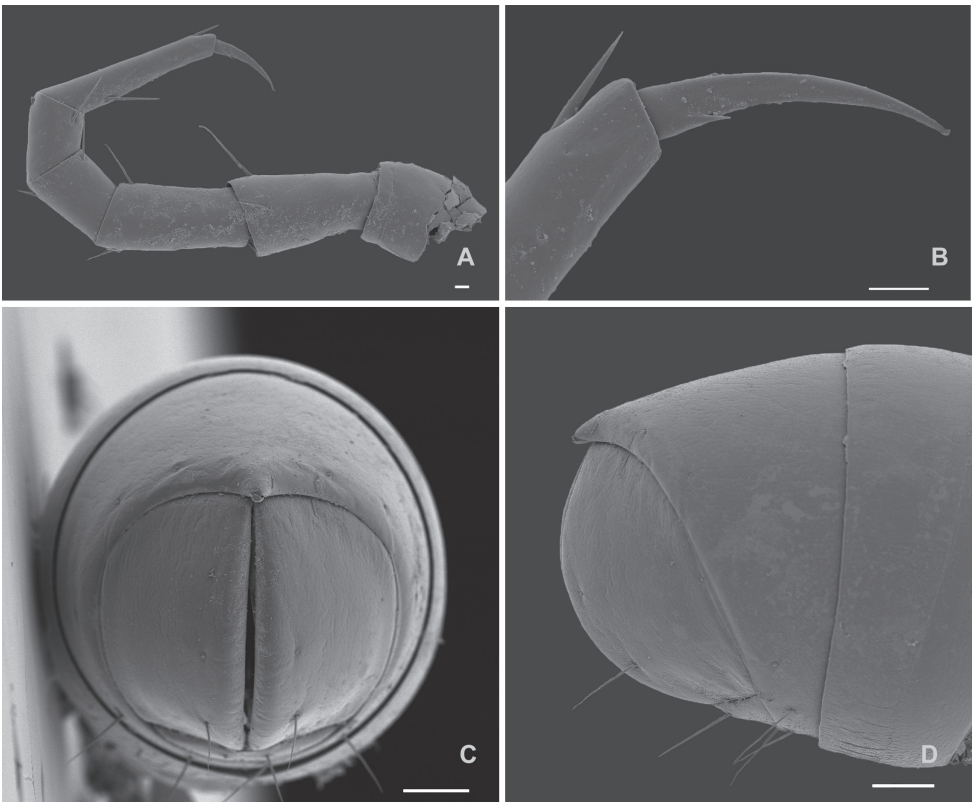

Figure 3. *Cylindroiulus villumi* sp. n. female paratype, SEM. **A** midbody leg **B** detail of the claw **C** posterior view of the anal valves **D** lateral view of the telson. Scale bars: 10 μm (**A, B**); 100 μm (**C, D**).

Gonopods (Figure 4): Promerite in anterior view (Figure 4D), higher than mesomerite (Figure 4D, E), with rugose area facing apical part of the mesomerite (Figure 4E). Mesomerite (Figure 4E): slender, shorter than, and fitting into, apical concavity of promerite. Paracoxal rim moderately developed. Paracoxal process not very prominent, rather short and mostly fused to solenomerite (Figure 4F). Solenomerite as in Figure 4A, B, C, F; very simple, subrectangular in lateral view, with denticles on anterior flagellum-conducting lamella (Figure 4C).

Vulvae (Figure 5A–B): Vulvae typical of the *C. perforatus*-group: glabrous operculum, bursa with a few setae and the receptaculum seminis as a stalked sphere with a small tubular appendix.

Etymology. The new species is dedicated to the VILLUM Foundation, named after Villum Kann Rasmussen (1909–1993), as recognition for the generous support to research in natural sciences.

Distribution. *Cylindroiulus villumi* sp. n. was discovered in the cave Algar do Pena, located in the Santo António plateau, the central sub-unit of the Estremenho

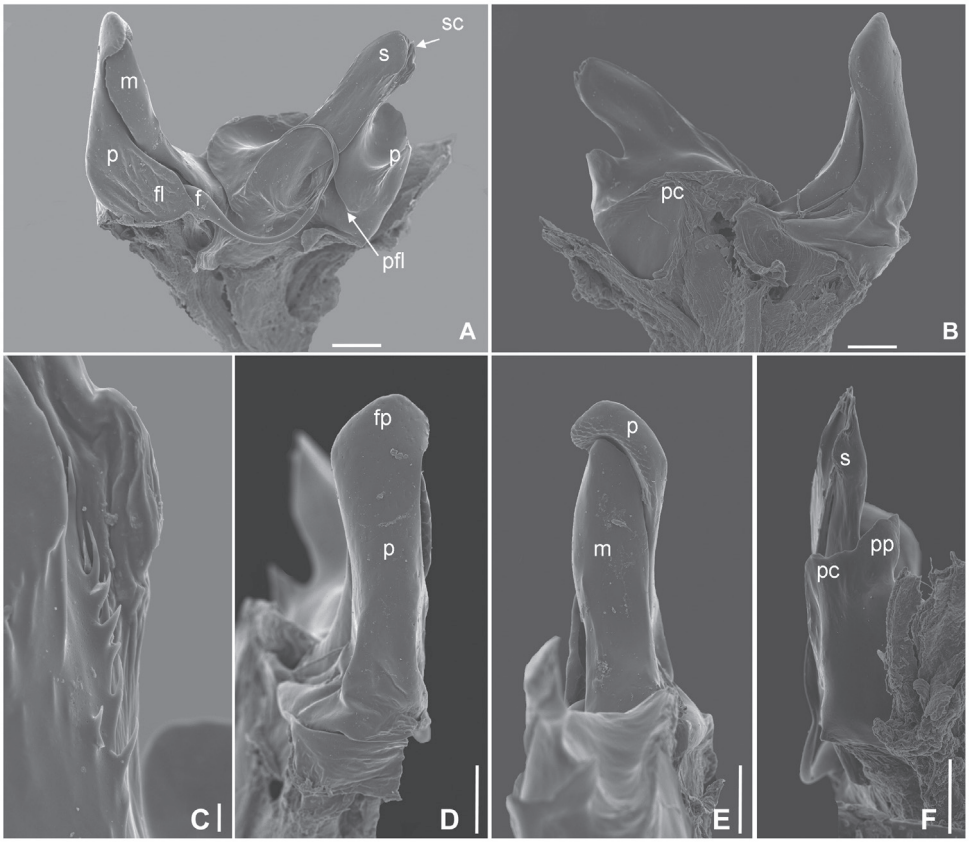

Figure 4. *Cylindroiulus villumi* sp. n. SEM of the male gonopod. **A** mesal view **B** lateral view **C** denticles on the anterior flagellum-conducting lamella of the solenomerite **D** pro- and mesomerite, anterior view **E** pro- and mesomerite, posterior view **F** opisthomerite, posterior view. Abbreviations: f: flagellum, fl: flagelliferous lobe of promerite, fp: finger-shapped projection of promerite, m: mesomerite, p: promerite, pc: lateral rim of paracoxite, pfl: posterior flagellum-conducting lamella, pp: paracoxal process, s: solenomerite, sc: sperm canal. Scale bars: 10 μm (**A, B, D, E, F**); 1 μm (**C**).

karst massif in central Portugal. It was found inside a big piece of deadwood located at the base of the entrance pit to the cave, at a depth of 33 meters below the surface.

Ecology. Algar do Pena is the largest underground chamber of Portugal. The temperature is very constant 13 ±1 °C and relative humidity close to saturation. It is a very oligotrophic cave where only a few cave-adapted species are recorded: the spider *Nesticus lusitanicus* Fage, 1931, the terrestrial isopod *Trichoniscoides meridionalis* Vandel, 1946, the springtail *Onychiurus confugiens* Gama, 1962; the dipluran *Podocampa* cf. *fragiloides* Silvestri, 1932; and the beetle *Trechus gamae* Reboleira & Serrano, 2009 (Reboleira 2007, 2012, Reboleira and Ortuño 2011, Reboleira et al. 2009, 2010, 2011). The holotype and a juvenile male paratype have 'Amphoromorpha' fungi on the head and antenna, similar to those observed by Enghoff and Reboleira (2017) on other millipedes.

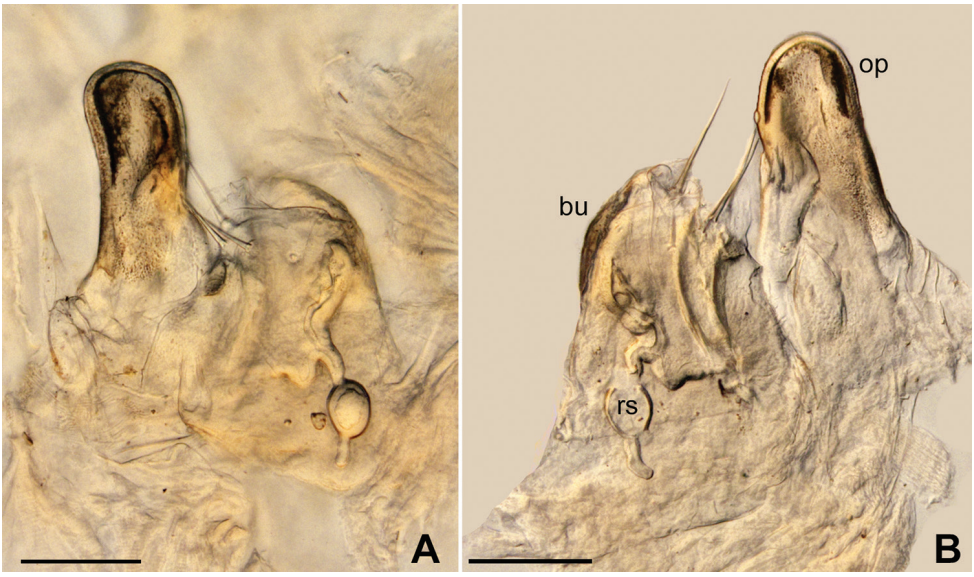

Figure 5. *Cylindroiulus villumi* sp. n. vulva, lateral view. Abbreviations: bu: bursa, op: operculum, rs: receptaculum seminis. Scale bar: 100 µm.

Discussion

The genus *Cylindroiulus* exhibits great morphological diversity concerning size, ocelli, number of segments, pigmentation, chaetotaxy, legs, accessory claws, and genital structures (Reboleira and Enghoff 2014c, Read 1989a, b); in the endemic *C. madeirae*-group from Madeira Island, part of the diversity can be seen as a result of niche segregation (Enghoff 1982, 1983, 2011). The new species *C. villumi* is the first representative of the genus with an exclusively subterranean life-style and corresponding troglomorphic characters (i.e., unpigmented, anophthalmic, elongated sensory cones on the antenna, and very short accessory claw) found in continental Europe. The new species can be distinguished from all congeners by the combination of anophthalmy and the shape of the male gonopods. The extremely short accessory claws, a trait believed to be associated with the ability to climb (Enghoff 1983), has also been observed in the other cave-adapted species of the genus (Reboleira and Enghoff 2014c).

Two anophthalmic, subterranean-adapted species of *Cylindroiulus*, *C. julesvernei* and *C. oromii,* are known from caves of Madeira Island (Reboleira and Enghoff 2014c). From the rest of the vast distribution area of *Cylindroiulus*, only two anophthalmic species are known: *C. vulnerarius* (Berlese, 1888), a species that has occasionally been found in caves but which is quite widespread in epigean soil habitats in West Europe (Schubart 1934, Kime and Enghoff 2017), and *C. gregoryi* Read, 2007 from the Galician province of Spain.

Cylindroiulus villumi sp. n. belongs to the nominal subgenus *Aneuloboiulus* Verhoeff, 1899 which is characterized by traits regarded as plesiomorphic (Enghoff 1982, Read 2007). Within this assemblage, *C. villumi* sp. n. may, with some uncertainty,

be placed in the Iberian *C. perforatus*-group. This group, which contains four Iberian species, is characterized by a "window", usually a perforation, in the gonopodal promerite; in other characters, the group is similar to the endemic Macaronesian *C. madeira*-group, notably by the presence of denticles on the flagellum-conducting lamella of the solenomerite, the naked vulvar operculum and the tubular appendix to the receptaculum seminis (Read 1989a, b, 2007). *Cylindroiulus villumi* does not have a perforated promite, but it does have denticles on the anterior flagellum-conducting lamella on the gonopod solenomerite like species of the *C. perforatus*-group; also the vulva of *C. villumi* sp. n. with the glabrous operculum and the subspherical receptaculum seminis with a small terminal appendix are typical of the *C. perforatus*-group. In these characters our new species is also similar to the Macaronesian *C. madeirae*-group (Enghoff 1982), presumably the sister-group of the *C. perforatus*-group (Read 1989a, b); however, the pilosity of the preanal ring in *C. villumi* sp. n. more resembles that of the *C. perforatus*-group.

The Algar do Pena Cave, where the new species was found, has been intensively sampled over the last decade, and only very recently this species was collected (Reboleira 2007, 2012). Several other caves in the same massif have been intensively sampled without retrieving any specimen of the new species. Only the troglophile chordeumatidan *Haplobainosoma lusitanum* Verhoeff, 1900 (family Haplobainosomatidae) has been recorded in caves of the same massif, while two epigean unidentified species of *Cylindroiulus* are also known from the mesovoid shallow substrate (MSS) in same massif (Reboleira and Enghoff 2014a).

Acknowledgements

We acknowledge the Natural Park of Serra de Aire e Candeeiros for all kinds of logistic support in fieldwork, and Josh Jenkins Shaw for English revision of the manuscript. ASR is supported by a research grant (15471) from VILLUM FONDEN. All specimens were collected under permits of the Instituto de Conservação da Natureza e das Florestas.

References

Akkari N, Enghoff H (2008) *Cylindroiulus mitta* n.sp., a new Tunisian millipede (Diplopoda, Julida: Julidae) and notes on the *Cylindroiulus distinctus* group. Zootaxa 1768: 61–68.

Berlese A (1888) *Mesoiulus vulnerarius* n.sp. Acari, Myriopoda et Scorpiones hucusque in Italia reperta 48(1): 1.

Brandt IF (1833) Tentaminum quorundam monographicorum Insecta Myriapoda Chilognatha Latreillii spectantium Prodromus. Bulletin de la Société Impériale des Naturalistes de Moscou 6: 194–209. [pl 5]

Curtis J (1845) Observations on the natural history and economy of the insects called wireworms, etc. Journal of the Royal Agricultural Society of England 5(1): 180–237.

Enghoff H (1982) The millipede genus *Cylindroiulus* on Madeira – an insular species swarm (Diplopoda, Julida: Julidae). Entomologica Scandinavica (Supplement No.) 18: 1–142.

Enghoff H (1983) Adaptive radiation of the millipede genus *Cylindroiulus* on Madeira: habitat, body size, and morphology (Diplopoda, Julida: Julidae). Revue d'écologie et de biologie du sol 20(3): 403–415.

Enghoff H (2011) The millipede genera *Cylindroiulus* and *Dolichoiulus* as examples of Macaronesian species swarms. In: Serrano ARM, Borges PAV, Boieiro M, Oromí P (Eds) Terrestrial arthropods of Macaronesia – Biodiversity, ecology and evolution. Sociedade Portuguesa de Entomologia, Lisboa, 231–247.

Enghoff H, Reboleira ASPS (2013) Subterranean species of *Acipes* Attems, 1937 (Diplopoda, Julida, Blaniulidae). Zootaxa 3652(4): 485–491. https://doi.org/10.11646/zootaxa.3652.4.6

Enghoff H, Reboleira ASPS (2017) Diversity of non–Laboulbenialean fungi on millipedes. Studies in Fungi 2(1): 130–137. https://doi.org/10.5943/sif/2/1/15

Fage L (1931) Araneae, 5e série, précédée d'un essai sur l'évolution souterraine et son déterminisme. In: Biospeologica, LV. Archives de Zoologie Expérimentale et Générale 71: 91–291.

Gama MM (1962) Collemboles des Grottes du Portugal. Voyage au Portugal du Dr. K. Lindberg. Boletim da Sociedade Portuguesa de Ciências Naturais 2 Sér, 9: 100–108.

Kime RD, Enghoff H (2017) Atlas of European millipedes 2: Order Julida (Class Diplopoda). European Journal of Taxonomy 346: 1–299. https://doi.org/10.5852/ejt.2017.346

Leach WE (1814) A tabular view of the external characters of four classes of animals, which Linné arranged under Insecta; with the distribution of the genera composing three of these classes into orders, etc. and descriptions of several new genera and species. Transactions of the Linnean Society of London 11(2): 306–400. https://doi.org/10.1111/j.1096-3642.1813.tb00065.x

Porat CO (1870) Om några Myriopoda från Azorerna. Öfversigt av Kongliga Vetenskaps. Akademiens Förhandlingar 1870(7): 813–823. [pl 10]

Read HJ (1989a) New species and records of the *Cylindroiulus madeirae*-group, with notes on the phylogenetic relationships (Diplopda, Julida: Julidae). Entomologica Scandinavica 19: 333–347. https://doi.org/10.1163/187631289X00212

Read HJ (1989b) The *Cylindroiulus perforatus*-group, with a description of a new species and notes on variation within *C. perforatus* Verhoeff, 1905 (Diplopda, Julida : Julidae). Entomologica Scandinavica 20: 243–249. https://doi.org/10.1163/187631289X00311

Read HJ (1990) The generic composition and relationships of the Cylindroiulini – a cladistic analysis (Diplopoda, Julida, Julidae. Entomologica Scandinavica 21: 97–112. https://doi.org/10.1163/187631290X00085

Read HJ (1992) The genus *Cylindroiulus* Verhoeff 1894 in the faunas of the Caucasus, Turkey and Iran. Senckenbergiana biologica 72: 373–433.

Read HJ (1994) The millipede genus *Cylindroiulus* Verhoeff, 1894, in Middle Asia (Diplopoda Julida Julidae). Arthropoda Selecta 3(1–2): 117–132.

Read HJ (2005) A revision of the *Cylindroiulus distinctus* Lucas group from north Africa, with descriptions of six new species (Diplopoda, Julida, Julidae). Journal of Natural History 39(18): 1491–1532. https://doi.org/10.1080/00222930420001936 89

Read HJ (2007) The millipede genus *Cylindroiulus* Verhoeff, 1894 in north-west Spain and northern Portugal: recent records and descriptions of four new species (Diplopoda, Julida, Julidae). Graellsia 63: 279–294. https://doi.org/10.3989/graellsia.2007.v63.i2.95

Reboleira ASPS (2007) Cave beetles (Insecta, Coleoptera) of Estremenho karstic massif: an approach to its biodiversity. M.Sc. thesis. Department of Biology, University of Aveiro, 74 pp. http://hdl.handle.net/10773/721

Reboleira ASPS (2012) Biodiversity and conservation of subterranean fauna of Portuguese karst. PhD Thesis, University of Aveiro, 333 pp. http://hdl.handle.net/10773/10865

Reboleira ASPS, Gonçalves F, Serrano A (2009) Two new species of cave-dwelling beetles *Trechus* Clairville of *fulvus*-group in Portugal. Deutsche Entomologische Zeitschrift 56(1): 101–107. https://doi.org/10.1002/mmnd.200900009

Reboleira ASPS, Sendra A, Gonçalves F, Oromí P (2010) The first hypogean dipluran from Portugal: description of a new species of the genus *Litocampa* (Diplura: Campodeidae). Zootaxa 2728: 50–56.

Reboleira ASPS, Ortuño VM (2011) Description of the larva and female genitalia of *Trechus gamae* with data on its ecology. Bulletin of Insectology 64(1): 43–52.

Reboleira ASPS, Borges PAV, Gonçalves F, Serrano A, Oromí P (2011) The subterranean fauna of a biodiversity hotspot region – Portugal: an overview and its conservation. International Journal of Speleology 40(1): 23–37. https://doi.org/10.5038/1827-806X.40.1.4

Reboleira ASPS, Enghoff H (2013a) The genus *Boreviulisoma* Brolemann, 1928 – an Iberian-N African outlier of a mainly tropical tribe of millipedes (Diplopoda: Polydesmida: Paradoxosomatidae). Zootaxa 3646: 516–528. https://doi.org/10.11646/zootaxa.3646.5.2

Reboleira ASPS, Enghoff H (2013b) A new cave-dwelling millipede of the genus *Scutogona* from central Portugal (Diplopoda, Chordeumatida, Chamaesomatidae). Zootaxa 3736(2), 175–186. https://doi.org/10.11646/zootaxa.3736.2.5

Reboleira ASPS, Enghoff H (2014a) Millipedes (Diplopoda) from caves of Portugal. Journal of Cave and Karst Studies 76(1): 20–25. https://doi.org/10.4311/2013LSC0113

Reboleira ASPS, Enghoff H (2014b) *Sireuma*, a new genus of subterranean millipedes from the Iberian Peninsula (Diplopoda, Chordeumatida, Opisthocheiridae). Zootaxa 3785(1): 79–86. https://doi.org/10.11646/zootaxa.3785.1.6

Reboleira ASPS, Enghoff H (2014c) Insular species swarm goes underground: two new troglobiont *Cylindroiulus* millipedes from Madeira (Diplopoda: Julidae). Zootaxa 3785(3): 481–489. https://doi.org/10.11646/zootaxa.3785.3.9

Reboleira ASPS, Enghoff H (2017) Subterranean millipedes (Diplopoda) of the Iberian Peninsula. Zootaxa 4317(2): 355–369. https://doi.org/10.11646/zootaxa.4317.2.10

Schubart O (1934) Tausendfüssler oder Myriapoda. I: Diplopoda. Tierwelt Deutchlands 28: 1–318.

Silvestri F (1896) Una excursion in Tunisia (Symphyla, Chilopoda, Diplopoda). Naturalista Siciliano An. I (Nuova Serie) (8–12): 143–161. [pl 7]

Silvestri F (1932) Campodeidae (Thysanura) de Espana (primera parte). Eos 8: 115–164.

Vandel A (1946) Crustacés isopodes terrestres (Oniscoïdea) épigés et cavernicoles du Portugal. Anais da Faculdade de Ciências do Porto 30: 135–427.

Verhoeff C (1891) Ein Beitrag zur mitteleuropäischen Diplopoden-Fauna. Berliner entomologische Zeitschrift 36(1): 115–166. [4 pls]

Verhoeff C (1894) Beiträge zur Systematik und Anatomie der Iuliden. Versuch einer natürlichen Gruppierung derselben. Verhandlungen der Zoologisch-Botanischen Gesellschaft in Wien 44: 137–162. [2 pls]

Verhoeff C (1899) Beiträge zur Kenntnis paläariktischer Myriopoden. IX. Aufsatz: Zur Systematik, Phylogenie und vergleichenden Morphologie der Juliden und über sinige andere Diplopoden. Archiv für Naturgeschichte 65(1): 183–220.

Verhoeff C (1900) Beiträge zur Kenntniss paläarktischer Myriopoden. XIII. Aufsatz: Zur vergleichenden Morphologie, Phylogenie, Gruppen- und Art-Systematik der Ascospermophora. Archiv für Naturgeschichte 66(1): 347–402.

Verhoeff KW (1905) Anmerkungen zu den Tafelwerken von C. L. Koch, die Myriapoden und A. Berlese (F. Silvestri) Acari, Miriapodi e Scorpioni italiani. Zur Klärung einiger Diplopoden-Gruppen und über einen neuen Iuliden. Notizen zu einigen neueren Arbeiten von C. Attems und übr zwei neue *Polybothrus*. Zoologischer Anzeiger 29(16): 497–514.

Wood HC (1864) Descriptions of new species of North American Iulidae. Proceedings of the Academy of Natural Sciences of Philadelphia 1864: 10–15.

ZooKeys 795: 105–114 (2018)
doi: 10.3897/zookeys.795.29140
http://zookeys.pensoft.net

RESEARCH ARTICLE

A peer-reviewed open-access journal
ZooKeys
Launched to accelerate biodiversity research

Description of a new species of *Dacus* from Sri Lanka, and new country distribution records (Diptera, Tephritidae, Dacinae)

Luc Leblanc[1], Camiel Doorenweerd[2], Michael San Jose[2], U.G.A.I. Sirisena[3], K.S. Hemachandra[4], Daniel Rubinoff[2]

1 *University of Idaho, Department of Entomology, Plant Pathology and Nematology, 875 Perimeter Drive, MS2329, Moscow, Idaho, 83844-2329, USA* **2** *University of Hawaii, Department of Plant and Environmental Protection Services, 3050 Maile Way, Honolulu, Hawaii, 96822-2231, USA* **3** *Department of Plant Sciences, Faculty of Agriculture, Rajarata University of Sri Lanka, Puliyankulama, Sri Lanka* **4** *Faculty of Agriculture, University of Peradeniya, Peradeniya, Sri Lanka*

Corresponding author: *Luc Leblanc* (leblancl@uidaho.edu)

Academic editor: *Martin Hauser* | Received 16 August 2018 | Accepted 22 October 2018 | Published 8 November 2018

http://zoobank.org/B96EFA27-3248-4A22-80C9-D96A7738E0AB

Citation: Leblanc L, Doorenweerd C, Jose MS, Sirisena UGAI, Hemachandra KS, Rubinoff D (2018) Description of a new species of *Dacus* from Sri Lanka, and new country distribution records (Diptera, Tephritidae, Dacinae). ZooKeys 795: 105–114. https://doi.org/10.3897/zookeys.795.29140

Abstract

A fruit fly survey in the Sinharaja and Knuckles National Parks in Sri Lanka (2016), using traps baited with the male lures methyl eugenol, cue-lure, and zingerone, yielded 21 species of Dacini fruit flies. Of these, three species, viz. *Bactrocera amarambalensis* Drew, *B. dongnaiae* Drew & Romig, and *B. rubigina* (Wang & Zhao), are new country occurrence records, and *Dacus* (*Mellesis*) *ancoralis* Leblanc & Doorenweerd, **sp. n.** is described as a new species. The Sri Lankan Dacini fruit fly fauna is now comprised of 39 species.

Keywords

Bactrocera, Dacini, pest, taxonomy, *Zeugodacus*

Copyright *Luc Leblanc et al.* This is an open access article distributed under the terms of the Creative Commons Attribution License (CC BY 4.0), which permits unrestricted use, distribution, and reproduction in any medium, provided the original author and source are credited.

Introduction

Dacine fruit flies are a large group of Old World tropical Diptera, with 932 described species, of which 83 are pests of fruit and fleshy vegetables (Vargas et al. 2015, Doorenweerd et al. 2018). Previous intensive surveys were carried out in Sri Lanka between 1993 and 1996 and resulted in a greatly improved understanding of the island's diversity of fruit flies, including the description of eleven new species (Tsuruta et al. 1997, 2005, Tsuruta and White 2001). This increased the number of known species for Sri Lanka to 35 (Drew and Romig 2013, 2016). We report here the results of new surveys carried out twenty years after the last one, which include three new country occurrence records, and we describe one new species of *Dacus*.

Materials and methods

We built traps from modified urine sample cups (described in Leblanc et al. 2015a) and deployed them along walking trails for 2–5 days in August 2015, to sample fruit flies in the Sinharaja National Park (40 sites) and the Knuckles National Park (31 sites). At each site, we maintained three traps, separately baited with the fruit fly lures methyl eugenol, cue-lure and zingerone. We used a 1×1 cm strip of dichlorvos insecticide to kill the flies entering traps. Collected specimens were preserved in 95% ethanol and later stored in a -20 °C freezer for long-term conservation, or double-mounted using 10 mm minuten pins. Prior to final mounting, we soaked minuten-pinned specimens for 3–12 hours in ethyl ether, to preserve the coloration. We identified flies using available keys (Tsuruta and White 2001, Drew and Romig 2016). We photographed the newly described species using a Nikon D7100 camera attached to an Olympus SZX10 microscope, with Helicon Focus pro v6.7.1 software used to stack photos taken at different focal planes. We took measurements using an ocular grid mounted on an Olympus SZ30 dissecting microscope. Morphological terms used in the description generally follow White (1999) and generic assignment for each species follows the checklist published by Doorenweerd et al. (2018). We extracted DNA and sequenced the mitochondrial COI-3P and COI-5P region from selected specimens to help confirm species identity. The entirety of the mitochondrial gene COI was sequenced using two PCR primers L1-DCHIM (5'-TCGCCTAAACTTCAGCCATT-3') and PAT-K508 (5'-TCCAATGCAC and two additional internal primers (HCO-2198, 5'-TAAACTTCAGGGTGACCAAAAAAT-CA-3' and HCO-2198RC 5'-TGATTTTTTGGTCACCCTGAAGTTTA-3') resulting in a 1,535 base-pair (bp) long fragment. We sequenced up to six additional genes (two fragments of CAD, Wingless, White-eye, PGD, EF1-alpha and Period) for selected representatives of all species, including the one described here, and already available from a published dataset (San Jose et al. 2018). Pairwise genetic distance (p-distance) between specimens was calculated in Geneious R10.2.3. We performed maximum likelihood analysis of 1535 base-pairs of COI (3P + 5P region) of the newly described species and several closely related congeners using RaxML v8.2.11 (Stamatakis 2014).

We repeated the best-scoring tree search 20 times and employed 1,000 multiparametric bootstrap searches with automatic halting following the extended majority rule criterion, halting the bootstraps after 200 searches, to estimate branch support. All specimen taxonomy and collecting data, as well as DNA sequences have been added to BOLD (dx.doi.org/10.5883/DS-DACANC) and the sequences have been deposited in Genbank (COI-5P: MH272136–MH272144 and COI-3P: MH272145–MH272155).

Results

We collected a total of 3,498 specimens representing 21 species; 14 species in Sinharaja N.P. and 15 in Knuckles N.P. (Table 1). The majority (76.0 %) belong to seven pest species, dominated (64.5%) by *Bactrocera kandiensis* Drew and Hancock. We treat the previously described *Bactrocera invadens* Drew, Tsuruta and White (Drew et al. 2005) as a junior synonym of *B. dorsalis* (see Schutze et al. 2015). Three species represent new country records: *B. rubigina* (Wang and Zhao), *B. dongnaiae* Drew and Romig, and *B. amarambalensis* Drew, and one new species, *Dacus ancoralis* Leblanc & Doorenweerd, is described below, increasing the number of species known to occur in Sri Lanka to 39 (Table 1).

One species not attracted to the traditional male lures, *B. syzygii* White & Tsuruta, was captured in zingerone-baited traps, as well as cue-lure responding *B. bipustulata* (Bezzi), *B. perigrapha* White & Tsuruta, *B. rubigina* (Wang & Zhao), and *Dacus discophorus* (Hering). The new species was also collected at zingerone. The specimen identified as *B. amarambalensis* Drew was collected in a cue-lure trap, whereas the two other known specimens (holotype and paratype) were collected at methyl eugenol. This may represent lure contamination or a superficially very similar species that shares the markings on postpronotal lobes and other distinctive features of the described species.

In addition to fruit flies, lacewings (Neuroptera: Chrysopidae) were collected in the methyl eugenol traps (133 specimens in Sinharaja N.P. and 55 in Knuckles N.P.). All specimens are consistent with *Ankylopteryx anomala*, a widely distributed species previously recorded from Sri Lanka (Breitkreuz et al. 2015), and for which attraction to methyl eugenol is well documented (Leblanc et al. 2015b).

Dacus (*Mellesis*) *ancoralis* Leblanc & Doorenweerd, sp. n.

http://zoobank.org/1AA99C05-4095-45F3-B508-774FAC0414C4

Holotype. Male. Labeled: "Sri Lanka: Sinharaja Forest Reserve, 6.3645N, 80.4786E, 22–24-viii-2016, D. Rubinoff, M. San Jose and U.G.A.I. Sirisena, FF638, zingerone trap, molecular voucher ms7321." Deposited in the University of Hawaii Insect Museum (UHIM).

Differential diagnosis. *Dacus ancoralis* is similar to other Asian species of *Dacus* with a red-brown scutum lacking the yellow medial and lateral vittae and with a costal

Table 1. Checklist of Dacine fruit flies of Sri Lanka, including three new country records and one new species, and number of specimens collected in Sinharaja and Knuckles National Parks in 2016.

Species	Distribution outside of Sri Lanka	PEST Status	Lure	Sinharaja N.P.	Knuckles N.P.
B. amarambalensis Drew*	Southern India	Non-pest	CL [1]	0	1
B. apicofuscans White & Tsuruta	Southern India	Non-pest	ME	0	1
B. bipustulata (Bezzi)	Southern India	Non-pest	CL, ZN [2]	233	57
B. brunneola White & Tsuruta	Endemic to Sri Lanka	Non-pest	0	0	0
B. ceylanica Tsuruta & White	Endemic to Sri Lanka	Non-pest	CL	0	4
B. correcta (Bezzi)	Widespread in Asia	Fruit pest (polyphagous)	ME	10	58
B. dongnaiae Drew & Romig*	Vietnam	Non-pest	CL	3	0
B. dorsalis (Hendel)	Widespread in Asia, invasive in Africa and Oceania	Fruit pest (polyphagous)	ME	174	91
B. fastigata Tsuruta & White	Southern India	Non-pest	CL	0	0
B. fernandoi Tsuruta & White	Endemic to Sri Lanka	Non-pest	CL	0	0
B. garciniae Bezzi	Endemic to Sri Lanka	Non-pest	No lure	0	0
B. hantanae Tsuruta & White	Endemic to Sri Lanka	Non-pest	CL	12	0
B. kandiensis Drew & Hancock	Endemic to Sri Lanka	Fruit pest (polyphagous)	ME	1709	542
B. latifrons (Hendel)	Widespread in Asia, invasive in Africa and Oceania	Fruit pest (oligophagous)	Latilure	0	0
B. nigrofemoralis White & Tsuruta	Pakistan, India, Bhutan	Non-pest	CL	2	0
B. nigrotibialis (Perkins)	India to Malaysia	Fruit pest (oligophagous)	CL	0	0
B. paraverbascifoliae Drew	Southern India	Non-pest	ME	0	0
B. perigrapha White & Tsuruta	Bhutan	Non-pest	CL, ZN [2]	119	100
B. profunda Tsuruta & White	Endemic to Sri Lanka	Non-pest	CL	0	0
B. rubigina (Wang & Zhao)*	Bangladesh to Vietnam, Taiwan (new record)	Non-pest	CL, ZN [2]	118	0
B. selenophora Tsuruta & White	Endemic to Sri Lanka	Non-pest	CL	1	0
B. syzygii White & Tsuruta	Vietnam (new record)	Non-pest	ZN [2]	42	144
B. versicolor (Bezzi)	Southern India	Fruit pest (sapodilla)	ME	0	0
B. zonata (Saunders)	Widespread in Asia, invasive in north Africa and Middle East	Fruit pest (polyphagous)	ME	0	1
D. ancoralis Leblanc & Doorenweld*	Endemic to Sri Lanka	Non-pest	ZN [2]	1	0
D. ciliatus Loew	Africa, Middle East, Indian subcontinent	Cucurbit fruit pest	No lure	0	0
D. discophorus (Hering)	Southern India	Non-pest	CL, ZN [2]	0	1
D. keiseri (Hering)	Endemic to Sri Lanka	Non-pest	No lure	0	0
D. persicus Hendel	Middle East, Pakistan, India	Non-pest	No lure	0	0
D. ramanii Drew & Hancock	Southern India	Non-pest	CL	0	0
Z. caudatus (Fabricius)	Widespread in Asia	Cucurbit flower pest	CL	0	1
Z. cucurbitae (Coquillett)	Widespread in Asia, invasive in Africa and Oceania	Cucurbit fruit pest	CL	50	9
Z. diaphorus (Hendel)	Widespread in Asia	Non-pest	CL	0	0
Z. diversus (Coquillett)	Pakistan to Thailand	Cucurbit flower pest	ME	0	0
Z. duplicatus (Bezzi)	Southern India	Non-pest	No lure	0	0
Z. gavisus (Munro)	India	Non-pest	CL	0	0
Z. tau (Walker)	Widespread in Asia	Cucurbit fruit pest	CL	12	1
Z. trilineatus (Hardy)	India, Thailand, Vietnam	Non-pest	CL	0	1
Z. zahadi (Mahmood)	Pakistan to Myanmar	Non-pest	CL	0	0

* New country occurrence records. [1] Uncertain lure record (see text). [2] New lure records. Lure abbreviations: CL = cue-lure, ME = methyl eugenol, ZN = zingerone

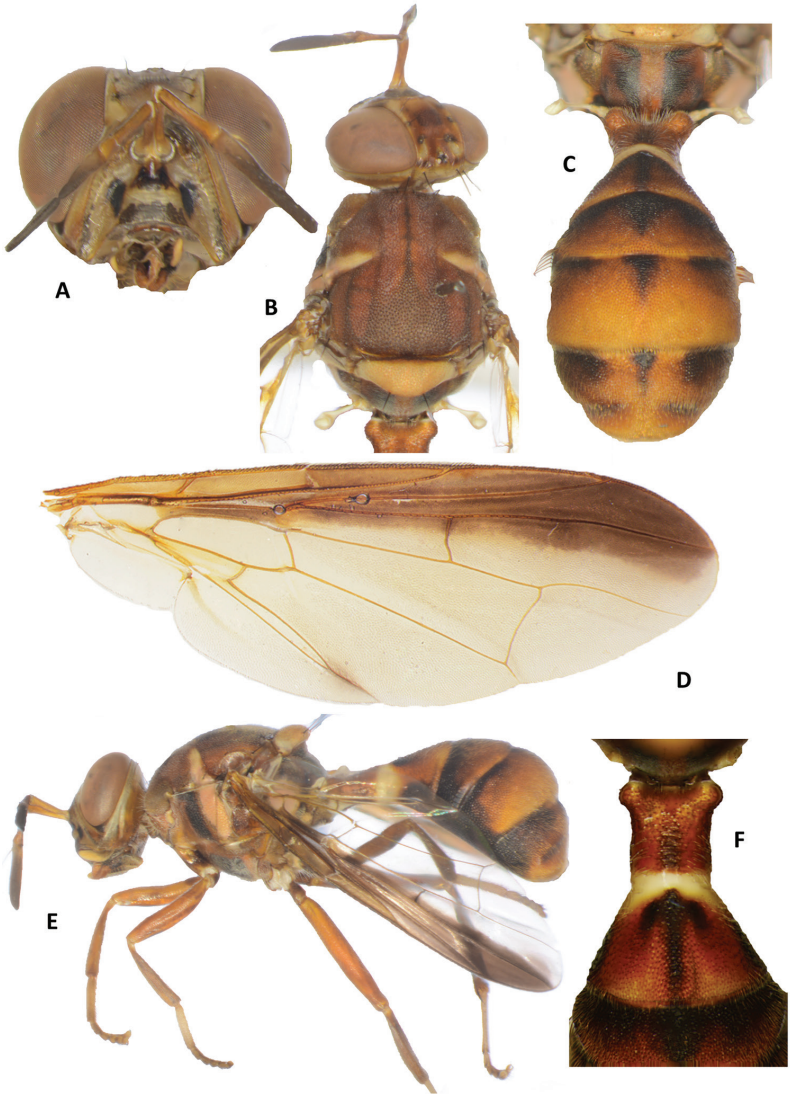

Figure 1. *Dacus* (*Mellesis*) *ancoralis* sp. n. **A** head **B** head and scutum **C** abdomen **D** wing **E** lateral view **F** Abdominal tergum II, with anchor-shaped marking.

band of uniform width that crosses vein R_{4+5} over the entire length of the wing, but does not reach vein M, and fuscous cells bc and c, such as *Dacus polistiformis* (Senior-White), *D. wallacei* White, *D. longicornis* Wiedemann, *D. insulosus* Drew and Hancock and *D. discretus* Drew and Romig. *Dacus ancoralis* differs from *D. polistiformis* and *D. wallacei* in lacking spines on the femur of the front legs, and it differs from all other aforementioned species by having dark fulvous postpronotal lobes. The closely related *D. vijaysegarani* (Figure 2A–E) Drew and Hancock is easily separated by its black scutum, mostly black abdomen and black legs.

Molecular diagnostics. Figure 3 shows the maximum likelihood tree based on combined COI-5P and COI-3P regions (1535 base-pairs [bp]) for *Dacus ancoralis* and the closest congeners in our dataset. In the COI-3P fragment (836 bp), the minimum p-distance to *Dacus vijaysegarani* is 1.38%, and in the COI-5p DNA barcode fragment (658 bp) it is 2.43%. Because there is only one specimen of *D. ancoralis* we cannot test for reciprocal monophyly. The overall next closest relative in our dataset is *D. siamensis*, at a minimum p-distance of 8.61% in COI-3P, 8.81% in COI-5P.

Description of adult. *Head* (Figure 1A). Vertical length 2.00 mm. Frons, of even width, length 1.06 times as long as broad; red-brown with fuscous around orbital setae and on anteromedial hump; latter covered by short red-brown hairs; orbital setae dark fuscous: one pair of superior and two pairs of inferior fronto-orbital setae present; lunule fulvous. Ocellar triangle dark fuscous. Vertex fuscous. Face fulvous with medium sized oval black spots in each antennal furrow, a fuscous band along lower margin between spots and a dark fuscous triangular marking below antennal sockets; length 0.55 mm. Genae red-brown, with fuscous subocular spot; dark fuscous seta present. Occiput fulvous and yellow along eye margins; occipital row with two parallel rows of adjacent setae (with 11 and 17 setae). Antennae with segments 1 (scape) and 2 (pedicel) fulvous and segment 3 (first flagellomere) fuscous; a strong red-brown dorsal seta on segment 2; arista black (fulvous basally); length of segments: 0.83 mm; 0.70 mm; 1.23 mm.

Thorax (Figure 1B, E). Scutum red-brown with a broad light fuscous lanceolate pattern on its posterior third, anteriorly prolonged into three very narrow lines reaching anterior margin, light fuscous narrow outer bands parallel to lanceolate pattern and reaching notopleural suture. Pleural areas red-brown except a broad vertical dark fuscous band in front of mesopleural stripe, a large dark fuscous spot occupying central portion of katepisternum, and a dark fuscous spot on katepimeron above hind coxa. Yellow markings as follows: notopleura (notopleural callus); narrow parallel-sided mesopleural (anepisternal) stripe, reaching midway between anterior margin of notopleura and anterior notopleural seta dorsally, continuing to katepisternum as a transverse spot and to scutum as moderately broad yellow markings along anterior margin of notopleural suture; lower 25% of anatergite (remainder dark fulvous); anterior 70 % of katatergite (remainder black). Postpronotal lobes dark fulvous. Medial and lateral postsutural vittae absent. Postnotum red-brown with two broad longitudinal fuscous bands. Scutellum yellow except for narrow black basal band. Setae (number of pairs): 1 scutellar; prescutellar absent; 1 intraalar; 1 posterior supraalar; 1 anterior supraalar; 1 mesopleural; 2 notopleural; 4 scapular; all setae well developed and black.

Legs (Figure 1E). Femora and tibiae orange-brown, except for fuscous ventral surface of hind femur; mid-tibiae each with an apical black spur; tarsi fulvous.

Wings (Figure 1D). Length 7.00 mm; basal costal (bc) and costal (c) cells fuscous and covered with microtrichia; remainder of wings colorless except dark fuscous subcostal cell, broad dark fuscous costal band overlapping R_{4+5} and of uniform width, not reaching vein M; anal streak absent; supernumerary lobe weakly developed.

Abdomen (Figure 1C, E, F). Elongate, clavate and petiolate; terga tightly joined but with medial protuberances; pecten of cilia present on tergum III; posterior lobe

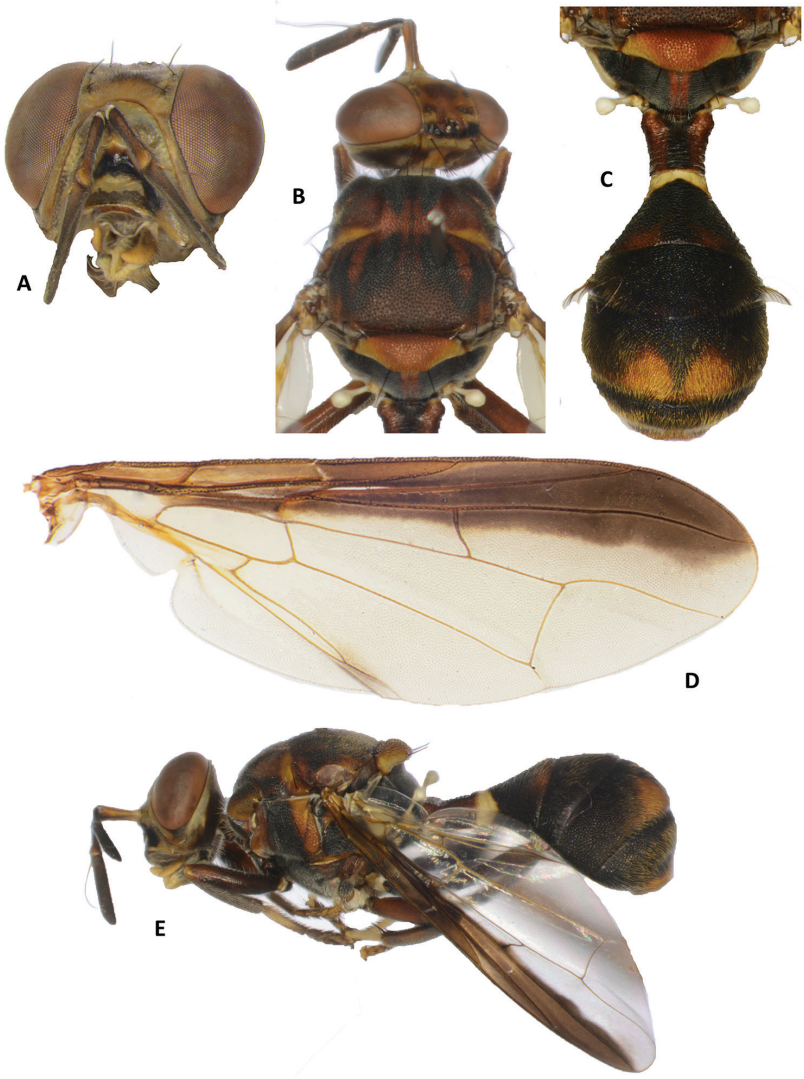

Figure 2. *Dacus* (*Mellesis*) *vijaysegerani* (Drew and Hancock). **A** head **B** head and scutum **C** abdomen **D** wing **E** lateral view.

of surstylus short; abdominal sternum V with a slight concavity on posterior margin. Tergum I and sterna I and II longer than wide. Tergum I orange-brown with apical third yellow and a median light fuscous band on apical half of red-brown portion. Tergum II orange-brown with medial dark fuscous narrow band and two short basal bands, lateral to medial band, forming an anchor-shaped pattern, and broad fuscous markings on lateral margins. Tergum III orange-brown with dark fuscous as along base and extended to whole lateral margins and into a triangular medial band. Tergum IV orange-brown with dark fuscous medial basal triangular marking, narrowly

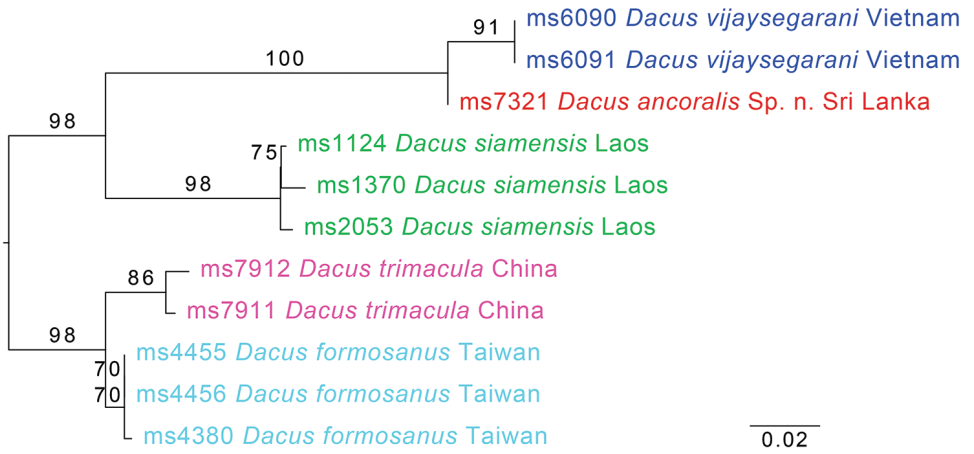

Figure 3. Maximum likelihood tree based on COI (1535 base-pairs) sequence data. Bootstrap support is indicated on the respective branches. Scale bar indicates substitutions per site.

along base of tergum and broadly along entire lateral margins. Tergum V orange-brown with dark fuscous medial basal triangular marking, and large lateral bands covering basal half of tergum and reaching lateral margins. A pair of basally fuscous and apically orange-brown ceromata (shining spots) on tergum V. Abdominal sterna dark except pale sternite II.

Etymology. The name *ancoralis* is a noun in apposition that refers to the anchor-shaped fuscous pattern on abdominal tergum II in the holotype (Figure 1F).

Notes. Although *Dacus ancoralis* is genetically closely related to *D. vijaysegarani* and there is only one specimen, they do not appear to be sympatric, with *D. vijaysegarani* only known from Malaysia, Thailand and Vietnam, and with the clear differences in coloration of all body parts we are confident in describing it as a new species. The holotype of *Dacus ancoralis* was referred to as "ms7321 *Dacus* (*Mellesis*) sp-78", sister to *D. vijaysegarani*, in the seven-gene phylogeny presented in San Jose et al. (2018). It keys to couplet 37 (p 467) in the Keys to the Fruit Flies of South-East Asia (Drew and Romig 2016), where it can be added as a unique combination of having dark fuscous postpronotal lobes and a red-brown scutum. *Dacus ancoralis* was collected in a trap with zingerone lure. A number of other species of *Dacus* were found to be drawn to zingerone in recent years (Doorenweerd et al. 2018), but because there is only one specimen known we cannot yet confirm it as a zingerone-attracted species. This species is assigned to subgenus *Mellesis*, as defined by Drew and Romig (2013) based on the petiolate abdomen with tergum I longer than wide and sternum V weakly concave apically, the presence of anterior supraalar setae and absence of prescutellar setae, the combined length of antennal segment greater than vertical length of face, and the absence of anal streak on wing. Its nearest relatives all belong to subgenus *Mellesis* (Figure 3).

Acknowledgements

We greatly appreciate help from Dan Nitta with molecular work. We thank Norman Barr for providing specimens of *Dacus trimacula* that we could use in the COI reference dataset. Funding for this project was provided by the United States Department of Agriculture (USDA) Farm Bill Section 10007 Plant Pest and Disease Management and Disaster Prevention Program in support of suggestion "Genomic approaches to fruit fly exclusion and pathway analysis": 3.0256-FY15 and 3.0497-FY17. These funds were managed as cooperative agreements between USDA Animal and Plant Health Inspection Service and the University of Hawaii's College of Tropical Agriculture and Human Resources (8130-0565-CA) and the University of Idaho's College of Agriculture and Life Sciences (8130-0665-CA). Additional funding was provided by the USDA Cooperative State Research, Education and Extension (CSREES) project HAW00942-H administered by the College of Tropical Agriculture and Human Resources, University of Hawai'i.

References

Breitkreuz LCV, Winterton SL, Engel MS (2015) Revision of the green lacewing subgenus *Ankylopteryx* (*Sencera*) (Neuroptera, Chrysopidae). ZooKeys 543: 111–127. https://doi.org/10.3897/zookeys.543.6476

Doorenweerd C, Leblanc L, Norrbom AL, San Jose M, Rubinoff R (2018) A global checklist of the 932 fruit fly species in the tribe Dacini (Diptera, Tephritidae). ZooKeys 730: 17–54. https://doi.org/10.3897/zookeys.730.21786

Drew RAI, Romig MC (2013) Tropical fruit flies of South-East Asia. CABI, Wallingford, 655 pp.

Drew RAI, Romig MC (2016) Keys to the Tropical Fruit Flies of South-East Asia. CABI, Wallingford, 487 pp.

Drew RAI, Tsuruta K, White IM (2005) A new species of pest fruit fly (Diptera: Tephritidae: Dacinae) from Sri Lanka and Africa. African Entomology 13: 149–154. https://hdl.handle.net/10520/EJC32620

Leblanc L, Fay H, Sengebau F, San Jose M, Rubinoff D, Pereira R (2015a) A survey of fruit flies (Diptera: Tephritidae: Dacinae) and their Opiine parasitoids (Hymenoptera: Braconidae) in Palau. Proceedings of the Hawaiian Entomological Society 47: 55–66. http://hdl.handle.net/10125/38673

Leblanc L, San Jose M, Bhandari BP, Tauber CA, Rubinoff D (2015b) Attraction of lacewings (Neuroptera: Chrysopidae) to methyl eugenol in Asia. Proceedings of the Hawaiian Entomological Society 47: 67–70. http://hdl.handle.net/10125/38674

San Jose M, Doorenweerd C, Leblanc L, Barr N, Geib SM, Rubinoff D (2018) Incongruence between molecules and morphology: A seven-gene phylogeny of Dacini fruit flies paves the way for reclassification (Diptera: Tephritidae). Molecular Phylogenetics and Evolution. https://doi.org/10.1016/j.ympev.2017.12.001

Schutze MK, Aketarawong N, Amornsak W, Armstrong KF, Augustinos AA, Barr N, Bo W, Bourtzis K, Boykin LM, Cáceres C, Cameron SL, Chapman TA, Chinvinijkul S, Chomic A, De Meyer M, Drosopoulou E, Englezou A, Ekesi S, Gariou-Papalexiou A, Geib SM, Hailstones D, Hasanuzzaman M, Haymer D, Hee AKW, Hendrichs J, Jessup A, Ji Q, Khamis FM, Krosch MN, Leblanc LUC, Mahmood K, Malacrida AR, Mavragani-Tsipidou P, Mwatawala M, Nishida R, Ono H, Reyes J, Rubinoff D, San Jose M, Shelly TE, Srikachar S, Tan KH, Thanaphum S, Haq I, Vijaysegaran S, Wee SL, Yesmin F, Zacharopoulou A, Clarke AR (2015) Synonymization of key pest species within the *Bactrocera dorsalis* species complex (Diptera: Tephritidae): Taxonomic changes based on a review of 20 years of integrative morphological, molecular, cytogenetic, behavioural and chemoecological data. Systematic Entomology 40: 456–471. https://doi.org/10.1111/syen.12113

Stamatakis A (2014) RAxML version 8: A tool for phylogenetic analysis and post-analysis of large phylogenies. Bioinformatics 30: 1312–1313. https://10.1093/bioinformatics/btu033

Tsuruta K, White IM, Bandara HMJ, Rajapakse H, Sundaraperuma, SAH, Kahawatta, SB-MUC, Rajapakse GBJP (1997) A preliminary note on the hosts of fruit flies of the tribe Dacini (Diptera, Tephritidae) in Sri Lanka. Esakia 37: 149–160.

Tsuruta K, White IM (2001) Eleven new species of the genus *Bactrocera* Macquart (Diptera: Tephritidae) from Sri Lanka. Entomological Science 4: 69–87.

Tsuruta K, Bandara HMJ, Rajapakse GBJP (2005) Notes on the Lure Responsiveness of Fruit Flies of the Tribe Dacini (Diptera: Tephritidae) in Sri Lanka. Esakia 45: 179–184.

Vargas RI, Pinero JC, Leblanc L (2015) An overview of pest species of *Bactrocera* fruit flies (Diptera: Tephritidae) and the integration of biopesticides with other biological approaches for their management with a focus on the Pacific region. Insects 6: 297–318. https://doi.org/10.3390/insects6020297

White IM (1999) Morphological Features of the Tribe Dacini (Dacinae): Their Significance to Behavior and Classification. In: Aluja M, Norrbom AL (Eds) Fruit Flies (Tephritidae): Phylogeny and Evolution of Behavior. CRC Press, 505–534. https://doi.org/10.1201/9781420074468.ch20

ZooKeys 795: 115–126 (2018)
doi: 10.3897/zookeys.795.28958
http://zookeys.pensoft.net

RESEARCH ARTICLE

A peer-reviewed open-access journal
ZooKeys
Launched to accelerate biodiversity research

Two new species of *Satsuma* A. Adams, 1868 from Taiwan (Pulmonata, Camaenidae)

Chung-Chi Hwang[1], Shu-Ping Wu[2]

1 *Department of Life Sciences, National University of Kaohsiung, No.700, Kaohsiung University Road, Nan-Tzu District, Kaohsiung 81148, Taiwan* **2** *Department of Earth and Life Sciences, University of Taipei, No.1, Ai-Guo West Road, Taipei 10048, Taiwan*

Corresponding author: *Shu-Ping Wu* (spwu@utaipei.edu.tw)

Academic editor: *Frank Köhler* | Received 8 August 2018 | Accepted 14 September 2018 | Published 8 November 2018

http://zoobank.org/F98D891E-C2B7-4141-9D8C-37CE8D30DA99

Citation: Hwang C-C, Wu S-P (2018) Two new species of *Satsuma* A. Adams, 1868 from Taiwan (Pulmonata, Camaenidae). ZooKeys 795: 115–126. https://doi.org/10.3897/zookeys.795.28958

Abstract

Two new sinistral species of the genus *Satsuma* A. Adams, 1868, *Satsuma squamigera* **sp. n.** and *Satsuma adiriensis* **sp. n.,** from southern Taiwan are described. *Satsuma squamigera* **sp. n.** is characterized by a microsculpture comprising coarse, irregularly-spaced ridges and dense, easily-dislodged triangular scales on its sinistral shell, an angulated periphery, and partly-opened umbilicus. This species inhabits secondary forests in lowland hills. *Satsuma adiriensis* **sp. n.** is characterized by a thin, fragile smooth shell with microsculpture of coarse, loose ridges, a rounded periphery, completely-opened umbilicus, and elongated penial verge formed by two main pilasters. This new species was collected in a mountainous, mid-elevation, broad-leafed forest.

Keywords

anatomy; Gastropoda; land snail; sinistral; Stylommatophora; taxonomy

Introduction

The family Camaenidae, which includes the confamilial Bradybaeninae, is widely distributed in Asia and Australasia (Wade et al. 2007). Recent studies have elucidated the systematics of this family by means of molecular tools (e.g., Wade et al. 2007,

Copyright *C.-C. Hwang, S.-P. Wu.* This is an open access article distributed under the terms of the Creative Commons Attribution License (CC BY 4.0), which permits unrestricted use, distribution, and reproduction in any medium, provided the original author and source are credited.

Hoso et al. 2010, Criscione and Köhler 2014), however significant gaps persist in the documentation of local faunas, such as in the genus *Satsuma* A. Adams, 1868. This genus is distributed in East Asia (Schileyko 2004), containing more than 100 species inhabiting Japan, China, Philippines, and Taiwan (Minato 1988, Wang et al. 2014, Adams and Reeve 1850). Some Vietnamese species, currently assigned to other genera, are likely part of genus *Satsuma* as well (Schileyko 2011). Species of *Satsuma* are characterized by conical, brownish shells varying in shape, size, color, chirality and banding (Schileyko 2004). The reproductive system of this genus features an epiphallic flagellum and a penial caecum, while dart sac, accessory sac, and mucous glands are absent (Kuroda and Habe 1949, Schileyko 2004).

To date, 46 species have been described from Taiwan; most of them are endemic to Taiwan and narrowly distributed (Hsieh et al. 2013, Wu and Tsai 2014, 2015, 2016, Wu and Wu 2017a, 2017b, Hwang et al. 2017). Previous studies have suggested that there are potentially undescribed species in Taiwan, especially in mountainous areas (Wu et al. 2007, 2008, Hwang et al. 2017). In this study, we describe two new Taiwanese species from mountainous areas of lowland and mid-elevation, based on shell morphology and genital anatomy.

Materials and methods

Specimens of the new species were collected in southern Taiwan (Figure 1). Live adults were drowned in water for 12 hours, then boiled briefly in hot water at 95 °C. Whole snails were fixed and preserved in 95% ethanol. Immediately before dissection, the snails' tissues were softened with warm water, and the body was removed from the shell. Empty shells were then cleaned, oven-dried, and stored at room temperature. Reproductive systems were dissected under a stereomicroscope (Leica MZ7.5). Drawings were made using a camera lucida attachment. We used the methods described by Kerney and Cameron (1979) to measure shell characteristics to 0.1 mm and to count the number of whorls to 0.25 whorls. Measurements of genitalia were obtained from the digital images using ImageJ 1.48k (Schneider et al. 2012). We followed Gómez's (2001) terminology in describing the reproductive system. The WGS84 coordinates of localities were recorded. A distribution map was created using the open-source software Quantum GIS 2.18.1 (QGIS Development Team 2016) with topographic databases ASTER GDEM V2 released by NASA and METI (downloadable from https://asterweb.jpl.nasa.gov) and GADM 2.8 released by Global Administrative Areas (downloadable from http://gadm.org/). The type specimens have been deposited in the National Museum of Natural Science, Taichung, Taiwan (NMNS).

Abbreviations

NMNS National Museum of Natural Science, Taichung, Taiwan.

Genitalia:

ag albumen gland;
at atrium;
bc bursa copulatrix;
ep epiphallus;
fl flagellum;
fod free oviduct;
p penis;
pc penial caecum;
pd pedunculus of the bursa copulatrix;
rm retractor muscle;
sod spermoviduct;
v verge;
va vagina;
vd vas deferens.

Shell measurements:

AH aperture height;
AW aperture width;
SH shell height;
SW shell width;
W# number of whorls

Systematics

Family Camaenidae Pilsbry, 1895

***Satsuma* A. Adams, 1868**

Type species. *Helix japonica* Pfeiffer, 1847, by subsequent designation (Kuroda and Habe 1949: 54)

***Satsuma squamigera* sp. n.**
http://zoobank.org/DAAF8145-928F-4755-8132-B1FDF89A4509
Figures 1–3

Type material. Holotype NMNS-7944-001, dry shell and dissected soft part in ethanol, coll. C. C. Hwang, 19 May 2016, collected from type locality; paratype NMNS- 7944-002, 1 specimen: dry shell and dissected soft part in ethanol, coll. S.P. Wu, 24 Jul 2014, collected from type locality; paratypes NMNS-7944-003, 5 specimens: 5 dry shells and 1 dissected soft part in ethanol, coll. S.T. Yang, 11 Feb. 2011, collected from type locality, paratypes NMNS-7944-004, 4 specimens: dry shells, coll. C. C. Hwang, 19 Aug 2014, collected from type locality, paratypes UTM2018001-5, 5 specimens: dry shells, coll. S. P. Wu, 11 May 2012, collected from type locality.

Type locality. Taiwan: Pingtung County, Shih-tze, Ka-yo-fong waterfall (also named Nei-shih waterfall), 22°17.55'N; 120°41.88'E, alt. 170 m, secondary lowland broad-leafed forest (Figure 1A).

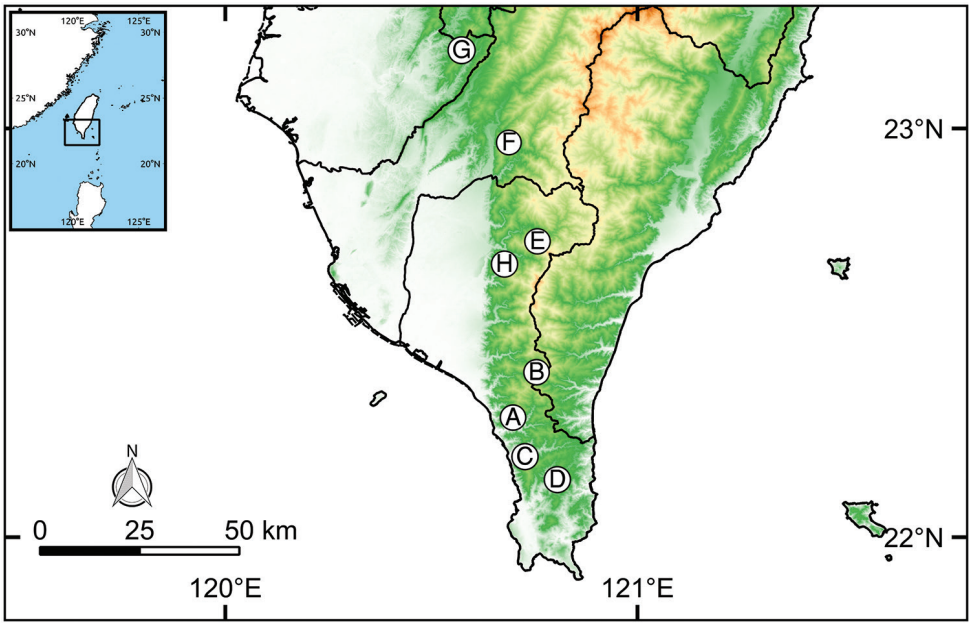

Figure 1. Distribution map of two *Satsuma* species in southern Taiwan. **A–D** *S. squamigera* sp. n.: **A** Kayo-fong waterfall, Shih-tze, Pingtung (type locality) **B** Da-han- shan forest road, Pingtung **C** Mt. Bei-li-long, Pingtung **D** Mu-dang, Pingtung; **E–H** *S. adiriensis* sp. n.: **E** A-li, Wu-tai, Pingtung (type locality) **F** Shan-ping, Liu-guei, Kaohsiung **G** Mt. Fan-bao-jian, Nan-xi, Tainan **H** Ma-jia, Pingtung.

Diagnosis. Shell sinistral with coarse and irregularly ridged and fine striations; surfaces with dense, fine, erected, triangular scales falling off easily; periphery angulated, umbilicus partly opened; penial caecum short, internally with elongated verge formed by two main pilasters.

Description. ***Shell.*** Measurements (n = 11): SH 12.1–13.9 mm, SW 18.5–20.7 mm, AH 6.9–8.2 mm, AW 11.0–12.2 mm, W# 5.5–5.75, SH/SW 0.61–0.71; sinistral, with low conical spire, light brown to dark brown with red-brown peripheral band and umbilicus spot. Apex obtuse. Whorls regularly increasing, slightly convex. Periphery angulated. Base of shell convex. Surface completely covered with dense, fine, erected, curved, triangular, easily-dislodged scales and leaving crescent-shaped trace; upper surface with coarse, oblique axial ridges; spiral striation absent. Aperture roundly lunate. Peristome expanded; outer lip smoothly curved; columellar lip oblique, curve, joining curved basal lip smoothly or in an angle. Parietal callus smooth, thin, transparent. Umbilicus open, 2.6–3.2 mm in width, 1/5 covered by reflected columellar lip.

External morphology. Light brown with irregular, small, dark brown spots and a distinct yellowish line running from head between tentacles to collar. Tentacles dark brown.

Reproductive system. Bursa copulatrix oval with long pedunculus of 27–30 mm. Free oviduct short. Vagina muscular, furrowed externally corresponding to internal folds, 10–12 mm in length. Atrium short, finely wrinkled inside. Penis slender, 10–12

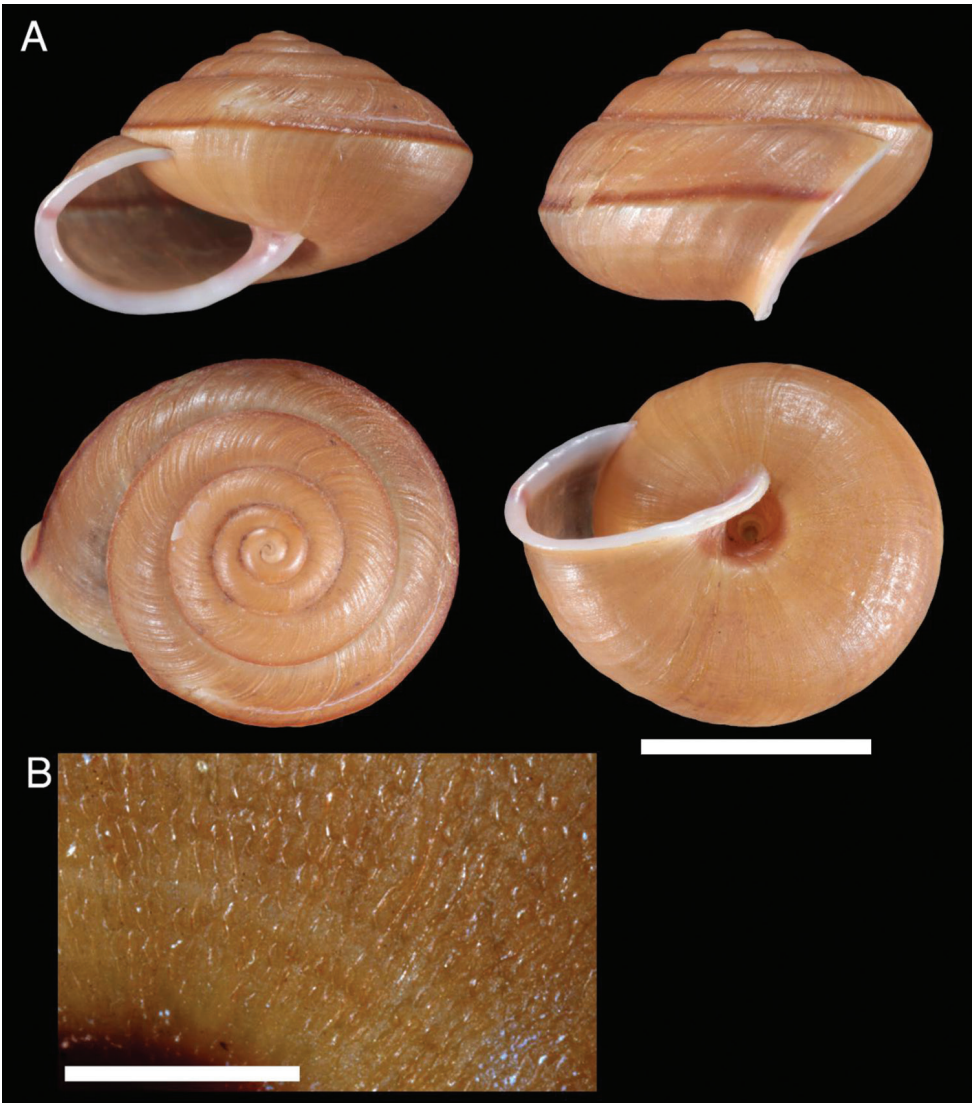

Figure 2. Shell of *Satsuma squamigera* sp. n. **A** shell of holotype (NMNS-7944-001) **B** scales on base of shell (paratype NMNS-794-002). Scale bar: 10 mm (**A**), 2 mm (**B**).

mm in length, evenly thickened, furrowed externally corresponding to 7–8 strong, straight, corrugated pilasters internally. Penial caecum short, protruding 2–3 mm. Verge extending along penial caecum, formed by two main pilasters, with wrinkled surface. Epiphallus slender, 15–17 mm in length, internally with 4 smooth pilasters. Penis retractor muscle attached at distal 1/4 of epiphallus. Flagellum short, tapering.

Etymology. From *squamigera* (Latin, adjective in the nominative feminine singular case) meaning scale-bearing, for the scaly shell surface.

Distribution. This species was found in southern Pingtung County, including the type locality, Da-han-shan forest road (22°24.20'N; 120°45.31'E, alt-1555 m),

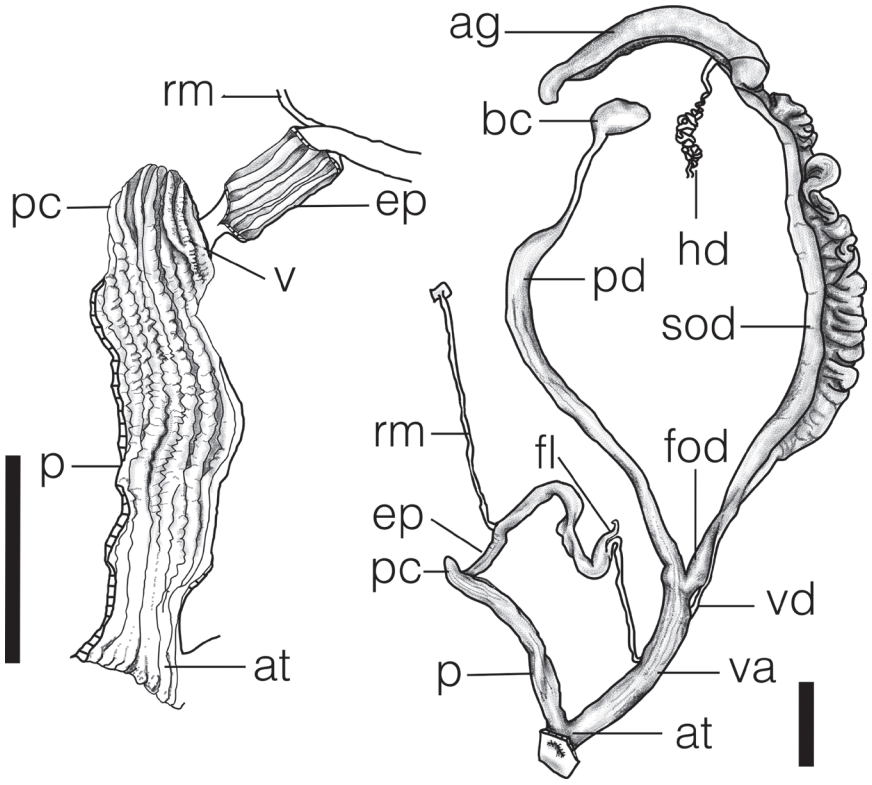

Figure 3. Reproductive system showing whole genitalia and opened penis of *Satsuma squamigera* sp. n. (holotype NMNS-7944-001). Scale bar: 5 mm.

Mt. Bei-li-long (22°11.81'N; 120°43.63'E, alt-320 m) and Mu-dang (22°8.43'N; 120°48.34'E, alt-240 m) (Figure 1A–D).

Ecology. All specimens were collected in mountainous, lowland, broad-leafed forest. Mature adults were collected in mid-May and February, from ground, rocks or fallen tree trunks. This species is sympatric with the congeners *Satsuma bacca* (Pfeiffer, 1866), *Satsuma batanica pancala* (Schmacker & Boettger, 1891) and *Satsuma longkiauwensis* Wu, Lin & Hwang, 2007.

Remarks. *Satsuma squamigera* sp. n. is distinguished from all other sinistral species by having dense and curved scales on the whole shell surface. When fully matured, the scales typically fall off, leaving crescent-shaped granules. Some intact scales may remain beside sutures, on the base of the last whorl or inside the umbilicus. The new species is similar to *S. pekanensis* (Rolle, 1911) and *S. submeridionalis* (Zilch, 1951) in shape of shell and angulated periphery. In comparison to *S. pekanensis,* the new species has a shortened spire and an extended flagellum (Chang 1989). The new species differs from *S. submeridionalis* in having a slender base of pedunculus of bursa copulatrix and a regularly thickened proximal vagina (Wang et al. 2014).

***Satsuma adiriensis* sp. n.**
http://zoobank.org/676C67FF-BC84-4DE6-9D6E-12C30768DBB9
Figures 4–5

Type material. Holotype NMNS-7945-001, dry shell, coll. C. C. Hwang, 24 Aug 1998, collected from type locality; paratype NMNS-7945-002, 1 specimen: dry shell and dissected soft part in ethanol, coll. S. C. Chang , 4 Jul 1997, Shan-ping, Liu-guei, Kaohsiung, 22°57.93'N; 120°41.28'E, alt. 850 m; paratype NMNS-7945-003, 1 dry shell, coll. C. C. Hwang, 25 May 1998, Mt. Fan-bao-jian, Nan-xi, Tainan, 22°71.48'N; 120°34.4'E, alt. 1000 m; paratype NMNS-7945-004, 1 dry subadult shell, coll. G. S. Hsiang, 29 Jun 1997, Ma-jia, Pingtung, 22°40.07'N; 120°40.65'E, alt. 1200 m.

Type locality. Taiwan: Pingtung County, Wu-tai, A-li, 22°43.42'N; 120°45.44'E, alt. 1350 m, disturbed primary broad-leaf forest.

Diagnosis. Shell sinistral, thin, fragile, smooth, with spaced, coarse ridges; periphery round, color band absent; umbilicus completely opened; penial caecum long, internally with elongated verge formed by two main pilasters.

Description. ***Shell.*** Measurements (n = 3): SH 10.8–12.9 mm, SW 17.4–20.6 mm, AH 6.9–8.5 mm, AW 8.6–10.3 mm, W# 5.5, SH/SW 0.61–0.68; sinistral, thin, fragile, semi-translucent, with low conic spire, light brown, without color band. Apex obtuse. Whorls regularly increasing, slightly convex. Periphery bluntly angulated on the first 3/4 of last whorl, becoming rounded 1/4 whorl before peristome. Base of shell convex. Surface covered with loose, coarse, oblique axial ridges, becoming thin on base; spiral striation absent. Aperture roundly lunate. Peristome expanded; outer lip smoothly curved; columellar lip sub-vertical, not reflected, joining with basal lip in a weak angle. Parietal callus smooth, thin, transparent. Umbilicus completely opened, 3.3–3.6 mm in width.

External morphology. Light brown with dense, irregular, dark brown to black spots and a distinct yellowish line running from head between tentacles to collar. Tentacles dark brown.

Reproductive system. Bursa copulatrix oval; pedunculus long, 31 mm in length, with slightly expanded base. Free oviduct short. Vagina thickened, smooth externally, with eleven internal pilasters, 11 mm in length. Atrium obvious, finely wrinkled inside. Penis muscular, 13 mm in length, evenly thickened, furrowed externally; distal half internally supporting three main, finely wrinkled pilasters; proximal half supporting eleven strong, corrugated pilasters. Penial caecum thickened, with blunt apex, protruding 7 mm. Verge extending along penial caecum, formed by two main pilasters. Epiphallus slender, 16 mm in length, internally with three smooth pilasters. Penis retractor muscle attached at distal 1/6 of epiphallus. Flagellum long, tapering, slightly wavy at middle portion.

Etymology. For Adiri, the indigenous Rukai name of the type locality, adjective of feminine gender.

Distribution. Known from mid-elevation forest of Kaohsiung, Tainan and Pingtung (Figure 1E–H).

Ecology. All specimens were collected in mountainous, mid-elevation, broad-leaf forest. The single live adult was collected in July, from a tree trunk. This species is sym-

Figure 4. Shell of *Satsuma adiriensis* sp. n. (holotype NMNS-7945-001). Scale bar: 10 mm.

patric with congeneric species *S. albida* (Adams, 1870) and *S. friesiana* (Moellendorff, 1884) at Shan-ping, *S. amblytropis* (Pilsbry, 1901) at Mt. Fan-bao-jian and an unknown *Satsuma* at the type locality A-li. Despite wide distribution in the mountainous areas of southwestern Taiwan, this species is quite rare.

Remarks. *Satsuma adiriensis* sp. n. is similar to *S. contraria* (Pilsbry & Hirase, 1909), distributed in Kenting, Pingtung, in having a sinistral, semi-transparent shell with completely open umbilicus. The new species, however, has smaller shell width, round periphery on the final 1/4 of the last whorl, a sub-vertical columellar lip, a sinuous upper lip, coarse ridges on the surface, a slender pedunculus of bursa copulatrix, and a longer penial caecum and flagellum and shorter penis than the latter species (Hwang and Ger 2018).

The new species shares a sinistral and depressed conic shell with *Satsuma formosensis* (Pfeiffer, 1866) and *S. yaeyamensis* (Pilsbry, 1894), which are found in northern Taiwan and the Ryukyu Islands. *Satsuma adiriensis* differs from these two species by its thin, semi-transparent shell with loose, coarse surface ridges, a sub-vertical columellar lip joining basal lip in a weak angle, and a bluntly angulated periphery on the first 3/4 of the last whorl.

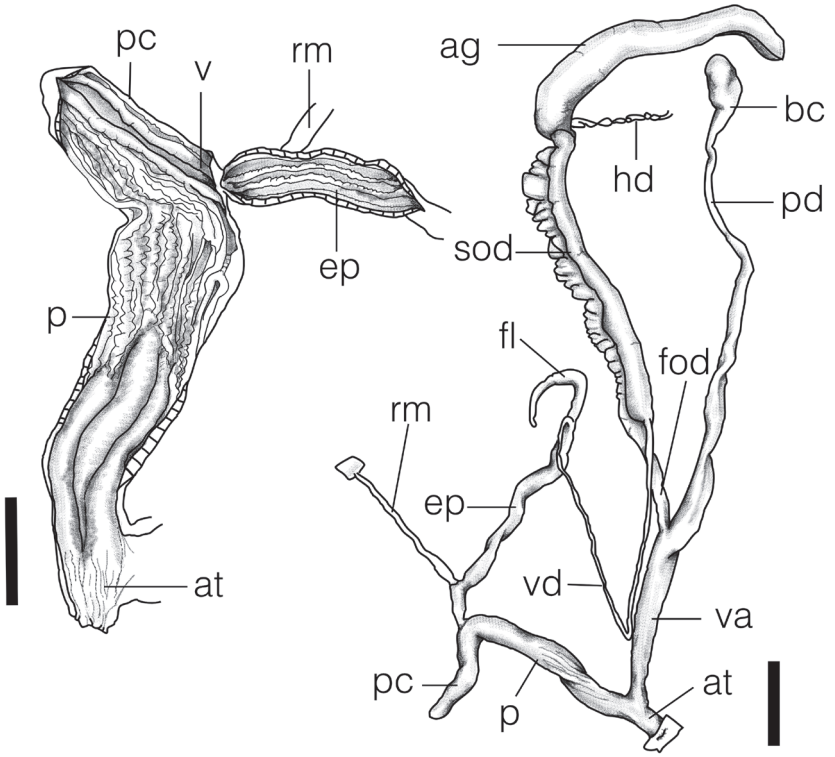

Figure 5. Reproductive system showing whole genitalia and opened penis of *Satsuma adiriensis* sp. n. (paratype NMNS-7945-002). Scale bar: 5 mm.

Discussion

In this study, two new species of sinistral *Satsuma* were described based on shell and reproductive system characteristics. This work has brought the number of known sinistral *Satsuma* species to seventeen. Among these seventeen species, eleven are distributed in Taiwan, three in the Ryukyu Islands, two in southern China, and one in Batan Island, Philippines. The diversification of *Satsuma* has been explained by allopatric speciation (Kameda et al. 2007), prey-predator coevolution and chirality (Hoso et al. 2010), and arboreal behavior (Wu et al. 2008).

Periostracal ornamentations such as granules and hairs are commonly seen in confamilial genera, e.g., *Chloritis* Beck, 1837, *Moellendorffia* Ancey, 1887, *Aegista* Albers, 1850 and many genera from Australia (Solem 1984, Hirano et al. 2014, Criscione and Köhler 2016). In the genus *Satsuma*, granules on embryonic whorls are commonly seen (personal observations), but rarely reported. This under-reporting may be due to the ease with which these granules wear off, or their simply being so small as to evade observation. Three sinistral species, *S. perversa* (Pilsbry, 1931), *S. yaeyamensis* and *S. batanica pancala* have been observed to have granulate embryonic whorls (Azuma

1995, personal observations), however these species do not have scales covering the whole shell surface, as does *S. squamigera* sp. n.

Short, hooked hairs have been observed over the entire shell surface of the sinistral species *S. uncopila* (Heude, 1882). Granules on the entire shell surface are also reported in some dextral species, e.g., *S. ferruginea* (Pilsbry, 1900), *S. textilis* (Pilsbry & Hirase, 1904), *S. japonica granulosa* (Pilsbry, 1902), *S. j. heteroglypta* (Pilsbry, 1900), *S. okiensis* (Pilsbry & Hirase, 1908) and *S. cristata* (Pilsbry, 1902). The hairs are thought to promote the snails' adherence to leaves when humidity levels are high (Pfenninger et al. 2005). The evolutionary significance of these varying ornamentations of size, shape, and position remains questionable. This question will not be adequately answered until more complete phylogeny and comparative studies of the *Satsuma* genus become available.

Author contributions

CC Hwang performed the anatomical studies, executed this study, and wrote the manuscript; SP Wu helped with the data collecting and paper writing.

Acknowledgements

We gratefully acknowledge the assistance of Dr. Hsueh-Wen Chang, Dr. Gao-Shih Hsiang, Ms. Su-Chin Chang, Mr. Chang-Yi Tsai (National Sun Yat-Sen University), Mr. Hsin-Te Yang (Da-Yeh University), Mr. Wei-Hsuan Tsai, Bo-An Lee, Wan-Bao Lee and Chi-Kai Liao (National University of Kaohsiung) and Mr. Chao-Ching Lee in the field works. Thanks are also due to Mr. James Bell for his editorial assistance. This study was partially supported by the Ministry of Science and Technology Grant (MOST 107-2321-B-845-001 -), We also wish to express our gratitude to Forestry Bureau and Taiwan Forestry Research Institute, Council of Agriculture for the permission for collection.

References

Adams A, Reeve L (1850) Mollusca, Part III. In: Adams A (Ed.) The Zoology of the Voyage of H.M.S. Samarang; Under the Command of Captain Sir Edward Belcher C.B., F.R.A.S., F.G.S., During the Years 1843–1846. Reeve, Benham & Reeve, London, 1–87.

Azuma M (1995) Colored Illustrations of the Land Snails of Japan. Hoikusha, 343 pp.

Chang KM (1989) Anatomy of *Coniglobus nux paiwanis* (Kuroda) and *Coniglobus pekanensis* (Rolle) from south Taiwan (Pulmonata: Camaenidae). Bulletin of Malacology 14: 1–8.

Criscione F, Köhler F (2014) Molecular phylogenetics and comparative anatomy of *Kimberleytrachia* Köhler, 2011 – a genus of land snail endemic to the coastal Kimberley, Western Australia with description of new taxa (Gastropoda, Camaenidae). Contributions to Zoology 83: 245–267. http://www.ctoz.nl/vol83/nr04/a03

Criscione F, Köhler F (2016) *Setobaudinia nicolasi* – a new species from Baudin Island, Kimberley, Western Australia (Stylommatophora, Camaenidae). Molluscan Research 36: 290–293. https://doi.org/10.1080/13235818.2016.1201037

Gómez BJ (2001) Structure and functioning of the reproductive system. In: Baker GM (Ed.) The Biology of Terrestrial Molluscs. CABI Publishing, Oxon, 307–330. https://doi.org/10.1079/9780851993188.0307

Hirano T, Kameda Y, Kimura K, Chiba S (2014) Substantial incongruence among the morphology, taxonomy, and molecular phylogeny of the land snails *Aegista*, *Landouria*, *Trishoplita*, and *Pseudobuliminus* (Pulmonata: Bradybaenidae) occurring in East Asia. Molecular Phylogenetics and Evolution 70: 171–181. https://doi.org/10.1016/j.ympev.2013.09.020

Hoso M, Kameda Y, Wu SP, Asami T, Kato M, Hori M (2010) A speciation gene for left-right reversal in snails results in anti-predator adaptation. Nature Communications 1: 133. https://doi.org/10.1038/ncomms1133

Hsieh BC, Wu SP, Tsai CL (2013) Land Snails of Taiwan (3rd edn). Forestry Bureau, Council of Agriculture, Executive Yuan, Taiwan, 381 pp.

Hwang CC, Ger MJ (2018) Reproductive system of land snail *Satsuma contraria* (Stylommatophora: Camaenidae). Bulletin of Malacology 41: 36–45.

Hwang CC, Okubo K, Tada A (2017) *Satsuma jinlunensis* – a new species from Taiwan (Stylommatophora: Camaenidae). Molluscan Research. https://doi.org/10.1080/13235818.2017.1358340

Kameda Y, Kawakita A, Kato M (2007) Cryptic genetic divergence and associated morphological differentiation in the arboreal land snail *Satsuma* (*Luchuhadra*) *largillierti* (Camaenidae) endemic to the Ryukyu Archipelago, Japan. Molecular Phylogenetics and Evolution 45: 519–533. https://doi.org/10.1016/j.ympev.2007.03.021

Kerney MP, Cameron RAD (1979) Land Snails of Britain & North-west Europe. Harper & Collins, London, 288 pp.

Kuroda T, Habe T (1949) Helicacea. Sanmeisha, Tokyo, 129 pp.

Minato H (1988) A Systematic and Bibliographic List of the Japanese Land Snails. Shirahama, Japan, 294 pp.

Pfenninger M, Hrabáková M, Steinke D, Dèpraz A (2005) Why do snails have hairs? A Bayesian inference of character evolution. BMC Evolutionary Biology 5: 59. https://doi.org/10.1186/1471-2148-5-59

QGIS Development Team (2016) QGIS Geographic Information System. Open Source Geospatial Foundation Project. http://www.qgis.org

Schileyko AA (2004) Treatise on Recent terrestrial pulmonate molluscs, Part 12: Bradybaenidae, Monadeniidae, Xanthonychidae, Epiphragmophoridae, Helminthoglyptidae, Elonidae, Humboldtianidae, Sphincterochilidae, Cochlicellidae. Ruthenica, supplement 2: 1627–1763.

Schileyko AA (2011) Check-list of land pulmonate molluscs of Vietnam (Gastropoda: Stylommatophora). Ruthenica 21: 1–68. https://biotaxa.org/Ruthenica/article/view/3603

Schneider CA, Rasband WS, Eliceiri KW (2012) NIH Image to ImageJ: 25 years of image analysis. Nature Methods 9: 671–675. https://doi.org/10.1038/nmeth.2089

Solem A (1984) Camaenid land snails from Western and central Australia (Mollusca: Pulmonata: Camaenidae). IV. Taxa from the Kimberley, Westraltrachia Iredale, 1933 and related genera. Records of the Western Australian Museum, Supplement 17: 427–705.

Wade CM, Hudelot C, Davison A, Naggs F, Mordan PB (2007) Molecular phylogeny of the helicoid land snails (Pulmonata: Stylommatophora: Helicoidea), with special emphasis on the Camaenidae. Journal of Molluscan Studies 73: 411–415. https://doi.org/10.1093/mollus/eym030

Wang P, Xiao Q, Zhou WC, Hwang CC (2014) Revision of three camaenid and one bradybaenid species (Gastropoda, Stylommatophora) from China based on morphological and molecular data, with description of a new bradybaenid subspecies from Inner Mongolia, China. ZooKeys 372: 1–16. https://doi.org/10.3897/zookeys.372.6581

Wu SP, Hwang CC, Lin YS (2008) Systematic revision of the arboreal snail *Satsuma albida* species complex (Mollusca: Camaenidae) with descriptions of 14 new species from Taiwan. Zoological Journal of the Linnean Society 154: 437–493. https://doi.org/10.1111/j.1096-3642.2008.00415.x

Wu SP, Lin YS, Hwang CC (2007) A new *Satsuma* species (Pulmonata: Camaenidae) endemic to Taiwan. Zootaxa 1608: 59–68.

Wu SP, Tsai CL (2014) A new sinistral *Satsuma* land snail (Pulmonata: Camaenidae) endemic to Taiwan. Bulletin of Malacology 37: 61–72.

Wu SP, Tsai CL (2015) A new endemic dextral *Satsuma* land snail (Pulmonata: Camaenidae) from Taiwan. Bulletin of Malacology 38: 41–48.

Wu SP, Tsai CL (2016) A new dextral species land snail of genus *Satsuma* (Pulmonata: Camaenidae) endemic to Taiwan. Bulletin of Malacology 39: 47–58.

Wu SP, Wu CC (2017a) A new and endemic sinistral *Satsuma* land snail (Pulmonata: Camaenidae) from South Taiwan. Bulletin of Malacology 40: 27–42.

Wu SP, Wu CC (2017b) A new dextral land snail of genus *Satsuma* (Pulmonata: Camaenidae) endemic to Taiwan. Bulletin of Malacology 40: 13–26.

ZooKeys 795: 127–157 (2018)
doi: 10.3897/zookeys.795.27070
http://zookeys.pensoft.net

RESEARCH ARTICLE

A peer-reviewed open-access journal
ZooKeys
Launched to accelerate biodiversity research

Overlooked gall-inducing moths revisited, with the description of *Andescecidium parrai* gen. et sp. n. and *Oliera saizi* sp. n. from Chile (Lepidoptera, Cecidosidae)

Gabriela T. Silva[1], Gilson R.P. Moreira[1], Héctor A. Vargas[2], Gislene L. Gonçalves[2,3], Marina D. Mainardi[4], Germán San Blas[5], Donald Davis[6]

1 *PPG Biologia Animal, Departamento de Zoologia, Instituto de Biociências, Universidade Federal do Rio Grande do Sul, Av. Bento Gonçalves 9500, Porto Alegre, RS, 91501-970, Brazil* **2** *Departamento de Recursos Ambientales, Facultad de Ciencias Agronómicas, Universidad de Tarapacá, Casilla 6-D, Arica, Chile* **3** *PPG Genética e Biologia Molecular, Departamento de Genética, Instituto de Biociências, Universidade Federal do Rio Grande do Sul, Av. Bento Gonçalves 9500, Porto Alegre, RS, 91501-970, Brazil* **4** *Ciências Biológicas, Instituto de Biociências, Universidade Federal do Rio Grande do Sul, Av. Bento Gonçalves, 9500, Porto Alegre, RS 91501-970, Brazil* **5** *Facultad de Ciencias Exactas y Naturales, CONICET, Universidad Nacional de La Pampa, La Pampa 6300, Argentina* **6** *Department of Entomology, National Museum of Natural History, Smithsonian Institution, Washington, DC 37012-7012, USA*

Corresponding author: *Gilson R.P. Moreira* (gilson.moreira@ufrgs.br)

Academic editor: *E. van Nieukerken* | Received 29 May 2018 | Accepted 17 September 2018 | Published 12 November 2018

http://zoobank.org/AC7C3779-0662-4D52-972F-F55556024CA1

Citation: Silva GT, Moreira GRP, Vargas HA, Gonçalves GL, Mainardi MD, Blas GS, Davis D (2018) Overlooked gall-inducing moths revisited, with the description of *Andescecidium parrai* gen. et sp. n. and *Oliera saizi* sp. n. from Chile (Lepidoptera, Cecidosidae). ZooKeys 795: 127–157. https://doi.org/10.3897/zookeys.795.27070

Abstract

There are still many gall systems associated with larvae of Lepidoptera in which the true gall-inducers have not been identified to species. Reports on misidentification of gall inducers have been recurrent for these galls, particularly in complex gall-systems that may include inquilines, kleptoparasites, and cecidophages, among other feeding guilds such as predators and parasitoid wasps. Here we describe and illustrate the adults, larvae, pupae and galls, based on light and scanning microscopy, of *Andescecidium parrai* **gen. et sp. n.** and *Oliera saizi* **sp. n.,** two sympatric cecidosid moths that are associated with *Schinus polygamus* (Cav.) Cabrera (Anacardiaceae) in central Chile. Adults, immatures, and galls of the former did not conform to any known cecidosid genus. Galls of *A. parrai* are external, spherical, and conspicuous, being known for more than one century. However, their induction has been mistakenly associated with either

Copyright *Gabriela T. Silva et al.* This is an open access article distributed under the terms of the Creative Commons Attribution License (CC BY 4.0), which permits unrestricted use, distribution, and reproduction in any medium, provided the original author and source are credited.

unidentified Coleoptera (original description) or *Oliera argentinana* Brèthes (recently), a distinct cecidosid species with distribution restricted to the eastern Andes. Galls of *O. saizi* had been undetected, as they are inconspicuous. They occur under the bark within swollen stems, and may occur on the same plant, adjacent to those of *A. parrai*. We also propose a time-calibrated phylogeny using sequences from mitochondrial and nuclear loci, including specimens of the new proposed taxa. Thus in addition to clarifying the taxonomy of the Chilean cecidosid species we also tested their monophyly in comparison to congeneric species and putative specimens of all genera of Neotropical and African cecidosids.

Keywords
Anacardiaceae, Cecidosid moths, insect galls, Neotropical microlepidoptera, *Schinus polygamus*

Introduction

Cecidosidae are a small group of ancient gall-inducing and stem-mining micromoths restricted in distribution to the Southern Hemisphere. They include seven genera and 19 species that are distributed in southern South America, southern Africa, and New Zealand (for taxonomic reviews see Davis 1988, Hoare and Dugdale 2003, Moreira et al. 2017). In spite of their interesting biology, close association with their Anacardiaceae host-plants (*Schinus* L.) and broad geographical distribution, the diversity of Cecidosidae remains mostly unexplored in the Neotropical region. Their galls may consist of complex ecological systems that involve additional organisms, in addition to the host-plant and corresponding gall-inducer. For example, other insects can act in multi-trophic levels in these galls, as inquilines, kleptoparasites, or cecidophages, among other feeding guilds, including predators, parasitoids or successors that use them just for shelter (Moreira et al. 2017). In the case of kleptoparasites and inquilines, the original inducer might be killed and thereafter the gall is usurped by the invader (Ronquist 1994, van Noort et al. 2007). This type of phenomenon may bring important taxonomic consequences, preventing the correct identification of the real inducer when such systems are undersampled. This situation is found for many gall-inducing insects, including other Lepidoptera (e.g., Morris 2000, van Noort et al. 2007, Luz et al. 2015). This was recently demonstrated in detail for *Cecidonius pampeanus* Moreira and Gonçalves, a cecidosid moth whose identity was overlooked for more than one hundred years, as its galls had been erroneously described as induced by their hymenopteran inquilines (Moreira et al. 2017).

A similar case of such a complex system was recently found for a cecidosid-induced gall in central Chile. In fact, such a spherical, external gall was briefly described for the first time by Kieffer and Herbst (1905), in association with the branches of the Anacardiaceae *Duvaua dependens* (Ortega) DC. [= *S. polygamus* (Cav.) Cabrera] as induced by an unidentified species of *Bruchus* L. (Coleoptera, Chrysomelidae). One year later, the same authors reported this type of gall again, providing in addition illustrations that included a cross-section view of it (Kieffer and Herbst 1906). In his monograph of galls from South and Central American plants later, Houard (1933) reproduced this description and illustrations, associated with the same country, gall-inducer, and host-plant. More than 50 years later, Núñez and Sáiz (1994) working with these galls in the Parque Nacional La Campana, Valparaiso Region, cited the corresponding findings that were

repeated by Houard (1933); however, a note was added by the authors recognizing that the true inducer of the galls belonged to Lepidoptera. Later, Sáiz and Núñez (1997) stated that these were in fact induced by Cecidosidae, but they did not describe the moth. Based on scarce material sent by these authors to the Universidad de Concepción, Parra (1998) described for the first time the corresponding gall-inducer cecidosid moth as conspecific to *Oliera argentinana* Brèthes, a species at that time only known to occur on the eastern side of the Andes (Argentina) and with poorly known immatures. He also synonymized *Oliera* Brèthes with *Cecidoses* Curtis, and proposed *Cecidoses argentinana* (Brèthes), thereafter considered to be the valid species responsible for the induction of *Schinus* galls in Chile. However, Moreira et al. (2012) in a broad study including abundant material of galls from Argentina and Brazil, also including type material, confirmed the original description of *O. argentinana* given by Brèthes (1916), showing that *Oliera* galls are formed under the bark instead, and have different morphology from material described by Parra (1998) based on the larvae, pupae and adults, thus revalidating the genus *Oliera*. In addition to morphological characters, Moreira et al. (2012) based their study on a preliminary analysis of mitochondrial (COI) DNA sequences, including putative members of the four Neotropical cecidosid genera recognized at that time. They also concluded that material described by Parra (1998) should belong to a different cecidosid genus yet to be identified, which is described in detail in the present study.

While searching later in the field for additional material of this new cecidosid genus, three of the authors of this study (G. R. P. Moreira, G. San Blas and H. A. Vargas) found that there was a second undescribed, cecidosid species in Chile occurring in sympatry, forming galls on swollen stems of the same *S. polygamus* plants, as already suggested by Sáiz and Núñez (1997). These internal, inconspicuous galls, from which Parra (1998) had not received material to work at that time, turned out to be an additional, unknown species of *Oliera* (Brèthes), which is also described here. Thus the main goal of this report is to clarify the peculiar and somewhat confused taxonomic history of these two cecidosid moths in Chile. Under light and scanning electron microscopy, their galls, larvae, pupae and adults are described and illustrated, and preliminary information on their life history is provided. A phylogenetic analysis of concatenated mitochondrial (COI and 16S) and nuclear (Wingless) DNA sequences, including putative members of all lineages of extant Cecidosidae from South America and Africa, was also conducted to provide support for the proposition of these new taxa.

Materials and methods

Morphology

Adults used in the study were reared by H.A. Vargas from galls either attached to *Schinus polygamus* branches or detached ones found in litter, under the canopy cover, which were maintained in small plastic vials at room temperature in the entomology laboratory of the Facultad de Ciencias Agronómicas, Universidad de Tarapacá, Arica,

Chile. They were periodically inspected for emerged adults, which were then pinned and dried. Larvae and pupae were obtained by dissecting additional galls. They were fixed in Kahle-Dietrich´s fluid and preserved in 70% EtOH. For DNA analyses, additional specimens were preserved in 100% EtOH at -20 °C.

For gross morphology studies, the specimens were cleared in a 10% potassium hydroxide (KOH) solution and mounted on slides with either glycerin jelly or Canada balsam. Observations were made with the aid of a Leica M125 stereomicroscope. Structures selected to be drawn were previously photographed with an attached Sony Cyber-shot DSC-H10 digital camera. The vectorized line drawings were made with the software CorelPhotoPaint X4, using the corresponding digitalized images as a guide. At least four specimens were used for the descriptions of each life stage. Measurements were made with an attached ocular micrometer; values are presented as mean ± standard deviation unless noted otherwise.

Specimens used in scanning electron microscope (SEM) analyses were dehydrated in a Bal-tec CPD030 critical-point dryer, mounted with double-sided tape on metal stubs and coated with gold in a Bal-tec SCD050 sputter coater. They were examined and photographed in a JEOL JSM6060 scanning electron microscope at Centro de MicroscopiaEletrônica (CME) of Federal University of Rio Grande do Sul, (UFRGS), Porto Alegre, RS, Brazil.

The material examined is deposited in the following collections:

IADIZA Instituto Argentino de Investigaciones de las Zonas Áridas, CCT-CONICET Mendoza, Mendoza, Argentina;
IDEA Colección Entomológica de la Universidad de Tarapacá, Arica, Chile;
LMCI Laboratório de Morfologia e Comportamento de Insetos /UFRGS, Porto Alegre, Brazil;
MNNC Museo Nacional de História Natural, Santiago, Chile;
UNCC Museo de Zoologia de la Universidad de Concepción, Concepción, Chile;
USNM United States National Museum-Smithsonian Institution, Washington DC, USA.

Molecular phylogeny

We assembled data from two mitochondrial loci and one nuclear protein-coding locus from 12 species representing all Neotropical lineages of Cecidosidae (*Cecidonius* Moreira & Gonçalves, *Cecidoses*, *Dicranoses* Kieffer & Jörgensen, *Eucecidoses* Brèthes and *Oliera*) to infer the relationship of *Andescecidium* gen. n. and the phylogenetic status of *A. parrai* sp. n. and its congeneric undescribed taxon *Andescecidium* sp. (Table 1). To infer the relationship of *O. saizi* sp. n., we added an undescribed taxon (*Oliera* sp.) in addition to the type species (*O. argentinana*). We also included distinct populations of *A. parrai* and *O. saizi* to cover putative geographic divergence. The South African genus *Scyrotis* Meyrick was also taken into account in the analysis. As outgroup, we in-

Table 1. Specimens used in this study for the phylogenetic inference in Cecidosidae.

Family	Genus	Species	Vouchers*	Pop (#) Locality	GenBank (accession number)			BOLD Systems
					COI	16S	Wg	COI-5P
Cecidosidae	*Andescecidium*	*parrai*	LMCI 231-5	Til-Til/ Rungue/ Chile	MH750899	–	MH750908	MISA020-18
			LMCI 233-5	Cuesta Barriga/ Chile	MH750900	–	MH750906	MISA021-18
			LMCI232-6	Cuesta La Dormida/ Chile	MH750901	–	MH750907	MISA022-18
		sp.	LMCI 163-15	Mendoza/ Argentina	MH750902	–	–	MISA023-18
	Cecidonius	*pampeanus*	LMCI 16-24	Eldorado do Sul/Brazil	MH750864	MH750886	MH750892	MISA024-18
		sp.	LMCI 14-72	Curitiba/ Brazil	MH750881	MH750887	MH750893	MISA025-18
	Cecidoses	*eremita*	LMCI 163-1	Mendoza/ Argentina	MH750879	MH750888	MH750895	MISA026-18
	Dicranoses	*congregatella*	LMCI 3-1	Canguçu/ Brazil	MH750880	MH750889	MH750896	MISA027-18
	Eucecidoses	*minutanus*	LMCI 163-21	Mendoza/ Argentina	MH750881	MH750890	MH750897	MISA028-18
	Oliera	*argentinana*	LMCI 6-11	Canguçu/ Brazil	MH750883	MH750891	MH750898	MISA029-18
		saizi	LMCI 232-2	Til-Til/ Rungue/ Chile	MH750904	–	MH750910	MISA030-18
			LMCI232-4	Cuesta La Dormida/ Chile	MH750905	–	MH750909	MISA031-18
		sp.	LMCI 163-13	Mendoza/ Argentina	MH750903	–	–	MISA032-18
	Scyrotis	*granosa*	LMCI 228-2	Tsitsikamma/South Africa	MH750885	–	–	MISA033-18
		pulleni	USNM 00907535	Transvaal / South Africa	-	–	–	LNAUT084-14
Adelidae	*Adela*	*septentrionella*	–	–	EU884115	–	–	–
Incurvariidae	*Incurvaria*	*masculella*	–	–	AF150926	–	–	–
Heliozelidae	*Antispila*	*ampelopsia*	RMNH.INS.30326	–	MF118352	–	–	HELA119-15
Prodoxidae	*Greya*	*enchrisa*	–	–	EU884123	–	–	–

cluded representative species of Adelidae, Incurvariidae, Heliozelidae, and Prodoxidae, which together with Cecidosidae comprise the superfamily Adeloidea (van Nieukerken et al. 2011, Regier et al. 2015). Voucher specimens used are listed in Table 1.

Total genomic DNA was purified from fresh larval tissue of *Andescecidium parrai*, *Andescecidium* sp. and two additional species of *Oliera* (*O. saizi* and *Oliera* sp.), using the PureLink genomic DNA kit (Life, Invitrogen, USA) following the manufacturer's instructions. Sequences of *Cecidonius pampeanus*, *Cecidonius* sp., *Cecidoses eremita* Curtis, *Dicranoses congregatella* (Brèthes), *Eucecidoses minutanus* Brèthes, *Oliera argentinana*, *Scyrotis granosa* (Meyrick) were previously generated by Moreira et al. (2017). Adelidae, Incurvariidae and Prodoxidae sequences were incorporated from the GenBank/NCBI databases, as well as the African cecidosid *S. pulleni* Mey.

Approximately 2.5 Kb of gene segments were amplified by polymerase chain reaction (PCR): 1421 bp of the cytochrome oxidase subunit I (COI), 474 bp of the 16S ribosomal RNA (16S) and 395 bp of the Wingless (Wg) gene loci, with primers and conditions described in Moreira et al. (2017). PCR products were purified using the enzymatic method (exonuclease and alkaline phosphatase), sequenced with BigDye chemistry, and analyzed in an ABI3730XL (Applied Biosystems Inc.). Chromatograms obtained from the automatic sequencer were read and sequences were assembled using the software CodonCode Aligner (CodonCode Corporation). Sequences generated in this study will be deposited in GenBank and BOLD (Table 1).

We used BEAST v2.02 (Bouckaert et al. 2014) to perform relaxed clock Bayesian analyses of the concatenated data and of each gene. Input files contained partitions for each codon position of each gene, which were selected by PartitionFinder v.1.1.1 (Lanfear et al. 2012). We linked site models in accordance with partitions identified by PartitionFinder, unlinked clock models across all partitions, and linked topology across all partitions. We tested the null hypothesis of a strict molecular clock for each gene (data not partitioned) using likelihood-ratio tests in MEGA v7 (Tamura et al. 2013) and found that all genes rejected the strict molecular clock hypothesis. Thus we used uncorrelated lognormal relaxed molecular clock models for all partitions, with mean rates estimated from a gamma distribution relative to a partition with an arbitrary fixed rate of 1. For a tree prior, we used a Calibrated Yule (pure-birth) model with random starting trees. Initial runs with BEAST showed that cecidosids did not remain monophyletic in relation to the outgroup taxa (Prodoxidae, Adelidae, Heliozelidae, and Incurvariidae). Because the monophyly of Cecidosidae is not in question in this study, we constrained it to be monophyletic in the analyses. To adjust the molecular clock we used the fossil calibration point of Adeloidea, about 120±10mya, with a log-normal distribution (Walhberg et al. 2013).We used 1×10^5 generations (sampled every 5,000) for each individual gene tree, with the number of generations increased to 2.5×10^5 for the concatenated analysis. We assessed convergence of BEAST analyses using Tracer v1.6 (Drummond and Rambaut 2007) to examine whether effective sample sizes exceed 200. We used TreeAnnotator v1.7.5 (Drummond et al. 2006) to summarize the posterior distribution of trees from individual MCMC analyses into maximum clade credibility trees using a burn-in fraction of 25%. Trees were observed and edited in FigTree v1.4.3 (Rambaut 2009). Clades with Bayesian Posterior Probability (BPP) ≥ 95% were considered strongly supported. Pairwise genetic distances (p-distances) among lineages were calculated in MEGA v7 with 1,000 bootstrap replications.

Results

Molecular phylogeny

The concatenated tree corroborated our hypothesis of monophyletic status for the new genus and species and their relationships within Cecidosidae with strong node support (BPP = 1) (Figure 1). Individual trees based on COI and 16S showed nearly identical topologies, with a slight difference for Wg (likely due to evolving at a slower rate than the other

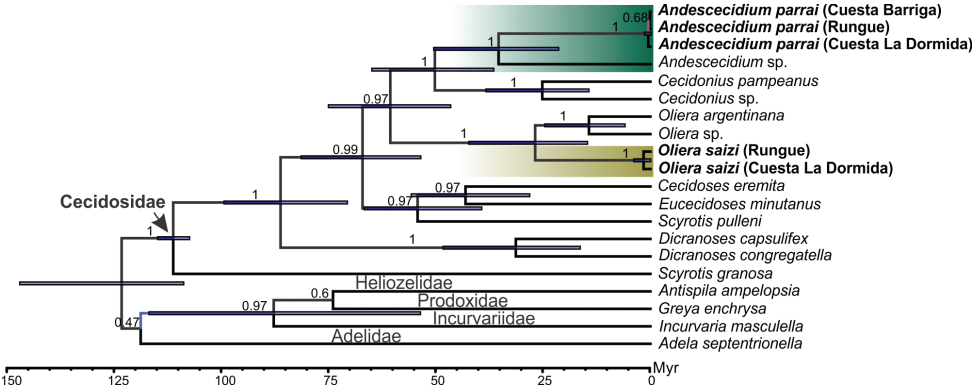

Figure 1. Molecular phylogeny of Cecidosidae showing monophyletic status and relationships of *Andescecidium* and *Oliera saizi* (highlighted by green and brown squares, respectively). Bayesian time-calibrated consensus tree based on cytochrome oxidase subunit I (COI), r16S ribosomal (16S), and Wingless (Wg) genes. Representative species of other Adeloidea families (Adelidae, Incurvariidae, Heliozelidae and Prodoxidae) were used to root the tree. Numbers above branches indicate posterior probability support for the equivalent node. Blue bars indicate confidence interval (95% HDP) for each node age estimate, presented in millions of years ago (Mya).

genes), resulting in weaker phylogenetic resolution than the concatenated tree; however, all retrieved the monophyletic status of the new taxa (data not shown). The concatenated time-tree indicates that *Andescecidium* is sister of *Cecidonius*, a Pampean lineage found in the grasslands of Southern Brazil, and emerged around 35 Mya (95% HDP 20.6–49.1). Genetic distances of the new genus to other cecidosids ranged from 12 to 27%; a lower divergence was observed in relation to *Oliera saizi* and highest to *Dicranoses* (both *D. congregatella* and *D. capsulifex*) and *Scyrotis* (both *S. pulleni* and *S. granosa* (Table 2).

Taxonomy

Andescecidium Moreira & Vargas, gen. n.

http://zoobank.org/5B581601-2C9E-42F7-9E89-1368F6EF38CC
Figs 2–8; Parra 1998: figs 1–4 as *Cecidoses* Curtis (misidentification).

Type species. *Andescecidium parrai* Moreira & Vargas, sp. n.

Diagnosis. *Andescecidium* gen. n. resembles *Cecidonius* in having pupae bearing strong spines on the anterior margins of the abdominal terga and larvae with two stemmata, which make them unique among cecidosids. However, *Andescecidium* shows several adult, larval, and gall features which in conjunction differentiate it from the latter. Adults are much larger, bear mandibular rudiments and have reduced three-segmented maxillary palpi, which are respectively absent and with two in the small *Cecidonius*. The ovipositor in *Andescecidium* is reduced in size, and associated with an inconspicuous dorsal crest in the oviscapt cone that is used to lay eggs on superficial external buds. The ovipositor of *Cecidonius* is very long, having the oviscapt cone dorsally

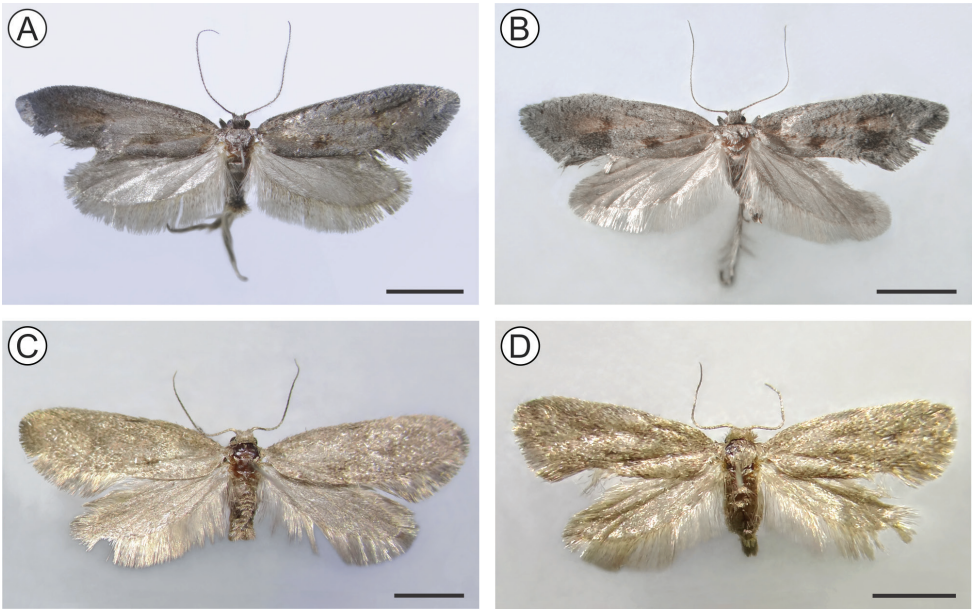

Figure 2. Pinned-dried males (holotypes, left) and females (paratypes, right) of *Andescecidium parrai* (**A, B**) and *Oliera saizi* (**C, D**), dorsal view. Scale bars: 2 mm (**A, B**), 1 mm (**C, D**).

Table 2. Estimates of pairwise genetic distance (%) among Cecidosidae lineages based on concatenated mitochondrial DNA sequences using p-distance.

		1.	2.	3.	4.	5.	6.	7.	8.	9.	10.	11.	12.	13.	14.	15.	16.
1.	*Andescecidium parrai*																
2.	*Andescecidium* sp.	9															
3.	*Cecidonius pampeanus*	12	12														
4.	*Cecidonius* sp.	14	15	7													
5.	*Cecidoses eremita*	16	15	14	15												
6.	*Dicranoses capsulifex*	19	18	19	21	21											
7.	*Dicranoses congregatella*	20	19	20	22	21	9										
8.	*Eucecidoses minutanus*	15	13	13	15	13	21	20									
9.	*Oliera argentinana*	11	13	10	11	12	19	18	11								
10.	*Oliera saizi*	11	12	11	12	12	18	18	13	5							
11.	*Oliera* sp.	12	11	12	15	13	19	18	12	4	6						
12.	*Scyrotis granosa*	21	20	20	23	22	22	23	23	21	20	19					
13.	*Scyrotis pulleni*	16	17	19	19	17	22	21	18	18	16	16	21				
14.	*Adela septentrionella*	20	19	19	21	21	21	21	21	19	16	16	18	21			
15.	*Incurvaria masculella*	20	20	19	22	20	23	24	20	18	19	19	21	22	17		
16.	*Antispila ampelopsia*	23	23	23	25	24	25	25	25	22	22	22	22	25	19	20	
17.	*Greya enchrysa*	19	18	18	21	21	23	24	21	18	20	20	19	21	18	14	18

anchored by a conspicuous crest, thus allowing oviposition deep into the stem. Contrary to the larvae of *Cecidonius*, which are unique among cecidosids in having setae of much longer size on the thorax, those of *Andescecidium* show these structures uniform on thorax and abdomen. The spherical galls of *Andescecidium* are associated with stem

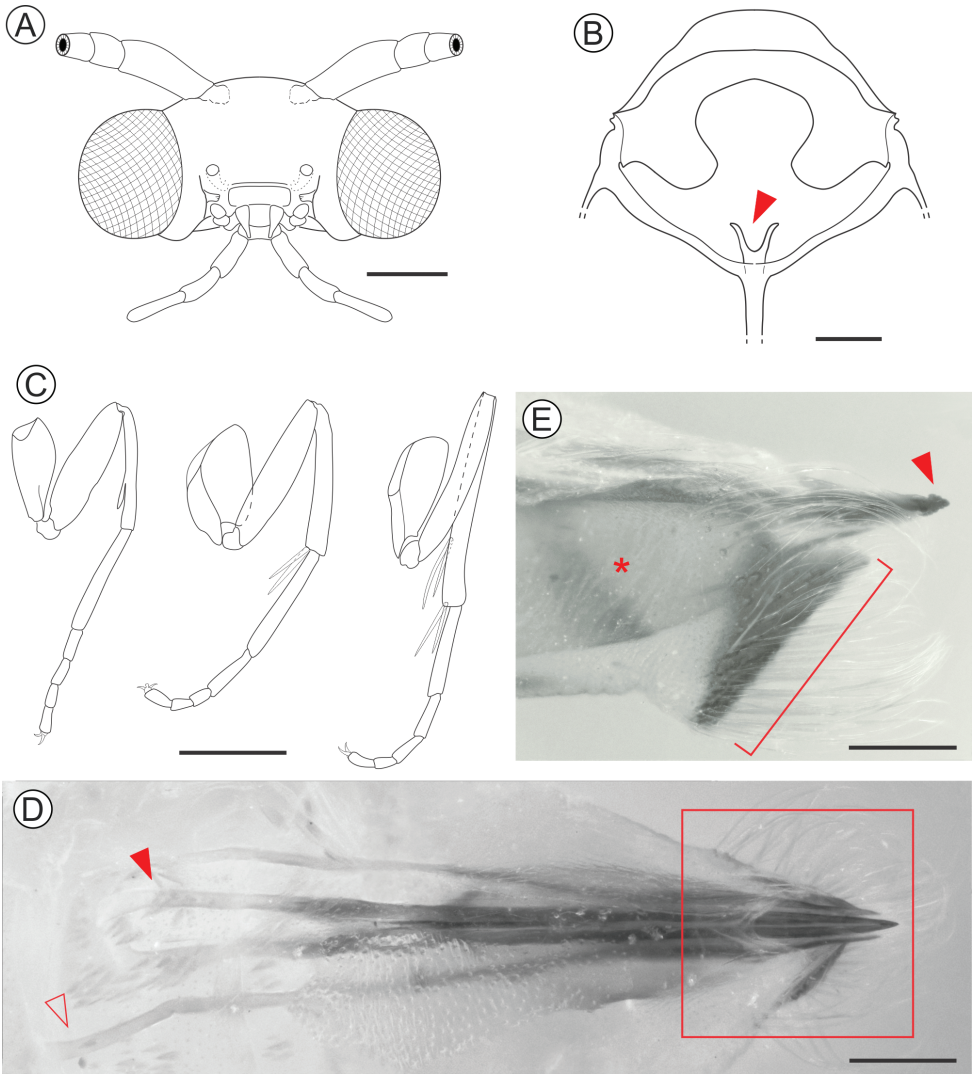

Figure 3. *Andescecidium parrai* adult morphology under light microscopy (LMCI 218-03). **A** head, anterior view **B** metathoracic furcasternum, posterior (closed arrow points to left furcal apophysis) **C** fore-, median- and hindlegs, from left to right, respectively **D** female genitalia, dorsal (open and closed arrows point to the anterior ends of left anterior and posterior right apophyses, respectively) **E** distal portion of female genitalia in detail, lateral (enlarged area marked by rectangle in **D**; closed arrow points to the ovipositor tip; asterisk identifies oviscapt seen by transparency; bracket indicates distal margin of sternum eight). Scale bars: 0.3 mm (**A, B**), 1 mm (**C**), 0.2 mm (**D, E**).

buds, growing on the external surface from the beginning; they are pedunculate and have fully developed walls. Those of *Cecidonius* grow initially under the bark, erupting through the stem surface later in ontogeny, and with their bases remaining open when mature, clogged with feces.

Description of adults (Figs 2A, B, 3). The adult male morphology was accurately described and illustrated in part by Parra (1998). We complement this description for

the male here, adding illustrations that were not provided by Parra, and we also describe the female for the first time.

Male. Forewing length ca. 12.1 mm (n = 1). *Head* (Figure 3A): vertex and frons covered by narrow, elongated dark brown scales with a few scattered whitish gray scales. Compound eyes black. Antennae filiform (~ 0.7× length of forewing), with dark brown scales on scape, pedicel and dorsal surface of basal half of flagellum; filiform sensilla on remaining dorsal and ventral surface of flagellum. Labrum semicircular, short. Mandibles poorly developed, as small stubs. Pilifers absent. Maxillae with galeae reduced to small lobes (~2/3 labial palpus length); maxillary palpi tri-segmented (ratios of segments from base ~1.0:0.8:0.8). Labial palpi tri-segmented (ratios of segments from base ~1.0:0.9:1.2). Maxillary and labial palpi with brownish gray scales. *Thorax*. Mostly with brownish gray scales. Anterior arms of latero cervical sclerites not observed. Metafurca (Figure 3B) with slender, elongate postero-dorsal apophyses, free from secondary arms. Forewings (Figure 2A, B) lanceolate, mostly covered with brownish gray scales; a broad dark brown spot close to the middle of the posterior margin of discal cell; a small dark brown spot at apex of discal cell. Hindwings lanceolate, brownish gray. Wing venation as described by Parra (1998: fig. 2). Prothoracic legs (Figure 3C) dark brown with a few scattered whitish gray scales, bearing an epiphysis on distal portion of tibia. Mesothoracic legs similar in coloration to prothoracic legs, with two whitish gray tibial spurs. Metathoracic legs whitish gray with two pairs of tibial spurs; tibia with longitudinal stripe of narrow, elongated hair-like whitish gray scales. Tibial length proportion (anterior / medium / posterior legs) ~ 0.6:0.7:1.0. Abdomen brownish gray with a few dark brown and scattered whitish gray scales. Male genitalia as described by Parra (1998: figs 2, 3, 4A).

Female. Forewing length ca. 11.5 mm (n = 2). Similar to male in general, except that sensilla are less abundant and smaller on the antennae, and abdominal sternum VII with caudal margin more sclerotized, bearing a dense ring of stout, elongate setae (Figure 3E). Female genitalia formed by an oviscapt cone (sensu Kristensen 2003, San Blas and Davis 2013), with weak internal dorsal crest, reaching the anterior margin of tergum seven. Anterior apophyses extending to anterior margin of sixth abdominal segment. Posterior apophyses ~1.3× length of anterior apophyses. Posterior apophyses are caudally fused to form the short, compressed, and sagittate apex of the ovipositor. Ductus and corpus bursae membranous, the latter saculiform, without signum.

Etymology. The genus name is derived from a composition between the Portuguese *Andes* and *Cecidia* (a gall; from the Greek *kekídion*). Thus, the epithet refers to the Andes Mountains where the galls of *Andescecidium* were first found.

Andescecidium parrai Moreira & Vargas, sp. n.

http://zoobank.org/6A158844-5CC2-4F30-AB27-665C2F33E1D8

Figs 2–8; Parra 1998: figs 1–4 as *Cecidoses argentinana* (Brèthes, 1916) (misidentification).

Diagnosis. As discussed for the monotypic genus.

Description of adults. As discussed for the monotypic genus.

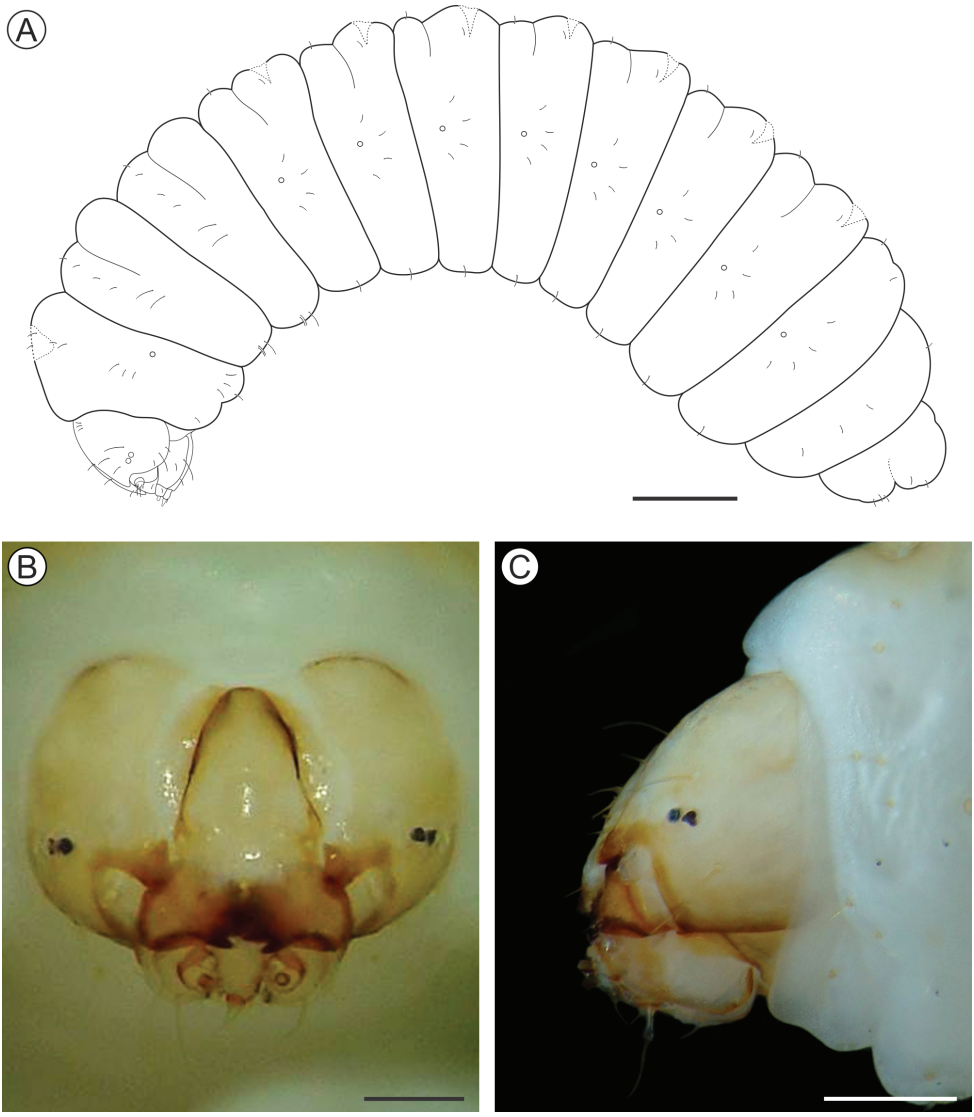

Figure 4. *Andescecidium parrai* last larval instar under light microscopy (LMCI 218-08). **A** general schematic representation, lateral view **B, C** head, anterior (**B**) and lateral (**C**). Scale bars: 1 mm (**A**), 0.3 mm (**B**), 0.2 mm (**C**).

Type material. Chile: Holotype ♂, Cuesta Barriga roadside, Padre Hurtado, Metropolitan Region, emerged June 2013, ex gall on *Schinus polygamus* collected 22.V. 2013, HA Vargas & GRP Moreira leg. (MNNC). Paratype: 1♀, same data as holotype (MNNC).

Non-type material. Immatures used for morphological description, fixed in Kahle-Dietrich's fluid, preserved in 70% EtOH: 33°31'24"S, 70°54'35"W, Cuesta Barriga roadside, Padre Hurtado, Metropolitan Region, HA Vargas & GRP Moreira leg., 13 larvae (22.V.2013, LMCI 218-3, 8, 9, 10, 12; 25.XI.2013, LMCI 231-5, 6), 5 pu-

pae (22.V.2013, LMCI 218-3, 5, 11, 14), 3 galls (22.V.2013, LMCI 218-5, 11, 13); 3°3'42"S, 71°0'35"W, roadside on Cuesta La Dormida, border Til-Til/Valparaiso, HA Vargas & GRP Moreira leg., 4 larvae (28.XI.2013, LMCI 233-6), 5 galls (22.V.2013, LMCI 216- 1 to 5, 11); 33°00'31"S, 70°53'52"W, 712m, roadside near Til-Til, Rungue, Metropolitan Region, HA Vargas & GRP Moreira leg., 6 larvae (26.XI.2013, LMCI 232-6, 7), 4 galls (26.XI.2013, LMCI 232-8), G San Blas leg., 12.X.2011, 3 larvae (donated to LMCI 163-14), 46 larvae (IADIZA), 5 galls (IADIZA), 7 pupae (extracted from dried galls on 3.V.2012, IADIZA), G San Blas leg., 15.III.2013, 3 dried pupae; 35°36'00"S, 71°07'17.02"W, 426m, Ruta J-65, 25km from Curicó, Maule Region, G San Blas leg., 12.X.2011, 16 larvae; 36°39'30"S, 72°16'41"W, 43m, roadside in Cruce Nebuco, Bio-Bio Region, HA Vargas, LE Parra & GRP Moreira leg., 2 galls (30.V.2013, LMCI 223-1); 35°31'53"S, 71°18'4"W and 35°31'29"S, 71°18'33"W, P. Sta. Edilia, San Clemente, Maule Region, LE Parra & GT Silva leg., 25.XI.2016, 2 larvae donated to LMCI (330-1, 2).

Additional larvae. Same data as above, fixed and preserved in 100% EtOH at -20 °C for DNA extraction: n = 2, LMCI 231-5; n = 6, LMCI 233-5, 6.

Additional adult material. Genitalia preparation on slide of male by LE Parra, UCCC, Parque Nacional La Campana, Sector Ocoa, Hijuelas, Valparaíso Region, L. Sáiz leg., March-April 1993, with label "*Cecidoses argentinana* (Brèthes), Det. LE Parra"; added label *"Andescecidium parrai* Moreira & Vargas, Det. GRP Moreira; 9.V.2018", 1♂ (LMCI 218-03-04) and 1♀ (LMCI 218-03-03), cleared in KOH 10%, preserved in 70% EtOH, same data as the holotype.

Etymology. Named in honor of Prof. Dr. Luis E. Parra, from the Universidad of Concepción, who for the first time characterized such a gall-inducing moth, for his great contribution to the development of Lepidopterology in Chile.

Description of immature stages. ***Last instar larva*** (Figs 4, 5). Body length = 8.10 ± 0.66 mm; head capsule width = 1.40 ± 0.04 mm (n = 4). *Head* (Figs 4B, C; 5A, B) yellowish with anterior margin light brown; lateral margins convex; frontoclypeus slightly bulged, subtriangular, with well-marked pigmented adfrontal sutures; ecdysial lines unpigmented. Two pairs of laterally located, well-developed stemmata (Figure 5C). Antennae (Figure 5D) 2-segmented; basal segment with one stout and one ~4× longer, filiform sensillum; distal segment with one stout sensillum on apex, flanked by two small filiform sensilla. Labrum slightly bilobed, with five pairs of small setae. Mandible well developed, with four cusps along distal margin (Parra 1998: fig. 4C), bearing one basal seta on external surface. Maxilla with palpus and galea reduced (Figure 5F). Spinneret conical-tubular (Figure 5E; Parra 1998: fig 4D); labial palpus one-segmented with well-developed apical seta. Chaetotaxy consisting of 15 pairs of setae: F group unisetose; C group unisetose; A group trisetose; AF group unisetose; P group trisetose, reduced in length; S group trisetose, middle one long; SS group trisetose, posterior one long.

Thorax (T) and abdomen (A) subcylindrical, creamy-white and covered with microtrichia (Figure 5I); thoracic setae small (Figure 5G), similar in size to abdominal ones. Prothoracic shield light yellow, weakly defined; thoracic legs and abdominal

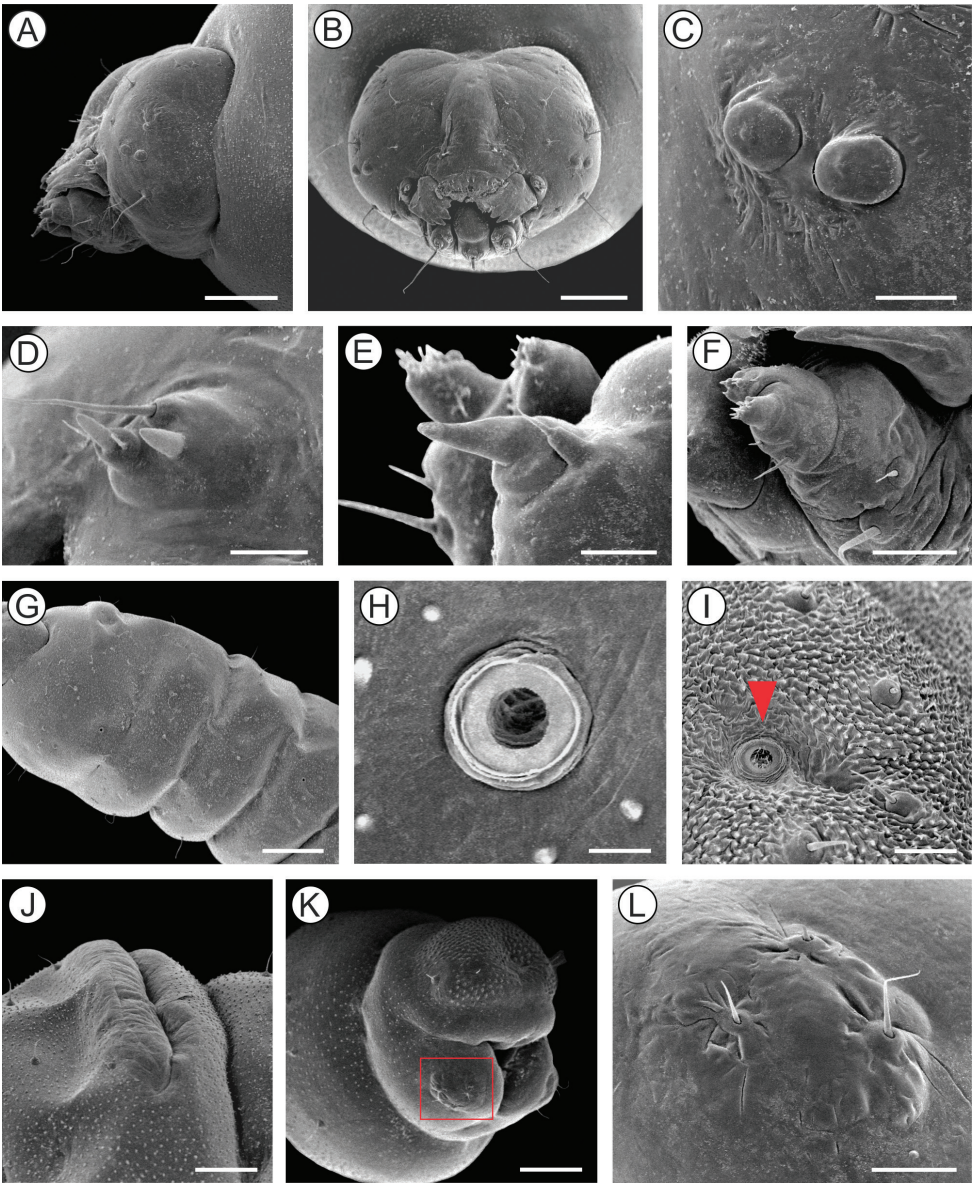

Figure 5. Morphology of *Andescecidium parrai* last larval instar under scanning electron microscopy. **A, B** head, lateral (**A**) and antero-dorsal (**B**) views **C** stemmata, lateral **D** antenna, lateral **E** labium, lateral **F** maxilla, lateral **G** thorax, lateral **H** first abdominal spiracle, lateral **I** detail of second abdominal segment, showing aligned setae (arrow indicates spiracle), lateral **J** callus of second abdominal tergum, latero-dorsal **K** last abdominal segments, postero-lateral **L** ventral lobe of tenth abdominal segment (enlarged area marked with rectangle in **K**). Scale bars: 150 μm (**A, B**), 30 μm (**C, L**), 20 μm (**D, E**), 50 μm (**F, I**), 300 μm (**G**), 10 μm (**H**), 100 μm (**J, K**).

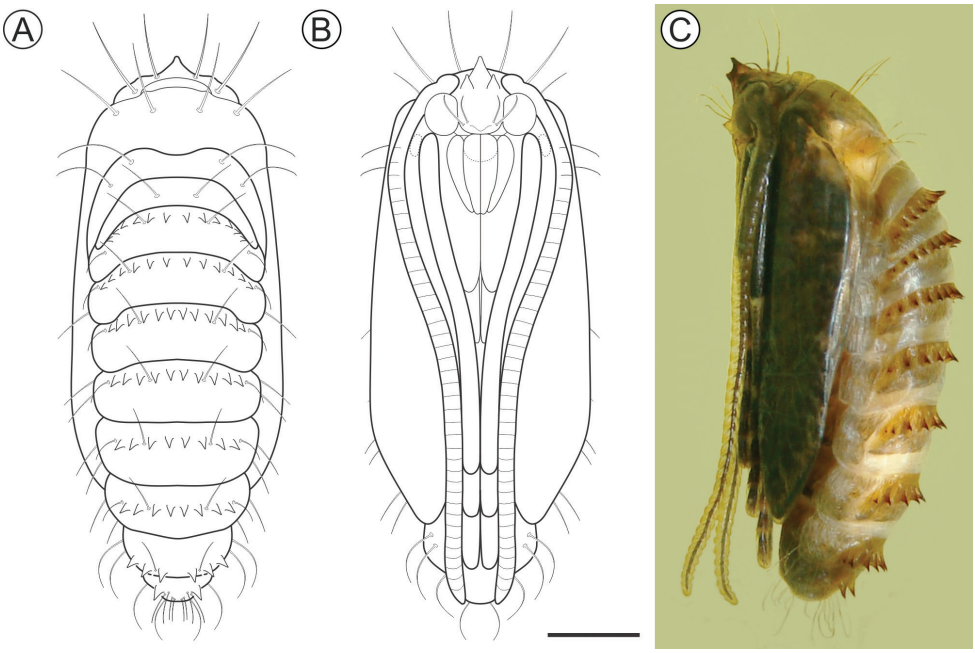

Figure 6. *Andescecidium parrai* pupa in dorsal (**A**), ventral (**B**), and lateral (**C**) views (LMCI 218-5). Scale bar: 1 mm.

prolegs absent; abdominal calli (Figure 5J) on segments A1–A7 located on posterior margin of terga. Last abdominal segment (Figure 5K, L) composed of three lobes, one dorsal, and two ventral, smaller. Spiracles (Figure 5H, I) laterally on T1, A1–A8, circular and without elevated peritreme. Chaetotaxy: T1 with twelve pairs of setae; D group bisetose, SD bisetose, outside prothoracic shield, L group trisetose, anterior to spiracle, SV group trisetose, MV unisetose, V unisetose. T2–3 with nine pairs of setae; D group bisetose, SD bisetose, L group bisetose, SV group bisetose, V unisetose. AB1–8 with seven pairs of setae; D group bisetose, L group tetrasetose, posterior to spiracles, V group unisetose. AB9 with four pairs of setae; D group unisetose, L group bisetose, SV group unisetose. A10 with five pairs of setae; SD group bisetose; SV trisetose.

Pupa (Figs 6, 7). Length = 12.3 + 0.4 mm; n = 3. Yellowish brown, with head, thorax, wings, and abdominal spines becoming dark brown near adult emergence. Head with frontal process (= gall-cutter) formed by three processes (Figure 7A–C); one large, subtriangular, located centrally at the anterior, which is flanked by the other two, shorter, located posteriorly at the base. Antennae narrow, long, slightly surpassing the end of abdomen; prothorax is a narrow transverse band between head and mesothorax; hindwings concealed by forewings, extending to sternum A8; pro-, meso- and metathoracic legs extending up to A6, A7 and A8, respectively. Frons with two pairs of setae laterally. Terga T2 and T3 with two pairs of setae, one dorsal and one laterodorsal. Abdominal segments with spiracular region covered with microtrichia; A2–9 with a transverse band of conspicuous spines (Figure 7E, F), near anterior margin of

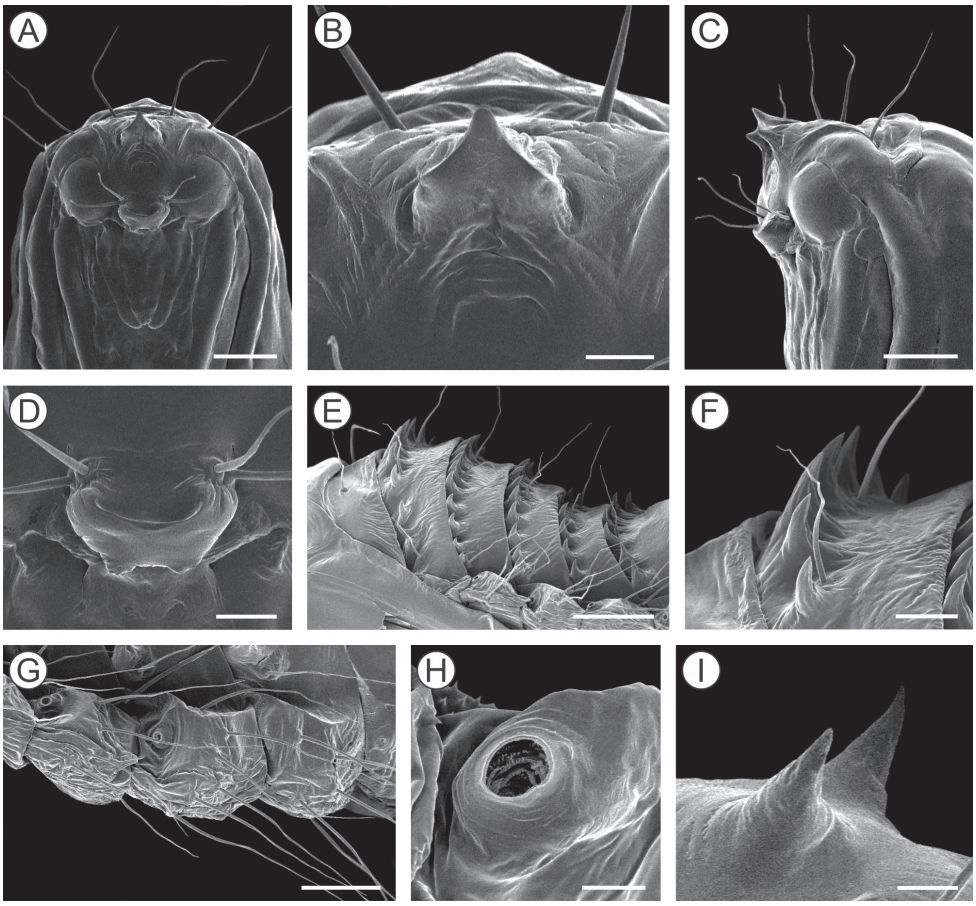

Figure 7. *Andescecidium parrai* pupal morphology with scanning electron microscopy. **A, C** head and prothorax, under ventral and lateral views, respectively **B** frontal process of head (= gall cutter), ventral **D** clypeus and labrum, ventral **E** abdominal terga, lateral **F** spines and setae of second abdominal tergum in detail, lateral **G** abdominal pleura and sterna, latero-dorsal **H** spiracle of third abdominal segment, dorsal **I** tergal spines of ninth abdominal segment, postero-lateral. Scale bars: 500 μm (**A, C, E**), 150 μm (**B, D, F**), 300 μm (**G**), 30 μm (**H**), 70 μm (**I**).

terga; tergum A9 with one pair of spines (Figure 7I) on posterior margin. Abdominal setae (Figs 6A, 7G) arranged in three rows (dorsal, supra and subspiracular); one dorsal pair on segments A1–8; one supra-spiracular pair on segments A2–8; four to six subspiracular pairs on segments A2–9; four pairs dorsally on A10; spiracles (Figure 7H) with slightly elevated peritreme, laterally on A2–8.

Life history. The large, short pedunculated galls of *A. parrai* develop externally from the beginning, on stem buds of *S. polygamus* terminal and sub-terminal branches (Figure 8B, C). A few galls of different sizes may be found on the same branch. They are elliptical and usually reddish when young, becoming to spherical and green when mature. The larval chamber is almost cylindrical in shape (maximum width and length

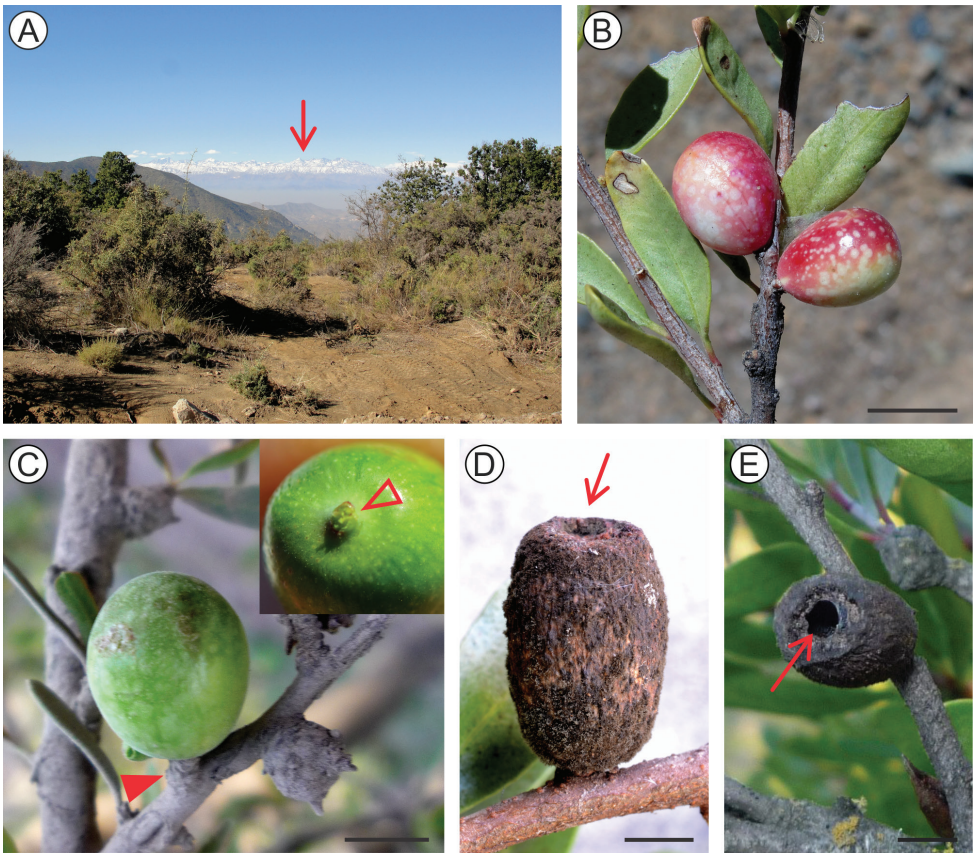

Figure 8. Natural history of *Andescecidium parrai* on *Schinus polygamus*. **A** host-plant habitat at Cuesta La Dormida, intersection Til-Til/Valparaíso, beginning of road to Rungue, Chile, 33°3'42"S, 71°0'35"W (seta on the horizon points to the El Altar mountain, Metropolitan region) **B** young, developing galls, lateral **C** mature gall, lateral, with pedunculus (indicated by arrow) in detail in the upper right corner **D, E** old, empty galls under lateral and posterior views, respectively (setae point to apical open). Scale bars: 4 mm (**B, C, E**), 3 mm (**D**).

varying from 9–10 and from 10–14 mm, respectively; n = 10), and transverse to the stem axis. Their external wall becomes dark brown and almost cylindrical during late development. At least some are apparently deciduous, falling to the ground. This morphotype has a rough external wall (Figure 8D), and was found among the litter under the *S. polygamus* plants, where they are easily confused with fecal pellets of the European rabbit (*Oryctolagus cuniculus* L.: Leporidae), that is abundant in the region. Like *C. pampeanus* galls, those of *A. parrai* also lack an operculum. Using the frontal process and abdominal spines present on the pupae to make pressure, together with body contortions, are likely the means the pupa uses to open an orifice on the distal, weaker wall (Figure 8E), in which it pushes itself partially out of the gall.

Little is known about biology of *A. parrai* galls. Our field observations suggest that the species is univoltine, galls starting to develop during late spring and summer, when

most leaf buds are found on *S. polygamus* plants (Sáiz and Núñez 1997). Deciduous galls were field-collected from the ground near the end of May, from which a few adults used here for description successfully emerged in the laboratory after ca. 25 days.

***Oliera* Brèthes**

***Oliera saizi* Moreira & Vargas, sp. n.**

http://zoobank.org/C959AC54-A09B-4EE5-A35C-2247A3D5744D
Figs 2, 9–14

Diagnosis. A typical member of *Oliera*, having two-segmented labial palpi, pupa with five-pointed frontal process and galls enclosed within swollen terminal branches of *Schinus* plants (for a generic review, see Moreira et al. 2012). It differs from *O. argentinana* by characteristics present on the adults, pupae, larvae, and galls. Contrary to adults of *O. argentinana* that vary from shiny copper to reddish brown, those of *O. saizi* are brownish gray in color. Adults of *O. saizi* (forewing length 5.5–6.3) are slightly larger than *O. argentinana* (forewing length 4.3 mm). Pupae of *O. saizi* have the two lateral units of the anterior row of the gall cutter short, ca. 1/3 the central one in length; in *O. argentinana* such processes are much longer, reaching ca. 3/4 the central in length. Furthermore, pupae of *O. saizi* bear long, conspicuous setae on the last abdominal segment, which are absent in *O. argentinana*. Larvae of *O. saizi* have the head with long, continuous and rectilinear, pigmented adfrontal sutures more or less parallel to the unpigmented ecdysial lines. Together they delimit two long adfrontal areas, which extend from the posterior margin of the labrum to the epicranial notch; in *O. argentinana*, the adfrontal sutures are marked only distally, delimiting two smaller, semicircular, posteriorly located adfrontal areas. In addition, the integument of *O. saizi* is covered by a greater number of rounded microtrichia that are finer and more regular in size compared to the less dense, larger in size and more irregular-shaped ones in *O. argentinana*. Galls of *O. saizi* are larger, and generally found on subterminal branches of *S. polygamus* plants, contrary to those of *O. argentinana* that occur commonly on narrower, terminal branches.

Description of adults. ***Male***. Forewing length varying from 5.5 to 6.3 mm (n = 3). *Head*: Vertex and frons covered with smooth, narrow, brownish gray scales. Compound eyes black. Antennae filiform, about half the length of forewing, with brownish gray scales dorsally, ventral half with short sensilla. Labrum semicircular, short. Mandibles poorly developed, as small stubs. Pilifers absent. Maxillae with galeae reduced to small lobes; maxillary palpi tri-segmented (ratios of segments from base ~1.0:0.9:0.6). Labial palpi tri-segmented (ratios of segments from base ~1.0:0.8:0.7). Maxillary and labial palpi with brownish gray scales. *Thorax*: Mostly with brownish gray scales. Wing venation (Figure 9A) as in *O. argentinana* (Moreira et al. 2012). Prothoracic legs with coxa, trochanter and femur dark gray (occasionally brownish gray); tibia and tarsus brownish gray; apex of tibial epiphysis reaching the apex of tibia. Mesothoracic leg brown-

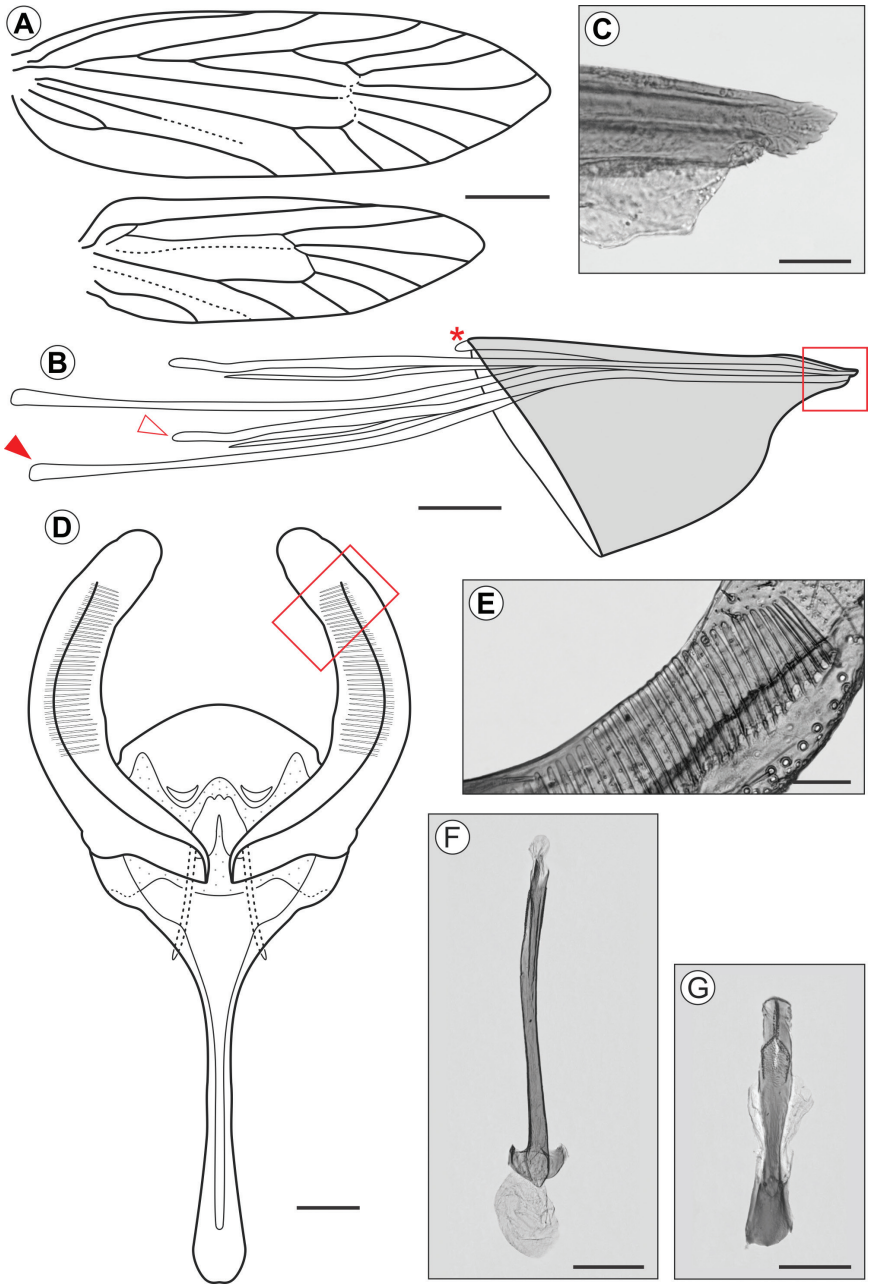

Figure 9. *Oliera saizi* adult morphology, under light microscopy (paratypes). **A** fore and hindwing venation, dorsal view **B** schematic representation of female oviscapt cone, lateral (asterisk indicates the distal end of internal dorsal crest; closed and open arrows point to the anterior ends of anterior and posterior left apophyses, respectively) **C** ovipositor tip in detail, lateral (enlarged area marked by rectangle in **B**) **D** male genitalia, ventral (phallus and juxta omitted) **E** distal section of right valva pectinifer in detail (enlarged area marked by rectangle in **D**) **F** phallus, ventral **G** juxta, ventral. Scale bars: 1 mm (**A**), 200 μm (**B**), 10 μm (**C**), 100 μm (**D, F, G**), 30 μm (**E**).

ish gray; one pair of tibial spurs. Metathoracic legs brownish gray; two pairs of tibial spurs; tibia with longitudinal band of narrow, elongated hair-like scales. Tibial length proportion (anterior / medium / posterior legs) ~ 0.5:0.6:1.0. Fore- and hindwings lanceolate, brownish gray. *Abdomen*: Brownish gray. Genitalia (Figure 9D) with narrow tegumen; uncus bilobed; socii as two small setigerous lobes. Saccus with dorsal arms narrow, U-shaped, with anterior projection prominent, slightly widened close to apex. Valva narrow, about 3/4 the length of the anterior projection of the saccus; dorsal and ventral margins sub-parallel, and distal portion dorsally dilated. Pectinifer (Figure 9E) as a straight band on the ventral part of the medial surface of the valva. Transtilla as an inverted "V", with ventral arms straight, slightly widened close the vertex. Juxta (Figure 9G) narrow, elongated, slightly spatulate distally. Phallus (Figure 9F) narrow, somewhat sinuous, with similar length to valva, with anterior apex laterally widened forming a semicircle; vesica without cornuti.

Female. Forewing length varying from 5.2 to 5.9mm (n = 7). Similar to male in general, but with abdominal sternumVII showing a ring of stout setae on caudal margin. Genitalia (Figure 9B) bearing an oviscapt cone (sensu Kristensen 2003, San Blas and Davis 2013), with weak internal dorsal crest, reaching the anterior portion of tergum seven. Posterior apophyses fused posteriorly, forming distally the laterally compressed, serrated apex of the ovipositor (Figure 9C). Anterior apex of posterior apophyses extend to abdominal segment VI; anterior apophyses project into the segment V. Internal reproductive system not represented, apparently as in *O. argentinana* (Moreira et al. 2012).

Type material. Chile: Holotype ♂, Cuesta Barriga roadside, Padre Hurtado, Metropolitan Region, emerged December 2013, ex gall on *Schinus polygamus* collected 25 November 2013, HA Vargas & GRP Moreira leg. (MNNC). Paratypes: 1♂, 2♀, same data as holotype (MNNC); 7♀, same data as holotype (IDEA); 1♂, roadside near Til-Til, Rungue, Metropolitan Region, emerged December 2013, ex gall on *Schinus polygamus*, collected 26 November 2013, HA Vargas & GRP Moreira leg. (IDEA).

Non-type material. Immature specimens used for descriptions: 33°31'24"S, 70°54'35"W, Cuesta Barriga roadside, Padre Hurtado, Metropolitan Region, HA Vargas & GRP Moreira leg., 6 larvae (25.XI.2013, LMCI 231-3, 4); 33°3'42"S, 71°0'35"W, roadside on Cuesta La Dormida, near border Til-Til/Valparaiso, Metropolitan Region, HA Vargas & GRP Moreira leg., 8 larvae (20.V.2013, LMCI 216-14), 2 pupae (28.XI.2013, LMCI 233-3); 33°00'31"S, 70°53'52"W, roadside near Til-Til, Rungue, Metropolitan Region, HA Vargas & GRP Moreira leg., 4 larvae (26.XI.2013, LMCI 232-4); 36°48'22"S, 71°44'36"W, roadside near Recinto, Bio-Bio Region, HA Vargas, LE Parra & GR. Moreira leg., 30.V.2013, 12 larvae (LMCI 222-2 to 6) and 2 pupal exuviae (LMCI 222-1).

Additional larvae. Data as above, fixed and preserved in 100% EtOH at -20 °C for DNA extraction (n = 2, LMCI 232-4; n = 2, LMCI 233-2).

Additional pinned-dried adults examined. Puente El Yeso, Cajón del Maipo, Metropolitan Region, R. Charling C. leg., 4 males, with one genitalia (DRD 16536) and one wing (DRD 29925) preparations; 2 females, with one wing and genitalia preparation (DRD 16537), USNM.

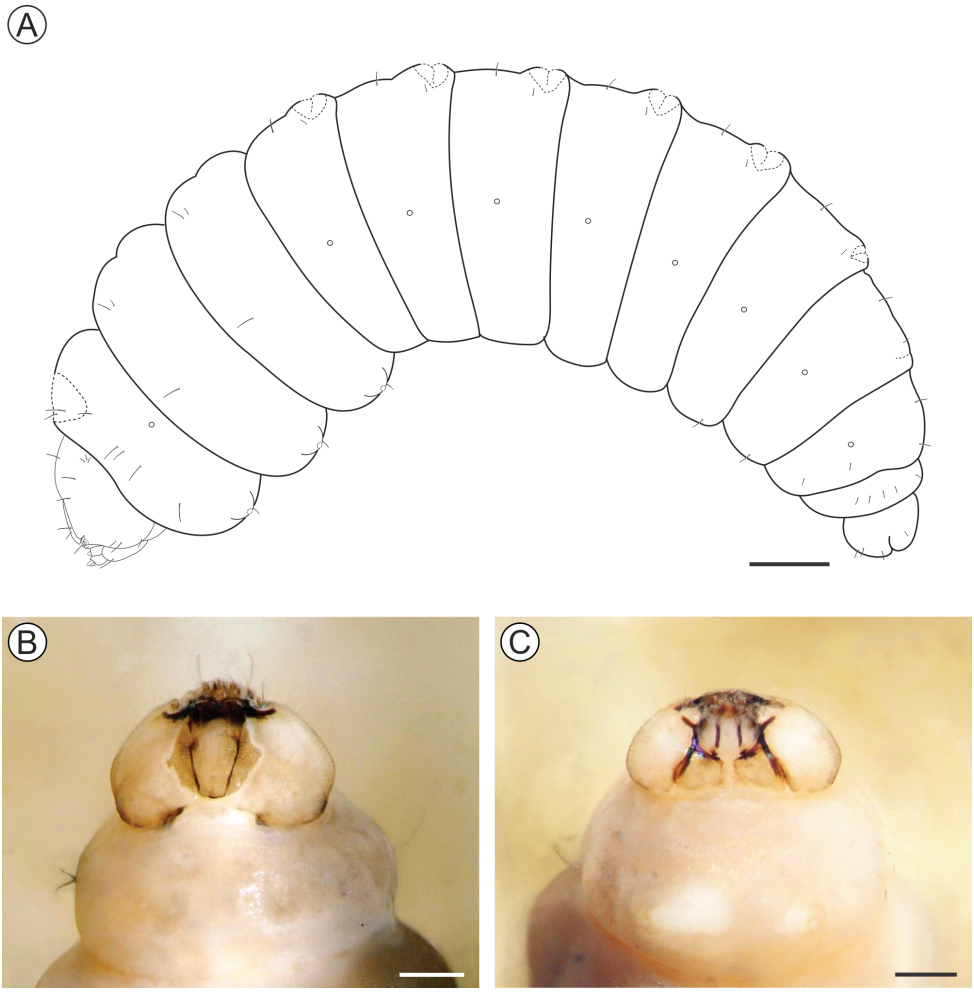

Figure 10. *Oliera saizi* last larval instar under light microscopy (LMCI 231-3). **A** general schematic representation, lateral view **B, C** head and prothorax, dorsal (**B**) and ventral (**C**). Scale bars: 0.5 mm (**A**), 0.3 mm (**B, C**).

Etymology. Named in honor of Prof. Dr. Francisco Sáiz, from the Universidad Católica de Valparaiso, who first noticed the existence of these galls, for his great contribution to the development of Cecidology in Chile.

Descriptions of immature stages. ***Last instar larva*** (Figs 10, 11). Body length = 3.99 ± 0.41 mm; head capsule width = 0.97 ± 0.02 mm (n = 3). Head (Figs 10B, C; 11A) creamy to light brown, ~ 2× broader than high, with convex lateral margins. Frontoclypeus triangular, marked by pigmented adfontral sutures extending to apex of epicranial notch that is paralleled by unpigmented ecdysial lines. Adfrontal sutures and ecdysial lines delimit two long adfrontal areas. Hypostomal ridges well marked and divergent; hypostomal lobes trapezoidal. Integument densely covered by rounded microtrichia (Figure 11F). Stemmata absent; antennae (Figure 11C) reduced, with five

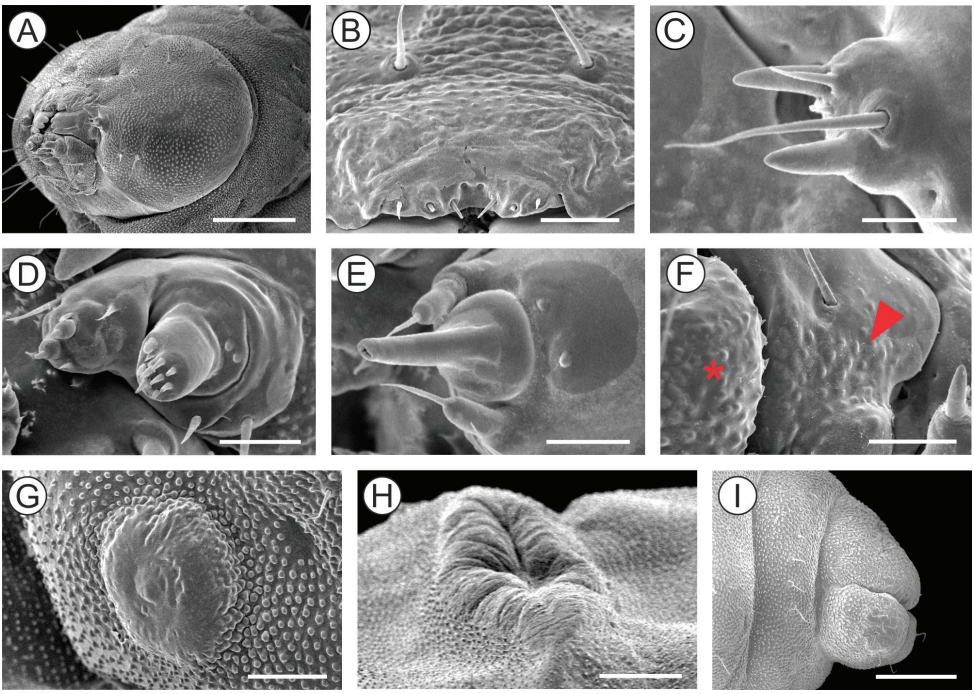

Figure 11. Morphology of *Oliera saizi* last larval instar under scanning electron microscopy. **A** head, antero-lateral view **B** labrum and clypeus, anterior **C** antenna, lateral **D** maxilla, anterior **E** labium, ventral **F** detail of maxilla (indicated by asterisk) and mandibula (pointed by arrow) bases, showing protuberances **G** mesothoracic leg rudiment, lateral **H** callus of third abdominal tergum, latero-dorsal **I** last abdominal segments, lateral. Scale bars: 250 μm (**A**), 40 μm (**B**), 20 μm (**C, E, F**), 30 μm (**D**), 60 μm (**G**), 100 μm (**H**), 200 μm (**I**).

sensilla, two stout and three filiform; labrum (Figure 11B) slightly bilobed, with three pairs of small setae on distal margin; mandible well developed with four cusps along distal margin and one small seta basally on external surface; maxilla (Figure 11D) with poorly developed palpus and galea; spinneret tubular; labial palpus one-segmented with well-developed apical seta (Figure 11E). Chaetotaxy consisting of 9 pairs of setae: F group unisetose, C group unisetose, AF group unisetose, A group unisetose, L group bisetose, S group trisetose.

Thorax (T) and abdomen (A) creamy white, mostly covered with rounded microtrichia; prothoracic shield weakly defined by a pair of slightly differentiate areas, with reduced microtrichia. A1–7 with well-developed callus (Figure 11H), mesally, close to posterior margin of terga. Thoracic legs (Figure 11G) reduced to circular, unsegmented tubercles; prolegs absent. Spiracles circular, without elevated peritreme, laterally on T1 and A1–8. Abdominal segment 10 composed of three lobes, one dorsal, wider and two ventral (Figure 11I). Chaetotaxy of thorax and abdomen composed of setae reduced in size. T1 with eight pairs of setae; XD group bisetose, SD group unisetose outside prothoracic shield, L group trisetose, SV group unisetose, V group unisetose. T2–3 with four pairs of setae; D group bisetose, L and V groups unisetose. A1–5 with two

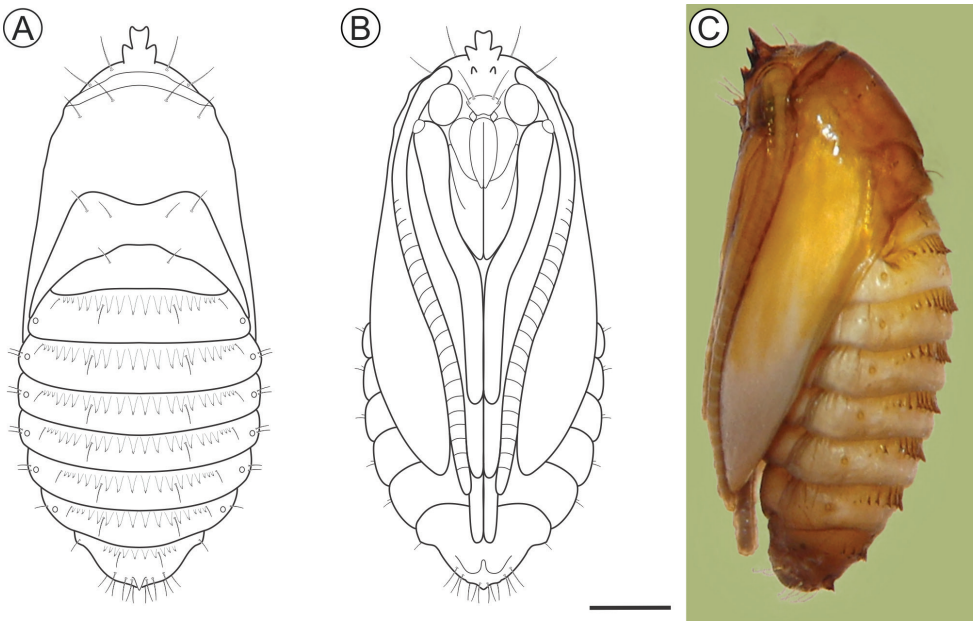

Figure 12. *Oliera saizi* pupa under light microscopy, in dorsal (**A**), ventral (**B**) and lateral (**C**) views (LMCI 233-3). Scale bar: 0.5 mm.

pairs of setae; D group bisetose. A6–7 with three pairs of setae, D group bisetose and V group unisetose. A8 with four pairs of setae; D group bisetose, L group unisetose and SV group unisetose. A9 with five pairs of setae; SD group unisetose and L group tetrasetose. A10 with four pairs of setae; SD unisetose, SV unisetose and V bisetose.

Pupa (Figs 12, 13). Length = 6.1 + 0.2mm; n = 3. Orange brown, becoming dark brown near adult emergence. Head with frontal process (= gall-cutter; Figure 13A–C) formed by five spines that are grouped into two parallel rows; the anterior row with three processes; middle process with a blunt apex, ca. 3/4 longer than lateral ones; posterior pair consists of two minute, pointed processes. Vertex with two pairs of setae laterally. Antennae narrow, long, with apex slightly surpassing forewing apex. Prothorax as a narrow transverse band between head and mesothorax; forewings reaching sternum A7; hindwings concealed by forewings; metathoracic legs reaching segment A9. Terga T2–3 with two pairs of latero-dorsal setae. Abdominal segments covered with microtrichia; A2–8 with a transverse band of spines (Figure 13E, F) near anterior margin of terga; tergum A9 with acute process (Figure 13H, I) on posterior margin. Setae relatively small, arranged in three rows, from A1 to A8 (dorsal, supra- and subspiracular): one dorsal pair on segments A1–8; one supra-spiracular pair on segments A2–8; two subspiracular pairs on segments A3–7 and one pair on A8. Six pairs of long and stout setaeon last segment (Figure 13J). Spiracles (Figure 13D) circular, without elevated peritreme, laterally on A2–8, and on A8, reduced.

Life history. *Oliera saizi* develops spindle-shaped galls enclosed within swollen stems of *S. polygamus* subterminal branches (Figure 14A, B). The larval chamber is

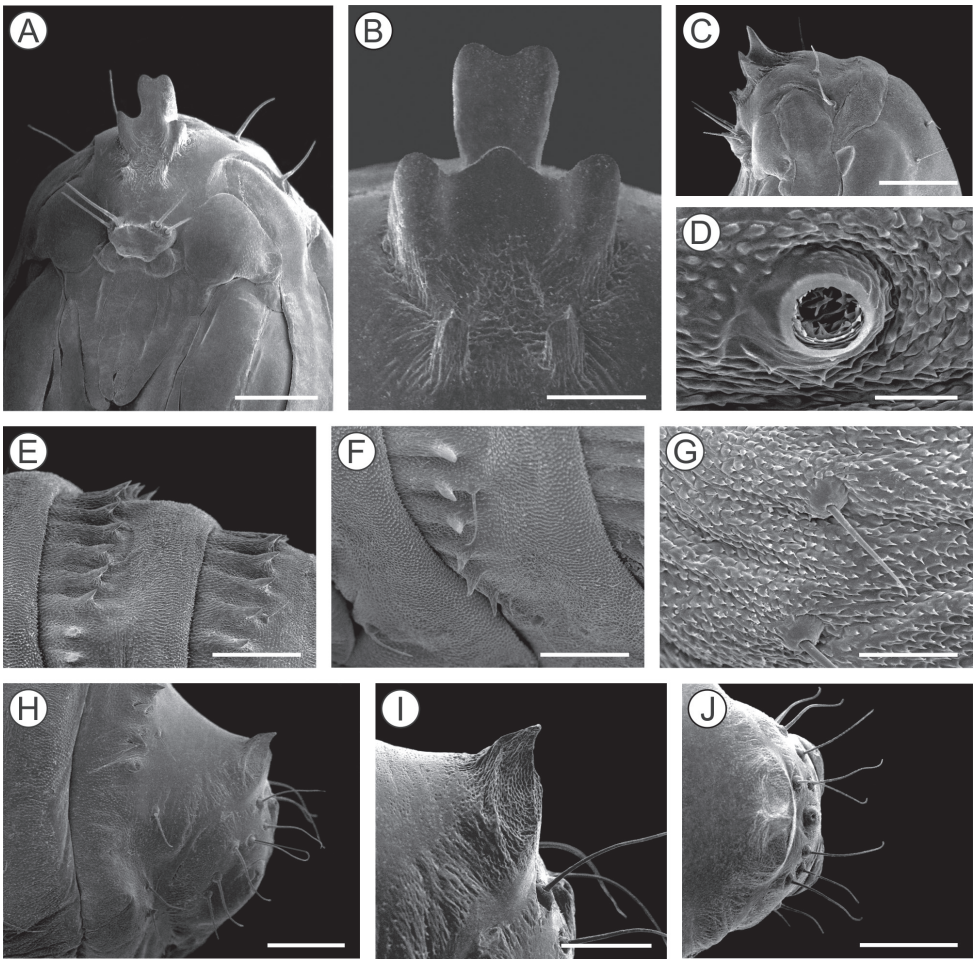

Figure 13. *Oliera saizi* pupal morphology using scanning electron microscopy. **A, C** head and prothorax, under ventral and lateral views, respectively **B** frontal processes of head (= gall cutter), ventral **D** spiracle of second abdominal segment, lateral **E** abdominal terga VI and VII, lateral **F** detail with supraspiracular setae and spines of abdominal tergum VI, lateral **G** detail with subspiracular setae of abdominal segment five, lateral **H, J** last abdominal segments, under lateral and dorsal views, respectively **I** single tergal spine on abdominal segment nine in detail, lateral. Scale bars: 250 μm (**A**), 100 μm (**B, I**), 350 μm (**C**), 30 μm (**D**), 200 μm (**E, H, J**), 150 μm (**F**), 50 μm (**G**).

elliptical in shape and transversally located in relation to the stem axis, and as in *O. argentinana*, the gall lacks an operculum. A progressive necrosis extends up the gall wall with the advent of pupation; meanwhile the pupa opens an orifice on the wall with the aid of its frontal process and through body contortions. The abdominal spines help the pupa during these movements to anchor itself on the wall; it pushes part of its body out of the gall, when the exuvia splits and the adult emerges (Figure 14B, D). The outer wall eventually collapses, leaving the empty galls appearing as small holes on the host plant branches (Figure 14E, F).

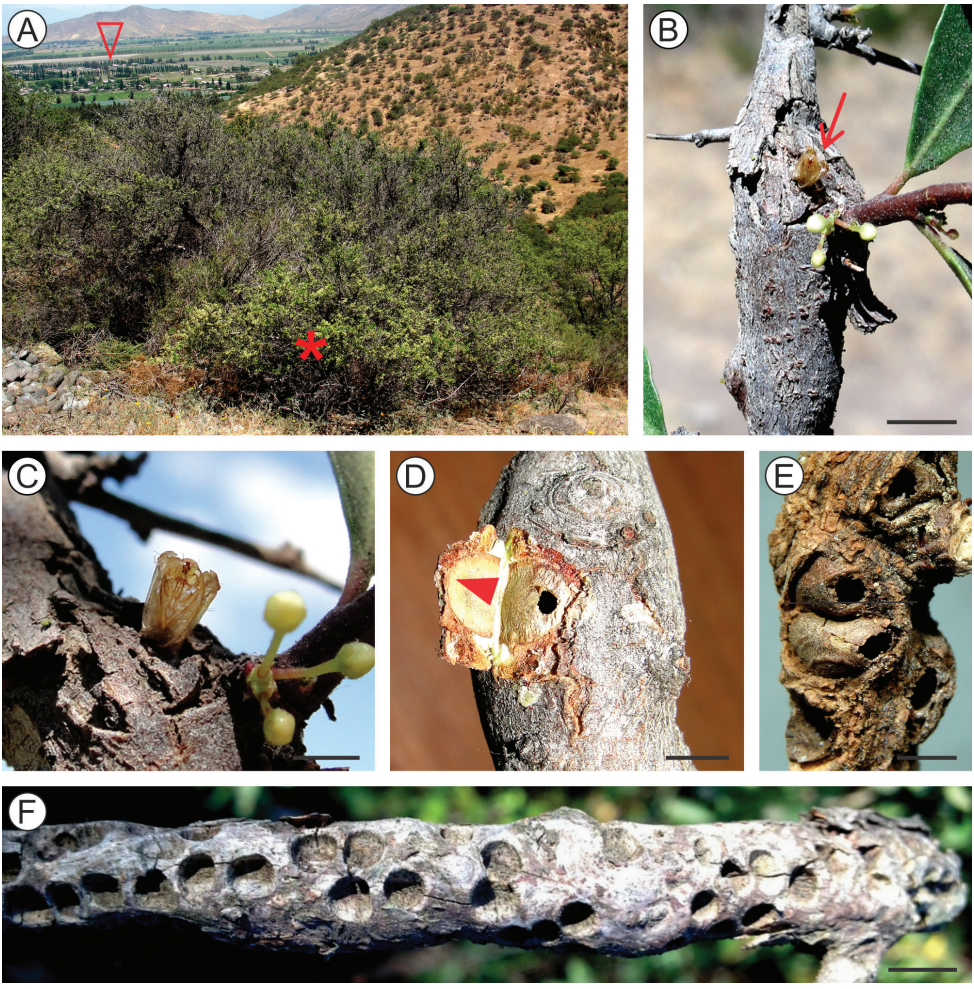

Figure 14. Natural history of *Oliera saizi* on *Schinus polygamus*. **A** host-plant habitat at Cuesta Barriga, near Santiago city, Chile, 33°31'24"S, 70°54'35"W (asterisk locates the plant; open arrow indicates commune of Padre Hurtado in the valley, Metropolitan region) **B** apical branches showing swollen stem with galls under bark **C** pupal exuvium protruded from the gall exit hole, just after the adult emergence (enlarged area pointed by arrow in (**B**) **D** intact empty gall, shown by detaching the bark (indicated by arrow) **E** empty galls, with decaying gall-wall still remaining, lateral **F** old gall signs appearing as small craters on surface of dried branch. Scale bars: 5 mm (**B**), 2 mm (**C**), 3 mm (**D, E**), 15 mm (**F**).

Little is also known about the biology of *O. saizi.* Similar to what has been found for *O. argentinana* (Moreira et al. 2012), their galls have been collected occasionally, either on isolated plants or in groups. They may occur at high densities per branch, sometimes adjacent to those of *A. parrai*. Our field collection data indicate that the species is univoltine, with adult emergence occurring from late spring to early summer (November / December). *Schinus polygamus* branches bearing galls with full-grown pupae were field-collected during November, from which a few adults used for description emerged under laboratory conditions ca. 25 days later.

Host plant and distribution of both species. Galls of both *A. parrai* and *O. saizi* have been found only on branches of *Schinus polygamus* (Cav.) Cabrera (Anacardiaceae), a small tree with single and glabrous leaves and slender spiny branches (Barkley 1957, Fleig 1989), commonly known in Chile as Huingan. The taxonomy of *Schinus* L. in southern South America is rather complex, as its wide geographic distribution and phenotypic plasticity have lead historically to a confused taxonomy. In fact, the genus is currently under review (CLS Luz, USP, pers. comm.), and *S. polygamus* (sensu lato; Cabrera 1938, Fleig 1987, 1989) may be split into several species, as already proposed by Barkley (1957). Nevertheless, according to this author in this case the true *S. polygamus* would be restricted in distribution to Chile. *Andescecidium parrai* and *O. saizi* galls were found on populations of *S. polygamus* on the central area, also known as the Mediterranean portion of the country (Quintanilla et al. 2012), which extends from 32°45'N to 37°30'S, abridging the V, VI, VII, VIII and Metropolitan (RM) regions (Figure 15). The main characteristics of this area are the presence of two mountainous ranges, the Andes on the east and the Coastal Range on the west, as well as the central valley located in between them. Plants bearing galls of both cecidosid species were found mainly in the Coastal Range (Figs 8A, 14A). The climate in these valleys is typically austral Mediterranean; the vegetation is autochthonous, composed of sclerophyllous forests, palm communities and coniferous forests and steppe at higher altitudes (Quintanilla et al. 2012, Valencia et al. 2015).

Discussion

This study illustrates further how important are intensive studies including the immature stages to achieve correct identification of true gall-inducing in Lepidoptera. It confirms preliminary findings of Sáiz and Núñez (1997), which were further supported by Parra (1998), showing that the cylindrical external galls associated with *S. polygamus* in Chile are induced by a cecidosid moth, and not by a beetle as originally suggested by Kieffer and Herbst (1905, 1906) and Houard (1933). In fact, during dissection of these galls we occasionally found an unidentified species of Coleoptera associated with them but only later in ontogeny; small, early developing galls always contained a larva of *Andececidium parrai*. We believe that this beetle acts as a kleptoparasite (sensu Luz et al. 2015), since apparently it does not change substantially the shape of the galls after usurping them. In addition, we found that galls of *A. parrai* may host other unidentified parasitoids, predators, and successors, thus being complex systems, similar to what has been previously demonstrated for *Cecidonius pampeanus* (Moreira et al. 2017). Thus we attribute in part the historical confusion involving the taxonomy of cecidosids in Chile to the scarce sampling activity from a taxonomic perspective in the past, and to the fact that galls of *A. parrai* and *O. saizi* are sympatric, occurring sometimes on the same host-plant and branch, as already mentioned. Furthermore, galls of the former are deciduous and those of the latter restricted to under bark, which makes them difficult to detect on plants in the field, and as a consequence also hard to be reared to the adult stage by non-specialists.

Andescecidium parrai and *O. saizi* resulted as unique lineages in the present study from both morphological and molecular analyses. The former appeared as one of the

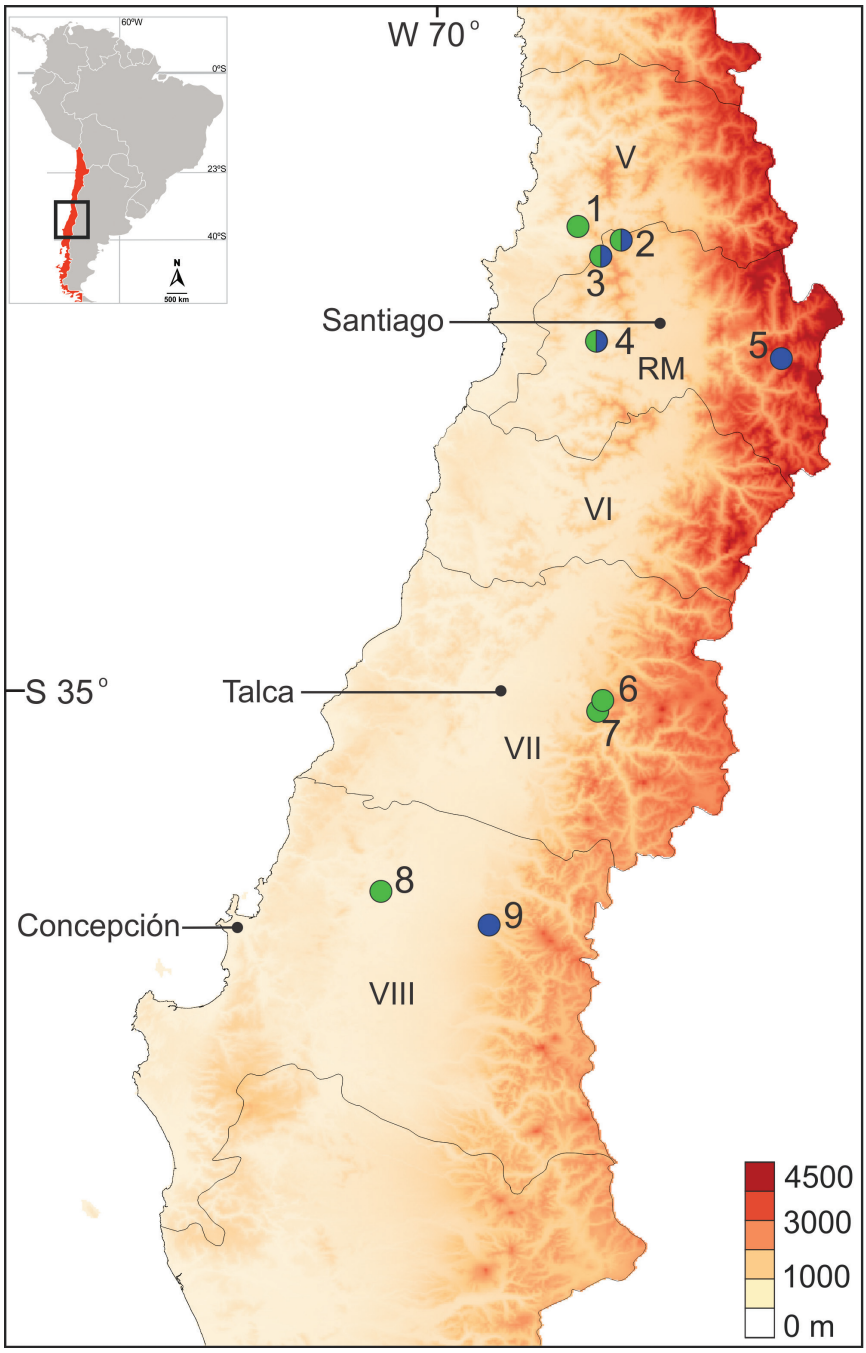

Figure 15. Geographic distribution of *Andescecidium parrai* (green circles) and *Oliera saizi* (blue circles) in central Chile. Regions are indicated by Roman numbers except for the Metropolitan (RM). Localities are indicated by cardinal numbers: **1** Parque Nacional La Campana **2** Cuesta La Dormida **3** Til-Til/Hungue **4** Cuesta Barriga **5** Cajón del Maipo **6** Curicó **7** San Clemente **8** Cruce Nebuco, and **9** Recinto; for a complete description of corresponding localities, see list of specimens examined.

most derived lineages to be evolved within the extant cecidosids. The genetic distance of *A. parrai* is ca. 10% from the nearest related species, an additional undescribed cecidosid existing in Mendoza, Argentina, which was included in the present study for comparison. *Oliera saizi* diverged ca. 6%, from an undescribed *Oliera* species collected at the same latitude in Argentina, and ca. 5% from the type species *O. argentinana*, sampled in southern Brazil. Thus molecular data suggest that although described as monotypic, there is at least one more species belonging to *Andescecidium*, and another to *Oliera*. In fact, these species share morphological characteristics with congenerics regarding the gall and larval stage, but unfortunately they have not been reared yet to the pupal and adult stages, upon which their descriptions are pending.

The present study also provides support to previous statements in the literature in the sense that inclusion of immature stages and galls is essential for elucidation of the taxonomy of Cecidosidae (Moreira et al. 2012, 2017). Our findings indicate that these moths have adults with relatively uniform morphologies, especially in relation to the genitalia, which apparently vary less compared to the immature stages at the generic level (see also Mey 2007). The adult mouth parts, frontal and caudal processes, tergal spines and arrangement of setae on the pupa, number and size of secondary setae on larva, and the plant tissue from which the galls are differentiated in association with their shape and size are apparently the main sources of morphological variation within the group. The wide genetic divergence among congenerics (6% in *Oliera*, 7% in *Cecidonius* and 10% in *Andescecidium*) found up to now at the molecular level (mitochondrial, COI sequences) is also notable, which demonstrates the importance of this kind of analysis in taxonomic studies.

A complete scenario of relationships within Cecidosidae, inferred in the Bayesian calibrated-time tree, retrieved high posterior probabilities for all nodes. It was somewhat unexpected to obtain a fully resolved genus-level tree, based on only two to three markers (see Kawahara et al. 2011). Therefore, results at this level in our study should be interpreted cautiously, as the support provided by the Markov Chain Monte Carlo-based Bayesian method may be overestimated, since it is more dependent on the model suitability than other methods, such as bootstrap (Simmons et al. 2004). The use of more loci usually increases the robustness of phylogenies, particularly the support of nodes (Regier et al. 2009, Kawahara et al. 2011, Zwick et al. 2011). Although COI alone may not accurately reflect the evolutionary relationships among species (Wahlberg and Wheat 2008), it is suitable as a simple estimate of genetic distance among moth lineages, as a first approach to evaluating the amount of difference. Regier et al. (2015) sequenced 15 nuclear genes (ca. 7,500 bp) in distinct Adeloidea families and found 25% of variation within Cecidosidae (*Cecidoses* vs. *Dicranoses*), quite similar to the 23% we found in COI. A comparative analysis using multilocus data generated by Regier et al. (2015) on variation within Adeloidea supports that Cecidosidae present greater variation in relation to the other families included (Adelidae, 13%; Incurvariidae, 13%; Prodoxidae, 17%). The high variation found by Regier et al. (2015) and in our study (also shown by long branches in the reconstructed phylogeny of Cecidosidae) might be related to the old age of this group (i.e. with more time to accumulate differences between lineages), incomplete sampling, and/or early extinctions. Additionally, differences in patterns and/or rates of molecular evolu-

tion of cecidosids (also observed in the genus *Scyrotis*, retrieved as polyphyletic) specifically related to COI might be due to metabolism-related factors (Pentinsaari et al. 2016).

In this study we recorded for the first time two new species of cecidosids for Chile that belong to two relatively recent genera (*Andescecidium* and *Oliera*) that apparently have representatives distributed on both the west and east sides of the Andes. Based on a broader survey exploring several southern South America biomes, Silva et al. (2018) suggested that the uplift of the Andes had a major role on speciation of *Eucecidoses* (Brèthes), a related genus with distribution restricted to the eastern Andes. Similar studies should be conducted for the west Andean cecidosid species described here. As already mentioned, galls induced by *O. saizi* had not been detected on *S. polygamus* before this study. But gall morphotypes similar to them, and also to those described in this study for *A. parrai*, were reported for the stems of *S. latifolius* (Gillies ex Lindl.) Engl. by Sáiz and Núñez (1997). The geographic distribution of *S. polygamus* is broader than that covered in this study, and there are a few other native species of *Schinus* in Chile (see Rodríguez et al. 2018), which should be also explored for galls. In other words, the diversity of cecidosids in Chile is believed to be greater, and thus should be better studied from a taxonomic perspective, involving other Anacardiaceae species, before a phylogeographic approach can be undertaken.

Acknowledgements

We thank the staff members of Centro de Microscopia Eletrônica and Thales O Freitas (UFRGS) for the use of facilities and assistance with scanning electron microscopy and molecular analyses, respectively. This work benefited from fruitful previous discussions with Francisco Sáiz (Universidad Católica de Valparaiso) and Luis E Parra (Universidad de Concepción) on the biology of cecidosid galls. The latter also kindly provided assistance with field work in the VII and VIII Regions of Chile. Thanks are also due to Francisco C Urra Lagos (Museu Nacional de História Natural, Santiago) and one anonymous reviewer for important suggestions made on the first version of the manuscript. We are also grateful to Lafayette Eaton for editing the manuscript. This research was supported in part by a PRONEX project (process 16/2551-0000485-4) from Fundação de Amparo à Pesquisa do Estado do Rio Grande do Sul (FAPERGS)/CNPq. GL Gonçalves, GT Silva and GRP Moreira were supported by fellowships from FAPERGS/CNPq, CAPES/PPGBan/UFRGS and CNPq, respectively. MD Mainardi was supported by the undergraduate research program of PROPESQ/UFRGS.

References

Barkley FA (1957) A study of *Schinus* L. Lilloa 28: 1–110.

Brèthes J (1916) Estudio fito-zoológico sobre algunos lepidópteros Argentinos productores de agallas. Anales de la Sociedad Científica Argentina 82: 113–140.

Bouckaert R, Heled J, Kuhnert D, Vaughan T, Wu C-H, Xie D, Suchard MA, Rambaut A, Drummond AJ (2014) BEAST 2: a software platform for Bayesian evolutionary analysis. PLoS Computational Biology 10: e1003537. https://doi.org/10.1371/journal.pcbi.1003537

Cabrera AL (1938) Revisión de las Anacardiáceas Austroamericanas. Revista del Museo de La Plata 2: 3–64.

Davis DR (1998) The monotrysian Heteroneura. In: Kristensen NP (Ed.) Lepidoptera, moths and butterflies, vol. 1: Evolution, systematics and biogeography. Handbook of Zoology 4(35). Walter de Gruyter, Berlin, 65–90. https://doi.org/10.1515/9783110804744.65

Drummond AJ, Rambaut A (2007) Beast: Bayesian evolutionary analysis by sampling trees. BMC Evolutionary Biology 7: 214. https://doi.org/10.1186/1471-2148-7-214

Drummond AJ, Ho SYW, Phillips MJ, Rambaut A (2006) Relaxed phylogenetics and dating with confidence. PLoS Biology 4: e88. https://doi.org/10.1371/journal.pbio.0040088

Fleig M (1987) Anacardiaceae. Boletim Instituto de Biociências 42: 1–72. [Flora Ilustrada do Rio Grande do Sul, 18]

Fleig M (1989) Anacardiáceas. In: Reitz R (Ed.) Flora Ilustrada Catarinense. Herbário Barbosa Rodrigues, Itajaí, 1–64.

Hoare RJB, Dugdale JS (2003) Description of the New Zealand incurvarioid *Xanadoses nielseni*, gen. n., sp. n. and placement in Cecidosidae (Lepidoptera). Invertebrate Systematics 17: 47–57. https://doi.org/10.1071/IS02024

Houard C (1933) Les zoocécidies des Plantes de l`Amérique du Sud et de l`Amérique Centrale. Librairie Scientifique Hermann et Cie, Paris, 519 pp.

Kawahara A, Ohshima I, Kawakita A, Regier JC, Mitter C, Cummings MP, Davis DR, Wagner DL, De Prins J, Lopez-Vaamonde C (2011) Increased gene sampling strengthens support for higher-level groups within leaf-mining moths and relatives (Lepidoptera: Gracillariidae). BMC Evolutionary Biology 11: 182. https://doi.org/10.1186/1471-2148-11-182

Kieffer JJ, Herbst P (1905) Ueber gallen und gallennerzeuger aus Chile. Zeischrift fur Wissenchaftliche Insektenbiologie 10: 63–66.

Kieffer JJ, Herbst P (1906) Description de Galles et d'Insectes gallicoles du Chili. Annales de la Société Scientifique de Bruxelles 30: 223–236. [figs 1–5, pl I]

Kristensen NP (2003) Skeleton and muscles: adults. In: Kristensen NP (Ed.) Lepidoptera: Moths and Butterflies, vol. 2: Morphology, Physiology, and Development. Handbook of zoology 4(36). Walter de Gruyter, Berlin, 39–131.

Lanfear R, Calcott B, Ho SYW, Guindon S (2012) PartitionFinder: combined selection of partitioning schemes and substitution models for phylogenetic analyses. Molecular Biology and Evolution 29: 1695–1701. https://doi.org/10.1093/molbev/mss020

Luz FA, Gonçalves GL, Moreira GRP, Becker VO (2015) Description, molecular phylogeny, and natural history of a new kleptoparasitic species of gelechiid moth (Lepidoptera) associated with Melastomataceae galls in Brazil. Journal of Natural History 49: 1849–1875. https://doi.org/10.1080/00222933.2015.1006284

Mey W (2007) Cecidosidae (Lepidoptera: Incurvarioidea). In: Mey W (Ed.) The Lepidoptera of the Brandberg Massif in Namibia. Esperiana Memoir 4: 31–48.

Moreira GRP, Gonçalves GL, Eltz RP, San Blas G, Davis DR (2012) Revalidation of *Oliera* Brèthes (Lepidoptera: Cecidosidae) based on a redescription of *O. argentinana* and DNA analysis of Neotropical cecidosids. Zootaxa 3557: 1–19.

Moreira GRP, Eltz RP, Pase RB, Silva GT, Bordignon SAL, Mey W, Gonçalves GL (2017) *Cecidonius pampeanus*, gen. et sp. n: an overlooked and rare, new gall-inducing micromoth associated with *Schinus* in southern Brazil (Lepidoptera, Cecidosidae). Zookeys 695: 37–74. https://doi.org/10.3897/zookeys.695.13320

Morris DC, Mound LA, Schwarz MP (2000) *Advenathrips inquilinus*: a new genus and species of social parasites (Thysanoptera: Phlaeothripidae). Australian Journal of Entomology 39: 53–57. https://doi.org/10.1046/j.1440-6055.2000.00146.x

van Nieukerken EJ, Kaila L, Kitching IJ, Kristensen NP, Lees DC, Minet J, Mitter C, Mutanen M, Regier JC, Simonsen TJ, Wahlberg N, Yen S-H, Zahiri R, Adamski D, Baixeras J, Bartsch D, Bengtsson BÅ, Brown JW, Bucheli SR, Davis DR, De Prins J, De Prins W, Epstein ME, Gentili-Poole P, Gielis C, Hättenschwiler P, Hausmann A, Holloway JD, Kallies A, Karsholt O, Kawahara AY, Koster SJC, Kozlov M, Lafontaine JD, Lamas G, Landry J-F, Lee S, Nuss M, Park K-T, Penz C, Rota J, Schintlmeister A, Schmidt BC, Sohn J-C, Solis MA, Tarmann GM, Warren AD, Weller S, Yakovlev RV, Zolotuhin VV, Zwick A (2011) Order Lepidoptera Linnaeus, 1758. In: Zhang Z-Q (Ed.) Animal biodiversity: An outline of higher-level classification and survey of taxonomic richness. Zootaxa 3148: 212–221. http://www.mapress.com/zootaxa/2011/f/zt03148p221.pdf

van Noort S, Stone GN, Whitehead VB, Nieves-Aldrey J-L (2007) Biology of *Rhoophilus loewi* (Hymenoptera: Cynipoidea: Cynipidae), with implications for the evolution of inquilinism in gall wasps. Biological Journal of the Linnean Society 90: 153–172. https://doi.org/10.1111/j.1095-8312.2007.00719.x

Núñez C, Sáiz F (1994) Cecidios en vegetación autoctona de Chile de clima mediterráneo. Anales del Museo de Historia Natural de Valparaíso 22: 57–80.

Parra LE (1998) A redescription of *Cecidoses argentinana* (Cecidosidae) and its early stages, with comments on its taxonomic position. Nota lepidopterologica 21: 206–214.

Pentinsaari M, Salmela H, Mutanen M, Roslin T (2016) Molecular evolution of a widely adopted taxonomic marker (COI) across the animal tree of life. Scientific Reports 6: 35275. https://doi.org/10.1038/srep35275

Quintanilla V, Cadiñanos JA, Latasa I, Lozano PJ (2012) Aproximación biogeográfica a lós bosques de la Zona Mediterránea de Chile: caracterización e inventário. Boletín de la Asociación de Geógrafos Españoles 60: 91–114. https://doi.org/10.21138/bage.1500

Rambaut A (2009) Molecular evolution, phylogenetics and epidemiology: FigTree. http://tree.bio.ed.ac.uk/software/figtree/

Regier JC, Zwick A, Cummings MP, Kawahara AY, Cho S, Weller S, Roe A, BaixerasJ, Brown JW, Parr C, Davis DR, Epstein M, Hallwachs W, Hausmann A, Janzen DH, Kitching IJ, Solis MA, Yen SH, Bazinet AL, Mitter C (2009) Towards reconstructing the evolution of advanced moths and butterflies (Lepidoptera: Ditrysia): an initial molecular study. BMC Evolutionary Biology 9: 280. https://doi.org/10.1186/1471-2148-9-280

Regier JC, Mitter C, Kristensen NP, Davis DR, Nieukerken EJ van, Rota J, Simonsen TJ, Mitter KT, Kawahara AY, Yen S-H, Cummings MP, Zwick A (2015) A molecular phylogeny for the oldest (nonditrysian) lineages of extant Lepidoptera, with implications for classification, comparative morphology and life-history evolution. Systematic Entomology 40: 671–704. https://doi.org/10.1111/syen.12129

Rodríguez R, Marticorena C, Alarcón D, Baeza C, Cavieres L, Finot VL, Fuentes N, Kiessling A, Mihoc M, Pauchard A, Ruizi E, Sanchez P, Marticorena A. (2018) Catálogo de las plantas vasculares de Chile. Gyana Botanica 70: 1–430.

Ronquist F (1994) Evolution of parasitism among closely related species: phylogenetic relationships and the origin of inquilinism in gall wasps (Hymenoptera, Cynipidae). Evolution 48: 241–266. https://doi.org/10.1111/j.1558-5646.1994.tb01310.x

San Blas G, Davis DR (2013) Redescription of *Dicranoses capsulifex* Kieffer and Jörgensen (Lepidoptera: Cecidosidae) with description of the immature stages and biology. Zootaxa 3682: 371–384. https://doi.org/10.11646/zootaxa.3682.2.9

Sáiz F, Núñez C (1997) Estudio ecológico de las cecidias del género *Schinus*, especialmente las de hoja y de rama de *S. polygamus* y *Schinus latifolius* (Anacardiaceae), en Chile Central. Acta Entomológica Chilena 21: 39–59.

Silva GT, San Blas G, Peçanha WT, Moreira GRP, Gonçalves GL (2018) Phylogeography of the gall-inducing micromoth *Eucecidoses minutanus* Brèthes (Cecidosidae) reveals lineage diversification associated with the Neotropical Peripampasic Orogenic Arc. PLoS ONE 13(8): e0201251. http://doi.org/10.1371/journal.pone.0201251

Simmons MP, Pickett KM, Miya M (2004) How meaningful are Bayesian support values? Molecular Biology and Evolution 21:188–199. https://doi.org/10.1093/molbev/msh014

Tamura K, Stecher G, Peterson D, Filipski A, Kumar S (2013) MEGA6: molecular Evolutionary Genetics Analysis version 6.0. Molecular Biology and Evolution 30: 2725–2729. https://doi.org/10.1093/molbev/mst197

Valencia PJLV, Aguirre JAC, Zaballos IL, Pérez VGQ, Rodríguez GM (2015) Valoración y evalución biogeográfica de diversos paisajes vegetales de la Región Mediterránea de Chile para su ordenación y gestión. Boletín de la Asociación de Geógrafos Españoles 67: 83–103.

Wahlberg N, Wheat CW (2008) Genomic outposts serve the phylogenomic pioneers: Designing novel nuclear markers for genomic DNA extractions of Lepidoptera. Systematic Biology 57: 231–242. https://doi.org/10.1080/10635150802033006

Walhberg N, Wheat CW, Peña C (2013) Timing and patterns in the taxonomic diversification of Lepidoptera (butterflies and moths). PLoS ONE 8: e80875. https://doi.org/10.1080/10635150802033006

Zwick A, Regier JC, Mitter C, Cummings MP (2011) Increased gene sampling yields robust support for higher-level clades within Bombycoidea (Lepidoptera). Systematic Entomology 36: 31–43. https://doi.org/10.1111/j.1365-3113.2010.00543.x